EVALUATING THE NEUROPROTECTIVE EFFECT OF CURCUMIN IN A PINK1 CELL MODEL OF PARKINSON'S DISEASE

by

Devina Chetty

Thesis presented in partial fulfilment of the requirements for the degree of Master of Science in the Faculty of Medicine and Health Sciences at Stellenbosch University

Supervisor: Prof. Soraya Bardien

Co-supervisors: Prof. Colin Kenyon and Dr. Shameemah Abrahams

April 2022

Declaration

By submitting this thesis electronically, I declare that the entirety of the work contained therein is my own, original work, that I am the sole author thereof (save to the extent explicitly otherwise stated), that reproduction and publication thereof by Stellenbosch University will not infringe any third-party rights and that I have not previously in its entirety or in part submitted it for obtaining any qualification.

April 2022

ABSTRACT

Parkinson's disease (PD) is a neurodegenerative disorder characterized by a loss of neurons producing the neurotransmitter dopamine. Notably, despite extensive studies that have revealed numerous dysregulated processes associated with PD, fundamental gaps still exist in our knowledge of the disease pathophysiology. Our understanding of the disease includes processes such as mitochondrial dysfunction causing increased oxidative stress and energy failure, as well as misfolded protein accumulation in large inclusions. However, the spatiotemporal sequence of events leading to PD and, importantly, the initial factors that trigger disease onset remain elusive. This challenges the development of effective therapeutic strategies to prevent and cure PD. Moreover, the various side effects associated with conventional pharmaceuticals currently used to treat this disease motivate the search for a natural treatment that can avoid augmenting the suffering associated with an already debilitating disease. It is evident that mitochondrial dysfunction and oxidative stress are likely to be involved in the disease pathogenesis, therefore studying these phenomena in PD may lead to the development of more effective therapeutic strategies.

Curcumin is a plant-based polyphenol that has been observed to have antioxidant properties, increase cell viability, and enhance mitochondrial function. Consequently, the aim of the present study was to create a PD cellular model and evaluate the potential protective effects of curcumin. Therefore, we sought to establish an appropriate PD model by transfecting SH-SY5Y cells with wild-type (WT) or G309D mutant PINK1 cDNA, of which the latter has been shown to upregulate dopamine and lead to cytotoxicity. Additionally, since several neurotoxins have been shown to trigger PD, the toxic herbicide paraquat was administered to complement the model with cellular damage and mitochondrial dysfunction. To confirm the model, we performed RT-qPCR to measure gene expression levels of *PINK1* and tyrosine hydroxylase (*TH*), an enzyme in the dopamine synthesis pathway. *PINK1* was significantly upregulated in the mutant, however, no significant difference in *TH* gene expression was observed between groups. We then sought to measure the levels of dopamine in transfected cells using liquid chromatography-mass spectrometry (LC-MS). Although no dopamine was detected using LC-MS, higher levels of phenylalanine, a precursor of dopamine, were observed in the mutant. Using this model, we sought to test the protective effects of curcumin using assays that measure cellular and mitochondrial health. A toxic paraquat concentration of 1.7 mM was chosen to elicit a 50 % decrease in cell viability for the model, while a curcumin concentration of 2.5 µM was chosen as it exhibited no toxic effects.

Following the establishment of the model, four treatment groups were established for all experiments thereon: untreated control, curcumin only treatment, paraquat only treatment, and pre-treatment (curcumin treatment followed by paraquat treatment). We found that curcumin was unable to significantly rescue the paraquat-induced reduction in cell viability and mitochondrial membrane

potential. The latter was significantly reduced in *PINK1* transfected groups, more so in the G309D mutant, indicating the toxic effects of the mutation. Thereafter, the effects of curcumin and polycaprolactone encapsulated nanocurcumin on cell viability were compared. Formulations of curcumin including nanocurcumin are postulated to improve the stability and efficacy of curcumin. Interestingly, curcumin had a greater protective effect, whereas nanocurcumin as well as the empty nanoparticles elicited toxicity. In fact, pre-treatment with the nanocurcumin prior to paraquat treatment caused a 30 % greater loss in cell viability compared to the paraquat treatment alone. Finally, a literature review was published, exploring the potential of consistent dietary consumption of curcumin as an alternative or supplement to existing therapies. We speculate that curcumin binds to α-synuclein protein (found to accumulate in PD) and that this complex is subsequently excreted from the body via the large intestine. In this view, replacing some of the PD drugs in an individual's treatment regime with a nutraceutical, or 'functional food', like curcumin may improve therapeutic benefits with fewer side effects. Considering these results and the published evidence for curcumin as a dietary 'nutraceutical', further studies are required to optimize curcumin treatment before advocation of its widespread use as a PD therapeutic agent. Study limitations include the use of an unverified WT plasmid and an undifferentiated cell line, which can be addressed in future work. The findings in this study are of importance as they may contribute to advancing the development of novel plant-based therapies to treat and potentially prevent this detrimental disease.

OPSOMMING

Parkinson se siekte (PS) is 'n neurodegeneratiewe versteuring wat gekenmerk word deur 'n verlies aan neurone wat die neurotransmitter dopamien produseer. Merkwaardig, ten spyte van omrykende studies wat talle gedisreguleerde prosesse verwant aan PS geopenbaar het, bestaan fundamentele gapings steeds in ons kennis van die siektepatofisiologie. Ons begrip van die siekte sluit prosesse soos mitochondriale disfunksie in wat verhoogde oksidatiewe stres en energiemislukking veroorsaak, asook verkeerde proteïenophoping in groot insluitings. Die tydruimtelike volgorde van gebeure wat tot PS lei en, belangriker, die aanvanklike faktore wat siekte-aanvang veroorsaak, bly egter ontwykend. Dit daag die ontwikkeling van effektiewe terapeutiese strategieë uit om PS te voorkom en te genees. Bowendien, het die huidige konvensionele farmaseutiese behandelinge vir PS tale newe-effekte. Dit dien as motivering vir soektogte na 'n natuurlike behandeling wat die aanvullende leiding kan verminder van 'n reeds afbrekende siekte. Dit is duidelik dat mitochondriale disfunksie en oksidatiewe stres betrokke is by die siekte se patologie, daarom kan die bestudering van hierdie verskynsels in PS lei tot die ontwikkeling van meer effektiewe terapeutiese strategieë.

Kurkumien is 'n plantgebaseerde polifenol wat waargeneem is om antioksidant eienskappe te toon, verhoog sel lewenskragtigheid en verbeter mitochondriale funksie. Gevolglik was die doel van die huidige studie om 'n PS-sellulêre model te skep en die potensiële beskermende effekte van kurkumien te evalueer. Daarom het ons probeer om 'n toepaslike PS-model te vestig deur SH-SY5Y-selle met wilde-tipe (WT) of G309D muteerde PINK1 cDNA te transreguleer, waarvan laasgenoemde dopamien op gereguleer het wat gelei het tot sitotoksiteit. Daarbenewens, aangesien verskeie neurotoksiene getoon is om PS te aktiveer, is die giftige onkruiddoder, parakwat, toegedien om die model aan te vul met sellulêre skade en mitochondriale disfunksie. Om die model te bevestig, het ons RT-qPCR uitgevoer om geen-uitdrukkingsvlakke van PINK1 en tyrosine hydroxylase (TH), 'n ensiem betrokke by die chemiese samestelling van dopamien, kwantitatief te meet. PINK1 was aansienlik opgereguleer in die muteerde, maar geen beduidende verskil was opgemerk in TH-geenuitdrukking tussen groepe nie. Ons het toe probeer om die vlakke van dopamien in transfekte selle te meet met behulp van vloeibare chromatografie-massaspektrometrie (VC-MS). Alhoewel geen dopamien opgespoor was met behulp van VC-MS nie, was hoër vlakke van fenylalanien, 'n voorloper van dopamien, in die muteerde waargeneem. Met behulp van hierdie model het ons probeer om die beskermende effekte van kurkumien te toets met behulp van eksperimente wat sellulêre en mitochondriale gesondheid kan bepaal. 'n Giftige parakwat konsentrasie van 1.7 mM was gekies om 'n 50% afname in sel lewensvatbaarheid in die model te ontlok, terwyl 'n kurkumien konsentrasie van 2.5 μM gekies was, aangesien dit geen giftige effekte getoon het nie.

Na die bevestiging van die model was vier behandelingsgroepe gestig vir alle eksperimente wat volg daarna, dit sluit in: onbehandelde kontrole, kurkumien alleenlik, parakwat alleenlik, en voor-

behandeling (kurkumien behandeling gevolg deur parakwat behandeling). Ons het gevind dat kurkumien nie merkwaardig die selle kon beskerm teen die verlaagde sel lewenskragtigheid en mitochondirale membraanpotentiaal wat geïnduseer was deur parakwat nie. Die mitochondriale membraanpotentiaal was aansienlik verminder in die PINK1-getransfekteerde groepe, meer so as in die G309D-muteerde, dit dui die giftige effekte van die mutasie aan. Daarna is die effek van kurkumien en policaprolactone ingeslote nanokurkumien op sel lewensvatbaarheid vergelyk. Formulerings van kurkumien, insluitend nanokurcumin, word gepostuleer om die stabiliteit en doeltreffendheid van kurkumien te verbeter. Interessant genoeg, kurkumien het 'n groter beskermende effek gehad, terwyl nanokurcumin sowel as die leë nanopartikels toksisiteit getoon het. In werklikheid, het die voorbehandeling met nanokurkumien (voor parakwat behandeling) 'n 30% groter verlies in sel lewenskragtigheid veroorsaak as die selle met slegs parakwat behandeling. Ten slotte is 'n literatuuroorsig gepubliseer, wat die potensiaal van konsekwente dieet verbruik van kurkumien ondersoek as 'n alternatief of aanvulling tot bestaande terapieë. Ons spekuleer dat kurkumien aan α-sinukleien proteien bind (gevind om te versamel in PS) en dat hierdie kompleks daarna uit die liggaam uitgeskei word deur die dikderm. Deur dit in ag te neem, kan die vervanging van sommige van die huidige PS-behandelinge met nutraceutiese produkte, of 'funksionele kos', soos kurkumien, voordelig wees en minder newe-effekte hê. Samevattend met hierdie resultate en die gepubliseerde bewyse vir kurkumien as 'n dieet 'nutraceutical', is verdere studies nodig om kurkumien behandeling te optimiseer voordat die wydverspreide gebruik daarvan as 'n PS terapeutiese middel kan gebeur. Studie beperkings sluit in die gebruik van 'n ongeverifieerde WT-plasmied en 'n ongedifferensieerde sellyn, wat in toekomstige werk aangespreek kan word. Die bevindings in hierdie studie is van belang, aangesien dit kan bydra tot die bevordering van die ontwikkeling van nuwe plantgebaseerde terapieë om hierdie nadelige siekte te behandel en moontlik te voorkom.

ACKNOWLEDGEMENTS

I would like to express my sincere appreciation to the following individuals and institutions for their support throughout this degree:

To my supervisor, Prof. Soraya Bardien. Thank you for being a role model for me - your work ethic and leadership inspired and pushed me to achieve this degree. Your kind nature and guidance are what I will always be thankful for.

To my co-supervisor, Prof. Colin Kenyon. Thank you for your enthusiasm and vast knowledge that you have conferred on me throughout this degree. You have helped me to work independently and improve my critical thinking skills.

To my co-supervisor, Dr. Shameemah Abrahams. Thank you for your continuous mentorship and support throughout this degree. I've been lucky to learn from such a knowledgeable and patient teacher.

Thank you to Stellenbosch University, the Department of Biomedical Sciences and the Division of Molecular Biology and Human Genetics for the use of their facilities. I would like to acknowledge Prof. Tromp for his assistance regarding statistical analysis.

Thank you to our collaborators at the University of Western Cape for providing us with nanocurcumin to use in this study. Special thanks to Dr. Sarah D'Souza who synthesized and validated the nanocurcumin.

I'd like to thank the members of the Parkinson's Disease Research Group for their moral support as well as advice and assistance in the laboratory.

To my colleagues in the MAGIC lab, thank you for help with my research project whenever needed, and for providing a pleasant working environment.

To my family and friends. Thank you for your unwavering support, love, and belief in me without which I could not have achieved this goal.

Finally, I would like to acknowledge my faith in God through whom I can do all things.

RESEARCH OUTPUTS

Publications:

Literature review: first author

Reference: **Chetty, D**., Abrahams, S., van Coller, R., Carr, J., Kenyon, C., & Bardien, S. (2021). Movement of prion-like α-synuclein along the gut-brain axis in Parkinson's disease: A potential target of curcumin treatment. The European journal of neuroscience, 54(2), 4695–4711. https://doi.org/10.1111/ejn.15324

Contribution to this output: compiling information from the literature writing of first draft, drawing figures, editing of manuscript, submission to journal, and responding to reviewers' comments.

Letter to the editor: third author

Reference: van Rensburg, Z.J., Abrahams, S., **Chetty, D**., Step, K., Acker, D., Lombard, C.J., Elbaz, A., Carr, J. and Bardien, S. (2021), The South African Parkinson's Disease Study Collection. Mov Disord. https://doi.org/10.1002/mds.28828

Contribution to this output: Writing of introduction, assisting with Graphical Abstract, reviewing final document.

TABLE OF CONTENTS

LIST OF FIGURES

LIST OF TABLES

LIST OF SYMBOLS AND ABBREVIATIONS

%	Percentage
+	Addition
=	Equal to
<	Smaller than
>	Greater than
°C	Degrees Celsius
µl	Microlitres
ml	Millilitres
µM	Micromolar
mM	Millimolar
©	Copyright
™	Trademark
s	Second
min	Minute
h	Hour
6-OHDA	6-hydroxydopamine
AADC	Aromatic acid decarboxylase
ALDH	Alcohol dehydrogenase
AMP	Adenosine 5'-monophosphate
AMPK	Adenosine 5'-monophosphate (AMP)-activated protein kinase (AMPK)
ANOVA	Analysis of variance
ATP	Adenosine triphosphate
BLAST	Basic Local Alignment Search Tool
BSA	Bovine serum albumin
CAF	Central Analytical Facilities
CCCP	Carbonyl cyanide 3-chlorophenylhydrazone
CNS	Central nervous system
CO_2	Carbon dioxide
COMT	Catechol-O-methyltransferase
CRISPR	Clustered regularly interspaced short palindromic repeats
DAC	Dopaminochrome
DAQ	Dopamine quinone
DASQ	Dopamine semiquinone
DAT	Dopamine transporter
DHI	5,6-dihydroxyindole
DHIQ	5,6-dihydroxyindole quinone
DMEM	Dulbecco's Modified Eagle's Medium
DMNV	Dorsal motor nucleus of the vagus nerve
DMSO	Dimethyl sulfoxide
DNA	Deoxyribonucleic acid
dNTP	Deoxynucleoside triphosphate
ddNTP	Dideoxyribonucleotide

DOPAC	3,4-dihydroxyphenylacetic acid
DOPAL	3,4-dihydroxyphenylacetaldehyde
DOPET	3,4-dihydroxyphenylethanol
DβH	Dopamine β-hydroxylase
EDTA	Ethylenediaminetetraacetic acid
FBS	Fetal bovine serum
FITC	Fluorescein isothiocyanate
GC	Gas chromatography
GI	Gastrointestinal
GPe	Globus pallidus pars externa
GPi	Globus pallidus pars interna
GSH	Glutathione
H_2O	Water
H_2O_2	Hydrogen peroxide
HO-1	Hemeoxygenase 1
HPLC	High performance liquid chromatography
HVA	Homovanillic acid
IMM	Inner mitochondrial membrane
iPSC	Induced pluripotent stem cell
JC-1	1,1',3,3'-Tetraethyl-5,5',6,6'-tetrachloroimidacarbocyanine iodide
LB	Lewy body
LC	Liquid chromatography
LC-MS	Liquid chromatography-mass spectrometry
LDAC	Leukodopaminochrome
L-DOPA	L-3,4-dihydroxyphenylalanine
L-Tyr	L-tyrosine
LUHMES	Lund human mesencephalic
MAO-B	Monoamine oxygenase B
MAPK	Mitogen-activated protein kinase
MOPAL	3-methoxy-4-hydroxyphenyl acetaldehyde
MPTP	1-methyl-4-phenyl-1,2,3,6-tetrahydropyridine
MS	Mass spectrometry
MTS	Mitochondrial targeting sequence
MTT	3-(4,5-Dimethylthiazol-2-yl)-2,5-diphenyltetrazolium bromide
MTY	Methoxytyramine
NAC	N-acetylcholine
NADPH	Nicotinamide adenine dinucleotide phosphate
NADH	Nicotinamide adenine dinucleotide
NCBI	National Centre for Biotechnology Information
NE	Norepinephrine
NHP	Non-human primate
NO	Nitrogen oxide
NP	Nanoparticle
O_2	Oxygen
OMIM	Online mendelian inheritance in man
OMM	Outer mitochondrial membrane

OMS	Membrane localization signal
PBS	Phosphate buffered saline
PC12	Pheochromocytoma
PCL	Polycaprolactone
PCR	Polymerase chain reaction
PD	Parkinson's disease
PDI	Polydispersity index
PE	R-phycoerythrin
PI3K/AKT/Nrf2	Phosphatidylinositol 3-kinase/protein kinase B/nuclear factor erythroid 2–related factor 2
PINK1	Phosphatase and tensin homolog (PTEN)-induced kinase 1
PPM	Parts per million
PTEN	Phosphatase and tensin homolog
PVA	Polyvinyl alcohol
RA	Retinoic acid
RNA	Ribonucleic acid
ROS	Reactive oxygen species
RT-qPCR	Real-time, quantitative, reverse transcription polymerase chain reaction
SA	South Africa
SARS-COV 2	Severe acute respiratory syndrome coronavirus 2
SEM	Scanning electron microscope
SFM	Serum-free media
SN	Substantia nigra
SNc	Substantia nigra pars compacta
SNr	Substantia nigra pars reticulata
SP	Sodium pyruvate
STN	Subthalamic nucleus
TFEB	Transcription factor EB
TH	Tyrosine hydroxylase
TMS	Transmembrane sequence
TRAP1	Tumor necrosis factor receptor-associated protein 1
UBL	Ubiquitin-like domain
VL	Ventrolateral nucleus
VMAT2	Vesicular monoamine transporter 2
WT	Wild-type
ZP	Zeta potential

CHAPTER 1: Introduction

1.1 Introduction to Parkinson's disease

Parkinson's disease (PD) is a common age-related motor disorder of the central nervous system (CNS), resulting from the mass degeneration of dopamine-producing neurons in the *substantia nigra pars compacta* (SNc). A pathological hallmark of PD is the formation of Lewy bodies (LBs) mainly containing α-synuclein protein (Marsden, 1982; van Laar & Berman, 2009). Dopamine acts as a neurotransmitter in regions of the brain such as the striatum which is involved in motor function (Park & Ellis, 2020), and progressive loss of dopaminergic neurons in the brain results in the manifestation of the main features of PD i.e., the motor symptoms which include reduced movement, tremor at rest, and rigidity (Rodriguez-Oroz et al., 2009). Furthermore, such degeneration causes characteristic depigmentation in the *substantia nigra* due to the loss of neuromelanin. Neuromelanin is a dark, complex, polymeric pigment that accumulates in dopaminergic neurons due to controlled dopamine oxidative processes (Zucca et al., 2017). The process of dopaminergic neurodegeneration in PD patients is relatively slow and it takes years to manifest the motor symptoms.

PD either presents as a familial or sporadic disease, each generally defined with an age at onset below and above 50 years of age, respectively (Wickremaratchi et al., 2011). Parkinsonism was first described by Dr. James Parkinson in 1817 who described a condition termed the "shaking palsy" (Parkinson, 2002). PD now affects approximately 1 % of the population over 60 years of age (Tysnes & Storstein, 2017). Despite decades of research, the exact mechanisms underlying the disease pathogenesis are yet to be elucidated (Hirsch & Hunot, 2009). This is complicated by a complex interplay of genetic and environmental factors that likely influence PD pathogenesis. As a result, effective disease-modifying treatments and preventative strategies have not yet been developed. This is especially alarming in Africa which is projected to experience a rise in neurodegenerative diseases due to an increasingly aging population (Dorsey et al., 2018). Consequently, there is an urgent need to develop and improve access to affordable, effective therapies to potentially help curb the increasing PD prevalence in Africa and around the globe (Hamid et al., 2021).

Therefore, in the present study, we aim to test the effects of a potential therapeutic drug, curcumin, for its antioxidant and neuroprotective effects. These effects will be evaluated using a PD cellular model using undifferentiated human neuroblastoma SH-SY5Y cells. In this study, the cellular model will be composed of three features: (1) overexpression of the phosphatase and tensin homolog (PTEN)-induced kinase 1 (*PINK1*) gene to represent familial PD; (2) toxicity which will be achieved by dopamine upregulation; and (3) an environmental stressor representing sporadic PD which will be caused by administration of the herbicide paraquat which has been shown to disrupt mitochondria and increase PD risk. *PINK1* mutations have been shown to cause familial PD and to be a model of

dopamine toxicity (Zhou et al., 2014). Paraquat is widely used to establish PD models due to its deleterious effects on mitochondrial function (Wang, Souders, et al., 2018). Notably and importantly, the societal movement away from artificially synthesized chemicals and toward more natural substances to treat medical conditions further enhances the attractiveness of plant-derived compounds, like curcumin, as a potential therapeutic strategy to treat PD.

1.1.1 *Dopamine deficiency in PD*

As seen in **Figure 1.1**, the cortex of the brain is responsible for voluntary body movement, and is connected to the *globus pallidus pars interna* (GPi) and *substantia nigra pars reticulata* (SNr) regions via the direct, hyperdirect, and indirect neural pathways (Rodriguez-Oroz et al., 2009).
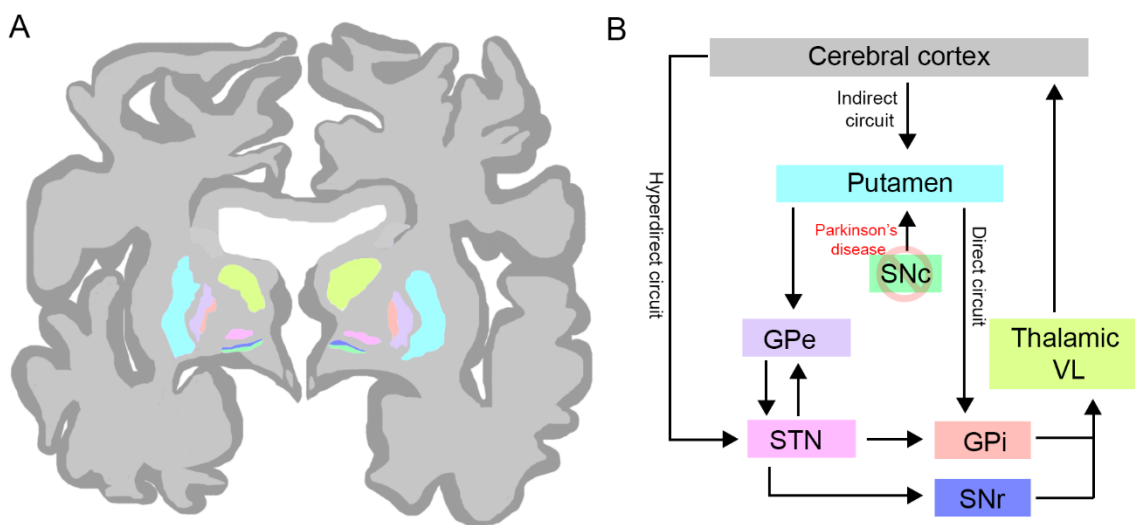
Figure 1.1 The classical physiological model of healthy neurons and the effect of PD. A – Frontal section of human brain. **B** – Activation of regions in the basal ganglia network. Neurons in the cerebral cortex extend to the putamen which sends projections to the GPi and SNr by the direct circuit (putamen-GPi) or indirect circuit (putamen-STN-GPi, SNr). Dopamine from the SNc facilitates neurons in the direct pathway and inhibits those in the indirect pathway. Activation of the direct pathway reduces firing in the GPi/SNr and aids movement. Conversely, activation of the indirect pathway suppresses movement. The STN can also be activated by the hyperdirect circuit (cortex-STN), reducing movement. In PD, the dopamine deficit increases activity in the indirect circuit, hyperactivates the STN, and reduces activity in the direct circuit. This results in increased inhibition of the thalamic VL and reduces activation of the cortex and motor regions in the brainstem. Abbreviations: GPe, globus pallidus pars externa; STN, subthalamic nucleus; GPi globus pallidus pars interna; SNc, substantia nigra pars compacta; SNr, substantia nigra pars reticulata; VL, ventrolateral nucleus (Rodriguez-Oroz et al., 2009).

Under normal conditions, dopamine in the SNc facilitates the direct circuit, thereby increasing neuronal firing in the GPi and SNr which in turn, raises activity in the cortex, and facilitates movement. In PD, loss of dopaminergic neurons in the SNc results in dopamine deficiency in the putamen and causes the manifestation of PD motor symptoms (Jankovic, 2008). Such a shortage of dopamine inactivates the direct circuit and activates the indirect circuit; thus, the ventral lateral (VL) nucleus is preferentially inhibited by GPi and SNr neurons. As a result, the cortex is activated to a lesser degree, and movement is suppressed. Levodopa (L-DOPA, **l**-3,4-dihydroxyphenylalanine), which is currently the gold-standard PD drug used for dopamine replacement therapy, cannot halt neuronal loss and results in involuntary muscle movement (dyskinesia), among other side effects. Therefore, a more effective PD treatment with fewer side effects is required for this already debilitating disease (Olanow, 2015).

1.1.2 *Accumulation of alpha-synuclein*

Along with dopaminergic neuronal loss, a distinct pathological hallmark of PD is the propagation of misfolded alpha-synuclein (α-synuclein) in the form of LBs and Lewy neurites along neural networks (Alafuzoff & Hartikainen, 2018). LB formation (**Figure 1.2**) involves the aggregation of misfolded α-synuclein and other proteins and cellular components into cytoplasmic inclusions (Luk et al., 2009).

In the cell, misfolded proteins can be degraded through the ubiquitin-proteasome system and autophagy (Ebrahimi-Fakhari et al., 2011). However, it has been hypothesized that when protein aggregate formation exceeds their degradation by autophagy, aggregates are transported to the microtubule-organizing center where they congregate to form large aggresomes (Kopito, 2000). These aggresomes are likely to be what is referred to as LBs (Tanaka et al., 2004). While properly folded α-synuclein plays a role in protection against neuronal damage and vesicle regulation, the toxic forms of α-synuclein produced during LB formation instigate cellular dysfunction culminating in cell death (Uversky & Eliezer, 2009; Gustot et al., 2015). Braak and colleagues proposed that LB propagation occurs in a staged manner, first affecting vulnerable brain regions such as the dorsal motor nucleus of the vagus nerve (DMNV) and olfactory bulb and thereafter, ascends rostrally to the cortex and prefrontal regions (Braak, del Tredici, et al., 2003). Braak and colleagues later hypothesized that LB formation begins in the enteric nervous system and thereafter, spreads to the brain (Braak, Rüb, et al., 2003). Although extensive progress has been made to elucidate the way Lewy pathology initiates and spreads, cell intrinsic factors may also play an important role in the formation of pathologic α-synuclein. These include mechanisms that increase endogenous α-synuclein levels, mutations and dysfunctional proteins associated with α-synuclein metabolism, and oxidative stress (Hijaz & Volpicelli-Daley, 2020).
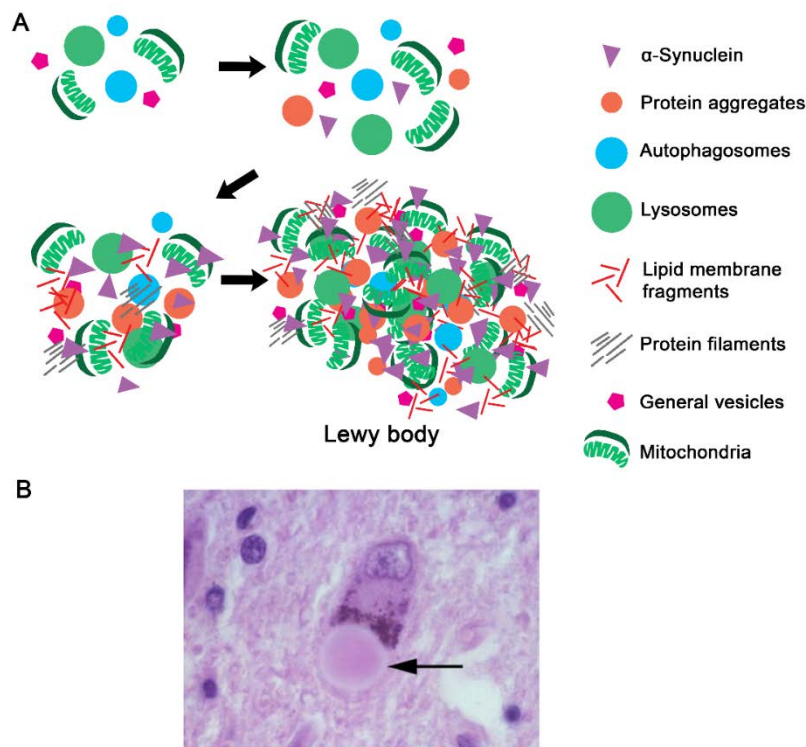
Figure 1.2 Possible mechanism of Lewy body formation. A - Organelles such as mitochondria, vesicles, and lysosomes in the cell, and the presence of pathological α-synuclein may lead to disruption of organelle membranes and further aggregation of cellular components. Large clumps of aggregated membranes and proteins compact over time and give rise to Lewy pathology (Shahmoradian et al., 2019). **B** – Light microscope image of a Lewy body found in a human midbrain (Dunn & Lewis, 2008). This figure was taken from an Open Access article distributed under the terms of the Creative Commons Attribution 4.0 International License. No changes were made.

1.1.3 *Mitochondrial dysfunction and PD*

Although the influence of numerous genetic factors and environmental exposures on PD pathogenesis have been suggested, a widely accepted theory of neuronal degeneration is free radical-induced oxidative stress. Mitochondrial dysfunction is directly linked to oxidative stress and is seen in both sporadic and familial PD (Larsen, Hanss & Krüger, 2018). Mitochondria are the main source of reactive oxygen species (ROS) which are produced as by-products of cellular metabolism (Islam, 2017). While low to moderate levels of ROS are essential for the maintenance of homeostasis, excessive ROS results in lipid, protein, and DNA damage, and may contribute to oxidative stress-induced cell death in PD (Murphy, 2009). Additionally, mitochondrial DNA (mtDNA) in neurons and glia of the SNc has a higher mutation rate than in any other brain region in PD patients (Soong et al., 1992). The role of mitochondria in PD pathology is further supported by the observation that

4

mitochondrial toxins such as paraquat, rotenone, and 1-methyl-4-phenyl-1,2,3,6-tetrahydropyridine (MPTP) can induce parkinsonism in humans and animals by increasing levels of ROS produced by the electron transport chain (Bové et al., 2005; Testa, Sherer & Greenamyre, 2005). In particular, paraquat undergoes redox cycling whereby it is reduced by nicotinamide adenine dinucleotide phosphate (NADPH) and is then oxidized to form highly reactive and damaging superoxide molecules (Dias, Junn & Mouradian, 2013). Such mitochondrial damage in the midbrain region has been linked to sporadic PD (Schapira, 2008). Finally, genes known to play important roles in mitochondrial function, such as *PRKN*, *LRRK2*, *DJ-1*, and *PINK1*, have been shown to cause PD (Cookson, 2012).

Pathogenic mutations in such genes as well as the mitochondrial dysfunction and oxidative stress that they initiate may seem indirectly related to LB propagation. However, extensive evidence supports an inextricable link to this hallmark of PD through various connected pathogenic events in the body (**Figure 1.3**), that ultimately result in dopaminergic cell death. Compromised cellular function (such as microtubule organization, cellular trafficking, and degradation pathways) may culminate in progressive accumulation of aberrant protein aggregates in PD (Esteves et al., 2011). Accordingly, neuronal dysfunction has been reported prior to α-synuclein aggregation in both PD patients and animal models (Paumier et al., 2013).
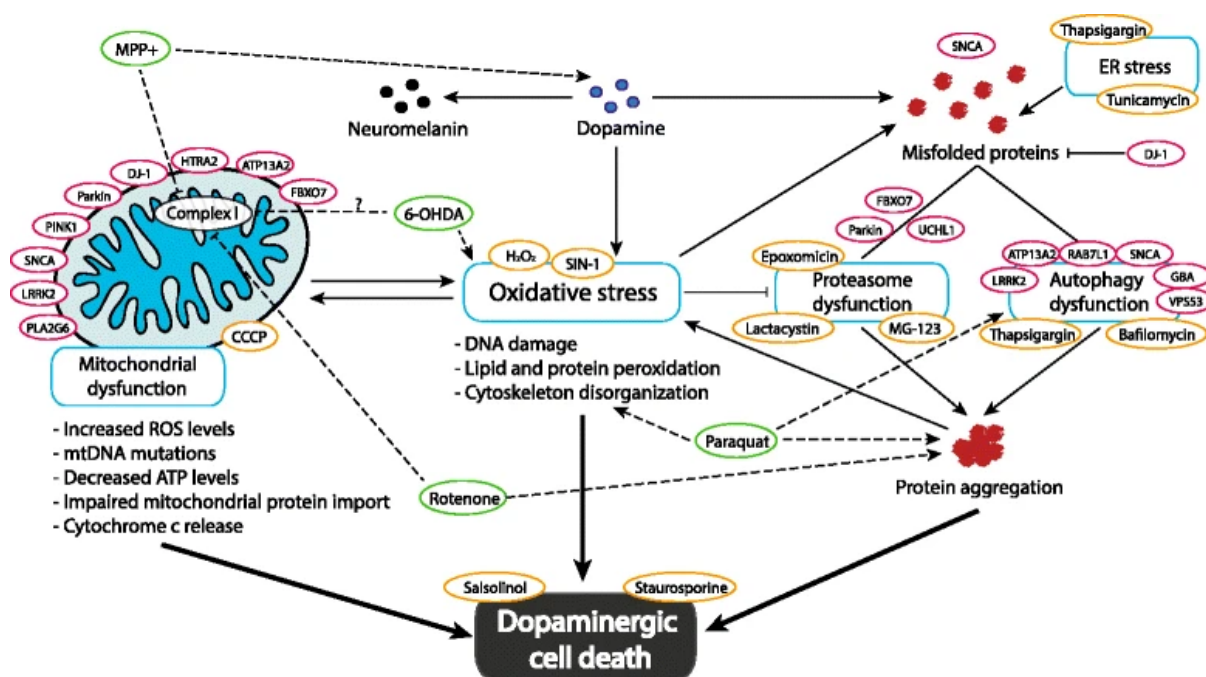
Figure 1.3. The molecular mechanisms that are dysregulated in PD (Xicoy, Wieringa & Martens, 2017)**.** Several interconnected cellular events culminate in dopaminergic cell death in PD, including dysfunction of mitochondria, proteasome system, autophagy as well as oxidative stress. This figure was taken from an Open Access article distributed under the terms of the Creative Commons Attribution 4.0 International License. No changes were made.

Therefore, mutations in key PD-related genes may initiate events such as mitochondrial dysfunction that later culminate in α-synuclein aggregation. Accordingly, the therapeutic potential of candidate drugs should be assessed in both specific PD models such as PINK1 but also for its broader application against widely observed pathologies such as protein aggregation. Studying the various molecular mechanisms associated with PD pathogenesis and progression is paramount to the development of effective therapies for this complex disease.

1.2 Cellular models to study PD

The relevance of the wide variety of pathways implicated in PD has led to prominent modeling of the disease to study PD pathogenesis and discover novel therapies. Models are useful research tools to enhance our understanding of PD pathophysiology and test potential interventions in order to develop novel therapeutics (Falkenburger, Saridaki & Dinter, 2016). Given that the underlying cause(s) of PD remains unknown, PD can only be partially represented in these models. Nevertheless, models greatly aid research as the use of individuals with PD in studies can be challenging due to variable disease stages, slow disease progression, the complexity of physiological features of neuronal systems, and vulnerability of elderly PD patients which complicates sampling (Bahmad et al., 2017). There are many types of models used in PD research, ranging from cellular/animal-based, genetic, and neurotoxic models (**Table 1.1**).

Table 1.1 Summary of advantages and limitations of animal/cell-based, neurotoxic, and genetic models in Parkinson's disease research (Chia, Tan & Chao, 2020)**.**

Model	Advantages	Limitations
Cell/animal models		
Rodents	Exhibit PD-like phenotype	Relatively expensive
	Established behavioral test	Long life cycle
	Availability of non-motor symptoms examination	
	Ease of genetic manipulation process	
Non-human primates (NHP)	Close similarity in genetic and brain anatomy to human	Laborious
		Very expensive
	Availability of disease assessment	Long life cycle
		Complicated genetic manipulation process
		Ethical considerations
Caenorhabditis (C.) elegans	Ease of genetic manipulation	Lack of α-synuclein

	Short life cycle	expression
	Low cost of maintenance	Difficult to target dopaminergic neuron
	Well-defined neuropathology and behavior	Neuronal connectivity differs from human
Drosophila	Availability of transgenic model	Lack of α-synuclein homolog
	Similar dopamine synthesis pathway	Limited cell death effectors
	Exhibit PD-like phenotype	
Zebrafish	Well-characterized dopaminergic neuron	Genetic and genomic research in progress
	Exhibit PD-like motor symptoms	
	Close genetic similarity	
iPSC	Ease of genetic manipulation	Lack of complete physiological connection that mimic brain
	Conduct study on patient's cells	
	Quickly and cost effective	Suitable for molecular study
	Suitable for large-scale screening	
Neurotoxic models		
6-OHDA	Able to induce massive destruction of dopaminergic neuron in SN	Lack of blood brain barrier penetration
	Able to induce major behavioral deficits seen in PD	Acute effect
		Lacks LB formation
MPTP	Can penetrate blood brain barrier	Lacks LB formation
	Similar topographic pattern of dopaminergic cell loss	
	Decreased striatal dopamine levels	
Paraquat	Induces age-dependent dopaminergic neuronal loss	Lack of striatal dopamine loss in some models
	Induces LB formation	
Rotenone	Behavioral impairment	Low reproducibility
	Dopaminergic neurodegeneration	Acute toxicity
Genetic models		
α-Synuclein	Useful to study α-synuclein-related degeneration and the association between genetic and environmental factors in PD	No significant dopaminergic neuron loss
		Exhibits different topography pattern of cell loss

7

LRRK2	Therapeutic target and useful for LRRK2 targeted drug test	No significant dopaminergic neuron loss
	Useful for LRRK2 functional study	Lack of α-synuclein inclusions
Parkin	Useful for Parkin functional study	Lack of important phenotype of PD
DJ-1	Useful to combine with neurotoxin models	Lack of nigral neurodegeneration
		Lack of inclusion bodies
PINK1	Dopamine reduction and decreased locomotor activity in G309D-PINK1 mice and Drosophila	Most PINK1 models do not show reduction of dopaminergic neuron and dopamine levels
	Useful to study the association of PINK1-Parkin pathway in PD	

This table was taken from an Open Access article distributed under the terms of the Creative Commons Attribution 4.0 International License. No changes were made.

Abbreviations: PD, Parkinson's disease; LB, Lewy body; NHP, non-human primate; iPSC, induced pluripotent stem cell; 6-OHDA, 6-hydroxydopamine; MPTP, 1-methyl-4-phenyl-1,2,3,6-tetrahydropyridine.

In comparison to animal models, cellular models are less costly, develop disease pathology quicker, and require less stringent ethical approval for use (Falkenburger, Saridaki & Dinter, 2016). Cellular models are important as they can represent PD through their cell type, electrical activity, behavior, and molecular basis (Falkenburger, Saridaki & Dinter, 2016). Depending on the aspect of PD pathobiology and the type of therapeutic agent to be studied, a suitable model must be chosen with regard to these factors (Ahmi, 2019). Manipulating DNA and testing pharmaceuticals are easier with cells than in animal models, allowing for rapid, large-scale experiments. Cells have been used in large high-throughput screening studies to identify drug candidates (Eglen & Reisine, 2011; He et al., 2018). Another advantage is the disease pathology can easily be monitored and manipulated as well as being amenable to testing multiple approaches at one time. Researchers are able to study a single cell type which is useful in identifying its role in PD pathology. Studying a therapeutic drug may be useful in a cellular model that has potential drug targets. However, since multiple cell types interact and result in PD pathogenesis and pathophysiology, these interactions can only be studied in animals or humans. Therefore, findings derived from cell models are usually validated in animal models and later in humans. Furthermore, cells develop rapidly which is the opposite *in vivo*, as PD is known to be a slowly progressive disease. Although it is difficult to make inferences about whole-body effects and system pathology, these simple models are suited to use in initial studies aiming to examine the cellular machinery involved in disease progression which can then be followed up by *in vivo* and

clinical trial phase studies. Overall, while cellular models have significant limitations for studying a complex disorder such as PD, they are still a useful tool in PD exploratory studies.

Cell types used in PD models include primary neurons and immortalized Lund human mesencephalic (LUHMES) SH-SY5Y, and Pheochromocytoma (PC12) cell lines (Falkenburger, Saridaki & Dinter, 2016). Primary mesencephalic cultures generally contain midbrain dopaminergic neurons that readily differentiate and form visible neurites and synapses (Falkenburger & Schulz, 2006). Midbrain dopaminergic cell cultures have been used to evaluate the neuroprotective effect of nicotine (Toulorge et al., 2011), and the antiepileptic drug valproate (Chen et al., 2006).

The characteristic dopaminergic deficit in PD patients has informed the use of catecholaminergic cells (dopaminergic and noradrenergic) such as LUHMES embryonic cells which are a widely used immortalized, dopaminergic precursor neuronal cell line (Lotharius et al., 2005). Differentiated LUHMES cells are similar to dopaminergic neurons in their neuronal markers, electrical properties and neuronal process morphology (Scholz et al., 2011). The SH-SY5Y neuroblastoma cell line and PC12 cell line produce and release catecholamines and can be differentiated to form neuron-like processes using retinoic acid and neuronal growth factor (Öz & Çelik, 2016; Yürekli, Gürler, Nazıroğlu, *et al.*, 2013). Differentiated SH-SY5Y cells have tyrosine hydroxylase (TH) and DA-β-hydroxylase activities (Xie, Hu & Li, 2010) and express several PD-causing genes (Krishna et al., 2014). Cheung *et al.* (2009) reported that undifferentiated SH-SY5Y cells were more susceptible to neurotoxins than their differentiated counterparts, thus may be more suited to model development to study toxicity (Cheung, Lau, Yu, *et al.*, 2009) and rescue effects with therapeutic intervention. SH-SY5Y cells have been used to test the neuroprotective properties of various therapeutic candidates such as nicotine and cotinine (Pogocki et al., 2007; Riveles, Huang & Quik, 2008) and Danshensu, an active component of the traditional Chinese medicinal herb Danshen (Wang, Li, et al., 2020). This highlights the versatility of SH-SY5Y cells as a model to test a wide variety of biological pathways and disease mechanisms.

Given the above, undifferentiated SH-SY5Y cells were selected for this study due to their catecholaminergic nature, suitability to study toxicity, ease of use, relatively low cost, and minimal maintenance requirements. Furthermore, this cell line has been widely used to test the neuroprotective effects of pharmaceutical candidates which suits this study's aims.

1.3 PINK1

As evidenced in **Table 1.1**, there are many genetic models of PD based on the expression of proteins that are known to be implicated in the disease. These include α-synuclein, LRRK2, Parkin, DJ-1, and PINK1. Encoded by the *PINK1* gene on chromosome 1, PINK1 is a serine-threonine kinase spanning 68-kDa and is localized to the mitochondria in the cell (Valente et al., 2004). This ubiquitin kinase is

composed of 581 amino acids and was first identified in cancer cells as a substrate for the PTEN protein. The structure of the PINK1 protein is shown in **Figure 1.4**.
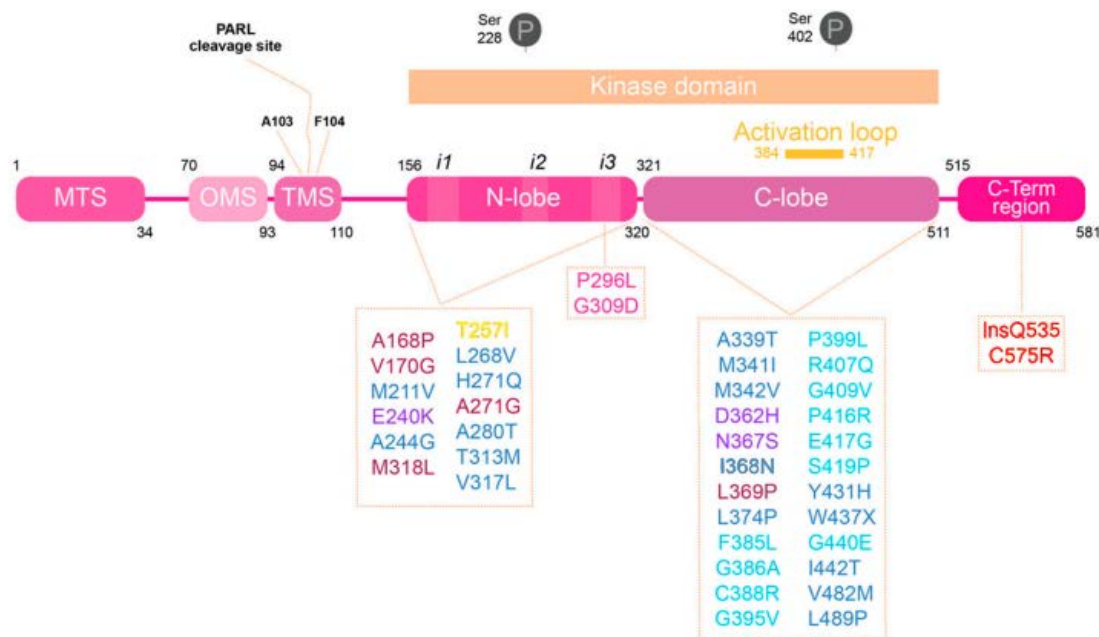
Figure 1.4 The two-dimensional structure of human PINK1 (hPINK1) protein and PD-associated mutations. The N-terminal contains several regions responsible for delivery of PINK1 to mitochondria, including the mitochondrial targeting sequence (MTS), membrane localization signal (OMS), and the transmembrane sequence (TMS). The kinase domain is divided into an N-lobe and C-lobe and contains phosphorylation and PD-associated mutation sites. The N-lobe contains three insertion sequences (i1, i2, and i3) while the C-lobe contains the activation loop responsible for changing the PINK1 protein conformation to the active state. PD-associated mutations can be categorized according to the region that they affect: ATP binding pocket (burgundy), kinase core (dark blue), catalytic mutations (purple), insert 2 (yellow), insert 3 (pink), activation loop (light blue) and C-terminal region (red) (Gonçalves & Morais, 2021). This figure was taken from an Open Access article distributed under the terms of the Creative Commons Attribution 4.0 International License. No changes were made.

Under normal physiological or homeostatic conditions, PINK1 is produced and degraded via a proteasome-dependent mechanism (Pickrell & Youle, 2015). Under stress-induced conditions when the mitochondria are damaged, PINK1 remains active and aids mitophagy, the process whereby dysfunctional mitochondria are degraded as illustrated in **Figure 1.5**. This is achieved by PINK1 recruiting autophagy receptors which then allows cytosolic Parkin, encoded by *PRKN*, to move to and tag damaged mitochondria with ubiquitin (Ub), and consequently triggering selective mitophagy (Lazarou et al., 2015).
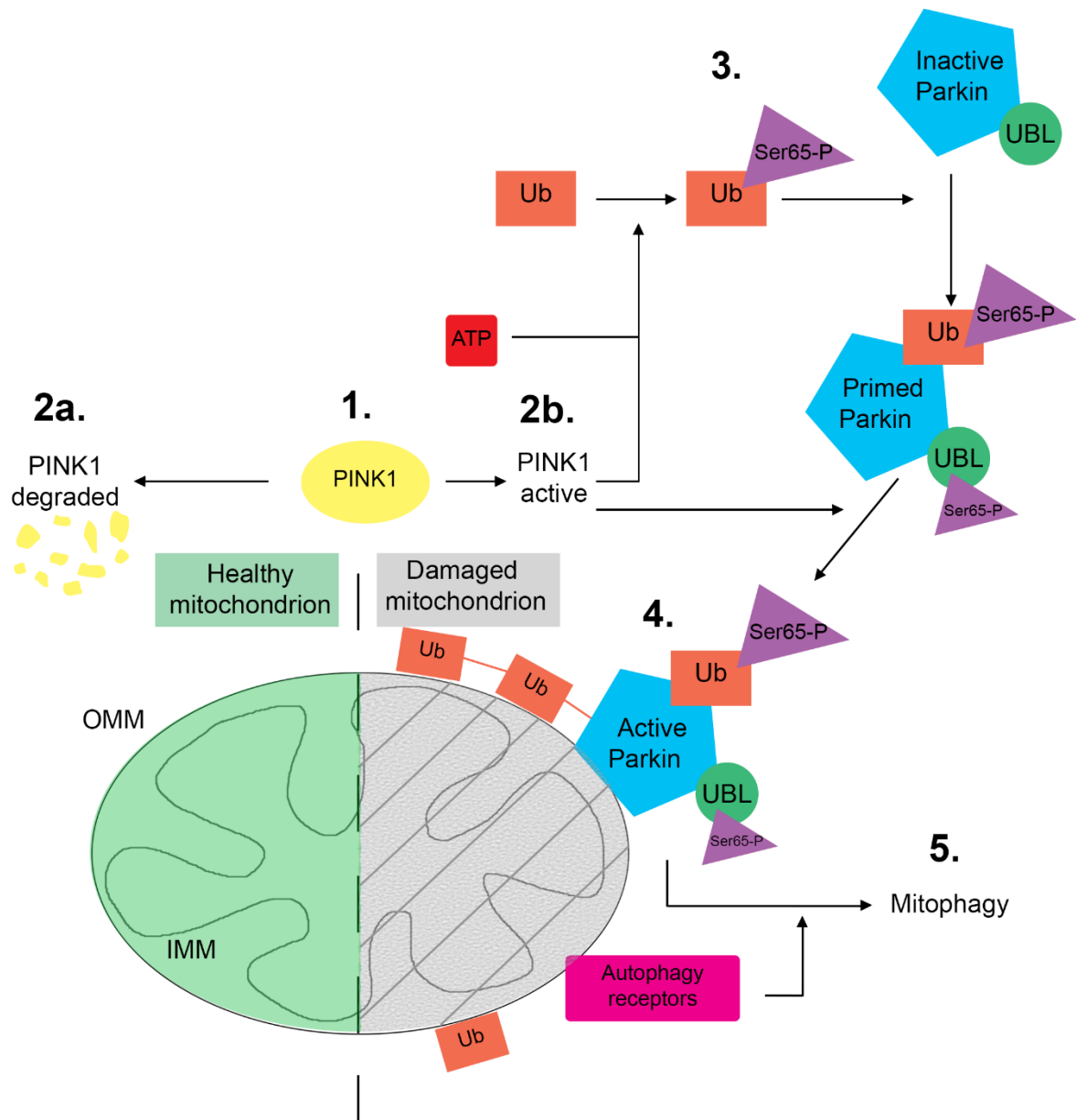
Figure 1.5 PINK1 regulation of Parkin-mediated mitochondrial clearance through mitophagy.
PINK1 protein (1) gets degraded when mitochondria are healthy (2a). However, when mitochondria become damaged, PINK1 remains active (2b) and a series of phosphorylation events occur (3) involving PINK1, Parkin, and Ub. (4) Active Parkin binds and creates Ub chains on damaged mitochondria. Autophagy receptors attach to the OMM and, together with active Parkin, lead to (5) the clearance of damaged mitochondria by mitophagy.

Abbreviations: ATP, adenosine triphosphate; IMM, inner mitochondrial membrane; OMM, outer mitochondrial membrane; Ub, ubiquitin; UBL, ubiquitin-like domain.

PINK1 binds ATP and phosphorylates Ub at its Ser65 domain and Parkin at its Ser65 equivalent residue, as illustrated in **Figure 1.5** (Kane et al., 2014; Kazlauskaite et al., 2014; Lazarou et al., 2015).

11

Parkin forms part of the E3 ubiquitin ligase multiprotein complex which is responsible for tagging proteins for breakdown by the ubiquitin-proteasome system (Wood-Kaczmar et al., 2008; Chan et al., 2011). Phosphorylation of both Parkin and Ub by PINK1 is necessary to maximize the E3 ligase activity of Parkin (Kane et al., 2014; Kazlauskaite et al., 2014; Lazarou et al., 2015). Once activated, Parkin ubiquitylates substrates in the outer mitochondrial membrane, thereby elongating pre-existing ubiquitin chains or creating new chains, either of which is also phosphorylated by PINK1. This process culminates in the recruitment of mitophagy adaptors that are required to complete mitochondrial degradation (Heo et al., 2015; Lazarou et al., 2015; Ordureau et al., 2015).

1.3.1 *PINK1 in PD*

At least 40 different PD-linked *PINK1* mutations have been identified, of which the majority constitute missense substitutions (Zhou et al., 2014). The serine-threonine kinase domain of the protein mainly has missense mutations and may be critical for PINK1 function (Mills et al., 2008). While studying consanguineous families in 2004, Valente and colleagues discovered the first homozygous PINK1 mutations, W437X and G309D, relating to autosomal recessive, early-onset PD (Valente et al., 2004). Thereafter, many *PINK1* mutations have likewise been found to cause this form of the disease (Bonifati et al., 2005).

Additionally, a major hallmark of PD is α-synuclein aggregates which have been implicated in PD pathogenesis on both a genetic and biochemical basis. Such involvement of α-synuclein in the disease development characterizes PD as a synucleinopathy. The fibrillization of this protein has been identified as a potential therapeutic target for PD (Goldberg & Lansbury Jr, 2000; Creed & Goldberg, 2018). However, despite decades of research, the role of α-synuclein aggregation in PD onset and progression remains elusive.

α-Synuclein has been shown to localize to the mitochondria (Devi et al., 2008), and mitochondrial function and morphology are affected by the loss of PINK1 and Parkin function (Dagda et al., 2009; Lutz et al., 2009). PINK1 was shown to bind to excess α-synuclein in the cytoplasm, preventing apoptosis by promoting autophagic removal of excess α-synuclein (Liu et al., 2017). Kamp and colleagues showed that mitochondrial fragmentation, due to increased expression of α-synuclein that binds to mitochondria, may be rescued by co-expression of the recessive PD-associated PINK1, Parkin, and DJ-1 genes (Kamp et al., 2010). These proteins may exert their protective effects, not by direct interaction between them but rather by the convergence of their pathways at the level of mitochondrial integrity. Their protection against mitochondrial stress could counteract the pathogenic effects of α-synuclein accumulation that render neurons susceptible in PD. Mutations in genes such as *PINK1* impair these protective functions. Through various pathways involving mitochondrial dysfunction, such mutations and many other causes of PD lead to toxic α-synuclein accumulation and

aggregation which is a frequent endpoint in PD pathophysiology and a major hallmark of PD (**Figure 1.3**).

PINK1 is involved in the maintenance of healthy mitochondria, which is the main source of endogenous ROS (Chen, Guo & Kong, 2012). ROS, such as free radicals (superoxide (O_2-), hydroxyl radical (•OH)) or reactive non-radicals (hydrogen peroxide, H_2O_2), are produced during oxygen metabolism in aerobic organisms (Halliwell, 1994). Although ROS are required for proper cellular function such as cell signaling and homeostasis, high levels of these reactive molecules can become deleterious to cell health (Chen, Guo & Kong, 2012). Oxidative stress results when pro-oxidant ROS and their reactive intermediates outbalance antioxidant species, resulting in cell demise and contribution to disease progression. PINK1 was reported to protect against oxidative stress by phosphorylating the mitochondrial chaperone tumor necrosis factor receptor-associated protein 1 (TRAP1) and suppressing mitochondrial cytochrome c release (Pridgeon et al., 2007). Zhou and colleagues demonstrated that stable overexpression of the PINK1 mutants, E231G, A339T, and G309D, upregulated levels of TH and dopamine in SH-SY5Y cells (Zhou et al., 2014). This renders these cells vulnerable due to reduced cell viability when exposed to stress. One possible explanation for this is the development of oxidative stress in the cell due to dysregulated ROS and reactive dopamine species which leads to cell death (Larsen *et al.*, 2002; Andersen, 2004; Lotharius *et al.*, 2005).

In mutant PINK1 SH-SY5Y cells, antioxidants sodium pyruvate (SP) and N-acetylcysteine (NAC) were shown to rescue apoptosis induced by H_2O_2 (McBurney et al., 2012). NAC is a scavenger of ROS which is important as iron species can lead to dopamine oxidation, ROS, and dopamine quinone (DAQ) formation, and even cell death (Zhou et al., 2010). Iron ions are a cofactor of the enzyme TH and thus are essential for TH-catalyzed dopamine production in dopaminergic neurons. However, ageing may result in toxic accumulation of this metal in the brain (Zecca et al., 2004). Significantly higher iron content has been found in the midbrains of individuals with early-onset PINK1 mutation-positive PD and autosomal recessive juvenile parkinsonism compared to both healthy controls and patients with sporadic PD (Takanashi et al., 2001). Thus, it is hypothesized that PINK1 mutations lead to iron accumulation in the *substantia nigra* which, in turn, results in dopamine oxidation and dopaminergic neurodegeneration. Therefore, studies investigating the protective effect of iron-chelating agents and DAQ-chelating antioxidants are important to determine if they can alleviate the neurodegeneration characteristic of PD-causing PINK1 mutations (Zhou et al., 2014). Given the role of PINK1 in mitophagy and protection against ROS and dopamine-induced oxidative stress, mutations in *PINK1* may lead to mitochondrial dysfunction, subsequent ROS imbalance, and oxidative stress, culminating in neuronal death in PD.

1.4 Dopamine

Dopamine was first discovered as a neurotransmitter by Nobel Prize winner Arvid Carlsson, following initial recognition as only a precursor in epinephrine and norepinephrine metabolism (Carlsson et al., 1958). Dopamine was linked to PD in 1960 (Ehringer & Hornykiewicz, 1960) and thereafter, the critical role of dopaminergic neurons in reward, cognition, and motor functions was described (Hornykiewicz, 2002). Dopaminergic neurons form nigrostriatal, mesolimbic, and mesocortical projections which branch out from the midbrain to the striatum, limbic system, and cortex, respectively (Jankovic, 2008). Locus coeruleus neurodegeneration in PD may precede the loss of dopaminergic neurons that causes the motor symptoms characteristic of the disease (Zarow et al., 2003; Pogocki et al., 2007). Neurons in the locus coeruleus interact with norepinephrine neurotransmitters and may also be responsible for the manifestation of motor and non-motor symptoms in PD (Jellinger, 1991). The extensive literature on the involvement of dopamine in PD pathophysiology emphasizes the importance of researching this aspect of the disease (Masato et al., 2019).

1.4.1 *Dopamine synthesis and metabolism*

Dopamine metabolism is one of the cellular events that has been proposed to be closely associated with PD pathobiology. The main pathway of dopamine synthesis in the CNS begins with L-tyrosine which is converted to L-DOPA through hydroxylation of its phenol ring by the TH enzyme, a process dependent on iron presence (**Figure 1.6**) (Daubner, Le & Wang, 2011). L-DOPA, as stated above, is currently the main drug treatment for PD. L-dopa is converted to dopamine and subsequently to norepinephrine by aromatic acid decarboxylase (AADC) and dopamine β-hydroxylase (DβH), respectively (Montioli et al., 2013). Two other minor pathways are also involved in dopamine synthesis, one of which is P450 cytochrome-dependent (Bromek et al., 2011), involving the decarboxylation of tyrosine to tyrosamine and then hydroxylation to dopamine. The other minor pathway involves the oxidation of phenylalanine to tyrosine by phenylalanine hydroxylase, an enzyme in the same family as TH (Daubner, Le & Wang, 2011). Dopamine is metabolized by MAO to produce ammonia, hydrogen peroxide, and 3,4-dihydroxyphenylacetaldehyde (DOPAL). The lattermost of which is converted to the corresponding 3,4-dihydroxyphenylacetic acid (DOPAC) by aldehyde dehydrogenase and thereafter, to non-reactive homovanillic acid (HVA) by catechol-O-methyltransferase (COMT) (Kingsbury et al., 2010; Nissinen, 2010). COMT is also involved in a minor dopamine degradation pathway, where dopamine is first converted to 3-methoxytyramine (MTY) and subsequently to 3-methoxy-4-hydroxyphenyl acetaldehyde (MOPAL), by monoamine oxidase B (MAO-B), and to HVA, by aldehyde dehydrogenase (Kingsbury et al., 2010; Meiser, Weindl & Hiller, 2013).

It must be noted that the pathways described above do not occur in the same cellular compartment (Monzani et al., 2019). In dopaminergic neurons, TH and AADC, enzymes responsible for dopamine biosynthesis, physically associate and interact with the vesicular monoamine transporter 2 (VMAT2) (Nissinen, 2010). The dopamine produced is largely stored in synaptic vesicles by VMAT2. This neurotransmitter is only released into the synaptic cleft when the presynaptic neuron is signaled to do so, to avoid unnecessarily stimulating the post-synaptic neuron.
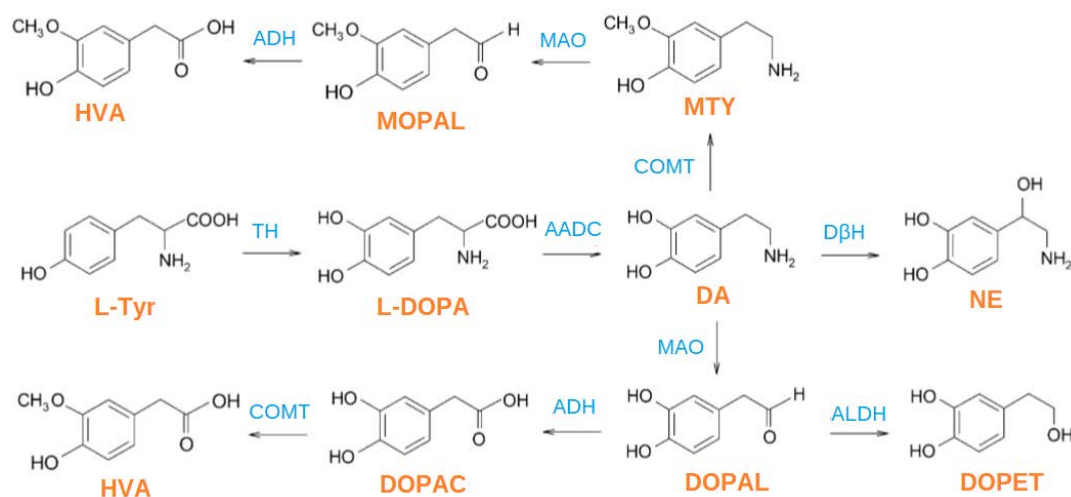
Figure 1.6. Summary of dopamine synthesis and metabolism pathways.

Abbreviations: L-Tyr, l-tyrosine; L-DOPA, **l**-3,4-dihydroxyphenylalanine; DA, dopamine; TH, tyrosine hydroxylase; AADC, aromatic acid decarboxylase; DOPAL, 3,4-dihydroxyphenylacetaldehyde; DOPAC, 3,4-dihydroxyphenylacetic acid; HVA, homovanillic acid; MAO, monoamine oxidase B; ADH, aldehyde dehydrogenase; COMT, catechol-O-methyltransferase; NE, norepinephrine; DβH, dopamine β-hydroxylase; DOPET, 3,4-dihydroxyphenylethanol; ALDH, alcohol dehydrogenase; MTY, methoxytyramine; MOPAL, 3-methoxy-4-hydroxyphenyl acetaldehyde (Monzani et al., 2019).

1.4.2 *Dopamine toxicity in PD*

Post-mortem PD brains have been shown to contain toxic dopamine species produced during dopamine oxidation (Spencer et al., 2002) which is one of several sources of ROS that may lead to disrupted redox homeostasis and neuronal death in PD (Jenner & Olanow, 2006). Excess dopamine that is not catabolized or packaged into vesicles can lead to neurotoxicity (Cobley, Fiorello & Bailey, 2018; Monzani et al., 2019). Such oxidative and nitrosative damage to dopaminergic axon terminals and their vesicles is triggered by the production of reactive molecules such as DAQ or dopamine semiquinones (DASQ). Redox-active metal ions, particularly copper and iron, promote dopamine

oxidation. Furthermore, dopamine spontaneously undergoes slow auto-oxidation which is enhanced with raised pH (Herlinger, Jameson & Linert, 1995), a phenomenon that occurs in brain regions affected by chronic disease (Monoranu et al., 2009; Genoud et al., 2017).

Neurodegeneration usually results from dyshomeostasis of redox-active metal ions and nitric oxide (NO)-derived species (such as peroxynitrite and nitrite) which enhance dopamine toxicity (Barnham & Bush, 2014; Ferrer-Sueta et al., 2018). A small number of DA-derived compounds account for post-transcriptional protein modification in PD and are involved in the following pathway: DAQ is cyclized to unstable leukodopaminochrome (LDAC) which is readily converted to stable dopaminochrome (DAC) (Segura-Aguilar et al., 2014). DAC accumulates and is converted to 5,6-dihydroxyindole (DHI) and further oxidizes to form a quinone (DHIQ) (Bisaglia et al., 2010). The reactivity of these species accounts for what is termed dopamine toxicity associated with PD (Monzani et al., 2019). The molecular basis and structural consequences of protein modification due to dopamine toxicity are not fully understood due to the lack of effective methods of investigating specific modification sites and types.

It is evident that excess dopamine, through overproduction and dysfunctional catabolism or reuptake, leads to the formation of radicals and reactive dopamine species, thereby resulting in dopaminergic neuron damage (Larsen et al., 2002; Andersen, 2004; Lotharius et al., 2005). The following section will provide an overview of current and potential PD drug treatments to prevent or combat neuronal damage, including curcumin.

1.5 Drug treatments for PD

Several drug therapies are currently used to relieve the symptoms of PD including L-DOPA, dopamine agonists, and inhibitors of MAO-B and COMT, which are administered based on age, the severity of motor symptoms, and various other clinical characteristics of the patient (summarized in

Table 1.2) (Jost, 2020). However, existing PD drugs do not halt disease progression and are generally associated with long-term side effects, as well as a loss in efficacy over time (Teo & Ho, 2013). Therefore, there is an urgent need to develop effective therapies that stop neuronal degeneration and elicit fewer side effects, for which plant-based compounds are now being investigated.

1.5.1 *Synthetic therapeutic compounds*

In the late 1960s, L-DOPA or levodopa was recognized as a drug to treat PD soon after the discovery of dopamine deficit pathology in PD. L-DOPA is still largely used today due to its efficacy in treating PD symptoms (Oertel & Schulz, 2016). L-DOPA may reduce motor symptoms by attempting to increase dopamine levels and normalize basal ganglia function, but it cannot stop disease progression.

This is due to the continued loss of striatal neuronal axons that release dopamine (Mosharov, Borgkvist & Sulzer, 2015; Olanow, 2015). Therefore, L-DOPA exerts its beneficial effects for only a limited time (Lane et al., 2008). Furthermore, several side effects of long-term L-DOPA use include the development of bradykinesia (or slowness of movement), dystonia, and on-off fluctuations of motor symptoms (Xu et al., 2016). L-DOPA treatment can be preceded by dopamine receptor agonist therapy as these molecules have longer plasma elimination half-lives than L-DOPA. They stimulate both pre- and post-synaptic dopamine receptors and thus, can improve drug delivery over longer periods (Stocchi, Vacca & Radicati, 2015). Treatment with L-DOPA and a peripheral dopa decarboxylase inhibitor appears to currently be the most effective strategy (Mizuno, 2020).

Since its discovery, the toxicity of L-DOPA has had researchers in debate. In pure neuronal-like cultures, this compound produces toxicity but triggers trophic effects when applied to glial cells (Falkenburger & Schulz, 2006). There is evidence of L-DOPA causing protein misfolding as it is a close analog of L-tyrosine (Rodgers & Dean, 2000). Due to this structural similarity (**Figure 1.6**), L-DOPA can be inserted into cellular proteins in place of L-tyrosine, leading to protein misfolding and dysfunction (Ozawa et al., 2005). With prolonged L-DOPA treatment, defective protein accumulation may contribute to increased neuronal dysfunction and PD progression (Giannopoulos et al., 2019). Giannopoulos *et al.* (2019) showed that SH-SY5Y cells treated with L-DOPA exhibited Ub accumulation, upregulation of the endosomal-lysosome degradation system, as well as dysfunctional and dysmorphic mitochondria. However, treatment with L-tyrosine protected against these side effects. If ongoing clinical trials reiterate these findings, L-tyrosine may be used in combination with L-DOPA to avoid these side effects in PD treatment, but this is yet to be reported.

As mentioned in section 1.4.1, MAO-B is involved in dopamine metabolism. MAO-B metabolizes dopamine into DOPAC and HVA. This compound also deaminates β-phenylethylamine, a compound that stimulates the release of dopamine and inhibits the uptake of neuronal dopamine (Fernandez & Chen, 2007). MAO-B inhibitors, which block this action of dopamine degradation, are used in combination with L-DOPA to treat PD. The drug selegiline is one such inhibitor that stabilizes dopamine levels in the synaptic cleft (Stocchi, Vacca & Radicati, 2015). However, as a derivative of methamphetamine, selegiline is metabolized to L-amphetamine products which may induce side effects such as insomnia (Kamada et al., 2002). MAO-B inhibitors, with few or well-tolerated adverse effects, may only be useful in selected PD patients such as younger individuals with mild symptoms, or to supplement with L-DOPA treatment (Teo & Ho, 2013).

COMT inhibitors block the action of the COMT enzyme which catalyzes the methylation of dopamine in the presence of Mg^{2+} ions during dopamine degradation (Guldberg & Marsden, 1975). However, COMT inhibitors like tolcapone, opicapone, and entacapone have several disadvantages including severe liver toxicity and augmented risk of dyskinesia (McBurney et al., 2012; Longo et al.,

2016; Fabbri et al., 2018). Therefore, it is yet to be elucidated whether safe and effective use of COMT inhibitors is possible for PD treatment (Wang, Wang, et al., 2021).

Table 1.2 Summary of commonly used PD drugs, their mechanisms of action, adverse effects, and recommended use.

Drug	Mechanism of action	Adverse effects	Recommended use	References
L-DOPA	Dopamine replacement	Bradykinesia Fluctuating motor symptoms	Precede by dopamine receptor agonist Supplement with a dopa decarboxylase inhibitor Supplement with tyrosine	(Mizuno, 2020)
Selegiline	MAO-B inhibitor	Insomnia	Supplement with L-DOPA	(Stocchi, Vacca & Radicati, 2015)
Rasagiline	MAO-B inhibitor	Few/Well-tolerated	Early treatment only	(Stocchi, Vacca & Radicati, 2015)
Safinamide	MAO-B inhibitor	Few/ Well-tolerated	Early treatment only Supplement with L-DOPA	(Parambi, 2020)
Tolcapone	COMT inhibitor	Severe liver toxicity Increased risk of dyskinesia	Supplement with L-DOPA	(McBurney et al., 2012)
Opicapone	COMT inhibitor	Increased risk of dyskinesia	Supplement with L-DOPA	(Fabbri et al., 2018)
Entacapone	COMT inhibitor	Increased risk of dyskinesia	Supplement with L-DOPA	(Longo et al., 2016)

Abbreviations: COMT, catechol-O-methyltransferase; MAO-B, monoamine oxidase B; L-DOPA, l-3,4-dihydroxyphenylalanine.

1.5.2 *Natural therapeutic compounds*

The absence of effective treatment strategies for PD that address disease progression and elicit fewer side effects has informed research into natural, plant-based compounds. In general, the wide biological activity, low cost, and high safety margins of natural compounds advocate for their use as treatment and/or prevention strategies in neurological diseases like PD (Sharma et al., 2013). Given the highly supported role of oxidative stress in disease pathogenesis, researchers have turned to natural antioxidants to investigate their therapeutic potential which has been reviewed previously (**Table 1.3**) (Park & Ellis, 2020). In theory, the antioxidant properties of such compounds are proposed to act in place of their endogenous counterparts, which are reduced in PD, and to counterbalance the excessive ROS which causes oxidative stress and cell death (Magalingam, Radhakrishnan & Haleagraha, 2013). Some of the more popular compounds are discussed briefly below.

Table 1.3 Summary of dietary plant-based compounds that may exert protective effects against PD pathophysiology.

Compound	Plant derived from	Protective effects	References
Rutin/sophorin, rutoside/quercetin-3-rutinoside	*Ruta graveolens* Oranges Lemons Cherries Peaches	Increases antioxidant enzymes Suppresses lipid peroxidation Anti-inflammatory	(Magalingam, Radhakrishnan & Haleagrahara, 2016) (Arowoogun et al., 2021)
Isoquercetin	*Ruta graveolens*	Increases antioxidant enzymes Suppresses lipid peroxidation	(Arowoogun et al., 2021)
Resveratrol	Grapes Raspberries Peanuts	Antioxidant Anti-inflammatory	(Arbo et al., 2020)
Vitamin E	Sunflower oil Leafy greens	Reduces synuclein oligomerization Protects against oxidative stress	(Jinsmaa et al., 2014) (Numakawa et al., 2006)
Vitamin C	Oranges Capsicum	Reduces synuclein oligomerization	(Jinsmaa et al., 2014)
Oleuropein	Olive oil	Stabilizes synuclein monomers and prevents toxic aggregation	(Palazzi et al., 2018)
Curcumin	Turmeric	Antioxidant Anti-inflammatory Promotes cancer cell death	(Jayaprakasha et al., 2002) (Anuchapreeda et al., 2008)

19

Rutin (3,3,4,5,7-pentahydroxyflavone-3-rhamnoglucoside) is a glycoside derived from quercitin and is also known as sophorin, rutoside, and quercetin-3-rutinoside (Harborne, 1986). This polyphenolic bioflavin is found in the *Ruta graveolens* plant after which it was named, as well as commonly consumed fruit such as oranges, lemons, cherries, and peaches (Ganeshpurkar & Saluja, 2017). Rutin has been shown to elicit antioxidant effects in several models. In a 6-hydroxydopamine (6-OHDA) model of PC12 cells, rutin and another quercetin derivative called isoquercetin were shown to significantly increase antioxidant enzymes such as superoxide dismutase and glutathione levels, as well as suppress lipid peroxidation, thereby preventing cell damage (Magalingam, Radhakrishnan & Haleagrahara, 2016). In addition, rutin was found to ameliorate copper sulfate-induced brain damage in rats through antioxidative and anti-inflammatory action (Arowoogun et al., 2021).

Resveratrol (3,4′,5-trihydroxy-*trans*-stilbene) is a stilbene, a subclass of phenolic compounds, commonly found in plants such as grapes, raspberries, and peanuts. The antioxidant and anti-inflammatory effects of resveratrol have been reported in several studies investigating its potential for neuroprotection in PD as well as other neurological diseases such as Alzheimer's disease (Arbo et al., 2020). This compound has been shown to protect against damage inflicted by 6-OHDA, MPTP, and rotenone both *in vitro* (Zhang et al., 2015; Zeng et al., 2017; Wang, Dong, et al., 2018) and in rodent models of PD (Guo et al., 2016; Palle & Neerati, 2018; Huang et al., 2019). However, the low bioavailability and rapid metabolism of resveratrol limit its clinical applications, informing research into alternative formulations to overcome these obstacles (Intagliata et al., 2019).

Several antioxidant vitamins found in fruits and vegetables have also been investigated for their neuroprotective effects in PD models, including vitamins C and E (Park & Ellis, 2020). Jinsmaa and colleagues showed that vitamin C treatment of PC12 cells reduced DOPAL-induced synuclein oligomerization caused by divalent metal ions (Jinsmaa et al., 2014). Vitamin E was reported to protect against oxidative stress-induced cell death in cortical neuron cultures (Numakawa et al., 2006). A study of $43,865$ individuals from the Swedish National March Cohort investigated the potential link between baseline vitamin intake and risk of PD. After a follow-up time of 17.5 years, only 465 cases of PD were reported, leading to the conclusion that dietary intake of vitamin C and E may be inversely associated with the risk of PD (Hantikainen et al., 2021). Conversely, the results of a study of 1036 PD patients in two cohorts, the Nurses' Health Study and the Health Professionals Follow-up Study, did not support the hypothesis of reduced PD risk with antioxidant intake (Hughes et al., 2016). Although promising, such conflicting studies necessitate further research into antioxidant vitamins as PD treatment or prevention strategies.

1.5.2.1 Curcumin, a plant-based therapeutic

20

For centuries, the turmeric plant (*Curcuma longa*) (**Figure 1.7**) has been used for its healing properties in Asia (Moselhy et al., 2018). In ancient Indian, or Ayurvedic, medicine, turmeric is used as an appetite-promoting, detoxifying, antacid, tonic, and stimulant (Bhowmik et al., 2009). Ancient Chinese medicine promotes turmeric as a medicinal agent that aids menstrual blood flow and pain relief (Chinese Pharmacopoeia Commission, 2005). Scientific research has corroborated many of these claims and the constituents of turmeric, particularly curcumin, have been found to be powerful antioxidant, anti-inflammatory, and chemo-preventative agents (Yue et al., 2010).

Figure 1.7. Turmeric (*Curcuma longa*) root and dried powder. Turmeric is an Asian food spice containing curcumin, a powerful antioxidant and anti-inflammatory compound. Photo taken by Devina Chetty.

Turmeric is composed of several yellow curcuminoids, of which curcumin is the most prominent (Tayyem et al., 2006). Curcumin (chemically known as (1,7-bis{4-hydroxy-3-methoxyphenyl}-1,6-heptadiene-3,5-dione) is a polyphenol extracted from the rhizome of the turmeric plant and is largely responsible for the characteristic yellow color of turmeric (**Figure 1.8**). This active compound has been used to color and preserve food for thousands of years, in addition to its application as an herbal medicine (Aggarwal, Sundaram, Malani, *et al.*, 2007; Singh, 2007).
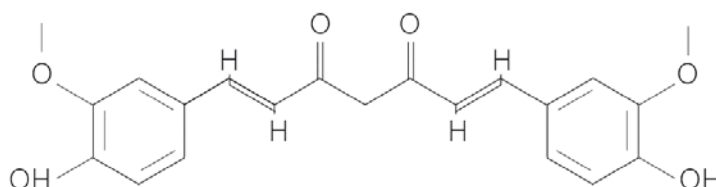
Figure 1.8. Two-dimensional chemical structure of curcumin, a polyphenol derived from the turmeric (*Curcuma longa*) plant.

Scientific studies have shown that curcumin is able to suppress tumor growth through the inhibition of signal transduction pathways (Mori et al., 2001). Other studies have reported that curcumin downregulates cell proliferation and increases the expression of anti-apoptotic genes by suppressing IκBα kinase (Aggarwal et al., 2006). In addition, curcumin has been shown to inhibit proliferation and promote cell death in human leukemic cell lines (Anuchapreeda et al., 2008), as well as several types of other cancer cells including human breast (Ramachandran et al., 2005), pancreatic (Kunnumakkara et al., 2007) and colon cells (Cheng et al., 2007). Furthermore, this compound has been found to control immune cell proliferation and cellular response (Bhaumik, Jyothi & Khar, 2000). In light of the severe acute respiratory syndrome coronavirus 2 (SARS-COV2) pandemic, turmeric extracts containing curcumin were recently shown *in vitro* to inhibit the chymotrypsin-like protease activity of this virus (Guijarro-Real et al., 2021). Additionally, curcumin has been shown to display antiplatelet (Lee, 2006) and antioxidant (Jayaprakasha et al., 2002) properties. Its antioxidant activity has been shown to include the scavenging of free radicals such as superoxide anions and hydroxyl radicals (Gibellini et al., 2015). Additionally, curcumin may relieve oxidative stress by upregulating the expression of cytoprotective proteins such as heme oxygenase and catalase, and by stabilizing antioxidant enzymes like glutathione peroxidase (Trujillo et al., 2014; Nawab et al., 2019).

1.5.2.2 Curcumin in PD treatment

With regards to PD, several studies have attested to the neuroprotective effects of curcumin in a wide range of models. This is well summarized in **Figure 1.9**, which illustrates the vast protection conferred by curcumin against the molecular events that are proposed to lead to neurodegeneration in PD (Mythri & Srinivas Bharath, 2012). This turmeric derivative has been shown to attenuate α-synuclein-induced toxicity, reduce ROS levels and protect against apoptosis in SH-SY5Y cells (Wang et al., 2010). In a mouse model of MPTP-induced toxicity, curcumin and its metabolite, tetrahydrocurcumin, were shown to reverse the accompanying dopamine and DOPAC depletion possibly due to MAO-B inhibition (Rajeswari & Sabesan, 2008). Curcumin was shown to successfully protect dopaminergic neurons in a 6-OHDA rat model of PD through iron chelation (Du et al., 2012). More recently, curcumin was reported to inhibit mitochondrial hexokinase release induced by fibrillation products of α-synuclein which trigger ROS formation (Dehghani et al., 2020). There is also evidence of the neuroprotection conferred by curcumin through the modulation of autophagy, a process known to be involved in several PD genes' functions and the removal of defective α-synuclein, as discussed in section 1.2 (Forouzanfar et al., 2020). However, a limitation of using curcumin as a therapeutic agent remains its restricted bioavailability. Low plasma and tissue levels of this compound may be attributed to rapid metabolism and systemic expulsion, and poor absorption (Anand et al., 2007). These limitations of native curcumin have led to the development of nanoparticle formulations such as nanocurcumin which exhibit increased bioavailability and solubility

(Maiti & Manna, 2014; Sookhaklari et al., 2019; Gao et al., 2020; Salehi et al., 2020). Studying the effectiveness of this compound, and its derivatives or bioavailable formulations, as a treatment for PD in cellular models is important and may lead to more effective treatments for PD in humans (Darvesh et al., 2012).
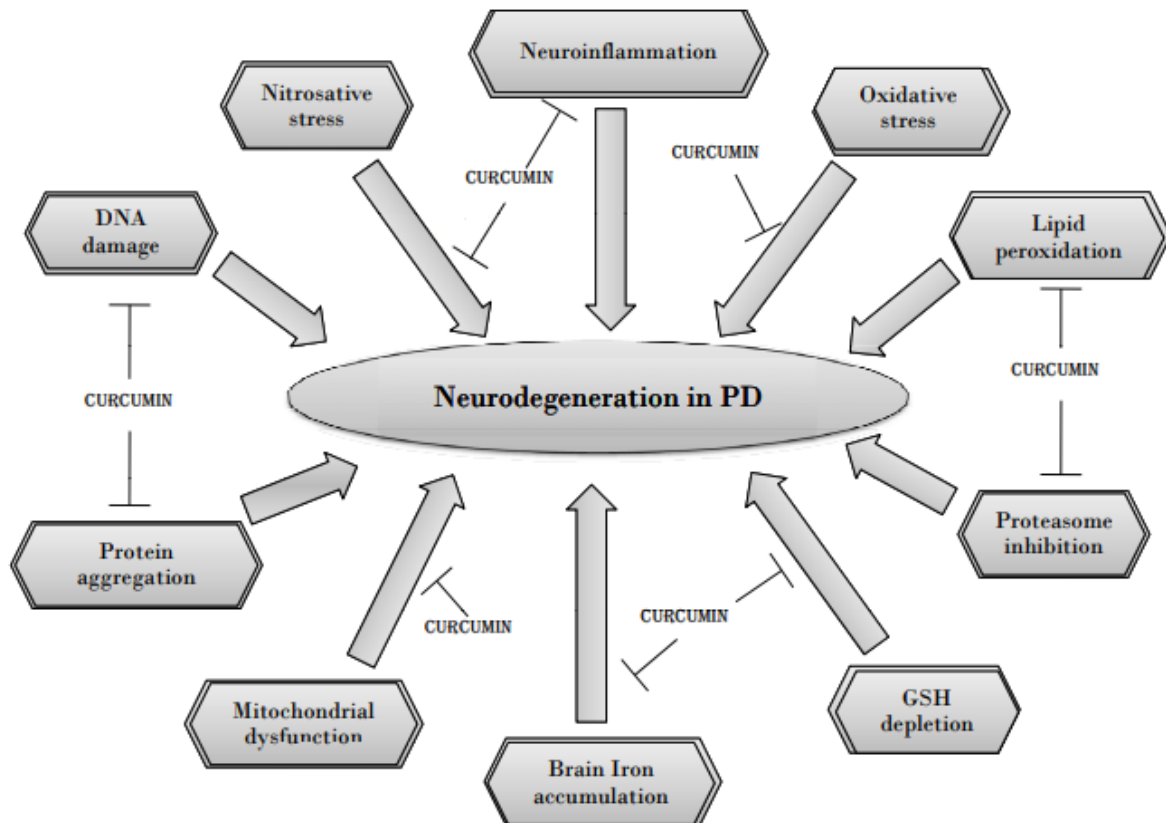
Figure 1.9. Schematic diagram showing the neuroprotective effects of curcumin against the causal molecular events responsible for neurodegeneration in Parkinson's disease. Reproduced with permission from (Mythri & Srinivas Bharath, 2012).

Abbreviations: GSH, glutathione.

Mounting evidence points to a protective effect of curcumin against damage caused by *PINK1* mutations. Curcumin was reported to rescue a *PINK1* knockdown SH-SY5Y model of PD from mitochondrial dysfunction and cell death (van der Merwe et al., 2017). In porcine intestinal epithelial (IPEC-J2) cells, curcumin was found to ameliorate H_2O_2 -induced oxidative stress, intestinal epithelial barrier injury, and mitochondrial damage in a manner dependent on PINK1-Parkin mediated mitophagy (Cao et al., 2020). The authors further confirmed these *in vitro* results in a pig model of the toxic herbicide diquat. They reported that dietary curcumin could protect against intestinal barrier function, enhance intestinal redox status, alleviate mitochondrial damage, initiate mitophagy, and

influence the adenosine 5'-monophosphate (AMP)-activated protein kinase (AMPK) transcription factor EB (TFEB) metabolic signaling pathway.

Curcumin has also been reported to have a positive therapeutic effect in PD through its interaction with α-synuclein. In transgenic *Drosophila* expressing human α-synuclein, curcumin was reported to increase lifespan and locomotor abilities as well as reduce oxidative stress and dopaminergic neuronal apoptosis (Siddique, Naz & Jyoti, 2014). Studies have shown that curcumin and its derivatives can not only prevent α-synuclein oligomer and fibril formation (Kamelabad et al., 2021), but further disintegrate these toxic protein forms thereby preventing aggregation and delaying PD onset (Pandey et al., 2008; Shrikanth Gadad et al., 2012). The value of curcumin for targeting α-synuclein as a PD treatment and prevention strategy is further discussed in the review article (Chapter 4).

Curcumin's protection against inflammation, oxidative stress, protein aggregation, and mitochondrial dysfunction may make this plant compound a candidate for reducing potential causative factors and symptoms of PD. This evidence warrants continued curcumin research to further elucidate its potential as a PD therapy.

1.6 The present study

The current global increase in population aging is resulting in an increased prevalence of age-related neurodegenerative diseases, including PD (Mythri & Srinivas Bharath, 2012). The United Nations estimated an increase in individuals over age 65 from 962 million in 2017 to 2.1 billion in 2050 (Bennett et al., 2017). This necessitates the search for a cure or preventative strategies for PD before the burden of this incurable disease becomes overwhelming to global health systems. From the research elucidated in the preceding sections, it is evident that oxidative stress may be an important contributing factor to the pathogenesis of PD. Dopaminergic neurons are particularly affected by oxidative stress due to dopamine biosynthetic pathways occurring within them, as well as their low mitochondrial reserve compared to other neuronal populations (Feng & Maguire-Zeiss, 2010). Furthermore, 'dopaminergic-like' cells such as the SH-SY5Y cell line are typically used as PD models as dopamine production is the hallmark of these neurons which characteristically degenerate in PD (Haque et al., 2008).

In the cellular model used in the present study, sources of oxidative stress include mitochondrial dysfunction (caused by *PINK1* mutation and paraquat exposure) and dopamine metabolism which produces ROS. Overexpression of mutant *PINK1* in the model represents the genetic causes of PD. This will upregulate dopamine production, causing increased dopamine auto-oxidation, enhancing oxidative stress, and thereby resulting in toxicity. Paraquat causes mitochondrial dysfunction and represents the environmental causes of sporadic PD. In this study, paraquat will be used as a mitochondrial stressor against which to assess the protective effects of curcumin. Paraquat is a toxic

herbicide having a similar chemical structure to MPP+, a compound that has been shown to induce the biochemical, neuropathological, and clinical characteristics of parkinsonism in human and non-human primates (Langston *et al.*, 1983). Paraquat contributes to oxidative stress through the reaction of paraquat cations with O_2, inducing the formation of superoxide and increasing mitochondrial membrane permeability as seen in PD (Cochemé & Murphy, 2008; Huang *et al.*, 2016). The numerous medicinal attributes of curcumin, particularly its antioxidant quality, makes this compound a potential therapeutic candidate for PD and a suitable compound to test in our model.

Also, as PD is a multi-faceted disease with many predicted etiologies, therapeutic candidates should be assessed for their protective effects across multiple disease pathologies. Therefore, to address these various etiologies, in this project we sought to investigate the effect of treatment on a genetic (*PINK1*) model of PD. In addition, we also reviewed its potential effects on toxic α-synuclein aggregation which is a pathological hallmark of the more common sporadic form of the disease and is triggered by an interplay of a wide variety of etiological factors – including genetic, environmental, and metabolic components.

The hypothesis for the present study is as follows:

1.6.1 Hypothesis

It is hypothesized that overexpression of mutant *PINK1* will produce a cellular model of dopamine accumulation, leading to mitochondrial dysfunction, which will be significantly rescued by curcumin.

1.6.2 Aim

Therefore, the aim of this study is to create a *PINK1-* and paraquat-induced model of cultured SH-SY5Y cells, which will be used to investigate the effects of curcumin on various cellular features such as cell viability and mitochondrial function.

1.6.3 Objectives

The aim will be achieved by executing the following objectives over the course of the study:

1. To acquire appropriate wild-type (WT) and mutant *PINK1* constructs for the cellular model to be used in this study

2. To culture SH-SY5Y cells and successfully transfect these cells with the constructs selected (viral plasmid pLenti6-DEST PINK1-V5 expressing either WT or mutant G309D PINK1) to produce excess dopamine, thereby creating a toxicity model of neuronal vulnerability.

3. To perform real-time quantitative RT-qPCR to quantify *PINK1* and *TH* gene expression in these cells.

4. To measure levels of dopamine using liquid chromatography-mass spectrometry (LC-MS) in these cells.

5. To produce dosage curves to determine optimum concentrations of curcumin, and the herbicide paraquat (as a mitochondrial stressor) for use in the study.

6. To determine the possible rescue effect of curcumin treatment on the metabolic activity of cells by performing the cell viability assay, 3-(4,5-Dimethylthiazol-2-yl)-2,5-diphenyltetrazolium bromide (MTT) assay.

7. To determine the possible rescue effect of curcumin treatment on mitochondrial membrane potential of the cells by performing a 1,1',3,3'-Tetraethyl-5,5',6,6'-tetrachloroimidacarbocyanine iodide (JC-1) assay.

8. To compare the rescue effects of curcumin and a modified, nanoparticle-encapsulated form of curcumin (nanocurcumin) on cell viability using the MTT assay

9. Finally, to write a review on the hypothesis that curcumin can also prevent misfolded α-synuclein accumulation and spread, a key pathological hallmark of PD.

CHAPTER 2:Materials and methods

2.1 Summary of methodology

This chapter provides a detailed description of the materials and methods used to evaluate the effect of curcumin on cell viability and mitochondrial function, as summarized in **Figure 2.1**.
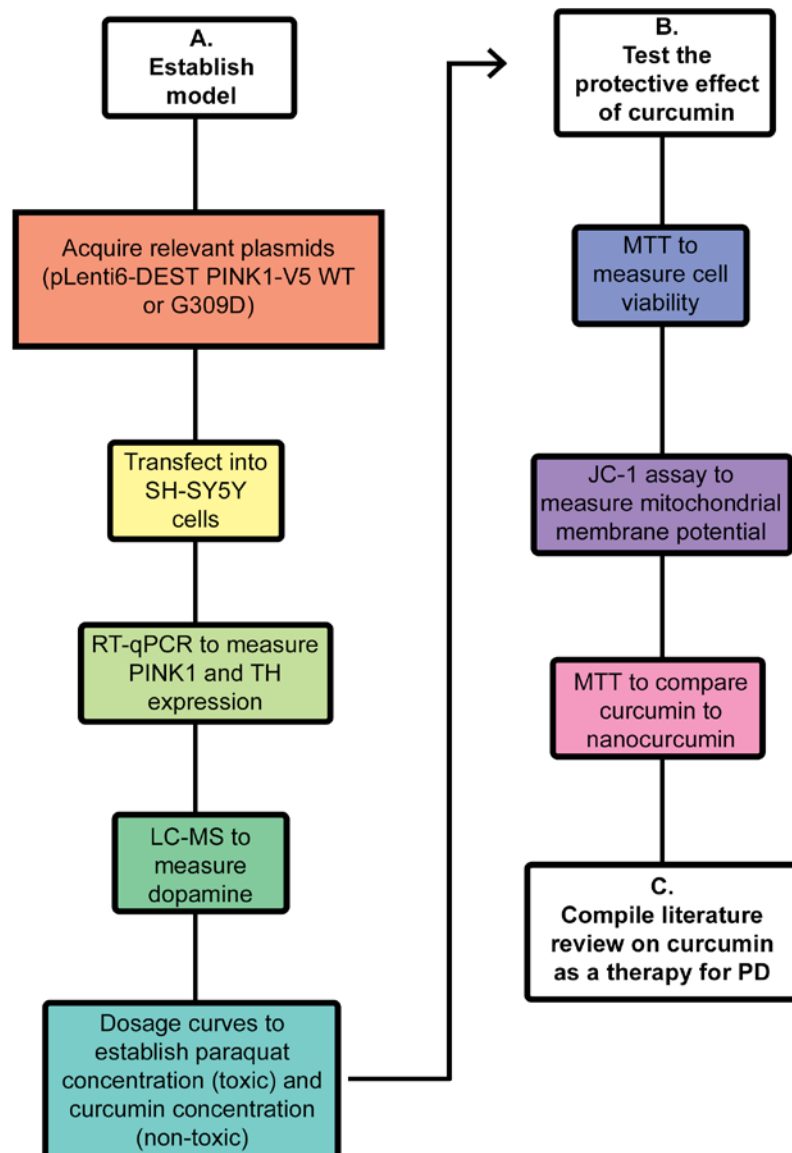
Figure 2.1 Summary of the study methodology. A-C refers to the main aspects of the project (establishing the model, testing the model and compiling a literature review).

Abbreviations: WT, wild-type; RT-qPCR, real time quantitative reverse transcription polymerase chain reaction; TH, tyrosine hydroxylase; PINK1, phosphatase and tensin homolog induced kinase 1; LC-MS, liquid chromatography-mass spectrometry; MTT, 3-(4,5-dimethylthiazol-2-yl)-2,5-diphenyltetrazolium bromide; tetraethylbenzimidazolylcarbocyanine iodide; JC-1, tetrachloro-1,1',3,3'tetraethylbenzimidazolylcarbocyanine iodide; PD, Parkinson's disease.

SH-SY5Y cells transfected with PINK1 plasmids were used to create the cellular PD model in an attempt to recapitulate the findings of Zhou *et al*. (2014) (Sections 2.2-2.4). PINK1 mutations, such as G309D PINK1, have been observed in connection with early-onset, recessive familial PD (Valente et al., 2004). The model was examined using RT-qPCR and LC-MS to assess levels of PINK1, as well as dopamine-related compounds to recapitulate the finding of dopamine toxicity observed by Zhou *et al*. (2014) (Sections 2.5 and 2.6). The 3-(4,5-dimethylthiazol-2-yl)-2,5-diphenyltetrazolium bromide (MTT) and CyQUANT assays were performed to determine appropriate treatment concentrations of curcumin and paraquat, a toxic herbicide used to create mitochondrial stress in the model (Section 2.7). After establishing the model, curcumin was investigated as a potential neuroprotective compound. The effect of curcumin treatment on cell viability and mitochondrial function in the model was investigated. This was achieved by measuring cell viability with the MTT assay (Section 2.8) and assessing mitochondrial membrane potential using the JC-1 assay (Section 2.9) in transfected and curcumin-treated cells. Finally, we compared the protective effects of nanocurcumin and curcumin on cell viability using the MTT assay (Section 2.10).

2.2 Plasmid acquisition

Zhou *et al.* (2014) published a study investigating neuronal vulnerability in a *PINK1* overexpression model. Overexpression is commonly used in *in vitro* studies of PD to model the pathogenesis of the disease. The authors reported that overexpression of mutant *PINK1* upregulated dopamine and TH, leading to neuronal vulnerability. We attempted to recapitulate this model using WT and mutant G309D PINK1, and then test the effects on curcumin exposure to determine the extent to which it could rescue the cell from paraquat toxicity by performing cell viability and mitochondrial membrane potential assays.

Lentiviral plasmids pLenti6-DEST PINK1-V5 containing subcloned WT PINK1 (Addgene; plasmid 13320) and the PINK1 mutant G309D (Addgene; plasmid 13318), both deposited by Professor Mark Cookson (Beilina *et al.*, 2005)), were purchased.

The plasmids were received as bacterial stabs of the *Escherichia coli* (*E. coli*) DH5α strain in order to propagate these constructs. A sterile inoculating loop was used to gather bacteria from the stab and streak onto an LB agar plate containing ampicillin for single colonies. Plates were incubated for 16 h at 37 °C. Bacterial glycerol stocks were made for long-term storage by adding 500 µl of overnight bacterial culture and 500 µl of 50 % glycerol to a cryovial and storing at -80 °C. Thereafter, to make new plates, an inoculating loop was used to select individual colonies from existing plates and inoculate 10 ml LB media containing 10 µl ampicillin (100 mg/ml) which were grown overnight at 37 °C (Appendix I). Approximately 150 µl of overnight bacterial culture were added to LB agar plates

containing selection antibiotic ampicillin to select transformed bacterial colonies. The plates were labeled, inverted, and incubated for 16 h at 37 °C.

The details of plasmid DNA extraction, sequencing, PCR, agarose gel electrophoresis, and restriction digest that were performed to verify the WT and mutant plasmid sequences are outlined below.

2.2.1 *Plasmid DNA extraction*

The techniques for plasmid DNA extraction are summarized in **Figure 2.2**. Single colonies were selected with an inoculating loop and used to inoculate centrifuge tubes containing 3 ml LB media and 3 µl ampicillin, which were grown overnight at 37 °C for use with the Zyppy™ Plasmid MiniPrep kit (Catalog ID D4036, Zymo Research, United States). A starter culture of single colonies in 5 ml LB media and 5 µl ampicillin was incubated for 8 h at 37 °C for use with the ZymoPURE™ II Plasmid Midiprep Kit (Zymo Research, United States). A volume of 100 µl starter culture was added to 100 ml LB media with ampicillin and incubated overnight. Thereafter, centrifuge tubes with bacterial culture were centrifuged for 10 min at maximum speed. The supernatant was discarded, and the pellet was resuspended in the remnants of supernatant. Plasmid DNA was extracted according to optimized manufacturers' instructions for each kit with plasmid DNA concentration and purity quantified using the Multiskan Sky microplate spectrophotometer (Thermo Fisher Scientific, United States).
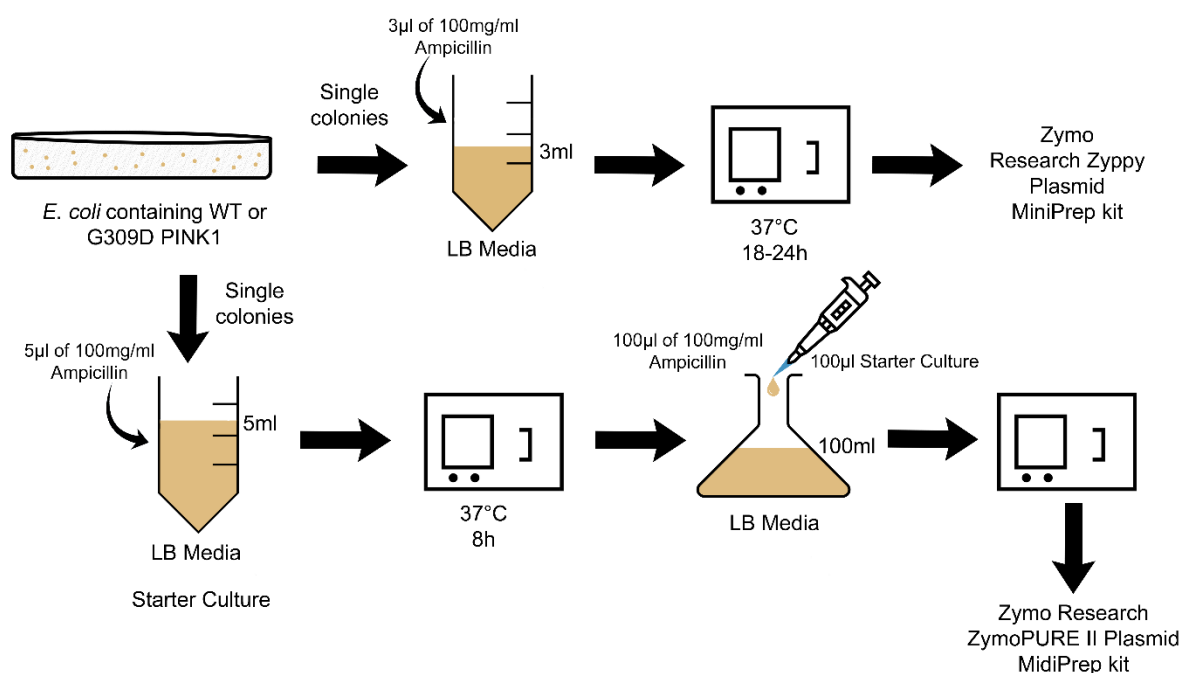
Figure 2.2 Methods used for plasmid DNA extraction in the present study.

2.2.2 *Sequencing primer design*

In addition to the known universal sequencing primers (CMV-F and pBABE3) available from Addgene https://www.addgene.org/mol-bio-reference/sequencing-primers/, primers across the plasmid construct were designed using sequence data obtained from the Online Mendelian Inheritance in Man (OMIM) database (https://www.omim.org/) and Ensembl Genome Browser database (http://www.ensembl.org). Primer3 software version 4.0.0 (http://primer3.ut.ee) (Koressaar and Remm, 2007), Primer-Basic Local Alignment Search Tool (BLAST) (https://www.ncbi.nlm.nih.gov/tools/primer-blast/), and Ensembl BLAST were used to determine primer length, GC content, melting temperature (T_m), and 3'self-complementarity and self-complementarity. The primers used to verify plasmid sequences and identify colonies containing the correct constructs by sequencing and PCR are shown in **Figure 2.3** and recorded in Appendix II, **Supplementary Table 2** and **Supplementary Table 3**.
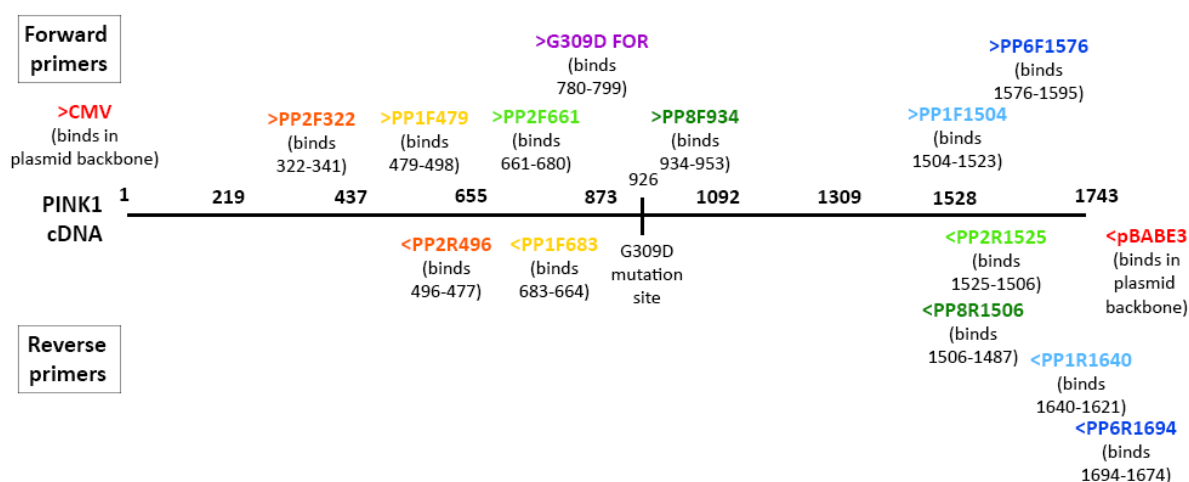
Figure 2.3 Schematic of PINK1 primers designed for Sanger sequencing and PCR of WT PINK1 and G309D PINK1. Matching colors indicate primer pairs composed of one forward and reverse primer. Universal primers included CMV and pBABE3.

Briefly, optimal primer design should yield primer pairs with several key properties (Dieffenbach, Lowe & Dveksler, 1993). A length of 18-24 bases is ideal as the longer the primers are, the less efficiently they will bind to the DNA target. A GC content of 40-60 % is required as the strong hydrogen binding between guanine and cytosine bases stabilizes the primer. However, excessive GC content above this range may cause primer-dimer formation which inhibits amplification. A T_m of 50-60 °C for each primer in a pair that differ by no more than 5 °C is required to separate the double-stranded DNA to allow primer annealing and is dependent on primer length. Lastly avoiding complementary regions within and between primers is essential to prevent secondary structures and

30

primer dimers. These properties ensure that the primers are suitable to achieve successful DNA amplification. A total of six primer pairs were designed to span the *PINK1* insert. An additional primer was designed around the mutation site in order to verify the presence of the G309D PINK1 mutation in the mutant and its absence in the WT plasmid. The G309D PINK1 mutant is characterised by a nonsynonymous substitution from guanine to adenine, resulting in an amino acid change from glycine (G**G**C) to aspartic acid (G**A**C). Primers were synthesized by Inqaba Biotechnical Industries (Pty) Ltd, Pretoria, SA.

2.2.3 *Sanger sequencing of plasmids*

Sanger sequencing was invented by Fredrick Sanger in 1977 as a method of determining the specific nucleotide sequence of DNA (Valencia et al., 2013). This technique involves the denaturation of double-stranded DNA and uses chain termination PCR to produce complementary single-stranded DNA using fluorescently labeled nucleotides (dNTPs) called dideoxyribonucleotides (ddNTPs). These ddNTPs lack the 3'-OH group required for phosphodiester bond formation between adjacent dNTPs. Therefore, when a ddNTP is incorporated at random, extension of the DNA strand ceases. The resulting chain-terminated oligonucleotides are separated by size via gel electrophoresis in which the DNA fragments are arranged from largest (top of gel), to smallest (bottom of gel). Since DNA polymerase only synthesizes DNA in the 5' to 3' direction beginning at a primer, each terminal ddNTP corresponds to a specific nucleotide in the original DNA sequence. The fluorescent signal emitted by each ddNTP is read by a computer which arranges the DNA sequence accordingly.

Plasmid DNA aliquots of 5 µl at a concentration of 100 ng/µl were sent to the DNA Sequencing Unit at the Central Analytical Facilities (CAF) at Stellenbosch University for sequencing. A total of eight primer pairs were designed, spanning the construct including the mutation site (**Figure 2.3**), and sent to CAF along with the plasmid DNA samples. Capillary electrophoresis was performed on a 3130 x1 Genetic Analyser (Applied Biosystems, CA, United States) using The BigDye Terminator Sequence Ready Reaction kit version 3.1 (Applied Biosystems, CA, United States). BioEdit v7.2.5 software (Hall, 1999) was used to analyze and align sequencing data to reference sequences obtained from the Ensembl Genome Browser database (http://www.ensembl.org).

2.2.4 *Polymerase chain reaction (PCR)*

For PCR, three primer pairs were chosen from the beginning, middle, and end of the plasmid (**Figure 2.3**). These primers were CMV-F and pBABE3, PP8F and -R, as well as PP1F and -R. The PCR product of CMV-F/pBABE3 was too large (1743 bp) to amplify consistently in PCR. Therefore, the primer pair PP2F661/PP2R1525 was used later instead as it yielded a smaller PCR product of 865 bp. Fragments of interest were amplified from plasmid DNA in a 40 µl PCR reaction containing 200 ng of

template genomic DNA, 20 µmol of each forward and reverse primer, 5 mM dNTPs (Promega, Madison, Wisconsin, United States), 1.5 mM $MgCl_2$, 1X Green GoTaq® Reaction Buffer (Promega, Madison, Wisconsin, United States), and 5 units of GoTaq® G2 Flexi DNA Polymerase (Promega, Madison, Wisconsin, United States). All PCR reactions that were performed included a non-template negative control to identify PCR contamination. Amplification was performed in an ABI 2720 Thermal Cycler (Applied Biosystems Inc., United States). PCR conditions comprised of an initial denaturation step at 92 °C, followed by 35 cycles of denaturation at 94 °C, primer annealing at the optimum temperature (Appendix II, **Supplementary Table 2** and **Supplementary Table 3**), and extension at 72 °C. A final extension step of 72 °C was performed for five minutes before a cooling step at 4 °C.

2.2.5 *Restriction enzyme digest*

To further confirm the presence of WT and mutant plasmid constructs, a restriction enzyme digest was also performed using EcoRV and BamHI enzymes (Thermo Fisher Scientific, United States; ER0301 EcoRV and ER0051 BamHI). The manufacturer's protocol was followed, and a digest was performed by combining the following reagents in a 1.5 ml centrifuge tube: 3 µl of restriction enzyme 10X buffer, 10 units of restriction enzyme, and 500 ng plasmid DNA, which was made up to a volume of 30 µl with dH_2O. The tubes were incubated for 2 h at 37 °C, and products were run on a 1 % agarose gel and visualized. Expected band sizes for EcoRV, which cuts the circular plasmid twice, were 6974 bp and 1873 bp. The expected band size for BamHI, which cuts the plasmid once, was 8811 bp (Appendix II, **Supplementary Figure 2**).

2.2.6 *Agarose gel electrophoresis*

Agarose gel electrophoresis was used to visualize plasmid DNA, PCR products, and restriction digest products. A 1 % agarose gel was made with agarose powder (SeaKem® LE, Lonza Bioscience, United States) dissolved in 1X sodium borate (SB) buffer by microwave heating (Appendix I). A volume of 6 µl GelStar dye (Lonza Bioscience, United States) was added and mixed into the warm agarose which was poured into a gel casting tray containing a 20-well gel comb. After solidifying, the gel was transferred to a gel tank containing 1X SB buffer for gel electrophoresis. Samples were prepared and loaded into the gel as follows: 6 µl diluted plasmid DNA, 6 µl restriction digest product, 5 µl PCR product, 1 µl of 1 kb DNA Ladder Ready to Load, or 1 µl of 100 bp DNA Ladder Ready to Load (Solis Biodyne, Estonia) (Appendix I, **Supplementary Figure 1**), mixed with 2 µl of 6X DNA gel loading dye (Thermo Fisher Scientific, United States).

2.3 Cell culture

2.3.1 *SH-SY5Y cell line*

The human neuroblastoma SH-SY5Y cell line (Cellonex, South Africa) was chosen as an *in vitro* model for this study as these cells are commonly used in PD research due to their 'dopaminergic-like' nature (Xie, Hu & Li, 2010). Cells were grown and cultured in Dulbecco's modified Eagle's medium (DMEM; Lonza Bioscience, Switzerland) supplemented with 10 % fetal bovine serum (FBS) (HyClone, Logan, Utah, United States) and 1 % penicillin (1000 U/ml) and streptomycin (1000 U/ml) solution at 37 °C in a 5 % CO_2 incubator. This will hereafter be referred to as the media. The SH-SY5Y cells were cultured for all experiments in 75 cm^2 culture flasks and handled in an Esco Airstream® Class II Biohazard Safety laminar flow cabinet (Esco Technologies Inc., United States) (Appendix V). Cells of passages 16-20 were used for the following experiments as loss of dopaminergic characteristics have been observed in cells at higher passages (Biedler et al., 1978).

2.3.2 *Cryopreservation and thawing of cells*

Cells were stored in stocks for later use in experiments using cryopreservation. The freezing medium consisted of 90 % FBS and 10 % dimethyl sulfoxide (DMSO) (Sigma-Aldrich, United States). Cells were trypsinized and centrifuged at 1006 x g in an Eppendorf Centrifuge 5810R (eppendorf, Germany). Following the discarding of the supernatant, the cell pellet was resuspended in 1 ml freezing media. The mixture was transferred into a 1.5 ml cryovial and placed into a Mr. Frosty Freezing Container (Thermo Fisher Scientific, United States) and stored in a -80 °C freezer. This preserves sample integrity by cooling the sample at a rate of -1 °C/minute.

To use cell stocks, frozen cryovials were quickly thawed at 37 °C with the addition of 1 ml warmed media. The mixture was transferred to a 15 ml polypropylene tube and centrifuged at 1006 x g for 5 min in an Eppendorf Centrifuge 5810R (eppendorf, Germany). The supernatant was discarded, and the pellet was resuspended in 2 ml warmed media. The resuspended mixture was pipetted into a 75 cm^2 culture flask containing 8 ml media and incubated at 37 °C, 5 % CO_2 in a Farma thermosteri-cycle humidified incubator (Thermo Fisher Scientific, United States).

2.3.3 *Passaging and seeding of cells*

Cells were grown to a confluency of 70-90 % after which one 75 cm^2 culture flask was subcultured into two new 75 cm^2 culture flasks. The media was removed from the flask, and the monolayer of cells was gently washed with phosphate-buffered saline (PBS, Whitehead Scientific, South Africa). A volume of 3 ml 1X trypsin-EDTA solution (Sigma-Aldrich, United States) was added to the flask and incubated for 5 min at 37 °C in a 5 % CO_2 incubator, to lift adherent cells off the flask surface. To

deactivate the trypsin, 4 ml media was added to the flask and the mixture was transferred to a 15 ml tube for centrifugation at 1006 x g. The supernatant was discarded, and the pellet was resuspended in 2 ml media. A volume of 1 ml of cell suspension was added to each of two 75 cm^2 culture flasks containing 9 ml pre-warmed media.

For experiments, cells were counted using trypan blue analysis to quantify live cells in suspension and were seeded into various cell culture plates. This is a dye exclusion test based on the principle that live cells are enclosed by intact cell membranes that prevent the entrance of certain dyes, such as trypan blue, but dead cells are not. This allows for the counting of viable and dead cells either manually or with a specialized, automated machine. Cells were harvested by adding trypsin and incubating for 5 min. Following deactivation of trypsin with media, centrifugation, and resuspension of the pellet, a volume of 1 µl of the cell suspension was combined with 9 µl trypan blue solution (0.4 % w/v) (Sigma-Aldrich, United States). This mixture was added to a cell counter chamber slide and placed in a Countess™ automated cell counter (Thermo Fisher Scientific, United States) and counted. At least 3 replicates were used for each sample.

Based on cell count, cells were seeded at optimum densities depending on the size of the tissue culture plate. Following seeding at an optimized density, flasks were incubated for 24 h to allow cells to grow to 80-90 % confluency for further experiments.

2.4 Transient PINK1-expressing SH-SY5Y cell lines

2.4.1 *Transient transfection of cells*

Successful transfection, or the introduction of genetic material into eukaryotic cells, is a reproducible procedure with many variations, although all are based on a few simple principles (Chu *et al.*, 1987). A net negatively charged DNA molecule must come into contact with the cell membrane of a cell to be transfected which also has a net negative charge. The protocol that was used in this study employs a transfection reagent called Lipofectamine 3000 which was used to aid in the uptake of DNA molecules into the cell by overcoming electrostatic repulsion (Dalby *et al.*, 2004).

SH-SY5Y cells were seeded at the optimized density of 125 000 cells/well in 24-well cell culture plates. Optimized volumes of 0.75 µl Lipofectamine 3000 and 1 µl P3000 reagent (Thermo Fisher Scientific, United States) with 5 ng plasmid DNA per well were separately incubated in 25 µl serum-free media (SFM), for 5 min at room temperature. The two volumes (SFM-Lipofectamine 3000 mixture and SFM-plasmid DNA mixture) were combined dropwise and gently mixed to form the transfection mixture. The transfection mixture was incubated for 20 min at room temperature. All media was removed by aspiration from each well of cells. Each well was rinsed with 100 µl DMEM containing 10 % FBS. A volume of 250 µl DMEM containing 10 % FBS was added to each well and

plates were returned to the incubator for 5-10 min. Following incubation, the transfection mixture was added dropwise to each well, ensuring that the mixture covered the well surface. The plates were incubated at 37 °C, 5 % CO_2 for 24 h. Following incubation to complete transfection, media was removed by aspiration and replaced with 1 ml pre-warmed complete media per well, ready for downstream experiments. Any unused plasmid DNA was stored in microcentrifuge tubes at -80 °C for later transfection of eukaryotic cells.

2.4.2 *Immunofluorescence for transfection efficiency*

To confirm successful transfection and to determine percentage efficiency, immunofluorescence was performed. Cells were seeded in 6-well plates containing a coverslip in each well at a density of 500 000 cells/well. Following a wash with PBS for 5 min, cells on the coverslip were fixed using 2 ml formaldehyde (3 %) in PBS for 20 min, at room temperature while shaking. The cells were then washed with shaking three times for 5 min each with 2 ml of PBS to remove loose cells. The fixed cells were permeabilized in 2 ml Triton X-100 (0.25 %) in PBS for 20 min at room temperature while shaking, and then washed three times for 5 min each with 2 ml of PBS. Blocking was performed with 2 ml BSA (0.5 %) in PBS for 30 min at room temperature while shaking, followed by a 5 min wash with 2 ml 1X PBS. Cells were incubated at 4 °C with shaking overnight in 500 µl diluted primary anti-V5 tag antibody (1:200; ab206566; Abcam, United Kingdom) per well, with the plates wrapped in wet paper towel to reduce evaporation. The anti-V5 antibody was used to target PINK1-V5 protein expressed by the plasmids (Appendix II, **Supplementary Figure 2**). Following overnight incubation, the cells were washed three times for 5 min each with 2 ml PBS to remove excess primary antibody. A volume of 500 µl Alexa Fluor 488 goat anti-rabbit IgG (1:500, Thermo Fisher Scientific, United States) antibody was added to each well and incubated for 1 h at room temperature in moist paper towel, wrapped in foil, and kept in the dark. Thereafter, the cells were washed with shaking three times for 5 min each with 2 ml 1X PBS to remove excess secondary antibody. In order to stain the cells, 1 ml PBS followed by 10 µl DAPI (10 µg/ml) were added to each coverslip and incubated for 5 min in the dark at room temperature. The cells were then washed with shaking four times for 5 min each with 2 ml PBS. Excess PBS was blotted off the coverslips and the cell-free side of each coverslip was dried. Each coverslip was mounted cell-side down on a clean microscope slide with 1 drop DAKO mounting medium containing 0.015 mol/L sodium azide (Agilent Technologies, United States) and allowed to set for at least 1 h, in the dark and at room temperature. The slides were covered and stored at 4 °C until ready to view, or for storage.

Slides were viewed under a Euromex Oxion inverso fluorescence microscope (Euromex, Netherlands). Brightfield (transmitted light) images were used to determine total cell count in untransfected, WT and G309D PINK1 images. Fluorescence images were used to determine fluorescent cell count in each group. The ratio of fluorescent cells to total cells was calculated for

each group. Autofluorescence, determined from the untransfected group, was subtracted from the WT and G309D PINK1 groups. The final ratios represented transfection efficiency of WT and G309D PINK1 DNA, and were reported as percentages.

2.5 Real time, quantitative, reverse transcription PCR (RT-qPCR)

Real-time, quantitative, reverse transcription polymerase chain reaction (RT-qPCR) is used for the sensitive, specific, and reproducible quantitation of genetic material. RNA is reverse transcribed into single-stranded cDNA. A DNA template, in the form of cDNA, is copied exponentially, resulting in a quantitative relationship between the amount of starting target DNA and accumulated product at any given cycle (Arya *et al.*, 2005). This technique was used to analyze *PINK1* and *TH* expression levels in the SH-SY5Y cells to establish the cellular model for the study.

2.5.1 *RNA extraction*

The RNeasy Mini kit (Qiagen, Germany) was used for the isolation and purification of total intracellular RNA from the SH-SY5Y cells. Following the 24 h transfection period (Section 2.4), cells were scraped from plate wells using Qiagen RLT lysis buffer supplemented with 10 µl/ml β-mercaptoethanol (Sigma-Aldrich, United States). The RNA was purified according to the manufacturer's instructions with several modifications to optimize yield and purity. Optimizations included performing all centrifugation steps for 1 min, and at 4 °C. Thereafter, a two-step RT-qPCR was performed. Any unused RNA was aliquoted and stored at -80 °C in RNase-free microcentrifuge tubes.

2.5.2 *Reverse transcription*

A Superscript IV VILO mastermix (Thermo Fisher Scientific, United States) was used to carry out reverse transcription, using 1 µg RNA for each 20 µl reaction. This kit provides a convenient procedure for effective first strand cDNA synthesis as well as effective genomic DNA (gDNA) elimination. The ezDNase enzyme contained in the master mix is a double-strand specific DNase that removes gDNA contamination from template RNA prior to reverse transcription. cDNA was aliquoted and stored at -80 °C until qPCR reactions were performed.

2.5.3 *cDNA optimization for RT-qPCR*

Since qPCR is a sensitive technique, cDNA usually requires dilution in preparation for amplification so as not to increase the background signal. An amount of cDNA should be chosen that yields a cycle threshold (Ct) value of between 15 and 25 cycles and has triplicates that are within 0.5 cycles of each other and do not diverge. To identify a suitable amount of cDNA for RT-qPCR, a 10X dilution series

of cDNA was created including neat, 1:10, 1:1000, and 1:10 000, using cDNA from untransfected cells. The *β-actin* and *TH* gene expression levels for all the samples were measured, and a cDNA dilution was chosen, according to the aforementioned criteria, for use in all subsequent RT-qPCR experiments. During this optimization experiment, gene expression was measured as both single and multiplex reactions to determine whether multiplex performance did not differ from singleplex reactions.

An assumption of the $2^{-\Delta\Delta Ct}$ method is that efficiencies of the targets and reference must be approximately equal (Livak & Schmittgen, 2001). The efficiency of qPCR refers to the rate at which the polymerase converts the DNA template and reaction reagents into amplicons (Taylor et al., 2010). The maximum increase in amplicon per cycle is 2-fold, indicating 100 % efficiency. Low reaction efficiencies (< 90%) may be caused by poor primer design, Taq inhibitors, suboptimal annealing temperatures and inactive Taq. Conversely, high efficiencies (> 110 %) usually result from primer dimers or nonspecific amplicons. Poor pipetting is a common cause for both low and high qPCR efficiencies. The qPCR efficiency for each gene was determined by performing qPCR on 10-fold dilutions on the cDNA and plotting the logarithm of the starting DNA copy number or dilution factor against Ct values obtained. The slope of the regression line is an indicator of qPCR efficiency. A slope of -3.32 is equivalent to 100 % efficiency which indicates doubling of DNA template with each cycle. In addition, the Pearson's correlation coefficient (r) or the coefficient of determination (r^2) value indicates how well the data fit the regression line and is a measure of replicate variability. A value of r >0.990 or r^2 value >0.980 is desirable for RT-qPCR.

2.5.4 *Real time quantitative PCR*

Fluorescently labeled probes for qPCR of cDNA were purchased as cataloged assays (Thermo Fisher Scientific, United States), and are listed below with their respective fluorescent dyes:

1. PINK1 TaqMan assay (Hs00260868_m1), FAM dye (Catalogue number 4331182)

2. TH TaqMan assay (Hs00165941_m1), FAM dye (Catalogue number 4331182)

3. Beta-actin (β-actin) TaqMan assay (Hs01060665_g1), VIC dye (Catalogue number 4448489)

TaqMan qPCR assays work similarly to SYBR green assays, however, TaqMan reagents allow for multiplexing as each gene can be specifically targeted with a unique probe sequence and dye combination. Therefore, multiplexing reactions requires less cDNA, mastermix, and time to prepare experimental plates. The TH assay (FAM) was multiplexed with β-actin (VIC), and the PINK1 assay (FAM) was performed as singleplex reactions on the same plate. To reduce pipetting error, one cocktail for each gene (singleplex) or gene combination (multiplex) was made by combining the appropriate multiple of a total volume of 18 µl per well, which included 10 µl TaqMan™ Fast

37

Advanced Master Mix (Applied Biosystems Inc., United States), 1 µl of each TaqMan assay, and nuclease-free H$_2$O. After vortexing, 18 µl of the cocktail was pipetted into each well in a 96-well plate (Lasec, SA). Thereafter, 2 µl of either cDNA or sterile H$_2$O was added to either experimental or control wells, in triplicate. The plate was centrifuged in an Eppendorf Centrifuge 5810R (eppendorf, Germany) at 112 x g for 15 s, and qPCR was performed.

All qPCR reactions were performed in a QuantStudio™ 5 real-time PCR detection system (Thermo Fisher Scientific, United States). The following amplification conditions were used: A hold stage at 50 °C for 2 min followed by an initial denaturation step at 95 °C for 2 min, and subsequently, 40 cycles of both 95 °C for 1 s and 60 °C for 20 s. Finally, a hold step at 4 °C completed the reactions. The reactions were performed in triplicate for each experimental group. To normalize the amplification products for the amount of starting RNA, the PCR amplification data were normalized to the geometric mean of the housekeeping gene, β-actin. Since we sought to recapitulate the results of Zhou *et al.* (2014), which showed upregulation of *PINK1* and *TH* in the mutant PINK1 group relative to the empty vector control, absolute quantification of transcript copy number was not necessary. Instead, the $2^{-\Delta\Delta CT}$ comparative method (Livak & Schmittgen, 2001) was used to determine the relative quantification of gene expression. For reporting, fold change in *PINK1* and *TH* expression levels in control cells were set to 100 %. Expression levels in WT and G309D PINK1 groups were expressed relative to this.

2.6 Liquid Chromatography-Mass Spectrometry (LC-MS) analysis of dopamine content in cells

LC-MS involves the separation of compounds in a mixture via liquid chromatography (LC), followed by identification of the separated compounds using mass spectrometry (MS) (Pitt, 2009). LC-MS is often preferred over standard LC due to its ability to handle complex mixtures with a high degree of specificity. Mass spectrometers convert the molecules in the sample to a charged state and analyze the ions produced based on their mass to charge ratio. Each vertical bar on the mass spectrum represents an ion with a specific ion ratio (relative to the main, or base, peak) and the bar height represents the abundance of the ion.

Approximately 3x10^5 cells were seeded in 12-well plates and transfected with either WT or G309D PINK1 in duplicate. As dopamine is a neurotransmitter that is active in the synapse between neurons, dopamine may be present in the media as well as within cells. Therefore, cells were scraped and collected with the overnight media in 5 ml centrifuge tubes. Four volumes of ice-cold 99.9 % acetone (HPLC-grade, Sigma-Aldrich, United States) were added to each tube, vortexed vigorously with glass beads, and allowed to stand at room temperature to precipitate proteins and cell debris. The tubes were incubated at 60 °C overnight to allow for evaporation of the methanol and water. Following

38

dehydration, the remaining residue was resuspended in HPLC-grade methanol (Sigma-Aldrich, United States) and centrifuged at 2796 x g to pellet particulates. The supernatant was filtered with a 0.2 µm nylon filter and pipetted into LC-MS tubes with glass inserts for storage and analysis at CAF at Stellenbosch University. LC-MS analysis was performed according to Zonyane *et al.* (2020) using a Waters UPLC HSS T3 column (1.7µm particle size, 2.1 x 100mm, Waters Corporation, United States) (Zonyane et al., 2020). The mobile phase consisted of water as eluent A and acetonitrile as eluent B.

The theoretical mass to charge ratio (m/z) of dopamine, was calculated using the Warwick mass error calculator (https://warwick.ac.uk/fac/sci/chemistry/research/barrow/barrowgroup/calculators/mass_errors/). The m/z of dopamine containing an additional hydrogen atom was determined, which is produced under positive electrospray ionization mode LC-MS. The mass to charge ratio, fragmentation data, retention time, and mass tolerance error were used to identify the dopamine peak on the resulting mass spectrum and relative dopamine levels were compared between untransfected and transfected groups. The retention time of dopamine of ~3.7 min was observed in previous literature (Chatterjee & Gerlai, 2009; Helmschrodt et al., 2020). Peak area is measured as the sum of the intensities of datapoints that make up a peak. Peak area was used as a measure of abundance relative to the untransfected group.

2.7 Cellular treatments of the PINK1 model

2.7.1 *Curcumin and paraquat treatment preparation*

Preparation of treatment stocks took place in low light to account for the light sensitivity of curcumin and safety precautions were taken when working with paraquat. Stocks were stored at -20 °C and protected from light. A curcumin stock of 20 mM was made and for the dosage curve, this 20 mM stock was diluted in DMSO (Sigma-Aldrich, United States) to make working stocks (0.125 mM to 2 mM) for each treatment. A paraquat stock of 50 mM was made up by dissolving 50 mg paraquat dichloride x-hydrate (molecular weight: 257.16 g/mol) (Sigma-Aldrich, United States) in 3.9 ml dH$_2$O. Dilutions using the 50 mg stock were made from 0.03 mM to 2.1 mM, with the addition of 1 % DMSO to each paraquat treatment to account for the effect of DMSO on curcumin. All treatments were made fresh, on the day of cell treatments, in 15 ml polypropylene tubes covered with foil.

For the curcumin dosage curve, cells were treated with 1.25 µM, 2.5 µM, 5 µM, 10 µM, or 20 µM. For the paraquat dosage curve, cells were treated with 0.03 mM, 0.07 mM, 0.13 mM, 0.26 mM, 0.52 mM, 1.05 mM, or 2.10 mM. For all experiments, cells were incubated with treatment solutions for 24 h. This was based on a previous study in which the effect of a range of curcumin treatments from 0 µg/ml to 12 µg/ml on SH-SY5Y cell viability was investigated (Yu et al., 2019). The authors reported

39

that cell viability is time-dependent, as cell viability did not significantly decrease after 24 h but was reduced after 48 h. Cell viability was also reported to be dose-dependent as an increased curcumin concentration of 16 µg/ml resulted in a significant decrease in cell viability.

2.7.2 *Curcumin and paraquat dosage curves*

The purpose of producing dosage curves is to determine optimum concentrations of both curcumin and paraquat so that curcumin is not cytotoxic, and paraquat is sufficiently toxic to challenge cells while avoiding excessive toxicity. Cells were seeded at a density of 30 000 cells/well in a 96-well plate and incubated overnight at 37 °C, 5 % CO_2. A vehicle control containing dH_2O and 1 % DMSO was included in each experiment. A 10 % DMSO positive control was used as this is a toxic concentration that induces cell death. Additionally, a blank control with media only without cells was included to remove the effect of the media's color from absorbance measures. After a period of 24 h following cell seeding, all media was removed from the incubated cells. A volume of 100 µl per well of treatments and controls were pipetted in triplicate in 96-well plates for curcumin and paraquat. The plates were incubated for 24 h. Thereafter, MTT assays were performed using a method described in section 2.8 below. Absorbance versus treatment graphs were drawn, and the optimum concentrations of curcumin and paraquat were derived from the graphs and used for subsequent treatment experiments. The curcumin concentration that exhibited the highest significant cell viability compared to the vehicle control indicated non-toxicity and was thereby chosen as optimal for treatment. The paraquat concentration that exhibited a 50 % significant decrease in cell viability compared to the vehicle control was chosen as a toxic dosage to induce mitochondrial stress.

In addition, a nanocurcumin treatment and unloaded nanoparticle control (without curcumin) were prepared at the same optimum concentration as curcumin determined by the curcumin dosage curve to allow for comparison. The 2.5 µM nanocurcumin was made by dissolving 25.7 µl nanocurcumin stock (1 mg/ml) (Appendix I) and 24 µl DMSO (Sigma-Aldrich, United States) in 2350.3 µl DMEM. Likewise, a 2.5 µM unloaded nanoparticle control was prepared by dissolving 17.9 µl nanoparticle stock (1 mg/ml) (Appendix I) and 18 µl DMSO in 1764.1 µl DMEM.

Thereafter in the study, cells were treated with optimized concentrations of curcumin and paraquat in five treatment groups including a vehicle control, curcumin only, curcumin pre-treatment, paraquat only, and a 10 % DMSO positive control. Curcumin pre-treatment involved 24 h curcumin treatment, followed by 24 h paraquat treatment. For the nanocurcumin experiment, the following treatment groups were included to supplement the aforementioned treatments: unloaded nanoparticle only, curcumin loaded nanoparticle only, and nanocurcumin pre-treatment. Nanocurcumin pre-treatment involved 24 h nanocurcumin treatment, followed by 18 h paraquat treatment to test the protective effects of nanocurcumin. The cells were incubated in a humidified incubator at 37 °C, 5 % CO_2.

2.8 MTT (3-(4,5-Dimethylthiazol-2-yl)-2,5-diphenyltetrazolium bromide) assay for cell viability

The MTT colorimetric assay is used to evaluate cell viability by determination of mitochondrial function as this assay measures the activity of mitochondrial enzymes such as succinate dehydrogenase. Mitochondrial activity is constant for most viable cells thus changes in mitochondrial activity reflect changes in cell viability. This assay is based on the ability of mitochondrial NADPH-dependent enzymes in metabolically active cells to reduce the yellow tetrazolium salt MTT into purple formazan crystals. These crystals are dissolved, and the concentration of the resulting solution is measured by the determination of its optical density at 570 nm which correlates with viable cell count (van Meerloo, Kaspers & Cloos, 2011). The MTT assay was used to determine the effects of PINK1 transfection as well as curcumin and nanocurcumin treatment on cell viability.

A 5 mg/ml MTT (Sigma-Aldrich, United States) solution was prepared (Appendix I) and used immediately or temporarily stored at 4 °C, in a dark or foil-wrapped bottle. A volume of 10 μl of MTT solution was added to each well containing 100 μl of culture media. Alternatively, pre-warmed sterile PBS was used to prepare a 1:10 dilution of the MTT stock which was pipetted in 100 μl volumes to each well. The plate was covered in aluminum foil and placed in a Farma thermosteri-cycle 5 % CO_2 humidified incubator for 3-4 h. Thereafter, the plate was centrifuged to prevent disturbance and loss of crystals during aspiration of the solution. The solution was removed and a volume of 50-100 μl DMSO (Sigma-Aldrich, United States) was added to each well to dissolve the purple formazan aggregates in the wells. The plates were incubated with shaking for 10 min in a Hybaid Midi Dual 14 incubator. The coloration that results was measured at 570 nm in a Synergy HT luminometer using Gen5™ software version 3.0. The absorbance was normalized by subtracting the negative control wells (blank) from the experimental wells.

2.8.1 *CyQUANT correction*

To account for cell density differences between wells in treated plates, a CyQUANT correction was performed with each MTT assay. CyQUANT ® is a dye that emits fluorescence when bound to nucleic acids. Measurement of the fluorescent emission and excitation wavelengths of the dye-nucleic acid complex is linearly correlated to the cell count, thereby quantifying the cell population (Jones et al., 2001). A 96-well plate was treated identically to the MTT assay plate, and a CyQUANT® NF cell proliferation kit (Thermo Fisher Scientific, United States) was used to normalize cell proliferation between plates. Following 24 h treatment with curcumin and paraquat, a volume of 50 μl dye binding solution (1X) was added to each well. The plate was covered with foil and incubated for 1 h at 37 °C, 5 % CO_2. Fluorescence was measured at an excitation wavelength of 480 nm and an emission wavelength of 530 nm with a Synergy HT luminometer and using Gen5™ software.

2.9 Mitochondrial membrane potential assay

Mitochondrial function is directly linked to the mitochondrial polarization state (Walsh et al., 2017). Intact mitochondria are polarized which means they sustain a highly charged membrane potential with an inner negative charge. This causes the inward transport of cations and outward transport of anions (Zorova et al., 2018). Depolarization is the process by which the mitochondrial membrane potential changes from negative to less negative. Mitochondrial membrane potential generated by proton pumps is vital to oxidative phosphorylation, the process whereby adenosine triphosphate (ATP) is formed through electron transfer.

The MitoProbe tetrachloro-1,1',3,3'tetraethylbenzimidazolylcarbocyanine iodide (JC-1) assay (Thermo Fisher Scientific, United States) was used to assess mitochondrial membrane potential in PINK1-transfected SH-SY5Y cells treated with curcumin. Briefly, cationic JC-1 dye is characterized by the potential-dependent accumulation in mitochondria as a monomer with green fluorescence emission at 529 nm, as well as the concentration-dependent formation of red aggregates exhibiting fluorescence at 590 nm (Sivandzade, Bhalerao & Cucullo, 2019). Depolarized mitochondria with low membrane potential, exhibit low internal concentrations of green JC-1 monomers. Conversely, polarized mitochondria with high membrane potential accumulate high concentrations of green JC-1 monomers, some of which transform into red aggregates. Therefore, mitochondrial depolarization is indicated by a decrease in the red/green fluorescence intensity ratio (**Figure 2.4**).

Following transfection and curcumin treatment of $0.5\text{-}1\text{x}10^6$ cells/ml per sample in 6-well plates, media was removed, and 1 ml warm PBS (37 °C) was added to each well. For the positive control, 1 μl of 50 mM carbonyl cyanide 3-chlorophenylhydrazone (CCCP), which is a potent mitochondrial membrane potential disrupter, was added and the cells were incubated at 37 °C for 5 min. A volume of 10 μl JC-1 solution (200 μM) was added to each well, and the cells were incubated at 37 °C, 5 % CO_2 for 15 to 30 min. The cells were washed once by adding 2 ml of warm PBS to each tube and thereafter pelleted by centrifugation for 5 min at 800 x g. The pellets were resuspended in 500 μl PBS by gently flicking the tubes. Cells were analyzed on a DxFLEX flow cytometer (Beckman Coulter, United States) with 488 nm excitation using emission filters appropriate for fluorescein isothiocyanate (FITC) and R-phycoerythrin (PE) at the CAF at Stellenbosch University.

Briefly, the flow cytometer uses lasers that excite to fluorescence the green JC-1 monomers and red JC-1 aggregates, which will be detectable in the FITC channel and PE channel, respectively. In our experiments, mitochondrial membrane potential was assessed by two measures: (1) the ratio of PE:FITC (or, red:green) fluorescence intensity, and (2) the ratio of PE events to FITC events occurring as a proportion of the total single cell events (i.e., frequency).

Flow cytometry optimization included the gating strategy for data analysis (Appendix III, **Supplementary Figure 6**). The first step in the gating strategy was to select cells and discard signal from cell debris from the total events detected by the flow cytometer. The CCCP positive control, as well as an unstained control (without JC-1) were used for gating to select cells of interest. Cell debris and other contaminants were excluded if displaying very small or large forward scatter (indicating cell size) or side scatter (indicating granularity), appearing as outliers to the majority of the densely positioned cell events. The population of cells was refined to contain only single cells ('singlets'), and the final refinement was to select singlet FITC and PE events.
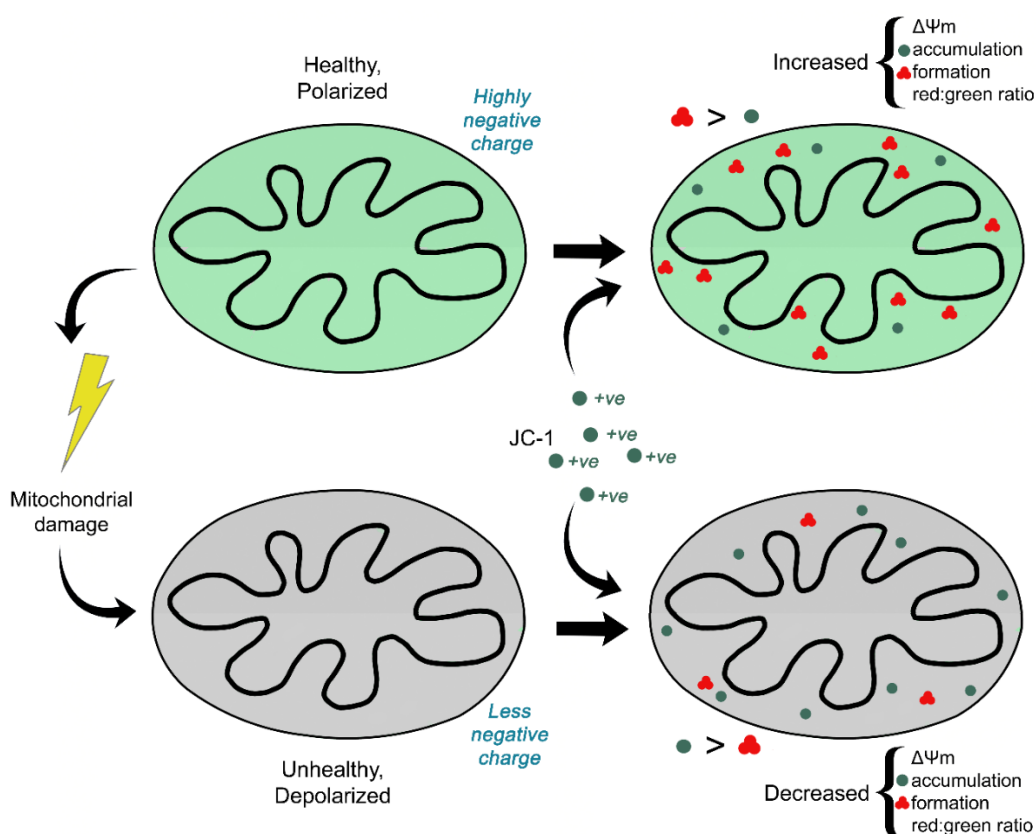
Figure 2.4 Action of JC-1 dye in healthy (green) versus depolarized (grey) mitochondria used to measure mitochondrial membrane potential (ΔΨm). JC-1 monomers (green) accumulate and aggregate into JC-1 aggregates (red) in healthy, polarized mitochondria, resulting in increased green fluorescence.

Abbreviations: JC-1, tetrachloro-1,1',3,3'tetraethylbenzimidazolylcarbocyanine iodide; ΔΨm, mitochondrial membrane potential.

2.10 Comparing curcumin and nanocurcumin

It is known that the protective capacity of curcumin is limited due to its poor solubility in water, low oral bioavailability, rapid metabolism, and sensitivity to heat and light (Flora, Gupta & Tiwari, 2013).

Therefore, alternative curcumin formulations have been developed to overcome these drawbacks. Nanocurcumin has been developed by encapsulating curcumin into various nanoformulations. The clinical trials on nanocurcumin have shown that this therapeutic modality improves clinical outcomes in cancer, multiple sclerosis, chronic kidney disease, and metabolic syndrome patients (Karthikeyan, Senthil & Min, 2020). However, more trials are required to determine its safety and efficacy in humans, and specifically in individuals living with PD.

In the present study, curcumin-loaded polycaprolactone (PCL) nanoparticles were synthesized by and obtained from Dr. Sarah D'Souza (University of Western Cape, South Africa). An outline of the method followed by Dr. D'Souza and the resulting nanoparticles are shown in **Figure 2.5** below.
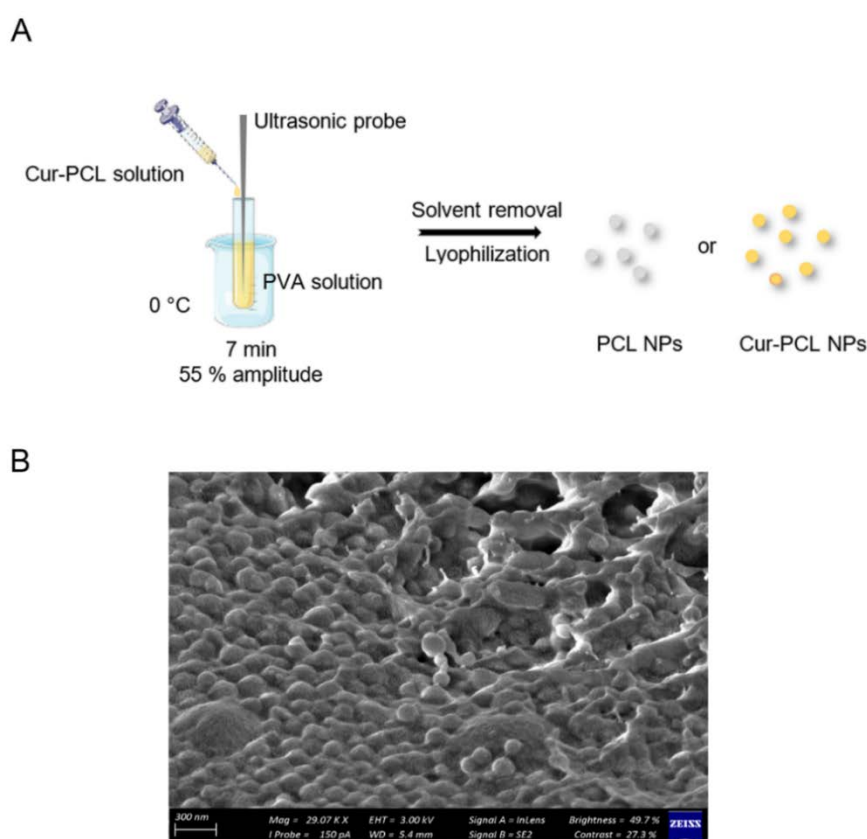
Figure 2.5 Synthesis of polycaprolactone nanoparticles. A – Schematic of the single emulsion-solvent evaporation method used by Dr. Sarah D'Souza for synthesizing nanocurcumin. **B** – Scanning electron microscope (SEM) image of synthesized polycaprolactone nanoparticles taken by Dr. Sarah D'Souza. The nanoparticles appeared to be smooth and spherical, with a small size range which correlates with the previous size and PDI measurements. The nanoparticles appeared to clump together which may be due to the use of sucrose as a stabilizer for lyophilization, as well as the sample preparation required for the synthesis technique. Images courtesy of Dr. Sarah D'Souza, University of Western Cape.

Abbreviations: Cur, curcumin; PCL, polycaprolactone; NPs, nanoparticles; PVA, polyvinyl alcohol; Mag, magnification; WD, working distance; EHT, electron high tension.

Briefly, a single emulsion-solvent evaporation technique was used to synthesize the nanoparticles. First, a PCL solution (1 % w/v) (Sigma-Aldrich, United States) containing curcumin (Sigma-Aldrich, United States) was made up in dichloromethane. Next, a polyvinyl alcohol (PVA) solution (0.5% w/v) was made by dissolving PVA (Sigma-Aldrich, United States) in de-ionized water obtained from a Barnstead EasyPure (II) UV-ultrapure water system (Thermo Fisher Scientific, United States). A volume of 2 ml of the PCL solution was added dropwise to 20 ml of the PVA solution under probe sonication for 7 min, 55 % power, 70 Watt (Bandelin Sonoplus UW2070 + HD 2070, Berlin, Germany). The PVA solvent was removed *in vacuo* at 35 °C and the mixture was centrifuged at 10 000 x g for 15 min to collect the nanoparticles. The curcumin-loaded nanoparticles were washed with de-ionized water and subjected to lyophilization for 72 h in the presence of sucrose (1% w/v) as a cryoprotectant. As a control, unloaded nanoparticles were likewise synthesized, however, curcumin was excluded from the PCL solution. Following synthesis, a Malvern Zetasizer Nano S (Malvern Instruments Ltd, UK) was used to determine the size, polydispersity index (PDI), and zeta potential (ZP) of the nanoparticles. The measurements were conducted at 25 °C in triplicate. Finally, nanoparticle morphology was characterized using scanning electron microscopy (SEM).

The therapeutic potential of nanocurcumin was assessed in comparison to curcumin by evaluating cell viability using the MTT and CyQUANT assays, as previously described in Section 2.8. The paraquat exposure time was reduced from 24 h to 18 h in order to evaluate the protective effects of nanocurcumin.

2.11 Statistical analysis

Depending on the number of groups, either a one-way or two-way analysis of variance (ANOVA) coupled with a post hoc test were performed using RStudio IDE Software version 4.0.3 (R Core Team, 2020) http://www.rstudio.com/. Post hoc tests included the Dunnett's test for comparisons to the control, or a Bonferroni post hoc test to test selected contrasts. The normality assumption of ANOVA was tested using the Shapiro Wilk test, while homogeneity of variances was assessed with the Levene's test. For non-parametric data, either the Kruskal Wallis test and Dunn's post hoc test were performed, or a robust linear model with Tukey's HSD post hoc test were implemented. All 'p' values less than or equal to 0.05 were considered statistically significant. An F-statistic was also reported as an indicator of variability within groups. The F statistic from the ANOVA with a small value close to 1 suggested that the null hypothesis of no difference was true. Conversely, a high F statistic indicated greater variation between group means than expected by chance.

Significant main effect/s of PINK1 transfection or curcumin treatment, or a significant interaction effect between these variables determined by the ANOVA were followed by post hoc analysis. This was performed to determine differences between the untransfected, untreated control compared to all

groups to ascertain whether the toxicity model was achieved with PINK1 alone or with both PINK1 expression and paraquat. Furthermore, we determined if curcumin could enhance cell health to or above baseline levels in the untreated control cells. Finally, differences between the paraquat and pre-treatment groups were determined to evaluate if curcumin's rescue ability could protect against the toxic effects of paraquat. The R script used in the present study can be found in Appendix VI. Box and whisker plots or scatterplots overlaying column graphs indicating mean and standard deviation were constructed with GraphPad Prism version 5.0.0 for Windows (GraphPad Software, San Diego, California, United States, www.graphpad.com).

CHAPTER 3: Results

3.1 Plasmid acquisition and sequence verification

Two commercially available plasmids containing WT PINK1 and G309D PINK1 DNA, respectively, were acquired from Addgene, United States of America. A series of problems were encountered with these plasmids and a range of experiments were undertaken to verify their sequences, as outlined in the sections that follow.

Briefly, the first batch of transformed bacterial clones that were purchased (WT-A and Mutant-A) did not grow well on selection media due to shipping and storage issues. They had arrived during the hard lockdown of the SARS-COV 2 pandemic and upon arrival in South Africa, were stored in the courier's warehouse at room temperature for several months before reaching our laboratory. Subsequently, Addgene sent a new batch of both WT and mutant transformed clones (WT-B and Mutant-B). Plasmid extraction, restriction enzyme digest, PCR, and sequencing were successful for Mutant-B, while these techniques produced unexpected results for WT-B.

Based on these problems, Addgene sent a third WT transformed clone (hereon referred to as WT-C). However, WT-C failed to grow in both liquid and solid media. Finally, on the premise that the plasmid DNA in their stock culture had undergone rearrangements, Addgene provided their WT PINK1 plasmid DNA (WT-D) for us to perform the bacterial transformation in our laboratory. However, this plasmid DNA needed to be transformed into Stbl3 *E. coli* which we did not have access to and, if ordered, could only be delivered to our laboratory in late 2021. We then contacted the authors of the paper who had originally described this model, Drs Zhou and Wuan-Ting (Duke-NUS Medical School, Singapore (Zhou et al., 2014)), who thereafter sent us their extracted WT and G309D PINK1 plasmid DNA (hereafter referred to as WT-Z and Mutant-Z). This DNA was then transformed into DH5α *E. coli,* but this was unsuccessful possibly due to lentiviral recombination.

The various WT and mutant PINK1 plasmids acquired for this project are summarized in **Table 3.1**, and further details on the troubleshooting are outlined in Appendix II **Supplementary Table 4** and the sections below.

Table 3.1 Summary of troubleshooting of WT and G309D (Mutant) PINK1 plasmids.

Plasmid	Date received	Source	Problem	Solution
WT-A (Transformed *E. coli* clone) **Mutant-A** (Transformed *E. coli* clone)	May 2020	Addgene, United States	Bacteria struggled to grow on selection media	Addgene agreed to send another batch of plasmids
WT-B (Transformed *E. coli* clone)	August 2020		Sequencing, PCR, and restriction digest failed	Addgene agreed to send another WT.
Mutant-B (Transformed *E. coli* clone)			Verified by sequencing, PCR, and restriction digest	These plasmids were chosen for use in all further experiments
WT-C (Transformed *E. coli* clone)	May 2021		Restriction digest failed and struggled to grow on selection media	Addgene sent WT plasmid DNA for transformation
WT-D (DNA)	June 2021		Stbl3 *E. coli* required for transformation	Wait for Stbl3 *E. coli*. Use WT-B in the interim
WT-Z (DNA)	June 2021	Dr. Zhi Dong Zhou, Dr. Saw Wuan-Ting (Duke-NUS Medical School, Singapore)	Restriction digest failed following DH5α *E. coli* transformation	Wait for Stbl3 *E. coli*. Use WT-B in the interim
Mutant-Z (DNA)			Not tested (functional mutant in use)	Not applicable

Abbreviations: WT, wild-type; PCR, polymerase chain reaction; *E. coli*, Escherichia coli.

3.1.1 *Plasmid DNA extraction*

A Zymo Research Zyppy MiniPrep kit yielding 30 µl of ~200 µg/ml of plasmid DNA as well as a Zymo Research ZympPURE MidiPrep kit yielding a greater volume (200 µl) of DNA were used for DNA extraction. Initial attempts at extracting WT PINK1 and G309D PINK1 DNA with the MiniPrep kit yielded less than 150 µg/ml of DNA each. It was proposed that incomplete cell lysis may explain the low DNA yield, therefore, lysis was performed for an extra 30s in addition to the standard 2 min for the MiniPrep kit. This resulted in highly concentrated and pure DNA (420 µg/ml).

Restriction digest of this plasmid extracted with prolonged lysis revealed that the expected bands for EcoRV and BamHI (Appendix III, **Supplementary Figure 3**) were not present. Instead of two products of 6974 bp and 1837 bp for EcoRV and one product of 8811 bp, additional bands of the wrong sizes were observed (**Figure 3.1**, lanes 4 and 11). Therefore, the plasmid DNA was likely degraded by prolonged lysis and was unusable.
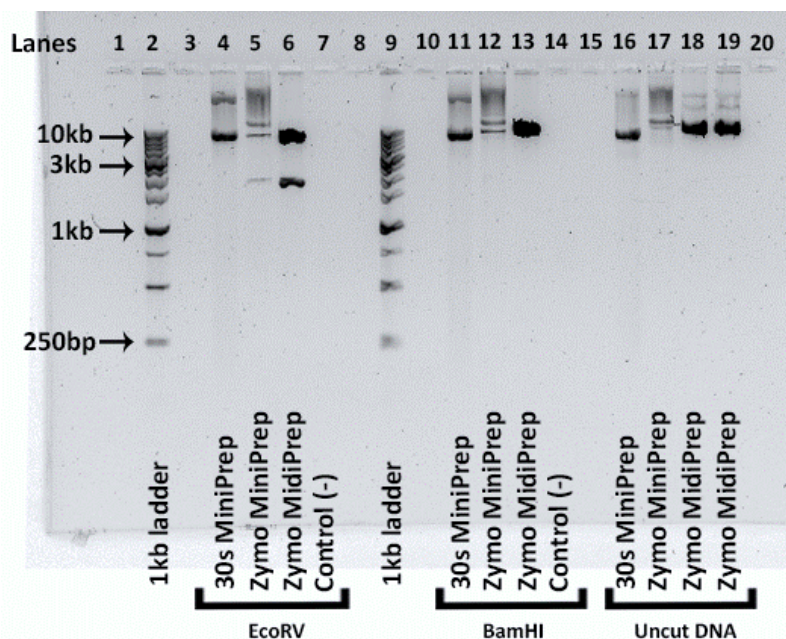
Figure 3.1 Optimized MidiPrep method yielded high concentration Mutant-B DNA. Lane 2: 1kb DNA ladder; Lanes 4-6: EcoRV (6974 bp and 1837 bp); Lanes 11-13: BamHI (8811 bp expected product); Lanes 16-19: Uncut G309D PINK1 DNA; Lanes 7 and 14: Negative control (Control (-)) Lanes 1, 3, 8, 10, 15, and 20: Blank.

Subsequently, the following alternative adjustments to the extraction protocol were made. The lysis buffer was warmed at 37 °C for 30 min before use to aid in lysis, and an extra centrifugation step was performed following washes to remove any residual buffer. The starting volume of culture was also reduced to 3 ml for the MiniPrep kit and to 40 ml for the MidiPrep kit to avoid clogging of the column. Notably, these adjustments (1) resulted in greater DNA yields for both kits and (2) produced the expected EcoRV and BamHI digest product sizes (**Figure 3.1**, lanes 16-19, 4-6 and 11-13). The MidiPrep kit (>550 µg/mL) yielded higher concentration DNA than the MiniPrep kit (>300 µg/ml). Thereafter, from these results, the optimized MidiPrep kit was used for DNA extraction for all subsequent experiments.

3.1.2 *WT and G309D PINK1 plasmid verification*

Following successful plasmid extraction, we sought to verify the plasmid sequences by PCR, Sanger sequencing, and restriction enzyme digest. Upon Sanger sequencing, the mutant-B PINK1 DNA sequence was identical to the reference sequence (NCBI Reference Sequence NM_032409.3), except for the mutation site which contained a single adenine nucleotide in place of a guanine nucleotide (**Figure 3.2**).

However, after multiple attempts, the WT-B plasmid sequence could not be verified by PCR, restriction enzyme digest, or sequencing. As seen in **Figure 3.3A**, both WT-A and WT-B uncut DNA appear to be smaller in size in comparison to Mutant-B. The mutant was ~9 kb in size which

49

approximated the actual size of the plasmid (8811 bp) **(Figure 3.3A** lane 10). Conversely, WT-A and WT-B were similar in size at < 3 kb (**Figure 3.3A** lanes 3, 5-8). Likewise, the expected products for BamHI and EcoRV restriction digests were observed for Mutant-B (as seen in **Figure 3.3B**, lanes 7 and 13). However, restriction enzyme digest on WT-A (data not shown) and WT-B (**Figure 3.3B**, lanes 5 and 11), as well as PCR (Appendix III, Supplementary Figure 3) and uncut plasmid DNA (**Figure 3.3A**), yielded incorrectly sized products. This indicated that WT-A and WT-B plasmids were either not the correct plasmids or that the plasmids had undergone rearrangement of their components.
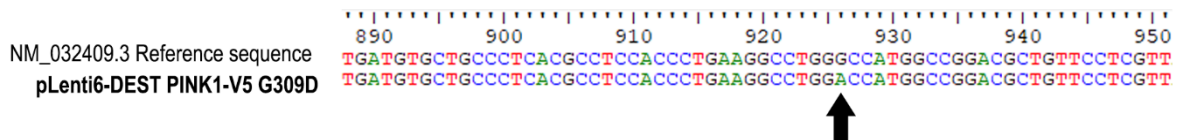
Figure 3.2 Mutant G309D PINK1 sequence verification. The G309D PINK1 mutation was present at position 926 which corresponds to amino acid position 309, exhibited by a single nucleotide change from guanine to adenine.
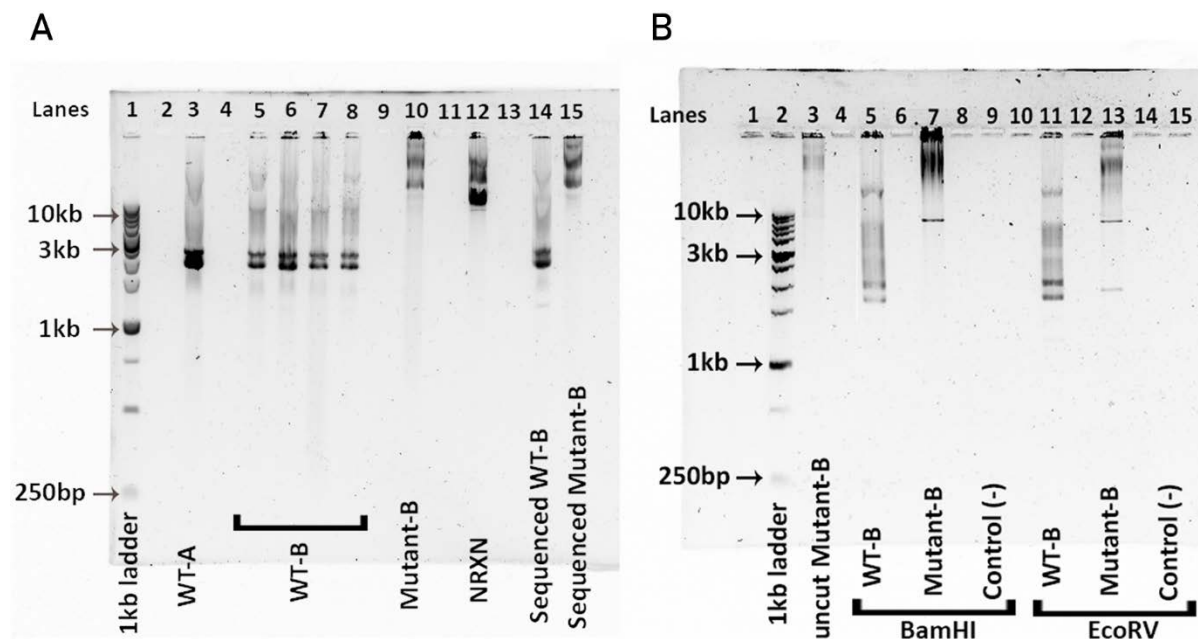
Figure 3.3 WT-A and WT-B are different to the Mutant-B PINK1 plasmid. A – Differences in uncut plasmid sizes observed for WT and G309D PINK1 DNA. Lane 1: 1 kb DNA ladder; WT-A PINK1 (128 µg/ml); Lane 5-8: WT-B (56.8, 301, 179, & 344 µg/ml); Mutant-B (169 µg/ml); Lane 12: positive control (NRXN2 plasmid DNA) (198 µg/ml); Lane 14-15: sequenced WT-B and Mutant-B; Lane 2, 4, 9, 11 & 13: Blank. The successfully sequenced Mutant-B ran high on the gel, closer to its expected 8811 bp size while all samples of the WT plasmids ran below 3 kb. WT NRXN2 was used as a positive control as its sequence and size were verified (>9 kb). **B** – Differences in restriction enzyme digestion products for WT and G309D PINK1. Lane 2: 1 kb DNA ladder; Lane 3: Uncut G309D-B DNA; Lane 5 and 7: BamHI (8811 bp expected product); Lane 11 and 13: EcoRV (6974 and 1837 bp expected products); Lanes 9 and 15: Negative control (Control (-)); Lane 1, 4, 6, 8, 10, 12, and 14: Blank

Upon receiving plasmid WT-C, we observed that the clones on the first streak plate directly from the agar stab grew well overnight at 37 °C. However, the bacteria struggled to grow on subsequent streak plates and in liquid media, both in the presence and absence of the bacterial selection agent ampicillin (**Figure 3.4**).
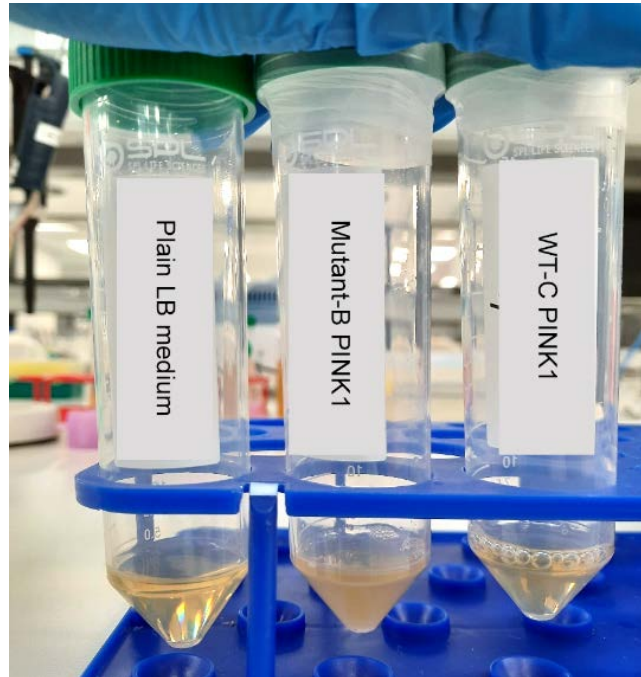
Figure 3.4 Comparison of plain LB medium, against Mutant-B and WT-C PINK1 overnight cultures. The Mutant-B PINK1 overnight culture was cloudy, indicating bacterial growth. However, the WT-C PINK1 culture was similar in opacity to plain LB medium, even after an extended 48 h incubation.

Drs Zhou and Wuan-Ting (Zhou et al., 2014) were then contacted and they sent us their WT and G309D PINK1 extracted DNA (WT-Z and mutant-Z). The plasmid DNA was transformed into standard DH5α *E. coli* and then verified with a restriction digest to confirm that the plasmids were intact. The restriction digest showed an incorrect number of bands on the gel, indicating possible plasmid rearrangements (**Figure 3.5**). Therefore, after these multiple attempts, we could not acquire a verifiable WT PINK1 plasmid.

Thus, in the absence of a more suitable option, we took the decision to proceed with the WT-B and the sequence-confirmed Mutant-B for all our subsequent experiments. WT-B was selected as it had arrived at the same time as Mutant-B and was the only WT plasmid that could be successfully and

repeatedly propagated in *E. coli*. Acknowledging this limitation, experiments with a verified WT were deferred for future work.
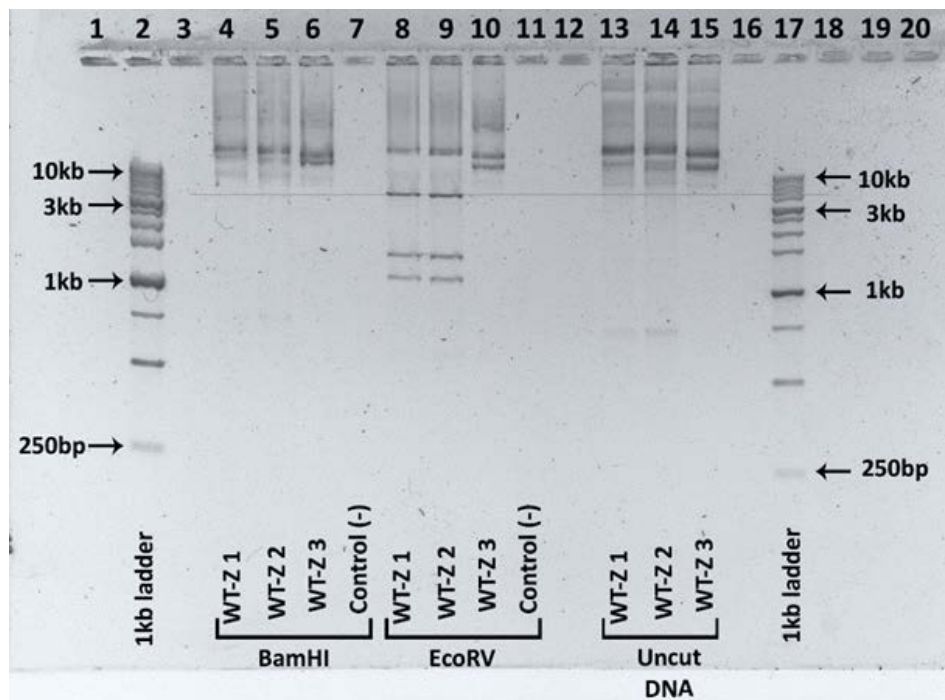
Figure 3.5 Restriction digest products of WT-Z PINK1 samples after DH5α *E. coli* transformation. Lane 2&17: 1kb DNA ladder; Lane 4-7: BamHI (8811 bp expected product); Lane 8-11: EcoRV (6974 and 1837 bp expected products); Lane 13-15: Uncut WT-Z PINK1 DNA; Lanes 7 and 11: Negative control (Control (-)); Lane 1, 3, 7, 12, 16, 18-20: Blank.

3.2 Transfection of SH-SY5Y cells with PINK1 plasmids

In objective 2 of the study, cells were transfected with the plasmids as detailed in Methods section 2.4, and transfection efficiency was calculated. Transfection efficiency was calculated as 42.1 % for the WT PINK1 plasmid, and 45.1 % for the G309D PINK1 plasmid (**Figure 3.6**). Since the transfection efficiencies were similar, we were able to proceed with the rest of the experiments.
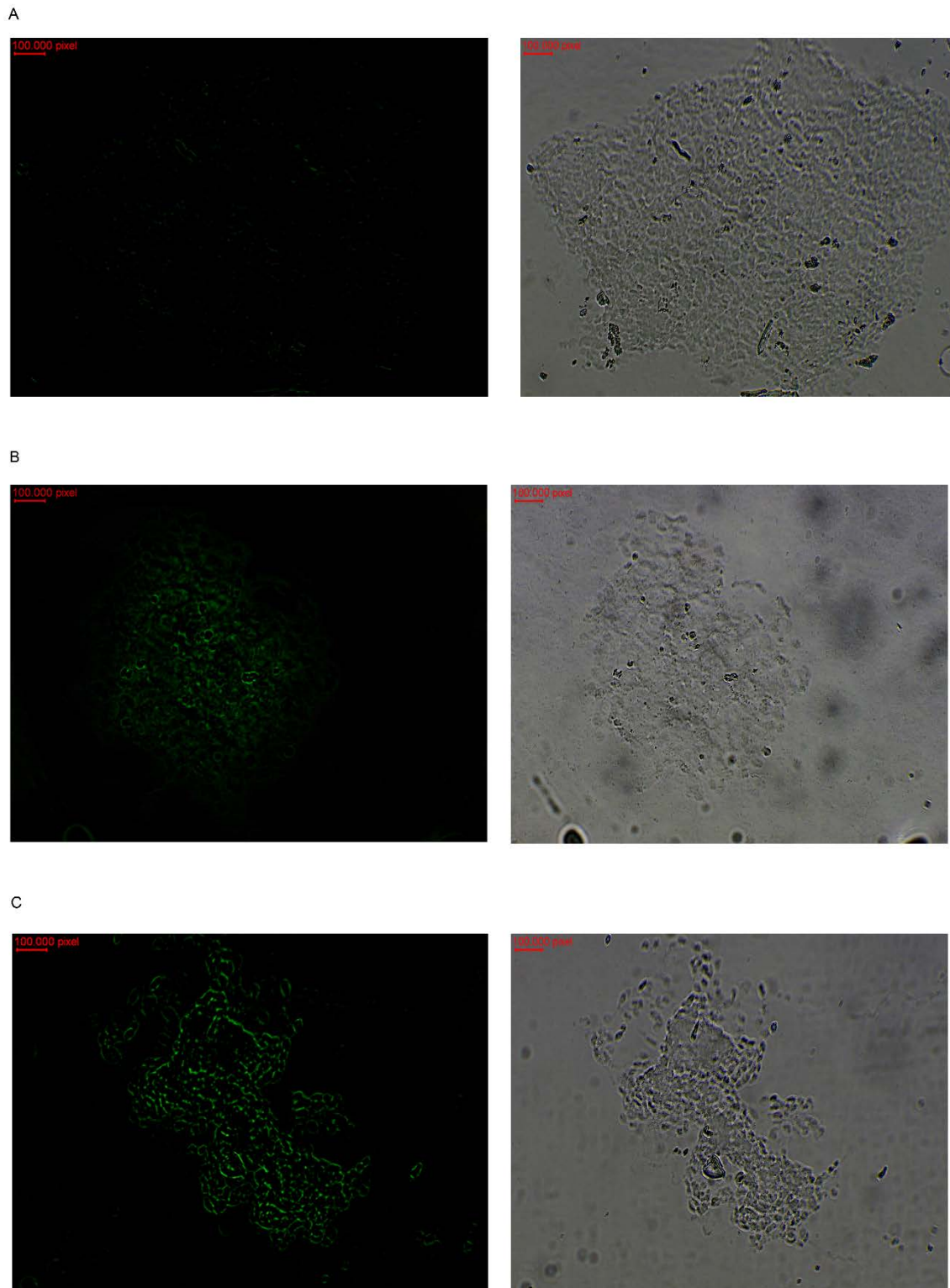
Figure 3.6 Immunofluorescence images of SH-SY5Y cells untransfected, or transfected with WT and G309D PINK1 plasmids. SH-SY5Y cells were seeded and (**A**) untransfected as a negative control, or transfected with either (**B**) WT PINK1 DNA or (**C**) G309D PINK1 DNA for 24 h. Cells were stained with anti-V5 tag antibody and Alexa Fluor 488 goat anti-rabbit IgG. Scale representing 100 000 pixels is displayed in red.

3.3 *PINK1* expression was upregulated in the mutant

We then sought to measure expression levels of *PINK1* and *TH* to confirm the PINK1 and dopamine toxicity model, as previously described in Zhou *et al.* (2014). Assessing *PINK1* expression would allow us to verify the toxicity model characterized by *PINK1* overexpression in the mutant. This causes dopamine toxicity by upregulating *TH* which is involved in dopamine metabolism (as shown in **Figure 1.6** in **Chapter 1**).

An increase in *TH* levels would indicate a possible increase in dopamine production. Optimization of the protocol for RT-qPCR was first performed and thereafter, gene expression levels were measured.

3.3.1 *RT-qPCR optimization*

Optimization of RT-qPCR was twofold. Firstly, to determine the optimal cDNA dilution for all RT-qPCR experiments, we performed qPCR on a 10-fold serial dilution (neat to 1: 10 000 dilutions) of cDNA from untransfected SH-Y5Y cells. Secondly, we assessed whether multiplex qPCR was equally as successful as the standard singleplex qPCR. For β-actin, amplification across all dilutions yielded acceptable Ct values within the optimal range of 15-25 cycles (**Figure 3.7A** and **B**).

However, only undiluted cDNA yielded a Ct value of less than 30 when amplifying *TH*. Therefore, undiluted cDNA was chosen for all RT-qPCR experiments. Replicates were closer together (within 0.5 cycles) in multiplex reactions for both *β-actin* and *TH* than in singleplex reactions. Therefore, multiplex qPCR was performed for all subsequent qPCR experiments. Additionally, several indicators of qPCR optimization were determined, including the qPCR efficiency and coefficient of determination (r^2). As seen in **Table 3.2**, the qPCR efficiency of *TH* was higher than expected but the other two qPCR efficiencies were within acceptable ranges, indicating that the RT-qPCR experiments could proceed.

Table 3.2 The qPCR validation through determination of reaction efficiency and data linearity.

Gene	Slope of regression line	qPCR efficiency	r^2
β-actin	-3.092	110.58%	0.9928
TH	-2.4679	154.22%	0.9559
PINK1	-3.2112	104.84%	0.8695

Abbreviations: r^2, coefficient of determination.

54
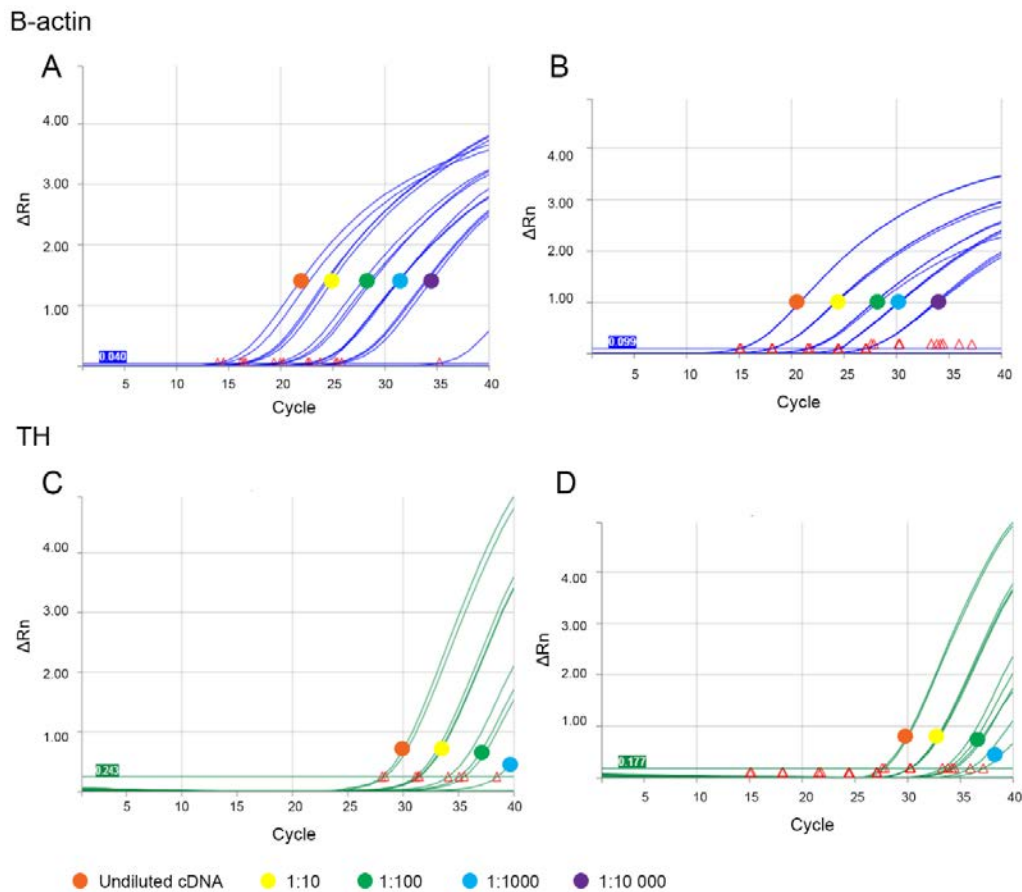
Figure 3.7 Singleplex and multiplex RT-qPCR analysis of *β-actin* and *TH* expression. A-B – Singleplex and multiplex RT-qPCR analysis of *β-actin* expression in untransfected SH-SY5Y cells, respectively. The *β-actin* gene was amplified with Ct values from ~15 to ~25 in both singleplex (**A**) and multiplex (**B**) reactions, while replicates were closer together for all dilutions in the multiplex reactions. **C-D** - Singleplex and multiplex RT-qPCR analysis of *TH* expression, respectively. The *TH* gene was amplified with Ct values from ~25 to ~35 in both singleplex (**C**) and multiplex (**D**) reactions, with closer replicates in the multiplex reactions and no evidence of amplification of the 1:10 000 dilution.

3.3.2 *PINK1 and TH gene expression with RT-qPCR*

As expected, RT-qPCR experiments revealed a 34-fold increase in *PINK1* gene expression in G309D PINK1 cells compared to the untransfected control (p < 0.001; **Figure 3.8A**). However, WT PINK1 cells exhibited no significant difference in *PINK1* expression compared to the control group. For *TH*, gene expression appeared to be lower in the WT PINK1 and G309D PINK1 compared to the control, but this was not significantly different (overall p = 0.244; **Figure 3.8B**). Therefore, these results indicate that the transfections were successful with increased *PINK1* expression observed for the mutant PINK1 compared to control. However, these RT-qPCR experiments could not verify

dopamine toxicity caused by increased *TH* expression in the mutant, as had been shown by Zhou and colleagues (Zhou et al., 2014).
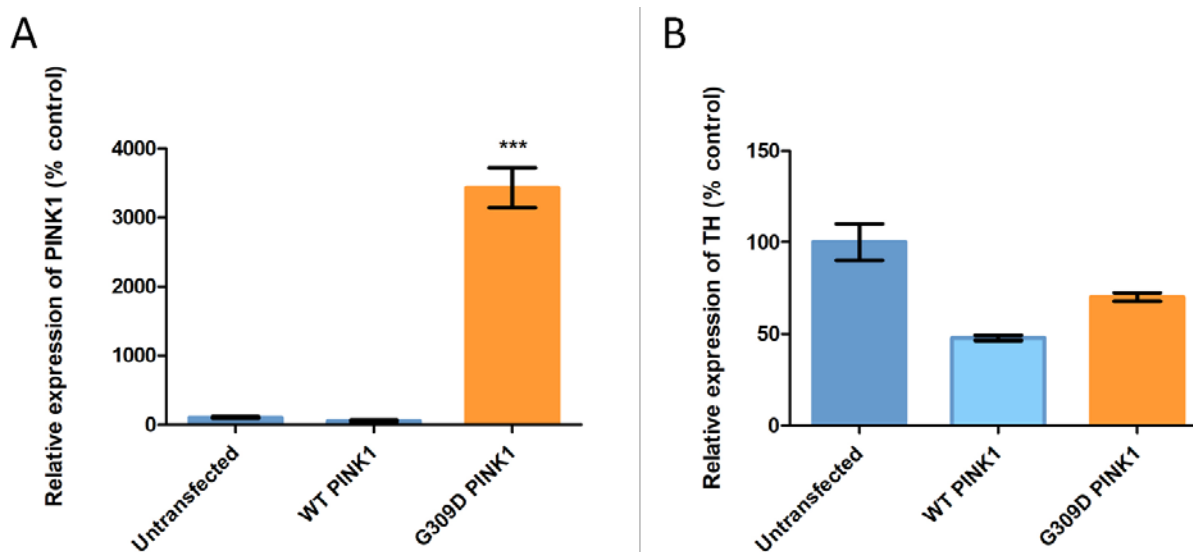
Figure 3.8 Reverse transcription quantitative real-time PCR (RT-qPCR) analysis of *PINK1* and *TH* gene expression in transiently transfected SH-SY5Y cells. RNA extracted from SH-SY5Y cells transiently expressing WT or G309D PINK1 was reverse transcribed and amplified using qPCR to assess *PINK1* and *TH* gene expression. **A** – A significant increase in *PINK1* gene expression was observed for cells expressing G309D PINK1 compared to the control ($p < 0.001$). **B** – No significant differences in *TH* gene expression were observed between all groups. One-way ANOVA statistical tests were performed, followed by Bonferroni post hoc analysis, with significance set at $p < 0.05$. *$p < 0.05$, **$p < 0.01$, ***$p < 0.001$: relative to untreated control

3.4 No increased dopamine levels detected by LC-MS

No significant difference in *TH* gene expression was detected between our PINK1 transfected groups and the control. Therefore, we sought to assess dopamine toxicity by measuring levels of dopamine in the transfected cells using LC-MS. The theoretical m/z of dopamine was calculated as 154.086, which is consistent with previous literature (Kim et al., 2014). The retention time of dopamine was previously found to be ~3.7 min (Chatterjee & Gerlai, 2009; Helmschrodt et al., 2020). However, dopamine could not be detected in the sample as the smallest compound had a m/z of only 158.12. Therefore, dopamine levels could not be evaluated in the samples as the extraction method failed to isolate such small molecules.

However, L-phenylalanine was identified with m/z ratio, retention time, and fragmentation data. The mass tolerance error was at an acceptable level of below 5 for all samples and the retention time was consistent (~2.3 min) for 88 % of samples (**Table 3.3**). The L- and D- enantiomers, or 'mirror image' structures, of this essential amino acid could not be differentiated by LC-MS. Levels of the amino

acid phenylalanine were found to be elevated in the mutant PINK1 group compared to both WT PINK1 and untransfected SH-SY5Y cells. These differences between groups remained after subtraction of the negative control, containing only DMEM media, in which phenylalanine was also detected. The presence of phenylalanine in the control is due to the fact that L-phenylalanine is used to manufacture DMEM culture medium (Appendix I, **Supplementary Table 1**). Notably, in the dopamine metabolism pathway phenylalanine is a precursor that is hydroxylated to tyrosine, which is converted to L-DOPA and is in turn, decarboxylated to dopamine (Daubner, Le & Wang, 2011). The relative abundance of phenylalanine was greater in the mutant (136.7 %) than in the WT PINK1 group (122.5 %) (**Table 3.3**; Appendix III, **Supplementary Table 6**). Furthermore, fragmentation ions with m/z ratios of 120.08 and 103.05 were observed in the samples (Appendix III, **Supplementary Figure 5**), consistent with previous literature (Zhang et al., 2019). This increase in phenylalanine could possibly indicate that dopamine toxicity is occurring in the model, but the timing for when this is measured may require optimization.

Table 3.3 The relative abundance of phenylalanine in media control, untransfected, WT, and G309D PINK1 groups.

Group	Observed m/z $[M+H]^+$	Molecular formula $[M+H]^+$	Theoretical m/z	Mass tolerance error (PPM)	Peak area	Mean peak area	Abundance relative to UT control (%)	RT (min)
Negative control 1	166.0874	$C_9H_{12}NO_2$	166.0868	3.59	11732.9	11535.1	75.3	2.71
Negative control 2	166.0869			0.58	11337.2			2.39
UT 1	166.0862			-3.63	14301.4	15315.7	100	2.35
UT 2	166.087			1.18	16330.1			2.35
WT PINK1 1	166.0871			1.78	17549.0	18758.4	122.5	2.34
WT PINK1 2	166.0876			4.79	19967.9			2.34
G309D PINK1 1	166.0876			4.79	20151.7	20936.7	136.7	2.33
G309D PINK1 2	166.0874			3.59	21721.7			2.33

Abbreviations: UT, untransfected; WT, wild-type; m/z, mass to charge ratio; PPM, parts per million; RT, retention time.

3.5 Curcumin and paraquat dosage determination

Next, we sought to establish an appropriate treatment protocol for the cellular model by testing a range of concentrations of curcumin and paraquat, over a 24 h exposure time. Optimum concentrations of these two compounds for the experiments were determined using the MTT assay.

For this model, a concentration of curcumin was required to evaluate its neuroprotective effects without being toxic to the cell. An overall significant effect on cell viability was observed with curcumin treatment (F = 65.95, $p < 0.0001$). **Figure 3.9A** and **B** show cell viability without and with CyQUANT correction, respectively. The 10 µM dosage was not significantly different to the control (**Figure 3.9B**). Conversely, a higher 20 µM curcumin concentration induced cellular toxicity indicated by significantly decreased cell viability by 32.2 % ($p < 0.01$), compared to the untreated control. Concentrations of 1.25 µM, 2.5 µM, and 5 µM of curcumin exhibited significant increases in viability ($p < 0.001$), with the 2.5 µM dosage causing the greatest increase of 77 % compared to the control. Therefore, an optimum concentration of 2.5 µM curcumin was chosen for use in our cellular model.
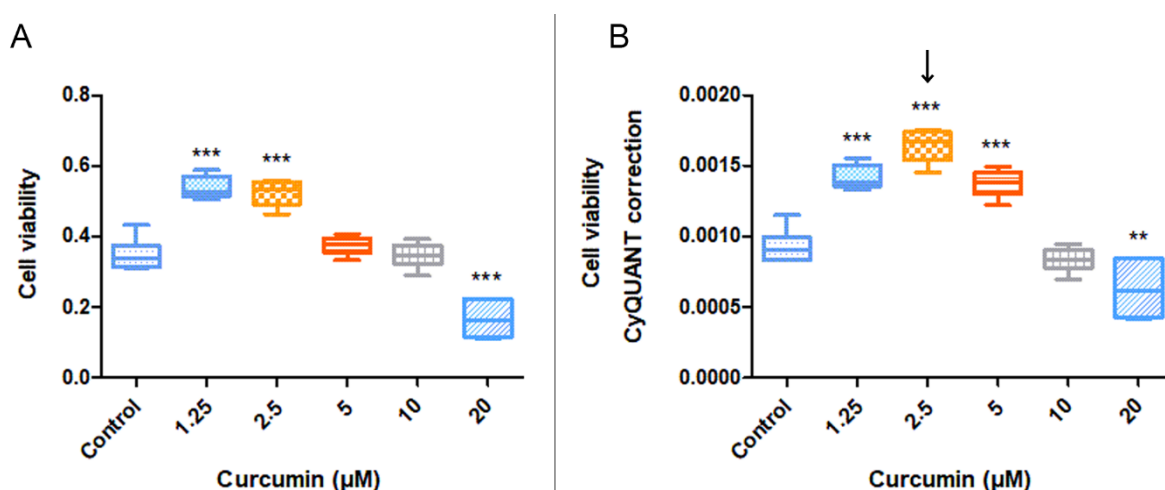
Figure 3.9 Assessment of the possible cytotoxic effect of curcumin using the MTT assay. SH-SY5Y cells received treatment concentrations of curcumin ranging from 1.25 µM – 20 µM for 24 h. **A** – A significant increase in cell viability was observed for the 1.25 µM and the 2.5 µM curcumin treatments compared to the control ($p < 0.001$). **B** – A similar trend to (**A**) was observed following CyQUANT correction ($p < 0.001$), accompanied by a significant increase in viability for the 5 µM treatment ($p < 0.001$) and a significant decrease with the 20 µM dosage ($p < 0.01$). One-way ANOVA statistical tests were performed, followed by Dunnett's test for post hoc analysis, with significance set at $p < 0.05$. The arrow indicates the chosen curcumin concentration for treatment.
*$p < 0.05$, **$p < 0.01$, ***$p < 0.001$: relative to untreated control

On the other hand, a paraquat toxin concentration was determined that was sufficiently high to decrease cell viability by ~ 50 %, thereby causing adequate cellular stress yet not excessive cell death. An overall significant effect on cell viability was observed with paraquat treatment (F = 66.90, $p <$ 0.0001). **Figure 3.10A** and **B** show cell viability without and with CyQUANT correction, respectively. High paraquat concentrations of 1.05 mM and 2.1 mM reduced cell viability by 28.7 %, and 59.0 %, respectively, compared to the control (**Figure 3.10B**, $p < 0.001$).
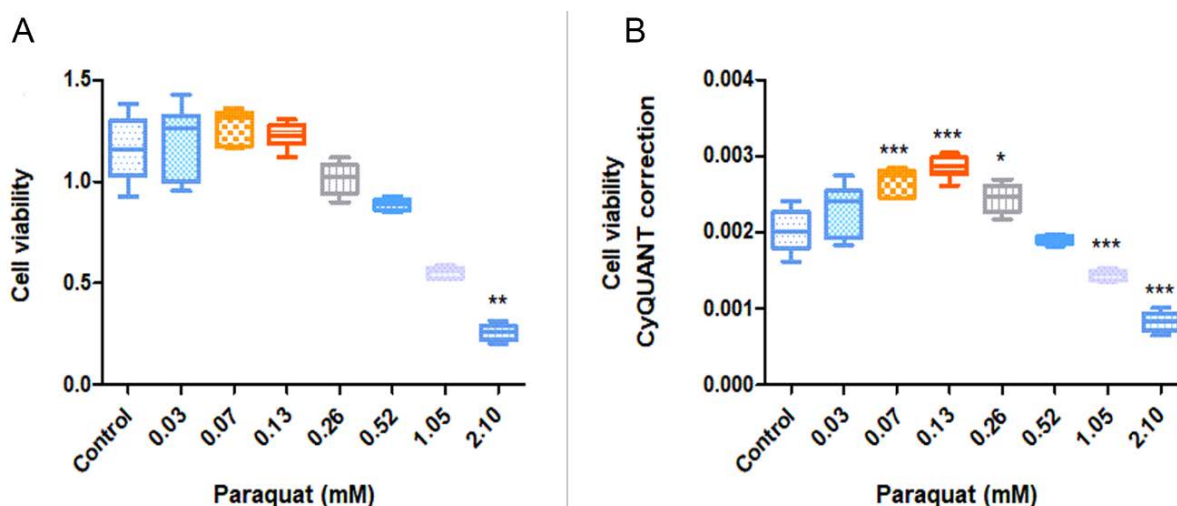
Figure 3.10 Assessment of the cytotoxic effect of paraquat using the MTT assay. SH-SY5Y cells received treatment concentrations of paraquat ranging from 0.03 mM – 2.10 mM for 24 h. **A** – A significant decrease in cell viability was observed for the 0.5 mM, 1.05 mM, and the 2.1 mM paraquat treatments compared to the untransfected control ($p < 0.001$). **B** – CyQUANT correction resulted in a significant decrease in viability for only the 1.05 mM and 2.10 mM treatments ($p < 0.001$). Significantly increased viability was observed for lower paraquat concentrations of 0.07 mM ($p <$ 0.001), 0.13 mM ($p < 0.001$) and 0.26 mM ($p < 0.05$) compared to the untransfected control. Non-parametric Kruskal Wallis statistical tests, followed by Dunn's post hoc analysis were performed for MTT data without CyQUANT correction which was not normally distributed. One-way ANOVA statistical tests followed by Dunnett's post hoc analysis were performed after CyQUANT correction with significance set at $p < 0.05$.
*$p < 0.05$, **$p < 0.01$, ***$p < 0.001$: relative to untreated control

To determine a final paraquat concentration at which a 50 % decrease in cell viability was expected, a regression of the absorbance values of all samples relative to the control set to 100, was plotted against paraquat concentration (**Figure 3.11**). The paraquat concentration exhibiting a 50 % loss in viability relative to the control was extrapolated as 1.7 mM from the regression line equation for subsequent use in the model.
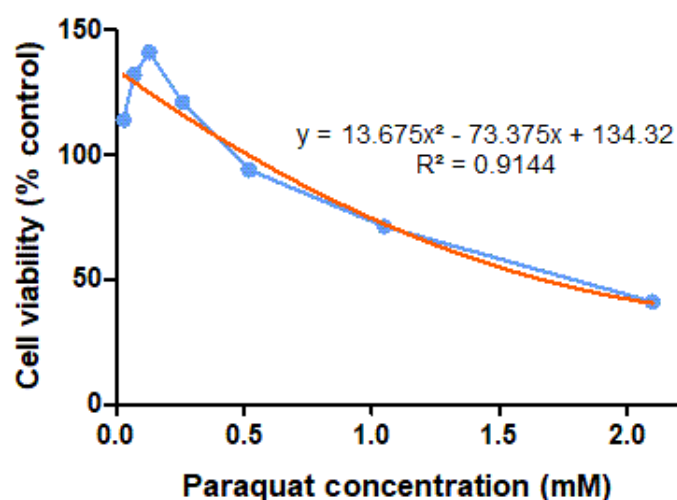
Figure 3.11 Regression of paraquat concentration and cell viability to determine the dosage that elicits a 50 % reduction in cell viability. According to the second-degree polynomial trendline equation (y = $13.675x^2 - 73.375x + 134.32$), the paraquat concentration that would lead to a 50 % loss in cell viability was 1.7 mM.

3.6 Curcumin pre-treatment could not significantly rescue cell viability

After establishing the PINK1 cellular model and optimum treatment conditions, we evaluated the potential protective effect of curcumin on cell viability by treating transfected cells in five groups as described in Methods Section 2.8. A significant main effect was found for both transfection status (F = 14.63, $p < 0.0001$) and treatment (F = 55.58, $p < 0.0001$; **Figure 3.12**). **Figure 3.12A** and **B** show cell viability without and with CyQUANT correction, respectively.

To determine if curcumin could increase cell viability, the 'curcumin only'-treated groups and curcumin pre-treatment groups were compared to the untransfected, untreated control. Notably, curcumin pre-treatment exhibited a significant decrease in cell viability in the untransfected and both PINK1 transfected groups ($p < 0.001$) compared to the control (**Figure 3.12B**). However, pre-treatment groups were not significantly different to the paraquat groups, indicating an inability of curcumin to sufficiently rescue paraquat-induced toxicity. The paraquat treatment significantly decreased cell viability compared to the untransfected, untreated control group in all transfected and untransfected groups ($p < 0.001$). Therefore, the paraquat treatment concentration and exposure time were appropriate to cause cellular stress in the model.
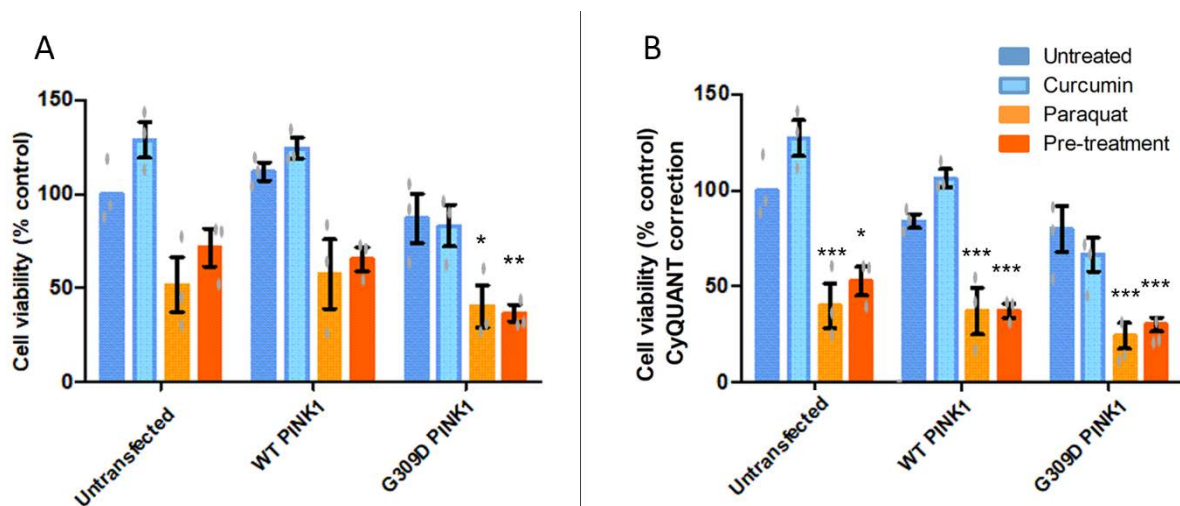
Figure 3.12 Effect of curcumin on transiently transfected SH-SY5Y cells expressing wild-type and mutant G309D PINK1. SH-SY5Y cells were either transfected with WT PINK1 or G309D PINK1 DNA for 24 h, and received treatment for 24 h of either 2.5 µM curcumin, 1.7 mM paraquat, or pre-treatment with curcumin (24 h) followed by paraquat (24 h). **A** – A significant decrease in cell viability was observed for the paraquat and pre-treatment groups in G309D PINK1 cells compared to the untransfected control ($p < 0.001$, $p < 0.01$). **B** – A similar trend to (**A**) was observed following CyQUANT correction except for all paraquat and pre-treatment groups ($p < 0.001$, $p < 0.01$). Two-way ANOVA statistical tests were performed, followed by the Bonferroni post hoc test, with significance set at $p < 0.05$.

*$p < 0.05$, **$p < 0.01$, ***$p < 0.001$: relative to untransfected, untreated control.

3.7 Curcumin pre-treatment could not significantly rescue mitochondrial membrane potential

While the MTT assay provides a reliable technique for the assessment of cell viability (Mosmann, 1983), the assay reflects only the mitochondrial metabolic activity of cells. We, therefore, sought to determine whether the protective effects of curcumin may be more evident in the assessment of other aspects of mitochondrial health such as mitochondrial membrane potential.

In our experiments, mitochondrial membrane potential was assessed by two measures: (1) fluorescence intensity, and (2) the ratio of % positive PE events to FITC events (i.e., frequency) as explained in Methods Section 2.9.

Regarding untreated groups, an overall significant effect on mitochondrial membrane potential was not observed with transfection status when assessing fluorescence intensity (F = 4.418, p = 0.066; **Figure 3.13A**) but was significant in the PE/FITC frequency data (F = 7.646, p = 0.022; **Figure 3.13B**). Transfection status significantly reduced PE/FITC frequency in the WT group and mutant

61

group compared to the untransfected control ($p < 0.05$). Therefore, the PINK1 model was characterized by a reduced measure of mitochondrial membrane potential.
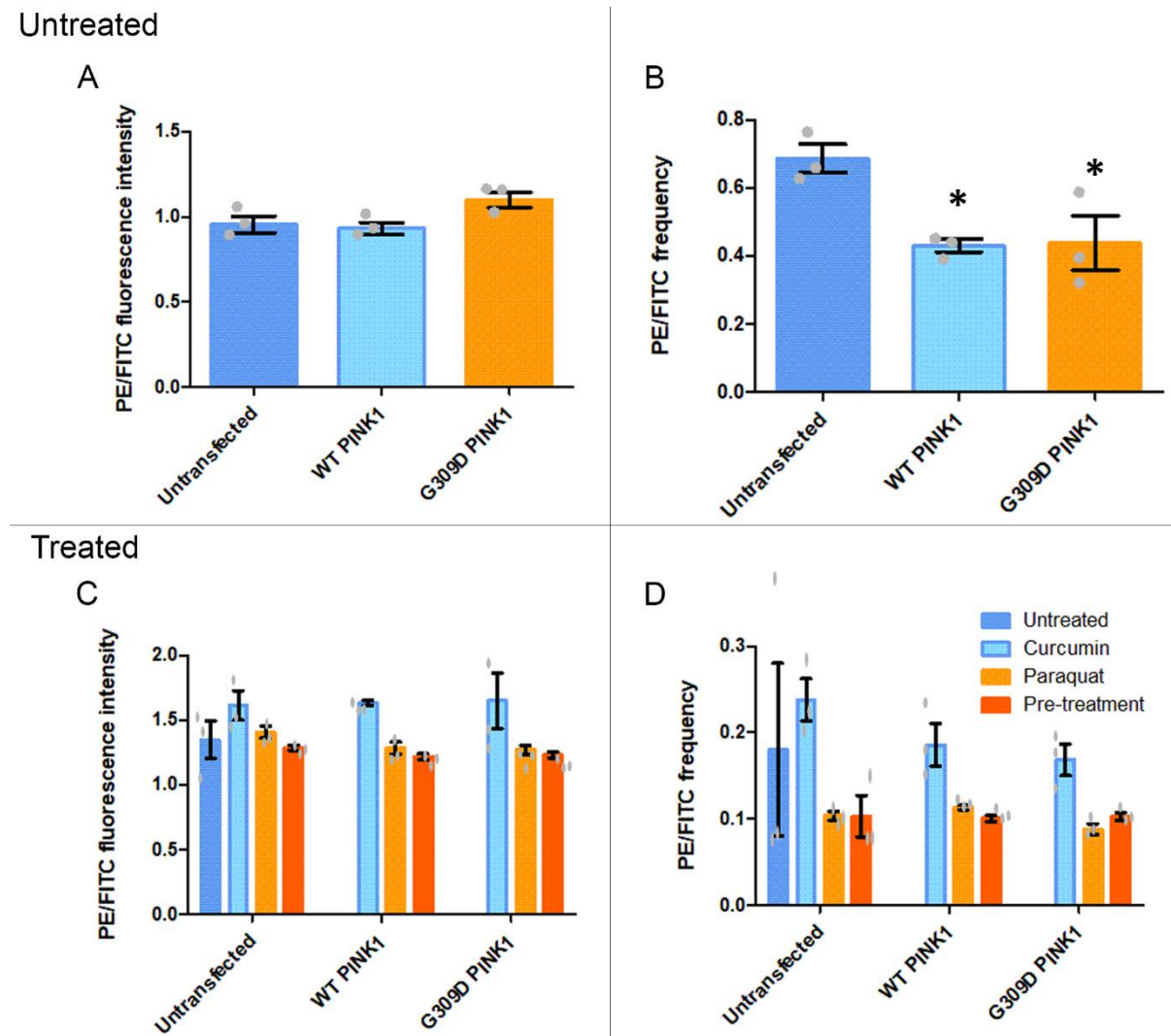
Figure 3.13 Flow cytometry analysis of mitochondrial membrane potential in transfected SH-SY5Y cells transiently expressing PINK1. Following 24 h PINK1 transfection and curcumin treatment, SH-SY5Y cells were stained with JC-1. The red/green fluorescence of PE/FITC fluorophores was measured using flow cytometry to assess mitochondrial membrane potential. **A** and **C** – No significant differences in PE/FITC fluorescence intensity were observed compared to the untransfected, untreated control. **B** – WT and G309D PINK1 transfected cells exhibited significantly lower fluorescence intensity than the untransfected control ($p < 0.05$). **D** – No significant differences in PE/FITC event frequency were observed between all groups compared to the untransfected, untreated control. One-way ANOVA (A-B), two-way ANOVA statistical tests (C), and a robust linear model (D) were performed, followed by Bonferroni or Tukey's HSD post hoc analysis, with significance set at $p < 0.05$.

$*p < 0.05$, $**p < 0.01$, $***p < 0.001$: relative to untransfected, untreated control.

Regarding the treated groups, a significant main effect of treatment was observed on both PE/FITC intensity (F = 9.829, p = 0.0003; **Figure 3.13C**) and frequency (F = 32.461, p < 0.0001; **Figure 3.13D**). Post hoc analyses revealed no significant differences in PE/FITC intensity between all treated groups compared to the control. However, paraquat and pre-treatment caused a non-significant trend of decreased PE/FITC frequency compared to the control.

Although not significant, curcumin pre-treatment showed a similar trend of PE/FITC frequency to paraquat in all groups (**Figure 3.13D**). This indicated curcumin's inability to sufficiently rescue paraquat's toxic effects on mitochondrial health. The lack of significance in the effect of paraquat and pre-treatment may be due to the variability in the control group as shown by the large error bar.

Consistent with the cell viability results, curcumin could not significantly increase mitochondrial membrane potential in all groups compared to the untreated control (**Figure 3.13C-D**). Nevertheless, curcumin did not cause a loss in mitochondrial membrane potential in the untransfected group. This further suggested that the curcumin concentration and exposure time were appropriate to avoid toxicity. As observed for cell viability (**Figure 3.12B**), curcumin was unable to increase mitochondrial membrane potential in the G309D PINK1 group compared to the untreated control, possibly due to the toxic effects of the mutation.

3.8 Nanocurcumin exhibits less protection than curcumin

Finally, since curcumin was not found to have a protective effect on cell viability in our cell model, we sought to evaluate if enhanced formulations of curcumin, which improve its oral bioavailability and solubility, could elicit a greater effect. We obtained a nanocurcumin preparation which had been synthesized and validated by Dr. Sarah D'Souza (University of Western Cape) (Appendix IV, **Supplementary Table 7**), and evaluated its effect on SH-SY5Y cell viability.

The unloaded nanoparticle without curcumin was used as a control to determine if the nanoparticle itself had an effect on cell viability. **Figure 3.14A** and **B** show cell viability without and with CyQUANT correction, respectively. An overall significant effect on cell viability was observed with treatment (F = 290.6, p < 0.0001; **Figure 3.14**). Also, several findings were consistent with the preceding cell viability experiments in the current study (Results Sections 3.5 and 3.6). Curcumin treatment exhibited a significant increase in viability compared to the untreated control (p < 0.001). Paraquat treatment caused cellular toxicity indicated by a significant 45 % decrease in cell viability compared to the untreated control (p < 0.001). In addition, the curcumin pre-treatment group was not significantly different to the paraquat group. Interestingly, the unloaded nanoparticle and nanocurcumin groups were not significantly different to each other, but reduced cell viability by 20 % compared to the untreated control (p < 0.001), possibly indicating mild toxic effects of the nanoparticle. Unlike pre-treatment with curcumin, which was similar to the paraquat group, pre-

treatment with nanocurcumin caused a significant 30 % reduction in cell viability compared to the paraquat group (p < 0.001).
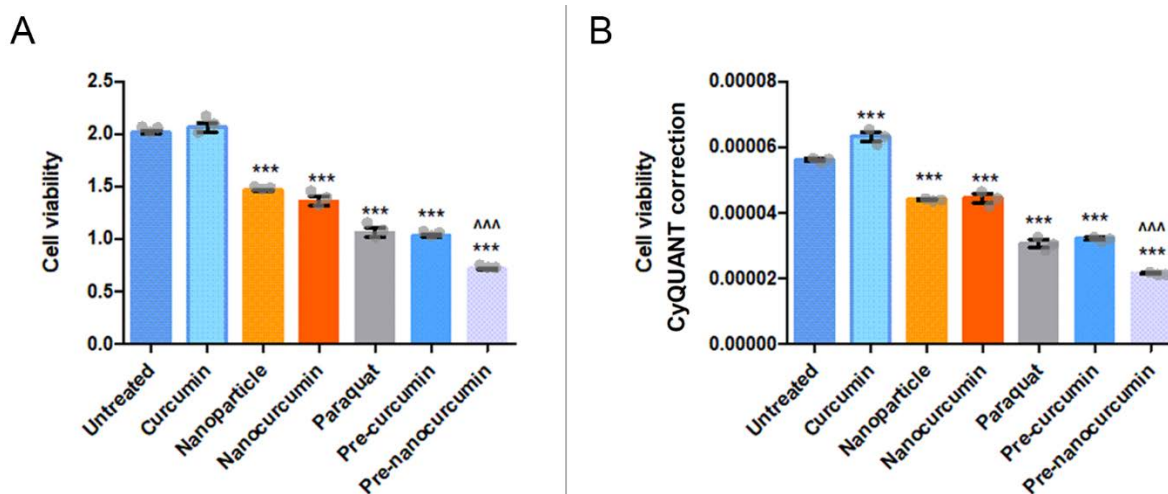
Figure 3.14 Comparing the effects of curcumin and nanocurcumin on SH-SY5Y cell viability. SH-SY5Y cells received treatment for 24 h of either 2.5 µM curcumin, 1.7 mM paraquat, or pre-treatment with curcumin or nanocurcumin followed by paraquat (24 h + 18 h). **A** – A significant decrease in cell viability was observed in the paraquat and curcumin pre-treatment groups compared to the untreated control (***p < 0.001). Nanocurcumin pre-treatment significantly reduced cell viability compared to the paraquat group (^^^p < 0.001). No significant difference was observed between the nanoparticle and nanocurcumin groups, as well as between the paraquat and pre-nanocurcumin groups. **B** – A similar trend to (**A**) was observed following CyQUANT correction for all groups. One-way ANOVA statistical tests were performed, followed by Bonferroni post hoc test, with significance set at p < 0.05.
*p < 0.05, **p < 0.01, ***p < 0.001: relative to untreated control
^p < 0.05, ^^p < 0.01, ^^^p < 0.001: relative to paraquat

These findings indicate that curcumin on its own was not toxic to the cell (and in fact improved the viability of the cells). Paraquat caused a ~50 % reduction in cell viability as expected. Interestingly, both the unloaded nanoparticle and the nanocurcumin were toxic to the cells although not as toxic as the paraquat treatment. Both pre-treatment groups could not rescue paraquat-induced toxicity, while pre-treatment with nanocurcumin resulted in significantly greater toxicity than paraquat alone.

CHAPTER 4: Literature review on curcumin's effect on α-synuclein in PD

Considering the wealth of evidence from individuals living with PD as well as from various cellular and animal models, it is clear that *PINK1* mutations lead to cellular dysfunction and PD development. Therefore, in the present study, we used a *PINK1* genetic model of PD to evaluate the therapeutic effect of curcumin. However, to address the need for effective, disease-modifying therapies for both genetic and environmental causes of the disease, we also assessed the possible broader therapeutic application of curcumin in other forms of PD. To this end, a literature review on this topic was compiled and subsequently published. Curcumin has been shown to bind toxic α-synuclein, which is a pathological hallmark of PD. In the review, we propose that by harnessing curcumin's rapid excretion from the body, curcumin can potentially bind to and eliminate α-synuclein thereby preventing its toxic build-up. Consequently, dietary supplementation with curcumin over one's lifetime has potential as a *novel, nutrient-based therapeutic approach* to complement existing PD treatment or initiate novel prevention strategies.

REVIEW ARTICLE

EJN European Journal of Neuroscience   FENS   WILEY

Movement of prion-like α-synuclein along the gut–brain axis in Parkinson's disease: A potential target of curcumin treatment

Devina Chetty[1] | **Shameemah Abrahams[1]** | **Riaan van Coller[2]** | **Jonathan Carr[3]** |
Colin Kenyon[1,4,5] | **Soraya Bardien[1]**

[1]Division of Molecular Biology and Human Genetics, Faculty of Medicine and Health Sciences, Stellenbosch University, Cape Town, South Africa

[2]Faculty of Health Sciences, School of Medicine, Department of Neurology, University of Pretoria, Pretoria, South Africa

[3]Division of Neurology, Department of Medicine, Faculty of Medicine and Health Sciences, Stellenbosch University, Cape Town, South Africa

[4]DST-NRF Centre of Excellence for Biomedical Tuberculosis Research, Division of Molecular Biology and Human Genetics, Faculty of Medicine and Health Sciences, South African Medical Research Council Centre for Tuberculosis Research, Stellenbosch University, Cape Town, South Africa

[5]South African Medical Research Council Centre for Tuberculosis Research, Stellenbosch University, Cape Town, South Africa

Correspondence
Devina Chetty and Soraya Bardien, Division of Molecular Biology and Human Genetics, Faculty of Medicine and Health Sciences, Stellenbosch University, Cape Town, South Africa.
Email: devinachetty@sun.ac.za (D. C.); sbardien@sun.ac.za (S. B.)

Abstract

A pathological hallmark of the neurodegenerative disorder, Parkinson's disease (PD), is aggregation of toxic forms of the presynaptic protein, α-synuclein in structures known as Lewy bodies. α-Synuclein pathology is found in both the brain and gastrointestinal tracts of affected individuals, possibly due to the movement of this protein along the vagus nerve that connects the brain to the gut. In this review, we discuss current insights into the spread of α-synuclein pathology along the gut–brain axis, which could be targeted for therapeutic interventions. The prion-like propagation of α-synuclein, and the clinical manifestations of gastrointestinal dysfunction in individuals living with PD, are discussed. There is currently insufficient evidence that surgical alteration of the vagus nerve, or removal of gut-associated lymphoid tissues, such as the appendix and tonsils, are protective against PD. Furthermore, we propose curcumin as a potential candidate to prevent the spread of α-synuclein pathology in the body by curcumin binding to α-synuclein's non-amyloid β-component (NAC) domain. Curcumin is an active component of the food spice turmeric and is known for its antioxidant, anti-inflammatory, and potentially neuroprotective properties. We hypothesize that once α-synuclein is bound to curcumin, both molecules are subsequently excreted from the body. Therefore, dietary supplementation with curcumin over one's lifetime has potential as a novel approach to complement existing PD treatment and/or prevention strategies. Future studies are required to validate this hypothesis, but if successful, this could represent a significant step towards improved

---

Abbreviations: ANS, autonomic nervous system; CJD, Creutzfeldt–Jakob disease; CNS, central nervous system; DMNV, dorsal motor nucleus of the vagus nerve; DNPR, Danish National Patient Registry; ENS, enteric nervous system; GI, gastrointestinal; LBs, Lewy bodies; mTOR/p70S6k, p70 ribosomal protein S6 kinase; NAC, non-amyloid β-component; PD, Parkinson's disease; PNS, peripheral nervous system; PPMI, Parkinson's Progression Markers Initiative; SNc, substantia nigra pars compacta; SNPR, Swedish National Patient Registry.

---

nutrient-based therapeutic interventions and preventative strategies for this debilitating and currently incurable disorder.

1 | INTRODUCTION

Parkinson's disease (PD) is an age-related neurological disorder characterized by loss of dopaminergic neurons, predominantly in the substantia nigra, leading to dopamine deficiency in the brain (Miyasaki et al., 2002). In 2016, 6.1 million individuals were living with PD, which is more than double the 1990 statistic of 2.5 million individuals (Dorsey et al., 2018), and this trend is set to continue. PD may not be caused by only one mechanism but rather several interdependent molecular events that result in the manifestation of the disease (Brundin & Melki, 2017). Neuronal degeneration in PD has been associated with various processes including oxidative stress, mitochondrial dysfunction, protein aggregation, proteasomal inhibition, and neuroinflammation (Mythri & Srinivas Bharath, 2012). A pathological hallmark of PD brains is the aggregation of misfolded α-synuclein protein in Lewy bodies (LBs). Notably, the presence of misfolded α-synuclein along the axis joining the gut and the brain suggests that the gut may play an important role in PD pathogenesis and progression.

In this review, we examine the evidence supporting the prion-like behavior of α-synuclein along the gut–brain axis, which may contribute to PD pathogenesis. Also described are the various clinical manifestations of gastrointestinal (GI) dysfunction experienced by individuals with PD. In addition, controversial evidence for the effect of various GI tract-associated surgeries and their effect on PD development are discussed. Furthermore, in this review, we explore the role of curcumin as a potential nutraceutical for the treatment of PD. Nutraceuticals are bioactive compounds in plant- or animal-based food that have beneficial pharmaceutical properties beyond their nutritional value (Biesalski et al., 2009). This therapeutic approach addresses possible long-term treatment options for PD based on the involvement of the gut and pathogenic α-synuclein in disease progression.

2 | α-SYNUCLEIN

Approximately, 5%–10% of PD cases have been linked to mutations in different genes. Genes that have been linked to PD pathogenesis include *SNCA* and *LRRK2*, responsible for autosomal dominant forms of PD, as well as *PINK1*, *PRKN*, *FBXO7*, and *DJ-1*, which cause autosomal recessive PD (Cherian & Divya, 2020). Juvenile onset parkinsonism

has been linked to *ATP13A2*, *SVE*, *DNAJC6*, and *SYNJ1* (Minakaki et al., 2020). Notably, the *SNCA* gene, which encodes α-synuclein, has point mutations as well as duplications and triplications that increase the production of this protein, resulting in toxic α-synuclein accumulation in the body that correlates with disease severity (Chartier-Harlin et al., 2004; Ibanez et al., 2004).

Although α-synuclein's precise role in the body remains unknown, it is a presynaptic nerve terminal protein believed to be involved in the release of dopamine, vesicle recycling, and membrane remodeling (Bourdenx et al., 2017). Native, or properly folded, forms of α-synuclein are thought to regulate the presynaptic vesicular pool and protect neuron terminals against injury (Uversky & Eliezer, 2009). As illustrated in Figure 1, the α-synuclein protein comprises an amphipathic amino terminal domain (amino acids 1–60) that contains PD-causing point mutations, a central non-amyloid β-component (NAC) domain (amino acids 61–95), and an acidic carboxyl terminal domain (amino acids 96–140) (Giasson et al., 2001).

Discovery of the causal link between α-synuclein assembly and synucleinopathies has led to several comparative studies on amyloid fiber aggregation (Boyer et al., 2019;
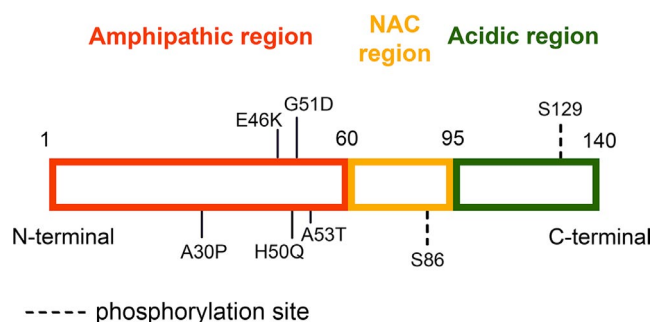
FIGURE 1 Protein domains of human α-synuclein. Schematic α-synuclein protein structure that is composed of the amphipathic amino terminal domain (orange), non-amyloid β-component (NAC) domain (yellow), and the acidic carboxyl terminal domain (green) (Flavin et al., 2017). The amphipathic amino terminal domain is lysine rich and is important for membrane interactions. The central NAC domain has hydrophobic and lipid sensing properties, modulates membrane binding affinity, and promotes protein aggregation (Giasson et al., 2001). The carboxyl terminal domain contains phosphorylation sites and plays a role in protein–protein interactions (Uversky & Eliezer, 2009). The numbers refer to amino acid positions, the solid lines refer to Parkinson's disease-causing point mutations, and the dashed lines refer to phosphorylation sites

Schweighauser et al., 2020). Structural analysis has revealed that variable fold forms of these fibers are possible and are affected by gene mutations, post-translational modifications, and non-proteinaceous molecules. Mutations may affect the hydrogen-bonding network within the filament rearrangements, as well as the kinetics of α-synuclein aggregation. This has been found in the α-synuclein associated with multiple system atrophy as well as the tauopathies of chronic traumatic encephalopathy and corticobasal degeneration (Falcon et al., 2019; Schweighauser et al., 2020; Zhang et al., 2020). Understanding the structural specificity of α-synuclein assembly in PD will facilitate defining the respective roles of mutations, aberrant α-synuclein expression regulation, and lifestyle on PD progression.

New data regarding the precise process of misfolding and aggregation of this protein into toxic β-rich intermediates and LBs are continually being elucidated. As seen in Figure 2, α-synuclein monomers can progressively be misfolded into toxic species due to many triggers, including neurotoxin exposure (e.g., paraquat, 1-methyl-4-phenyl-1,2,3,6-tetrahydropyridine [MPTP], and rotenone), and mutations in the gene encoding α-synuclein, *SNCA* (Ingelsson, 2016). The NAC domain of α-synuclein is responsible for the conformational change of the protein from the random coil structure of monomers and dimers to the β-sheet conformation of oligomers (Fusco et al., 2014). β-Sheet-rich oligomers grow into

protofibrils and continue to polymerize to form LBs (Lashuel et al., 2013). LBs (proteinaceous structures with radiating filaments) and Lewy neurites (less structured fibrillary inclusions) are predominantly composed of insoluble α-synuclein, ubiquitin, tau protein, and phosphorylated neurofilaments (Alafuzoff & Hartikainen, 2018; del Tredici et al., 2002). The toxic species of α-synuclein produced during misfolding and polymerization lead to cellular dysfunction and, eventually, cell death (Gustot et al., 2015).

Neuronal loss and Lewy pathology in the brainstem and cerebral cortex are pathognomonic for PD (Ruffmann & Parkkinen, 2016). However, alternative, less invasive methods are being explored to identify LBs and α-synuclein outside the central nervous system (CNS). Extensive research has been undertaken to investigate the possibility that α-synuclein pathology in PD may even begin in the gut (Chandra et al., 2017; Holmqvist et al., 2014; Lionnet et al., 2018). Notably, dysfunction of the GI system gives rise to symptoms that may precede the motor features of the disease by decades (Houser & Tansey, 2017). The GI tract represents a more accessible region than the CNS, which would be valuable for early detection of PD (Mukherjee et al., 2016). Therefore, elucidation of the involvement and role of the GI tract in PD pathology could provide a major stepping stone towards the goal of developing more effective methods of detecting, treating, and even preventing the disease.
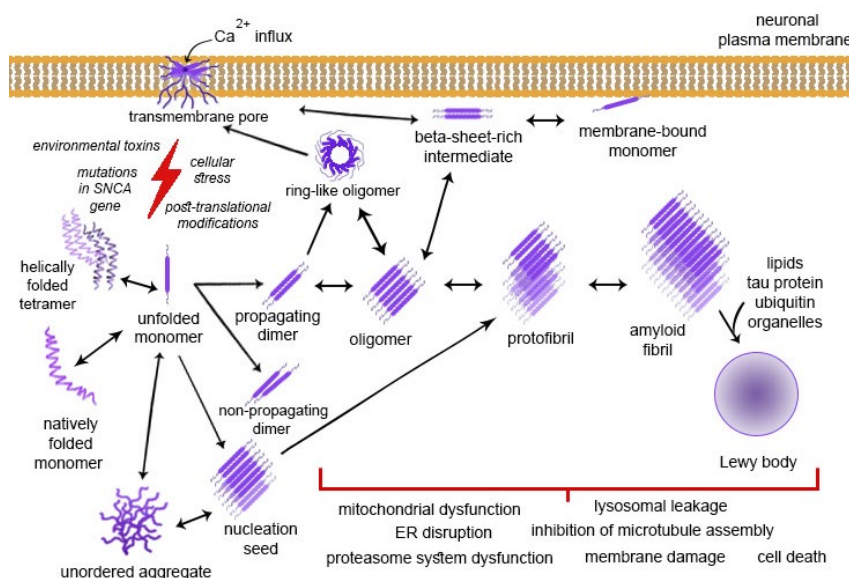
FIGURE 2 Process of α-synuclein misfolding and aggregation into pathogenic intermediates and, finally, Lewy bodies that are characteristic of Parkinson's disease. Native α-synuclein exists in the cytosol as an unordered monomer, a folded monomer, an unordered aggregate (Swart et al., 2014), or as a degradation-resistant, helically folded tetramer (Bartels et al., 2011). A pre-formed fibril or fibril fragment, known as a seed, accelerates fibril formation by the dominant process of secondary nucleation. Secondary nucleation involves aggregate formation from surface monomers (Gaspar et al., 2017). The toxic species produced during polymerization may damage mitochondria and lysosomes (Hashimoto et al., 2004; Hsu et al., 2000), disrupt microtubules (Alim et al., 2004), promote aggregate formation (Bousset et al., 2013; Brehme et al., 2014), cause organelle dysfunction (Flavin et al., 2017), and trigger inflammation and eventual cell death (Gustot et al., 2015). Ca^{2+}, calcium; ER, endoplasmic reticulum; SNCA, α-synuclein

3 | α-SYNUCLEIN FOUND IN THE GUT OF PD PATIENTS

Support for the gut's involvement in PD is derived, in part, from studies in which pathogenic α-synuclein has been found in the GI tracts of PD patients. Stockholm and colleagues studied this protein in a total of 57 PD patients and 90 controls from the Danish National Pathology Registry (Stokholm et al., 2016). Pathogenic phosphorylated α-synuclein was found in 22 of 39 (56%) PD patients who had tissue removed during the prodromal phase (early stage of the disease prior to disease diagnosis) compared with only 23 of 90 (26%) age- and sex-matched controls. The tissue samples were taken from a variety of anatomical regions including the nose and mouth regions, salivary glands, esophagus, stomach, small intestine, colon, and appendix. Importantly, this study identified Lewy pathology in the GI tract up to 20 years before patients were diagnosed with PD (Stokholm et al., 2016). This correlates with the reported prodromal period for PD of over 20 years, in which early signs and symptoms are present but a classical diagnosis based on fully developed motor impairment is not yet possible (Berg et al., 2015; Schenck et al., 2013). Hilton and colleagues reported α-synuclein accumulation in the bowel of PD patients and suggested this as an accessible biomarker for studying early stages of PD (Hilton et al., 2014). Further reports identified pathogenic phosphorylated α-synuclein deposits in the submandibular gland (Adler & Beach, 2016), as well as the myenteric plexus, submucosal layer, and mucosal nerve fibers of the intestine in individuals living with early untreated PD (Shannon et al., 2012).

In a large study measuring the PD diagnostic sensitivity and predictive ability of α-synuclein in different tissue biopsies, the sensitivity of colon biopsies (24%) was lower than skin and submandibular gland biopsies, with a negative predictive value of 67% (Chahine et al., 2020). A meta-analysis reported that only nine of 16 studies showed a positive association between the presence of gut α-synuclein and PD diagnosis (Bu et al., 2019). Specifically, colon α-synuclein had the highest degree of discrimination between PD and controls, with a specificity of 81.9% but a low sensitivity of only 56.8%. Biopsy site and histochemical technique can be confounders. Taken together, these findings show that the variable sensitivity and specificity reported for α-synuclein-positive colon biopsies raises questions for this technique as an early diagnostic or biomarker for PD (Chung et al., 2016; Lee et al., 2017; Visanji et al., 2015).

Moreover, although α-synuclein occurs at a statistically higher level in the enteric nervous system (ENS) of PD patients compared with control individuals (Aldecoa et al., 2015), the presence of α-synuclein aggregates throughout the body in healthy individuals raises further concerns about its use as a biomarker for PD. Even though α-synuclein's expression is highest in the brain, it is known to be expressed throughout the body in non-diseased individuals (https://www.proteinatlas.org/ENSG00000145335-SNCA/tissue). Consequently, improved methods for a detailed structural analysis to discriminate between pathogenic and non-pathogenic forms of this protein on the cellular and biochemical levels are necessary before interpreting the role of α-synuclein in PD diagnosis (Schaeffer et al., 2020).

3.1 | α-synuclein distribution in the brain and gut

The distribution of α-synuclein in the gut generally follows a rostrocaudal (top to bottom) gradient, with more misfolded protein found in the upper than the lower GI tract (Cersosimo, 2015). Studies have reported that the greatest levels of pathogenic α-synuclein are in the submandibular gland and lower esophagus of PD patients, followed by the stomach, small intestine, colon, and rectum (Beach et al., 2010).

In monogenic PD, neuropathological findings of synuclein deposition range from being characteristic of *SNCA* mutations (Duda et al., 2002) to relatively uncommon in cases with *PRKN* mutations (Seike et al., 2021) and are frequently variable in *LRRK2* mutations (Wszolek et al., 2004). LBs are not restricted to cases of PD, as Lewy-type pathology is well described in Alzheimer's disease, both sporadic and genetic forms (Compta & Revesz, 2021). Many cases of sporadic PD likely arise in patients with an incidental "Lewy Body State" (de la Fuente-Fernandez et al., 1998). In sporadic PD, LBs are distributed throughout the brainstem (substantia nigra, raphe nuclei, mesopontine tegmentum, locus coeruleus, and dorsal motor nucleus of the vagus nerve [DMNV]) and basal forebrain (N basalis Meynert) (Dickson, 2018); additional cortical LBs are found in the amygdala and neocortex. Lewy neurites, largely representing disrupted axonal processes, are an important source of synuclein pathology and are commonly identified in the anterior olfactory nucleus and other sites (Braak, del Tredici, et al., 2003). Synuclein pathology is largely found in neurons and not glia, and the presence of cytoplasmic inclusions reflects displacement of synuclein from its location in the presynaptic terminals (Dickson, 2018).

In addition to the brain and the gut, α-synuclein pathology is also distributed throughout the body, particularly in the spinal cord, the sympathetic ganglia, skin, the vagus nerve, and endocrine organs (Beach et al., 2010). Similar changes are also frequently found in the spinal cord and sympathetic ganglia in incidental LB disease (Beach et al., 2010). These pathological findings, together with clinical evidence of prodromal autonomic dysfunction and abnormal metaiodobenzylguanidine (MIBG) cardiac imaging showing postganglionic sympathetic cardiac denervation (Yoshita, 1998),

point to early involvement of the autonomic nervous system (ANS) by α-synuclein pathology.

Lewy pathology is usually restricted to certain cell types; for example, within the DMNV, only the cholinergic and catecholaminergic neurons are affected, whereas neurons producing γ-aminobutyric acid are not (Kingsbury et al., 2010). The selective vulnerability of cells in individuals living with PD may be explained in part by the proposal made by Braak et al. that a relationship exists between axonal characteristics of neurons and susceptibility to pathogenic α-synuclein (Braak et al., 2003). The vagus nerve contains long, thin, poorly myelinated fibers of the visceromotor system. These fibers appear to be more susceptible to LB pathology than the myelinated fibers that relay viscerosensory inputs or fibers derived from the nucleus ambiguus. It is speculated that this phenomenon may be related to the bioenergetic demands of sustaining electrical excitability along these axons or the physiological traits of neurons, such as slow calcium oscillations, leading to mitochondrial oxidative stress (Breen et al., 2019). However, at this stage, it remains unclear why only certain cells are affected by α-synuclein pathology.

4 | PRION-LIKE MOVEMENT OF α-SYNUCLEIN IN PD

In 1976, it was established that diseases such as Creutzfeldt–Jakob disease (CJD) could be transmitted through direct intracerebral injection of brain tissue from affected patients (Gibbs et al., 1968; Masters et al., 1981). Stanley B. Prusiner discovered a transmissible agent unlike bacteria or viruses that consists of protein, which he named a "prion"—an amalgamation of the words "protein" and "infectious" (Prusiner, 1982). Prions are known to be proteinaceous infectious agents that are responsible for several fatal neurological diseases in humans. Prions lack nucleic acids and are instead solely composed of misfolded, host-encoded prion protein, which is a glycoprotein expressed in all vertebrates (Wickner et al., 2011). Interestingly, a recent study reported a case of variant CJD that was diagnosed 7.5 years after accidental occupational exposure to bovine spongiform encephalopathy prions from infected mice brain tissue, which emphasizes the need to improve identification and prevention strategies for prion disease transmission to humans (Brandel et al., 2020). The understanding of prion diseases is still incomplete, and the existence of prion-like mechanisms in PD pathology remains unknown (Collinge, 2016; Jucker & Walker, 2013).

4.1 | PD and the prion hypothesis

Several features are shared between PD and prion diseases, and these similarities have been reviewed previously (Brundin

& Melki, 2017; Olanow & Brundin, 2013; Prusiner, 2001). Human prion disease and PD are neurodegenerative disorders in which the affected neurons display selective vulnerability. Both pathologies are characterized by propagating protein deposits that can be taken up by neurons and transferred to unaffected cells nearby. Misfolded prions may migrate along the peripheral nerves and up the spinal cord in prion diseases (Olanow & Brundin, 2013). At the cellular level, this migration and transmission of the prion protein can occur horizontally from one cell to its neighbors as well as vertically when a single cell divides into identical daughter cells, although the exact mechanisms underlying these processes remain unclear. It is hypothesized that pathogenic α-synuclein spreads from the gut and olfactory bulb to the CNS in PD (Niu et al., 2018).

Animal studies have demonstrated cell-to-cell transmission and centripetal spread of α-synuclein in a prion-like fashion (Ayers et al., 2017; Breid et al., 2016). Human studies have also provided evidence for a possible prion-like spread of α-synuclein through observations of neural grafts in PD patients. Specifically, α-synuclein-positive LBs and Lewy neurites were identified in fetal neuronal grafts in three PD patients 11–16 years after transplantation (Kordower et al., 2008; Li et al., 2008).

PD pathology and symptoms are known to worsen as the disease progresses. The healthy donor-grafted neurons may undergo a similar neurodegenerative process to that present in PD with synuclein pathology becoming evident following the graft. Although insufficient epidemiological evidence currently exists on the infectious transmission of synucleinopathies between humans (Beekes et al., 2014; Irwin et al., 2013), the evidence from human neural grafts and animal models provides support that there is similarity in the mechanism of spread of α-synuclein pathology in PD and prion pathology in prion diseases. From the above, it appears that although there is much evidence for the prion hypothesis in PD (Brundin & Melki, 2017), the alternative argument that PD is not simply a prion disorder and could be due to regional or cell-autonomous factors such as specific vulnerability of neurons (Surmeier et al., 2017) should also be considered.

The similarities between prion disease and PD suggest that the prion-like movement of α-synuclein partly contributes to PD pathogenesis and spread of pathology. However, α-synuclein will as yet only be referred to as a "prion-like," or "prionoid," protein (Ma et al., 2019).

5 | MOVEMENT OF α-SYNUCLEIN ALONG THE GUT–BRAIN AXIS

As noted previously, α-synuclein is found in the GI tracts of many PD patients, and it is believed that the physical connection between the brain and the gut may shed light onto

the pathophysiological mechanisms that allow gut involvement in this neurodegenerative disease. The gut–brain axis (Figure 3) refers to a complex, bidirectional line of communication between the CNS, ANS, and GI tract (Carabotti et al., 2015). Gut–brain crosstalk regulates GI homeostasis by monitoring intestinal permeability, immune activation, entero-endocrine signaling, and enteric reflex. The vagus nerve is composed of 80% afferent and 20% efferent fibers and plays an important role in the regulation of parasympathetic activity such as digestion and heart rate (Babic & Browning, 2014; Bonaz et al., 2018).

α-Synuclein inclusions are proposed to form initially in nerve terminals of the ENS and then spread via autonomic connections to the medulla and spinal cord (Borghammer, 2018). However, staging is made complex by the range of patterns of synuclein deposition, which may be limbic or neocortical predominant (Beach et al., 2009). A major distinction may lie between two subtypes in which dysfunction originates either in the peripheral ANS, and subsequently ascends via autonomic afferents to the brain, and one in which the pathology arises in the brain itself (Horsager et al., 2020). This may be illustrated by premotor rapid eye movement (REM) sleep behavior disorder, which is postulated to be a prominent premotor marker of onset in the peripheral ANS and gut, spreading to the brainstem (Horsager et al., 2020).

Perturbation of the gut–brain axis has been implicated in the pathophysiology of GI disorders such as inflammatory bowel disease (Bonaz et al., 2017) and several neurological diseases, including PD (Cenit et al., 2017; Kobayashi et al., 2017; Quigley, 2017). Evidence of the involvement of the gut in PD pathophysiology is mounting, particularly placing the gut or ENS as the possible starting point of PD pathology. This stems from the finding of misfolded α-synuclein in nerves of the enteric system before it appears in the brain (Chandra et al., 2017). The vagus nerve may act as a path whereby PD pathology can spread from the GI tract to the CNS (Mukherjee et al., 2016). However, a recent primate study investigated the injection of α-synuclein-containing LB extracts from patients with PD and found no α-synuclein pathological lesions in the primate vagus nerve (Arotcarena et al., 2020). Furthermore, there is some *debate regarding the direction of α-synuclein movement along the gut–brain axis.*

Inoculation of duodenal walls with α-synuclein fibrils has been shown to lead to increased progression of α-synuclein histopathology in the midbrains of aged mice, indicating caudorostral, or gut to brain, movement of α-synuclein pathology (Challis et al., 2020). This is one of the many studies that support this direction of α-synuclein spread along the gut–brain axis (Chandra et al., 2017; Holmqvist et al., 2014; Ulusoy et al., 2013). Conversely, a small number of studies have demonstrated the movement of α-synuclein pathology from
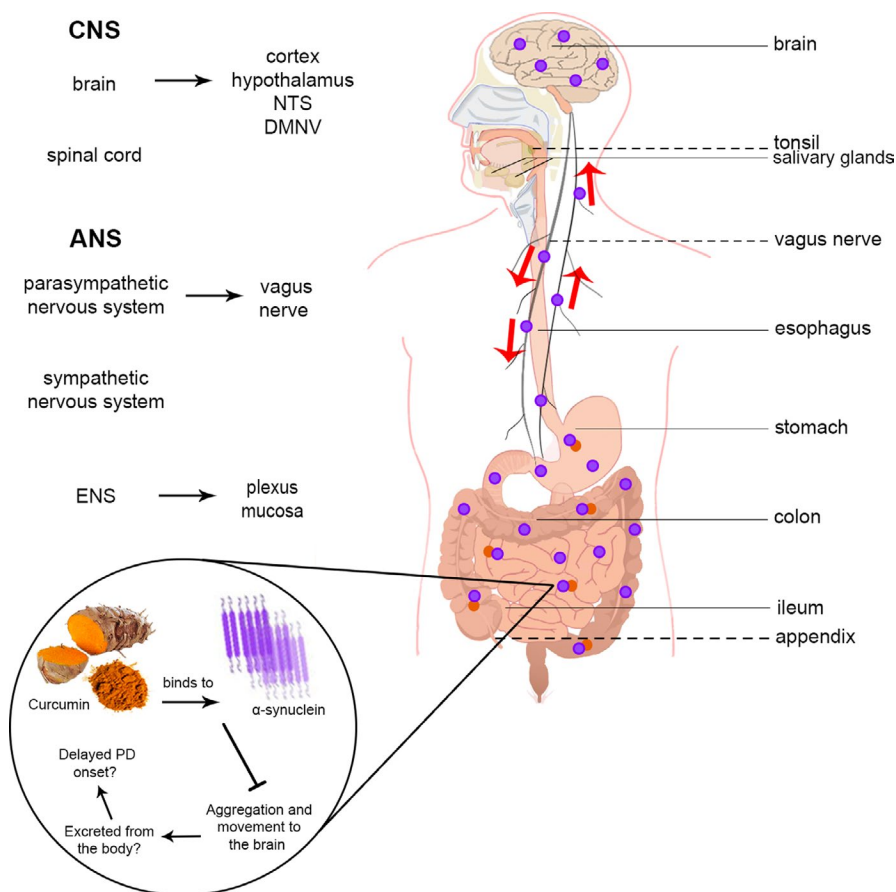
FIGURE 3 Bidirectional movement of α-synuclein along the gut–brain axis via the vagus nerve, and potential intervention with curcumin. Following oral consumption, curcumin (orange dots) binds to α-synuclein (purple dots), thereby preventing aggregation and movement to the brain. Thereafter, it is hypothesized that the curcumin–α-synuclein complex is excreted from the body due to the rapid metabolism of curcumin in the body. Red arrows along the vagus nerve indicate the direction of α-synuclein movement: gut-to-brain or vice versa. Gut components that may be linked to Parkinson's disease risk following surgical alteration or removal are indicated (dashed line). ANS, autonomic nervous system; CNS, central nervous system; DMNV, dorsal motor nucleus of the vagus nerve; ENS, enteric nervous system; NTS, nucleus tractus solitarius

the brain to the gut along the course of the vagus nerve. One such study used rat models to show that the DMNV may be a relay center for α-synuclein transmission from central to peripheral tissues (Ulusoy et al., 2017). Despite these conflicting reports, it remains probable that the vagus nerve and LB movement along this track are implicated in PD pathology.

In 2003, Braak et al. published their hypothesis regarding the staged manner in which PD pathology may spread in the brain (Braak, del Tredici, et al., 2003). They noted the pathological findings of α-synuclein-immunopositive LBs and Lewy neurites initially appearing in the DMNV, the glossopharyngeal nerve, and the olfactory bulb. Thereafter, rostral regions of the brainstem and cortical and prefrontal regions sequentially became affected. However, it was unclear as to the origin of abnormal α-synuclein deposition in the caudal brainstem and olfactory bulb, and subsequently, Braak, Rüb, et al., (2003) proposed that LB formation might begin in the ENS and then spreads to the brain. They speculated that this could arise following the ingestion of an exogenous pathogen that triggered abnormal α-synuclein accumulation (Braak, Rüb, et al., 2003). Such a pathogen would potentially have prion-like properties and would consist of α-synuclein fragments (Liautard, 1991). With some modifications, the proposal was that α-synuclein might cross the mucosal barrier of the gut and then travel along enteric neurons and preganglionic fibers of the vagus nerve to the CNS in a prion-like manner (Braak, Rüb, et al., 2003; Braak et al., 2006). This retrograde axonal and transneuronal movement resulted in the deposition of α-synuclein in the vulnerable subcortical nuclei of the brainstem, triggering disease onset and furthering disease progression. In vitro and in vivo clinical evidence has accumulated to support this hypothesis (Rietdijk et al., 2017).

However, some skepticism remains regarding the validity of the prion-like, gut-to-brain hypothesis of α-synuclein movement, and therefore, further experimental evidence is required for its wider acceptance. Another possibility is that the gut–brain axis may provide a pathway by which α-synuclein travels bidirectionally from either the brain or the gut to trigger PD (Arotcarena et al., 2020). In support of this view, Borghammer and van den Berge describe a theory wherein PD is separated into two subtypes based on the region in which α-synuclein initially appears in the patient: CNS-first and peripheral nervous system (PNS)-first (Borghammer & van den Berge, 2019). Additionally, there is the threshold theory, whereby both the CNS and PNS degenerate simultaneously, albeit with different thresholds for emergence of symptoms related to dopamine reserves (Engelender & Isacson, 2017). These thresholds are based on compensatory mechanisms that tolerate a certain level of neuronal damage before symptoms manifest. The PNS appears to have a lower threshold because less neuronal damage (20% reduction) is required to elicit prodromal non-motor symptoms. By contrast, the CNS has a higher threshold

requiring over 50% loss in dopaminergic neurons to elicit the classical motor symptoms of PD. Furthermore, the role of the brain–gut–microbiota axis in PD (Mulak & Bonaz, 2015) has gained traction from a study that found changes in the microbiome following nigral injection of α-synuclein in rat brains (O'Donovan et al., 2020). Such a study suggests a potential role of the microbiome in PD, but factors such as dopaminergic medication, GI motility, and the translatability of animal model findings to human diseases make interpretation difficult. Therefore, longitudinal studies in large cohorts (Wallen et al., 2020) including prodromal subjects are recommended to clarify the relationship between the microbiome and α-synuclein and ultimately its role in PD pathogenesis and progression (Keshavarzian et al., 2015).

6 | CLINICAL MANIFESTATIONS OF GI AND MOTOR DYSFUNCTION IN PD

Cardinal motor symptoms such as tremor and bradykinesia are frequently observed at clinical diagnosis (Darweesh et al., 2016). However, many non-motor symptoms manifest in the prodromal phase before PD diagnosis. One such symptom is GI dysfunction that affects 80% of PD patients over the course of the disease (Cersosimo et al., 2013). Defecatory dysfunction (Savica et al., 2009) and gastric dysfunction are common in both early and late stages of the disease (Heetun & Quigley, 2012; Marrinan et al., 2014; Tanaka et al., 2011). This leads to early satiety and dysphagia, which contribute to reduced appetite and malnutrition (Sheard et al., 2013). Malnutrition, as well as immobility and lack of sunlight, are also correlated with vitamin D deficiencies, which are common among PD patients (Lv et al., 2014).

Furthermore, delayed gastric emptying (Pasricha & Parkman, 2015) impairs levodopa absorption, contributing to symptom fluctuations (Doi et al., 2012). Constipation has been found to occur as early as 20 years prior to motor symptoms, making it one of the earliest non-motor symptoms in PD (Savica et al., 2009). It is evident that many components of the GI system are affected in PD, from the salivary glands and stomach (dysphagia and gastroparesis) to the colon and rectum (constipation and defecatory dysfunction) (Pfeiffer, 2003). This suggests that the GI tract may play a role in the pathogenic mechanisms underlying PD (Schaeffer et al., 2020).

7 | EFFECTS OF GI TRACT SURGERIES ON PD RISK

Several medical procedures including vagotomy, appendectomy, and tonsillectomy have been investigated for their

effect on an individual's risk of subsequently developing PD (Breen et al., 2019). It should be noted that, due to inconsistent findings, it remains controversial as to whether these surgeries are truly beneficial in delaying or preventing PD onset. Furthermore, epidemiological studies only infer associations, which makes it challenging to deduce causality from this type of study (Grimes & Schulz, 2012). Therefore, unless conclusive evidence is produced through large, matched-cohort studies that accurately account for all potential confounders, these surgeries should not be promoted as prevention or treatment strategies against this disease.

7.1 | Appendectomy

The appendix was identified as having particularly enriched α-synuclein staining with immunohistochemistry in its mucosal plexus, suggesting that it might be involved in enteric α-synuclein aggregation (Gray et al., 2014).

Subsequently, it was reported that appendectomy might delay the onset of PD (Mendes et al., 2015). In a group of 295 PD patients, appendectomy in those with PD onset after the age of 55 had a delayed onset of PD with a hazard ratio (HR) of 0.63 (95% confidence interval [CI] 0.41–0.98). Appendectomy appeared to be associated specifically with delayed onset of motor symptoms in patients with late onset of PD. The authors recognized the possibility that α-synuclein spread may have occurred prior to the surgical procedure. In a subsequent population-based study from Ontario, no differences were found in the risk of PD when comparing those who had undergone appendectomy with those who had undergone cholecystectomy. The authors did find a higher risk of PD shortly after appendectomy but noted that it was probable that PD was already present at the time of surgery in those developing the disease within 5 years after appendectomy.

As with the Canadian study, when the issue was examined over a 30-year period reviewing data from the Danish National Patient Registry (DNPR), the results were in the opposing direction to the initial findings of Mendes et al., (2015), in that appendectomy was associated with a slightly *increased* risk of PD (adjusted HR 1.14; 95% CI 1.03–1.27). Nearly 266,000 individuals underwent appendectomy, of whom 786 had a diagnosis of PD, resulting in a PD incidence rate of 0.16 per 1,000 person years, versus a lower PD incidence of 0.15 for the general population (Svensson et al., 2016).

In a further report derived from participants in the Nurses' Health Study and the Health Professionals Follow-up Study (Palacios et al., 2018), appendectomy in women related to actual appendicitis was associated with a modestly elevated risk of PD (HR 1.23, 95% CI 1.00–1.50). However, a subsequent study (Killinger et al., 2018) reviewed data from the Swedish National Patient Registry (SNPR) and the Parkinson's Progression Markers Initiative (PPMI). From the

SNPR cohort, the cumulative prevalence of PD was reduced by 16.9% compared with the general population, and age at PD diagnosis was 1.6 years later in those who had undergone surgery 20 years or more prior as compared with those without appendectomy. This finding of delayed onset of PD was replicated in the PPMI cohort, including confirmation of nigral cell loss by nuclear imaging. In a further study using data from 78,650 PD patients in the SNPR, there was a 16% lower risk of PD linked to previous appendectomy (odds ratio [OR] = 0.84, 95% CI 0.80–0.88), and temporal analyses confirmed the finding at 5, 10, and 20 years following surgery (Liu et al., 2020).

7.2 | Vagotomy

The vagus nerve controls acid secretion and gastric motility. Truncal vagotomy refers to resection of the trunks of the anterior and posterior nerves and, therefore, removes all vagal and parasympathetic supply to the abdominal contents except for the gut distal to the transverse colon, which receives parasympathetic outflow from the sacral segments of the spinal cord. Selective vagotomy refers to resection of the fibers supplying only the stomach, and in highly selective or superselective vagotomy, only nerve branches to the esophagus, fundus, and body are divided, sparing the antrum and pylorus (Seeras & Prakash, 2019).

The effect of these procedures on the risk of PD has been studied in large national registries available in Nordic countries that have allowed for the examination of the uncommon association of vagotomy with PD (Liu et al., 2017; Svensson et al., 2015). The initial analysis was performed using the DNPR and analyzed a cohort of patients who underwent vagotomy between 1977 and 1995. This analysis showed that if a diagnosis of PD was made 5 years or more after a vagal resection, those with a truncal vagotomy compared with superselective vagotomy had a lower risk of being diagnosed with PD (HR 0.85, although this did not reach significance in both groups). At the 20-year follow-up after surgery, the cumulative incidence of PD in individuals who had the superselective vagotomy (0.96 per 1,000 person years) was similar to that of the general population (0.87 per 1,000 person years), versus an incidence of 0.65 per 1,000 person years for those with truncal vagotomy (Svensson et al., 2015). However, in a further analysis of the same Danish registry, but which assembled a cohort of patients over an extended period (1977–2011), no significant finding was found in any group, including those with a 20-year follow-up after surgery (Tysnes et al., 2015).

When a similar analysis was carried out using the SNPR, almost 5,000 cases of PD were identified, of whom only 101 also had a vagotomy (Liu et al., 2017). The crude incidences for PD were 80.4 (per 100,000 person years) for truncal

vagotomy, 55.1 for selective vagotomy, with an intermediate value (67.5) for matched cases from the general population without vagotomy. Cumulative incidences were similar to the Danish study for the different types of vagal surgery, with selective vagotomy again resembling the general population, and with a lower risk of PD >5 years after truncal vagotomy (HR 0.59, 95% CI 0.37–0.93).

7.3 | Tonsillectomy

Like the appendix, tonsils are also part of the gut-associated lymphoid tissues but are not directly innervated by the vagus nerve (Breen et al., 2019). However, prion infection in variant CJD is identified in the tonsils and may spread rostrally to the brain through autonomic fibers and the spinal cord. Using the DNPR, approximately 195,000 patients who had undergone tonsillectomy (median age 17 years) were each compared with five age- and sex-matched controls (Svensson et al., 2018). The risk of PD was similar in patients who had undergone tonsillectomy and controls. However, the study population was relatively young, and PD cases may have been missed as a result.

A further analysis was carried out in the SNPR, and although there was a trend of prior tonsillectomy being associated with a lower risk for PD, associations did not reach statistical significance (Liu et al., 2020).

8 | CURCUMIN AS A NUTRACEUTICAL APPROACH TO PD TREATMENT AND PREVENTION

Levodopa and other commonly used PD drugs may be associated with significant side effects with long-term use. In addition, none of these drugs halt or slow down disease progression by protecting against the degeneration of remaining neurons (Bharath, 2008). Therefore, developing alternative treatment strategies is important to reduce morbidity and mortality associated with PD. Treatments that target the gut have become an area of interest for therapeutic interventions to prevent or slow the progression of the disease.

Nutraceuticals, dietary supplements, and "functional foods" have gained popularity over the past few decades due to the potential health benefits of these natural products, which are believed to be less toxic than synthetic derivatives (Santini et al., 2017). A popular nutraceutical with a wide variety of therapeutic properties is curcumin, a component of the spice turmeric, which is derived from the *Curcuma longa* Linn. rhizome (Kochhar, 2008). The well-known issue of curcumin's low bioavailability has largely been overcome with the development of several formulations of curcumin such as nanoparticles, adjuvants, complexes with other

molecules, and microemulsions (Govindaraju et al., 2019; Panahi et al., 2014; Tapal & Tiku, 2012; Xiao et al., 2013). Curcumin is proposed here as a potentially effective approach to PD treatment and management. We speculate that curcumin may serve a protective role as it could act on α-synuclein in the gut and remove it from the body (illustrated in Figure 3).

The prevalence of neurological diseases in countries that consume more turmeric has been investigated (Ganguli et al., 2000; Ng et al., 2006). Turmeric and red chilies are the most commonly used spices in Indian households (Bhathal et al., 2020; Siruguri & Bhat, 2015), where the average intake can be as high as 2000–2500 mg/day (Basnet & Skalko-Basnet, 2011). Comparisons of the elderly in Eastern and Western populations have shown that frequent consumption of dietary curcumin in India may be linked to a lower risk of Alzheimer's disease and a delay in age-related cognitive impairments than North American populations (Ganguli et al., 2000; Ng et al., 2006). Although the prevalence and incidence of PD in India are reported to be low (Bharucha et al., 1988; Das et al., 2010; Razdan et al., 1994; Surathi et al., 2016), larger multi-center studies across India are required to produce more accurate epidemiological data on PD and to establish whether turmeric consumption is linked to lower PD prevalence and incidence rates.

A global paradigm shift is occurring away from monotherapy, in which compounds target one particular cellular pathway, to multi-therapy based on several targets, thereby increasing the likelihood of success (Bang et al., 2019). Plant-based medicines such as curcumin align with this concept and, thus, are being studied to develop better therapies for human diseases (Kumar, 2006; Sparreboom et al., 2004). Curcumin has been shown to target multiple pathways implicated in PD pathobiology (Mythri & Srinivas Bharath, 2012) and may prove useful for long-term PD treatment due to its effect on both α-synuclein and the GI tract, which will be discussed below.

8.1 | Effect on α-synuclein

Curcumin and its derivatives have been shown in multiple studies to inhibit the aggregation of α-synuclein in vitro (Figure 3) (Ahmad & Lapidus, 2012; Jha et al., 2016; Pandey et al., 2008; Sharma & Nehru, 2018; Singh et al., 2013). In addition, curcumin has been reported to protect against mutant A53T α-synuclein-induced toxicity in cell models (Liu et al., 2011). Furthermore, it acts to protect against α-synuclein-induced toxicity by downregulating the mammalian target of the rapamycin/p70 ribosomal protein S6 kinase (mTOR/p70S6k) signaling pathway and promoting the recovery of suppressed macroautophagy pathways (Jiang et al., 2013). Curcumin has been shown to bind strongly to the

NAC domain of α-synuclein thereby reducing α-synuclein aggregation (Figure 3) (Kamelabad et al., 2020). Although using curcumin as an aggregation inhibitor is promising, the precise structures of monomeric and oligomeric α-synuclein are still poorly defined, thus limiting their use in rational drug design to target early protein aggregation (Tuttle et al., 2016).

8.2 | Effect on GI health

Dysbiosis in the gut can lead to intestinal hyperpermeability, or "leaky gut," a condition frequently found in PD patients (Maes, 2008; Thevaranjan et al., 2017). The mucosal barrier of the intestines is a single layer of epithelium that allows for nutrient absorption while preventing the entry of exterior antigens from the intestinal lumen into the host. However, when this barrier is compromised, the individual develops a "leaky gut" and foreign antigens enter host tissues and can initiate an immune response (Peterson & Artis, 2014). Curcumin has been found to relieve leaky gut in rats with intestinal ischemia-reperfusion injury, by reducing changes in intestinal tumor necrosis factor-α (TNF-α). This results in an improvement in the histological abnormalities present in intestinal mucosa and restores tight junction protein zonula occludens-1 expression (Tian et al., 2016). Rats have also been shown to have a reduction in methotrexate-induced damage to the intestinal mucosa barrier following treatment with curcumin (Song et al., 2010). Constipation may also be treated by curcumin as it has been shown to have a dose-dependent mild laxative effect (Bhowmik et al., 2009; Srinivasan, 1972). In addition, the lack of vitamin D found in many PD patients may be relieved by supplementation with curcumin, which is reportedly taken up by intestinal epithelia and binds to the vitamin D receptor, thereby enhancing vitamin D signaling (Bartik et al., 2010).

In "diabetic" rats, in which GI complications were induced, the antioxidant properties of curcumin were found to successfully restore body weight, gastric emptying, and intestinal transit, all of which could also benefit PD patients (Kochar et al., 2014). Therefore, curcumin has the potential to relieve GI complications in individuals living with PD, but further studies, particularly in humans, are needed to show its efficacy and its possible adverse effects.

9 | CONCLUDING REMARKS

The gut is affected both early and extensively in PD and appears to play a role in disease pathogenesis and progression. There is ample evidence for the presence of pathogenic forms of α-synuclein, a hallmark of PD, in the gut, which may travel between the gut and the brain. There are, however, a number of theories to account for the development of PD, including the threshold theory (simultaneous degeneration in the CNS and PNS) and the brain–gut–microbiota axis theory, and further studies are therefore required to elucidate whether it is the gut, the brain, or a region in between that acts as a starting point for α-synuclein movement. It is plausible that the initiation site and the pattern of α-synuclein progression may vary between patients, which may explain, in part, the clinical heterogeneity observed in the disease (Uversky & Eliezer, 2009). Notably, postmortem tissue gives a static view of this dynamic process, and therefore, improved methods for detection of α-synuclein throughout the body and the ability to distinguish between pathological and native forms of this protein are needed to shed light on this topic (Schaeffer et al., 2020).

Notably, gut dysfunction is known to contribute significantly to the morbidity and complications experienced by persons living with PD. Despite numerous studies, the possible protective effect of gut-associated surgeries against PD remains controversial. In India, gut dysfunction is traditionally treated with turmeric, which is used to promote digestion, detoxify the liver and gallbladder, and improve intestinal flora (Bhowmik et al., 2009)—benefits that may be attributable to its polyphenolic curcuminoids including curcumin. Turmeric-derived curcumin is one of many nutraceuticals that have become compelling therapeutic candidates in the treatment of several disorders including PD. Curcumin's low bioavailability may not limit its potential as a nutraceutical to treat disorders such as PD if the gut is the preferred site of action. In the gut, curcumin is able to bind α-synuclein over longer periods of time through life-long dietary intake and attenuate the initiation and spread of Lewy pathology. However, larger studies in humans need to be performed to investigate the long-term safety and efficacy of curcumin as a nutraceutical in vivo. If curcumin's beneficial properties are validated, it is proposed that life-long dietary supplementation with curcumin is an attractive therapeutic modality for PD. It is hypothesized that curcumin may bind to α-synuclein in the gut and be excreted from the body, thereby reducing the risk of PD or at least delaying disease onset. Consequently, this compound has the potential to slow disease progression and improve quality of life through the relief of gut dysfunction, thereby bridging PD prevention and management.

CONFLICT OF INTEREST
The authors do not have any financial disclosures or conflicts of interest concerning the research related to this article.

AUTHOR CONTRIBUTIONS

PEER REVIEW

ORCID

Devina Chetty https://orcid.org/0000-0003-4541-3696
Shameemah Abrahams https://orcid.org/0000-0002-1120-678X
Riaan van Coller https://orcid.org/0000-0001-6250-363X
Jonathan Carr https://orcid.org/0000-0002-7677-426X
Colin Kenyon https://orcid.org/0000-0003-1590-7230
Soraya Bardien https://orcid.org/0000-0002-3508-3438

REFERENCES

Adler, C. H., & Beach, T. G. (2016). Neuropathological basis of nonmotor manifestations of Parkinson's disease. *Movement Disorders*, *31*, 1114–1119. https://doi.org/10.1002/mds.26605

Ahmad, B., & Lapidus, L. J. (2012). Curcumin prevents aggregation in α-synuclein by increasing reconfiguration rate. *Journal of Biological Chemistry*, *287*, 9193–9199. https://doi.org/10.1074/jbc.M111.325548

Alafuzoff, I., & Hartikainen, P. (2018). Alpha-synucleinopathies. In G .G. Kovacs & I. Alafuzoff (Eds.), *Handbook of clinical neurology* (pp. 339–353). Elsevier. https://doi.org/10.1016/B978-0-12-802395-2.00024-9

Aldecoa, I., Navarro-Otano, J., Stefanova, N., Sprenger, F. S., Seppi, K., Poewe, W., Cuatrecasas, M., Valldeoriola, F., Gelpi, E., & Tolosa, E. (2015). Alpha-synuclein immunoreactivity patterns in the enteric nervous system. *Neuroscience Letters*, *602*, 145–149. https://doi.org/10.1016/j.neulet.2015.07.005

Alim, M. A., Ma, Q.-L., Takeda, K., Aizawa, T., Matsubara, M., Nakamura, M., Asada, A., Saito, T., Kaji, H., Yoshii, M., Hisanaga, S., & Uéda, K. (2004). Demonstration of a role for α-synuclein as a functional microtubuleassociated protein. *Journal of Alzheimer's Disease*, *6*, 435–442.

Arotcarena, M. L., Dovero, S., Prigent, A., Bourdenx, M., Camus, S., Porras, G., Thiolat, M. L., Tasselli, M., Aubert, P., Kruse, N., Mollenhauer, B., Trigo Damas, I., Estrada, C., Garcia-Carrillo, N., Vaikath, N. N., El-Agnaf, O. M. A., Herrero, M. T., Vila, M., Obeso, J. A., … Bezard, E. (2020). Bidirectional gut-to-brain and brain-to-gut propagation of synucleinopathy in non-human primates. *Brain*, *143*, 1462–1475. https://doi.org/10.1093/brain/awaa096

Ayers, J. I., Brooks, M. M., Rutherford, N. J., Howard, J. K., Sorrentino, Z. A., Riffe, C. J., & Giasson, B. I. (2017). Robust central nervous system pathology in transgenic mice following peripheral injection of α-synuclein fibrils. *Journal of Virology*, *91*, e02095–e2116. https://doi.org/10.1128/JVI.02095-16

Babic, T., & Browning, K. N. (2014). The role of vagal neurocircuits in the regulation of nausea and vomiting. *European Journal of Pharmacology*, *722*, 38–47. https://doi.org/10.1016/j.ejphar.2013.08.047

Bang, S., Son, S., Kim, S., & Shin, H. (2019). Disease pathway cut for multi-target drugs. *BMC Bioinformatics*, *20*, 74. https://doi.org/10.1186/s12859-019-2638-3

Bartels, T., Choi, J. G., & Selkoe, D. J. (2011). α-Synuclein occurs physiologically as a helically folded tetramer that resists aggregation. *Nature*, *477*, 107–110. https://doi.org/10.1038/nature10324

Bartik, L., Whitfield, G. K., Kaczmarska, M., Lowmiller, C. L., Moffet, E. W., Furmick, J. K., Hernandez, Z., Haussler, C. A., Haussler, M. R., & Jurutka, P. W. (2010). Curcumin: A novel nutritionally derived ligand of the vitamin D receptor with implications for colon cancer chemoprevention. *Journal of Nutritional Biochemistry*, *21*, 1153–1161. https://doi.org/10.1016/j.jnutbio.2009.09.012

Basnet, P., & Skalko-Basnet, N. (2011). Curcumin: An anti-inflammatory molecule from a curry spice on the path to cancer treatment. *Molecules*, *16*, 4567–4598. https://doi.org/10.3390/molecules16064567

Beach, T. G., Adler, C. H., Lue, L. F., Sue, L. I., Bachalakuri, J., Henry-Watson, J., Sasse, J., Boyer, S., Shirohi, S., Brooks, R., Eschbacher, J., White, C. L., Akiyama, H., Caviness, J., Shill, H. A., Connor, D. J., Sabbagh, M. N., & Walker, D. G. (2009). Unified staging system for Lewy body disorders: Correlation with nigrostriatal degeneration, cognitive impairment and motor dysfunction. *Acta Neuropathologica*, *117*, 613–634. https://doi.org/10.1007/s00401-009-0538-8

Beach, T. G., Adler, C. H., Sue, L. I., Vedders, L., Lue, L. F., White III, C. L., Akiyama, H., Caviness, J. N., Shill, H. A., Sabbagh, M. N., & Walker, D. G. (2010). Multi-organ distribution of phosphorylated α-synuclein histopathology in subjects with Lewy body disorders. *Acta Neuropathologica*, *119*, 689–702. https://doi.org/10.1007/s00401-010-0664-3

Beekes, M., Thomzig, A., Schulz-Schaeffer, W. J., & Burger, R. (2014). Is there a risk of prion-like disease transmission by Alzheimer-or Parkinson-associated protein particles? *Acta Neuropathologica*, *128*, 463–476. https://doi.org/10.1007/s00401-014-1324-9

Berg, D., Postuma, R. B., Adler, C. H., Bloem, B. R., Chan, P., Dubois, B., Gasser, T., Goetz, C. G., Halliday, G., Joseph, L., Lang, A. E., Liepelt-Scarfone, I., Litvan, I., Marek, K., Obeso, J., Oertel, W., Olanow, C. W., Poewe, W., Stern, M., & Deuschl, G. (2015). MDS research criteria for prodromal Parkinson's disease. *Movement Disorders*, *30*, 1600–1611. https://doi.org/10.1002/mds.26431

Bharath, M. (2008). Therapeutic strategies in Parkinson's disease. *Recent Patents on Endocrine, Metabolic & Immune Drug Discovery*, *2*, 135–147.

Bharucha, N. E., Bharucha, E. P., Bharucha, A. E., Bhise, A. V., & Schoenberg, B. S. (1988). Prevalence of Parkinson's disease in the Parsi community of Bombay, India. *Archives of Neurology*, *45*, 1321–1323. https://doi.org/10.1001/archneur.1988.00520360039008

Bhathal, S. K., Kaur, H., Bains, K., & Mahal, A. K. (2020). Assessing intake and consumption level of spices among urban and rural households of Ludhiana district of Punjab, India. *Nutrition Journal*, *19*, 121. https://doi.org/10.1186/s12937-020-00639-4

Bhowmik, D., Kumar, K. P., Chandira, M., & Jayakar, B. (2009). Turmeric: A herbal and traditional medicine. *Archives of Applied Science Research*, *1*, 86–108.

Biesalski, H.-K., Dragsted, L. O., Elmadfa, I., Grossklaus, R., Müller, M., Schrenk, D., Walter, P., & Weber, P. (2009). Bioactive compounds: Definition and assessment of activity. *Nutrition*, *25*, 1202–1205. https://doi.org/10.1016/j.nut.2009.04.023

Stellenbosch University https://scholar.sun.ac.za

12 WILEY—EJN European Journal of Neuroscience FENS CHETTY ET AL.

Bonaz, B., Bazin, T., & Pellissier, S. (2018). The vagus nerve at the interface of the microbiota-gut-brain axis. *Frontiers in Neuroscience*, *12*. https://doi.org/10.3389/fnins.2018.00049

Bonaz, B., Sinniger, V., & Pellissier, S. (2017). Vagus nerve stimulation: A new promising therapeutic tool in inflammatory bowel disease. *Journal of Internal Medicine*, *282*, 46–63. https://doi.org/10.1111/joim.12611

Borghammer, P. (2018). How does parkinson's disease begin? Perspectives on neuroanatomical pathways, prions, and histology. *Movement Disorders*, *33*, 48–57. https://doi.org/10.1002/mds.27138

Borghammer, P., & van den Berge, N. (2019). Brain-first versus gut-first Parkinson's disease: A hypothesis. *Journal of Parkinson's Disease*, *9*, S281–S295. https://doi.org/10.3233/JPD-191721

Bourdenx, M., Koulakiotis, N. S., Sanoudou, D., Bezard, E., Dehay, B., & Tsarbopoulos, A. (2017). Protein aggregation and neurodegeneration in prototypical neurodegenerative diseases: Examples of amyloidopathies, tauopathies and synucleinopathies. *Progress in Neurobiology*, *155*, 171–193. https://doi.org/10.1016/j.pneurobio.2015.07.003

Bousset, L., Pieri, L., Ruiz-Arlandis, G., Gath, J., Jensen, P. H., Habenstein, B., Madiona, K., Olieric, V., Böckmann, A., & Meier, B. H. (2013). Structural and functional characterization of two alpha-synuclein strains. *Nature Communications*, *4*, 1–13.

Boyer, D. R., Li, B., Sun, C., Fan, W., Sawaya, M. R., Jiang, L., & Eisenberg, D. S. (2019). Structures of fibrils formed by α-synuclein hereditary disease mutant H50Q reveal new polymorphs. *Nature Structural & Molecular Biology*, *26*, 1044–1052. https://doi.org/10.1038/s41594-019-0322-y

Braak, H., de Vos, R. A. I., Bohl, J., & del Tredici, K. (2006). Gastric α-synuclein immunoreactive inclusions in Meissner's and Auerbach's plexuses in cases staged for Parkinson's disease-related brain pathology. *Neuroscience Letters*, *396*, 67–72. https://doi.org/10.1016/j.neulet.2005.11.012

Braak, H., del Tredici, K., Rüb, U., de Vos, R. A. I., Steur, E. N. H. J., & Braak, E. (2003). Staging of brain pathology related to sporadic Parkinson's disease. *Neurobiology of Aging*, *24*, 197–211. https://doi.org/10.1016/S0197-4580(02)00065-9

Braak, H., Rüb, U., Gai, W. P., & del Tredici, K. (2003). Idiopathic Parkinson's disease: Possible routes by which vulnerable neuronal types may be subject to neuroinvasion by an unknown pathogen. *Journal of Neural Transmission*, *110*, 517–536. https://doi.org/10.1007/s00702-002-0808-2

Brandel, J.-P., Vlaicu, M. B., Culeux, A., Belondrade, M., Bougard, D., Grznarova, K., Denouel, A., Plu, I., Bouaziz-Amar, E., Seilhean, D., Levasseur, M., & Haïk, S. (2020). Variant creutzfeldt-jakob disease diagnosed 7.5 years after occupational exposure. *New England Journal of Medicine*, *383*, 83–85. https://doi.org/10.1056/NEJMc2000687

Breen, D. P., Halliday, G. M., & Lang, A. E. (2019). Gut–brain axis and the spread of α-synuclein pathology: Vagal highway or dead end? *Movement Disorders*, *34*, 307–316. https://doi.org/10.1002/mds.27556

Brehme, M., Voisine, C., Rolland, T., Wachi, S., Soper, J. H., Zhu, Y., Orton, K., Villella, A., Garza, D., & Vidal, M. (2014). A chaperome subnetwork safeguards proteostasis in aging and neurodegenerative disease. *Cell Reports*, *9*, 1135–1150.

Breid, S., Bernis, M. E., Babila, J. T., Garza, M. C., Wille, H., & Tamgüney, G. (2016). Neuroinvasion of α-synuclein prionoids after intraperitoneal and intraglossal inoculation. *Journal of Virology*, *90*, 9182–9193. https://doi.org/10.1128/JVI.01399-16

Brundin, P., & Melki, R. (2017). Prying into the prion hypothesis for Parkinson's disease. *Journal of Neuroscience*, *37*, 9808–9818. https://doi.org/10.1523/JNEUROSCI.1788-16.2017

Bu, J., Liu, J., Liu, K., & Wang, Z. (2019). Diagnostic utility of gut α-synuclein in Parkinson's disease: A systematic review and meta-analysis. *Behavioural Brain Research*, *364*, 340–347. https://doi.org/10.1016/j.bbr.2019.02.039

Carabotti, M., Scirocco, A., Maselli, M. A., & Severi, C. (2015). The gut-brain axis: Interactions between enteric microbiota, central and enteric nervous systems. *Annals of Gastroenterology*, *28*, 203–209.

Cenit, M. C., Sanz, Y., & Codoñer-Franch, P. (2017). Influence of gut microbiota on neuropsychiatric disorders. *World Journal of Gastroenterology*, *23*, 5486. https://doi.org/10.3748/wjg.v23.i30.5486

Cersosimo, M. G. (2015). Gastrointestinal biopsies for the diagnosis of alpha-synuclein pathology in Parkinson's disease. *Gastroenterology Research and Practice*, *2015*, 476041.

Cersosimo, M. G., Raina, G. B., Pecci, C., Pellene, A., Calandra, C. R., Gutiérrez, C., Micheli, F. E., & Benarroch, E. E. (2013). Gastrointestinal manifestations in Parkinson's disease: Prevalence and occurrence before motor symptoms. *Journal of Neurology*, *260*, 1332–1338. https://doi.org/10.1007/s00415-012-6801-2

Chahine, L. M., Beach, T. G., Brumm, M. C., Adler, C. H., Coffey, C. S., Mosovsky, S., Caspell-Garcia, C., Serrano, G. E., Munoz, D. G., White, C. L., Crary, J. F., Jennings, D., Taylor, P., Foroud, T., Arnedo, V., Kopil, C. M., Riley, L., Dave, K. D., & Mollenhauer, B. (2020). In vivo distribution of α-synuclein in multiple tissues and biofluids in Parkinson disease. *Neurology*, *95*, e1267–e1284.

Challis, C., Hori, A., Sampson, T. R., Yoo, B. B., Challis, R. C., Hamilton, A. M., Mazmanian, S. K., Volpicelli-Daley, L. A., & Gradinaru, V. (2020). Gut-seeded α-synuclein fibrils promote gut dysfunction and brain pathology specifically in aged mice. *Nature Neuroscience*, *23*, 327–336. https://doi.org/10.1038/s41593-020-0589-7

Chandra, R., Hiniker, A., Kuo, Y.-M., Nussbaum, R. L., & Liddle, R. A. (2017). α-Synuclein in gut endocrine cells and its implications for Parkinson's disease. *JCI Insight*, *2*, e92295. https://doi.org/10.1172/jci.insight.92295

Chartier-Harlin, M.-C., Kachergus, J., Roumier, C., Mouroux, V., Douay, X., Lincoln, S., Levecque, C., Larvor, L., Andrieux, J., Hulihan, M., Waucquier, N., Defebvre, L., Amouyel, P., Farrer, M., & Destée, A. (2004). α-synuclein locus duplication as a cause of familial Parkinson's disease. *The Lancet*, *364*, 1167–1169. https://doi.org/10.1016/S0140-6736(04)17103-1

Cherian, A., & Divya, K. P. (2020). Genetics of Parkinson's disease. *Acta Neurologica Belgica*, *120*, 1297–1305. https://doi.org/10.1007/s13760-020-01473-5

Chung, S. J., Kim, J., Lee, H. J., Ryu, H.-S., Kim, K., Lee, J. H., Jung, K. W., Kim, M. J., Kim, M.-J., Kim, Y. J., Yun, S.-C., Lee, J.-Y., Hong, S.-M., & Myung, S.-J. (2016). Alpha-synuclein in gastric and colonic mucosa in Parkinson's disease: Limited role as a biomarker. *Movement Disorders*, *31*.

Collinge, J. (2016). Mammalian prions and their wider relevance in neurodegenerative diseases. *Nature*, *539*, 217–226. https://doi.org/10.1038/nature20415

Compta, Y., & Revesz, T. (2021). Neuropathological and biomarker findings in Parkinson's disease and Alzheimer's disease: From protein aggregates to synaptic dysfunction. *Journal of Parkinson's Disease*, *11*, 107–121. https://doi.org/10.3233/JPD-202323

Darweesh, S. K. L., Verlinden, V. J. A., Stricker, B. H., Hofman, A., Koudstaal, P. J., & Ikram, M. A. (2016). Trajectories of prediagnostic

functioning in Parkinson's disease. *Brain*, *140*, 429–441. https://doi.org/10.1093/brain/aww291

Das, S. K., Misra, A. K., Ray, B. K., Hazra, A., Ghosal, M. K., Chaudhuri, A., Roy, T., Banerjee, T. K., & Raut, D. K. (2010). Epidemiology of Parkinson disease in the city of Kolkata, India: A community-based study. *Neurology*, *75*, 1362–1369. https://doi.org/10.1212/WNL.0b013e3181f735a7

de la Fuente-Fernandez, R., Schulzer, M., Mak, E., Kishore, A., & Calne, D. B. (1998). The role of the Lewy body in idiopathic Parkinsonism. *Parkinsonism & Related Disorders*, *4*, 73–77. https://doi.org/10.1016/S1353-8020(98)00016-9

del Tredici, K., Rub, U., de Vos, R. A., Bohl, J. R., & Braak, H. (2002). Where does parkinson disease pathology begin in the brain? *Journal of Neuropathology and Experimental Neurology*, *61*, 413–426. https://doi.org/10.1093/jnen/61.5.413

Dickson, D. W. (2018). Neuropathology of Parkinson disease. *Parkinsonism & Related Disorders*, *46*, S30–S33. https://doi.org/10.1016/j.parkreldis.2017.07.033

Doi, H., Sakakibara, R., Sato, M., Masaka, T., Kishi, M., Tateno, A., Tateno, F., Tsuyusaki, Y., & Takahashi, O. (2012). Plasma levodopa peak delay and impaired gastric emptying in Parkinson's disease. *Journal of the Neurological Sciences*, *319*, 86–88. https://doi.org/10.1016/j.jns.2012.05.010

Dorsey, E. R., Elbaz, A., Nichols, E., Abd-Allah, F., Abdelalim, A., Adsuar, J. C., Ansha, M. G., Brayne, C., Choi, J.-Y., Collado-Mateo, D., Dahodwala, N., Do, H. P., Edessa, D., Endres, M., Fereshtehnejad, S.-M., Foreman, K. J., Gankpe, F. G., Gupta, R., Hankey, G. J., … Murray, C. J. L. (2018). Global, regional, and national burden of Parkinson's disease, 1990–2016: A systematic analysis for the Global Burden of Disease Study 2016. *The Lancet Neurology*, *17*, 939–953. https://doi.org/10.1016/S1474-4422(18)30295-3

Duda, J. E., Giasson, B. I., Mabon, M. E., Miller, D. C., Golbe, L. I., Lee, V.-M.-Y., & Trojanowski, J. Q. (2002). Concurrence of α-synuclein and tau brain pathology in the Contursi kindred. *Acta Neuropathologica*, *104*, 7–11. https://doi.org/10.1007/s00401-002-0563-3

Engelender, S., & Isacson, O. (2017). The threshold theory for Parkinson's disease. *Trends in Neurosciences*, *40*, 4–14. https://doi.org/10.1016/j.tins.2016.10.008

Falcon, B., Zivanov, J., Zhang, W., Murzin, A. G., Garringer, H. J., Vidal, R., Crowther, R. A., Newell, K. L., Ghetti, B., Goedert, M., & Scheres, S. H. W. (2019). Novel tau filament fold in chronic traumatic encephalopathy encloses hydrophobic molecules. *Nature*, *568*, 420–423. https://doi.org/10.1038/s41586-019-1026-5

Flavin, W. P., Bousset, L., Green, Z. C., Chu, Y., Skarpathiotis, S., Chaney, M. J., Kordower, J. H., Melki, R., & Campbell, E. M. (2017). Endocytic vesicle rupture is a conserved mechanism of cellular invasion by amyloid proteins. *Acta Neuropathologica*, *134*, 629–653. https://doi.org/10.1007/s00401-017-1722-x

Fusco, G., de Simone, A., Gopinath, T., Vostrikov, V., Vendruscolo, M., Dobson, C. M., & Veglia, G. (2014). Direct observation of the three regions in α-synuclein that determine its membrane-bound behaviour. *Nature Communications*, *5*, 1–8. https://doi.org/10.1038/ncomms4827

Ganguli, M., Chandra, V., Kamboh, M. I., Johnston, J. M., Dodge, H. H., Thelma, B. K., Juyal, R. C., Pandav, R., Belle, S. H., & DeKosky, S. T. (2000). Apolipoprotein E polymorphism and Alzheimer disease: The Indo-US Cross-National Dementia Study. *Archives of Neurology*, *57*, 824–830. https://doi.org/10.1001/archneur.57.6.824

Gaspar, R., Meisl, G., Buell, A. K., Young, L., Kaminski, C. F., Knowles, T. P. J., Sparr, E., & Linse, S. (2017). Secondary nucleation of monomers on fibril surface dominates α-synuclein aggregation and provides autocatalytic amyloid amplification. *Quarterly Reviews of Biophysics*, *50*, e6.

Giasson, B. I., Murray, I. V. J., Trojanowski, J. Q., & Lee, V.-M.-Y. (2001). A hydrophobic stretch of 12 amino acid residues in the middle of α-synuclein is essential for filament assembly. *Journal of Biological Chemistry*, *276*, 2380–2386. https://doi.org/10.1074/jbc.M008919200

Gibbs, C. J., Gajdusek, D. C., Asher, D. M., Alpers, M. P., Beck, E., Daniel, P. M., & Matthews, W. B. (1968). Creutzfeldt-Jakob disease (spongiform encephalopathy): Transmission to the chimpanzee. *Science*, *161*, 388–389. https://doi.org/10.1126/science.161.3839.388

Govindaraju, R., Karki, R., Chandrashekarappa, J., Santhanam, M., Shankar, A. K. K., Joshi, H. K., & Divakar, G. (2019). Enhanced water dispersibility of curcumin encapsulated in alginate-polysorbate 80 nano particles and bioavailability in healthy human volunteers. *Pharm Nanotechnol*, *7*, 39–56. https://doi.org/10.2174/2211738507666190122121242

Gray, M. T., Munoz, D. G., Gray, D. A., Schlossmacher, M. G., & Woulfe, J. M. (2014). Alpha-synuclein in the appendiceal mucosa of neurologically intact subjects. *Movement Disorders*, *29*, 991–998. https://doi.org/10.1002/mds.25779

Grimes, D. A., & Schulz, K. F. (2012). False alarms and pseudo-epidemics: The limitations of observational epidemiology. *Obstetrics & Gynecology*, *120*, 920–927. https://doi.org/10.1097/AOG.0b013e31826af61a

Gustot, A., Gallea, J. I., Sarroukh, R., Celej, M. S., Ruysschaert, J.-M., & Raussens, V. (2015). Amyloid fibrils are the molecular trigger of inflammation in Parkinson's disease. *Biochemical Journal*, *471*, 323–333. https://doi.org/10.1042/BJ20150617

Hashimoto, M., Kawahara, K., Bar-On, P., Rockenstein, E., Crews, L., & Masliah, E. (2004). The role of α-synuclein assembly and metabolism in the pathogenesis of Lewy body disease. *Journal of Molecular Neuroscience*, *24*, 343–352.

Heetun, Z. S., & Quigley, E. M. M. (2012). Gastroparesis and Parkinson's disease: A systematic review. *Parkinsonism & Related Disorders*, *18*, 433–440. https://doi.org/10.1016/j.parkreldis.2011.12.004

Hilton, D., Stephens, M., Kirk, L., Edwards, P., Potter, R., Zajicek, J., Broughton, E., Hagan, H., & Carroll, C. (2014). Accumulation of α-synuclein in the bowel of patients in the pre-clinical phase of Parkinson's disease. *Acta Neuropathologica*, *127*, 235–241. https://doi.org/10.1007/s00401-013-1214-6

Holmqvist, S., Chutna, O., Bousset, L., Aldrin-Kirk, P., Li, W., Björklund, T., Wang, Z.-Y., Roybon, L., Melki, R., & Li, J.-Y. (2014). Direct evidence of Parkinson pathology spread from the gastrointestinal tract to the brain in rats. *Acta Neuropathologica*, *128*, 805–820. https://doi.org/10.1007/s00401-014-1343-6

Horsager, J., Andersen, K. B., Knudsen, K., Skjærbæk, C., Fedorova, T. D., Okkels, N., Schaeffer, E., Bonkat, S. K., Geday, J., Otto, M., Sommerauer, M., Danielsen, E. H., Bech, E., Kraft, J., Munk, O. L., Hansen, S. D., Pavese, N., Göder, R., Brooks, D. J., … Borghammer, P. (2020). Brain-first versus body-first Parkinson's disease: A multimodal imaging case-control study. *Brain*, *143*, 3077–3088. https://doi.org/10.1093/brain/awaa238

Houser, M. C., & Tansey, M. G. (2017). The gut-brain axis: Is intestinal inflammation a silent driver of Parkinson's disease pathogenesis?

NPJ Parkinson's Disease, *3*, 1–9. https://doi.org/10.1038/s4153 1-016-0002-0

Hsu, L. J., Sagara, Y., Arroyo, A., Rockenstein, E., Sisk, A., Mallory, M., Wong, J., Takenouchi, T., Hashimoto, M., & Masliah, E. (2000). α-Synuclein promotes mitochondrial deficit and oxidative stress. *The American Journal of Pathology*, *157*, 401–410.

Ibanez, P., Bonnet, A. M., Debarges, B., Lohmann, E., Tison, F., Agid, Y., Dürr, A., Brice, A., Pollak, P., & Group, F. P. D. G. S. (2004). Causal relation between α-synuclein locus duplication as a cause of familial Parkinson's disease. *The Lancet*, *364*, 1169–1171. https://doi.org/10.1016/S0140-6736(04)17104-3

Ingelsson, M. (2016). Alpha-synuclein oligomers—neurotoxic molecules in Parkinson's disease and other lewy body disorders. *Frontiers in Neuroscience*, *10*. https://doi.org/10.3389/fnins.2016.00408

Irwin, D. J., Abrams, J. Y., Schonberger, L. B., Leschek, E. W., Mills, J. L., Lee, V.-M.-Y., & Trojanowski, J. Q. (2013). Evaluation of potential infectivity of Alzheimer and Parkinson disease proteins in recipients of cadaver-derived human growth hormone. *JAMA Neurology*, *70*, 462–468. https://doi.org/10.1001/jamaneurol.2013.1933

Jha, N. N., Ghosh, D., Das, S., Anoop, A., Jacob, R. S., Singh, P. K., Ayyagari, N., Namboothiri, I. N. N., & Maji, S. K. (2016). Effect of curcumin analogs onα-synuclein aggregation and cytotoxicity. *Scientific Reports*, *6*, 1–15. https://doi.org/10.1038/srep28511

Jiang, T.-F., Zhang, Y.-J., Zhou, H.-Y., Wang, H.-M., Tian, L.-P., Liu, J., Ding, J.-Q., & Chen, S.-D. (2013). Curcumin ameliorates the neurodegenerative pathology in A53T α-synuclein cell model of Parkinson's disease through the downregulation of mTOR/p70S6K signaling and the recovery of macroautophagy. *Journal of Neuroimmune Pharmacology*, *8*, 356–369. https://doi.org/10.1007/s11481-012-9431-7

Jucker, M., & Walker, L. C. (2013). Self-propagation of pathogenic protein aggregates in neurodegenerative diseases. *Nature*, *501*, 45–51. https://doi.org/10.1038/nature12481

Kamelabad, M. R., Sardroodi, J. J., & Ebrahimzadeh, A. R. (2020). The interaction of curcumin and rosmarinic acid with non-amyloid-component domain of alpha-synuclein: A molecular dynamics study. *ChemistrySelect*, *5*, 3312–3320. https://doi.org/10.1002/slct.201904799

Keshavarzian, A., Green, S. J., Engen, P. A., Voigt, R. M., Naqib, A., Forsyth, C. B., Mutlu, E., & Shannon, K. M. (2015). Colonic bacterial composition in Parkinson's disease. *Movement Disorders*, *30*, 1351–1360. https://doi.org/10.1002/mds.26307

Killinger, B. A., Madaj, Z., Sikora, J. W., Rey, N., Haas, A. J., Vepa, Y., Lindqvist, D., Chen, H., Thomas, P. M., Brundin, P., Brundin, L., & Labrie, V. (2018). The vermiform appendix impacts the risk of developing Parkinson's disease. *Science Translational Medicine*, *10*, eaar5280. https://doi.org/10.1126/scitranslmed.aar5280

Kingsbury, A. E., Bandopadhyay, R., Silveira-Moriyama, L., Ayling, H., Kallis, C., Sterlacci, W., Maeir, H., Poewe, W., & Lees, A. J. (2010). Brain stem pathology in Parkinson's disease: An evaluation of the Braak staging model. *Movement Disorders*, *25*, 2508–2515. https://doi.org/10.1002/mds.23305

Kobayashi, Y., Sugahara, H., Shimada, K., Mitsuyama, E., Kuhara, T., Yasuoka, A., Kondo, T., Abe, K., & Xiao, J. (2017). Therapeutic potential of Bifidobacterium breve strain A1 for preventing cognitive impairment in Alzheimer's disease. *Scientific Reports*, *7*, 1–10. https://doi.org/10.1038/s41598-017-13368-2

Kochar, N. I., Gonge, K., Chandewar, A. V. & Khadse, C. (2014). Curcumin ameliorates gastrointestinal dysfunction and oxidative damage in diabetic rats. *International Journal of Pharmacology Research*, *4*, 53–60.

Kochhar, K. P. (2008). Dietary spices in health and diseases: I. *Indian Journal of Physiology and Pharmacology*, *52*, 106–122.

Kordower, J. H., Chu, Y., Hauser, R. A., Freeman, T. B., & Olanow, C. W. (2008). Lewy body–like pathology in long-term embryonic nigral transplants in Parkinson's disease. *Nature Medicine*, *14*, 504–506. https://doi.org/10.1038/nm1747

Kumar, V. (2006). Potential medicinal plants for CNS disorders: An overview. *Phytotherapy Research*, *20*, 1023–1035.

Lashuel, H. A., Overk, C. R., Oueslati, A., & Masliah, E. (2013). The many faces of α-synuclein: From structure and toxicity to therapeutic target. *Nature Reviews. Neuroscience*, *14*, 38–48.

Lee, J. M., Derkinderen, P., Kordower, J. H., Freeman, R., Munoz, D. G., Kremer, T., Zago, W., Hutten, S. J., Adler, C. H., Serrano, G. E., & Beach, T. G. (2017). The search for a peripheral biopsy indicator of α-synuclein pathology for Parkinson disease. *Journal of Neuropathology & Experimental Neurology*, *76*, 2–15. https://doi.org/10.1093/jnen/nlw103

Li, J.-Y., Englund, E., Holton, J. L., Soulet, D., Hagell, P., Lees, A. J., Lashley, T., Quinn, N. P., Rehncrona, S., Björklund, A., Widner, H., Revesz, T., Lindvall, O., & Brundin, P. (2008). Lewy bodies in grafted neurons in subjects with Parkinson's disease suggest host-to-graft disease propagation. *Nature Medicine*, *14*, 501–503. https://doi.org/10.1038/nm1746

Liautard, J.-P. (1991). Are prions misfolded molecular chaperones? *FEBS Letters*, *294*, 155–157. https://doi.org/10.1016/0014-5793(91)80657-O

Lionnet, A., Leclair-Visonneau, L., Neunlist, M., Murayama, S., Takao, M., Adler, C. H., Derkinderen, P., & Beach, T. G. (2018). Does Parkinson's disease start in the gut? *Acta Neuropathologica*, *135*, 1–12. https://doi.org/10.1007/s00401-017-1777-8

Liu, B., Fang, F., Pedersen, N. L., Tillander, A., Ludvigsson, J. F., Ekbom, A., Svenningsson, P., Chen, H., & Wirdefeldt, K. (2017). Vagotomy and Parkinson disease: A Swedish register–based matched-cohort study. *Neurology*, *88*, 1996–2002. https://doi.org/10.1212/WNL.0000000000003961

Liu, B., Fang, F., Ye, W., & Wirdefeldt, K. (2020). Appendectomy, tonsillectomy and Parkinson's disease risk: A Swedish register-based study. *Frontiers in Neurology*, *11*, 510. https://doi.org/10.3389/fneur.2020.00510

Liu, Z., Yu, Y., Li, X., Ross, C. A., & Smith, W. W. (2011). Curcumin protects against A53T alpha-synuclein-induced toxicity in a PC12 inducible cell model for Parkinsonism. *Pharmacological Research*, *63*, 439–444. https://doi.org/10.1016/j.phrs.2011.01.004

Lv, Z., Qi, H., Wang, L., Fan, X., Han, F., Wang, H., & Bi, S. (2014). Vitamin D status and Parkinson's disease: A systematic review and meta-analysis. *Neurological Sciences*, *35*, 1723–1730. https://doi.org/10.1007/s10072-014-1821-6

Ma, J., Gao, J., Wang, J., & Xie, A. (2019). Prion-like mechanisms in Parkinson's disease. *Frontiers in Neuroscience*, *13*, 552. https://doi.org/10.3389/fnins.2019.00552

Maes, M. (2008). The cytokine hypothesis of depression: Inflammation, oxidative & nitrosative stress (IO&NS) and leaky gut as new targets for adjunctive treatments in depression. *Neuroendocrinology Letters*, *29*, 287–291.

Marrinan, S., Emmanuel, A. V., & Burn, D. J. (2014). Delayed gastric emptying in Parkinson's disease. *Movement Disorders*, *29*, 23–32. https://doi.org/10.1002/mds.25708

Masters, C. L., Gajdusek, D. C., & Gibbs, C. J Jr (1981). Creutzfeldt-Jakob disease virus isolations from the Gerstmann-Sträussler syndrome: With an analysis of the various forms of amyloid plaque deposition in the virus-induced spongiform encephalopathies. *Brain*, *104*, 559–588. https://doi.org/10.1093/brain/104.3.559

Mendes, A., Gonçalves, A., Vila-Chã, N., Moreira, I., Fernandes, J., Damásio, J., Teixeira-Pinto, A., Taipa, R., Lima, A. B., & Cavaco, S. (2015). Appendectomy may delay Parkinson's disease onset. *Movement Disorders*, *30*, 1404–1407. https://doi.org/10.1002/mds.26311

Minakaki, G., Krainc, D., & Burbulla, L. F. (2020). The convergence of alpha-synuclein, mitochondrial, and lysosomal pathways in vulnerability of midbrain dopaminergic neurons in Parkinson's disease. *Frontiers in Cell and Developmental Biology*, *8*, 580634-undefined. https://doi.org/10.3389/fcell.2020.580634

Miyasaki, J. M., Martin, W., Suchowersky, O., Weiner, W. J., & Lang, A. E. (2002). Practice parameter: Initiation of treatment for Parkinson's disease: An evidence-based review: Report of the Quality Standards Subcommittee of the American Academy of Neurology. *Neurology*, *58*, 11–17. https://doi.org/10.1212/WNL.58.1.11

Mukherjee, A., Biswas, A., & Das, S. K. (2016). Gut dysfunction in Parkinson's disease. *World Journal of Gastroenterology*, *22*, 5742. https://doi.org/10.3748/wjg.v22.i25.5742

Mulak, A., & Bonaz, B. (2015). Brain-gut-microbiota axis in Parkinson's disease. *World Journal of Gastroenterology*, *21*, 10609–10620. https://doi.org/10.3748/wjg.v21.i37.10609

Mythri, R. B., & Srinivas Bharath, M. M. (2012). Curcumin: A potential neuroprotective agent in Parkinson's disease. *Current Pharmaceutical Design*, *18*, 91–99.

Ng, T. P., Chiam, P. C., Lee, T., Chua, H. C., Lim, L., & Kua, E. H. (2006). Curry consumption and cognitive function in the elderly. *American Journal of Epidemiology*, *164*, 898–906. https://doi.org/10.1093/aje/kwj267

Niu, H., Shen, L., Li, T., Ren, C., Ding, S., Wang, L., Zhang, Z., Liu, X., Zhang, Q., Geng, D., Wu, X., & Li, H. (2018). Alpha-synuclein overexpression in the olfactory bulb initiates prodromal symptoms and pathology of Parkinson's disease. *Translational Neurodegeneration*, *7*, 25. https://doi.org/10.1186/s40035-018-0128-6

O'Donovan, S. M., Crowley, E. K., Brown, J. R., O'Sullivan, O., O'Leary, O. F., Timmons, S., Nolan, Y. M., Clarke, D. J., Hyland, N. P., Joyce, S. A., Sullivan, A. M., & O'Neill, C. (2020). Nigral overexpression of α-synuclein in a rat Parkinson's disease model indicates alterations in the enteric nervous system and the gut microbiome. *Neurogastroenterology and Motility*, *32*, e13726. https://doi.org/10.1111/nmo.13726

Olanow, C. W., & Brundin, P. (2013). Parkinson's disease and alpha synuclein: Is Parkinson's disease a prion-like disorder? *Movement Disorders*, *28*, 31–40. https://doi.org/10.1002/mds.25373

Palacios, N., Hughes, K. C., Cereda, E., Schwarzschild, M. A., & Ascherio, A. (2018). Appendectomy and risk of Parkinson's disease in two large prospective cohorts of men and women. *Movement Disorders*, *33*, 1492–1496. https://doi.org/10.1002/mds.109

Panahi, Y., Saadat, A., Beiraghdar, F., & Sahebkar, A. (2014). Adjuvant therapy with bioavailability-boosted curcuminoids suppresses systemic inflammation and improves quality of life in patients with solid tumors: A randomized double-blind placebo-controlled trial. *Phytotherapy Research*, *28*, 1461–1467. https://doi.org/10.1002/ptr.5149

Pandey, N., Strider, J., Nolan, W. C., Yan, S. X., & Galvin, J. E. (2008). Curcumin inhibits aggregation of α-synuclein. *Acta Neuropathologica*, *115*, 479–489. https://doi.org/10.1007/s00401-007-0332-4

Pasricha, P. J., & Parkman, H. P. (2015). Gastroparesis: Definitions and diagnosis. *Gastroenterology Clinics*, *44*, 1–7. https://doi.org/10.1016/j.gtc.2014.11.001

Peterson, L. W., & Artis, D. (2014). Intestinal epithelial cells: Regulators of barrier function and immune homeostasis. *Nature Reviews Immunology*, *14*, 141–153. https://doi.org/10.1038/nri3608

Pfeiffer, R. F. (2003). Gastrointestinal dysfunction in Parkinson's disease. *The Lancet Neurology*, *2*. https://doi.org/10.1016/S1474-4422(03)00307-7

Prusiner, S. B. (1982). Novel proteinaceous infectious particles cause scrapie. *Science*, *216*, 136–144. https://doi.org/10.1126/science.6801762

Prusiner, S. B. (2001). Neurodegenerative diseases and prions. *New England Journal of Medicine*, *344*. https://doi.org/10.1056/NEJM200105173442006

Quigley, E. M. M. (2017). Microbiota-brain-gut axis and neurodegenerative diseases. *Current Neurology and Neuroscience Reports*, *17*, 94. https://doi.org/10.1007/s11910-017-0802-6

Razdan, S., Kaul, R. L., Motta, A., Kaul, S., & Bhatt, R. K. (1994). Prevalence and pattern of major neurological disorders in rural Kashmir (India) in 1986. *Neuroepidemiology*, *13*, 113–119. https://doi.org/10.1159/000110368

Rietdijk, C. D., Perez-Pardo, P., Garssen, J., van Wezel, R. J. A., & Kraneveld, A. D. (2017). Exploring Braak's hypothesis of Parkinson's disease. *Frontiers in Neurology*, *8*, 37. https://doi.org/10.3389/fneur.2017.00037

Ruffmann, C., & Parkkinen, L. (2016). Gut feelings about alpha-synuclein in gastrointestinal biopsies: Biomarker in the making? *Movement Disorders*, *31*, 193–202.

Santini, A., Tenore, G. C., & Novellino, E. (2017). Nutraceuticals: A paradigm of proactive medicine. *European Journal of Pharmaceutical Sciences*, *96*, 53–61. https://doi.org/10.1016/j.ejps.2016.09.003

Savica, R., Carlin, J. M., Grossardt, B. R., Bower, J. H., Ahlskog, J. E., Maraganore, D. M., Bharucha, A. E., & Rocca, W. A. (2009). Medical records documentation of constipation preceding Parkinson disease: A case-control study. *Neurology*, *73*, 1752–1758. https://doi.org/10.1212/WNL.0b013e3181c34af5

Schaeffer, E., Kluge, A., Böttner, M., Zunke, F., Cossais, F., Berg, D., & Arnold, P. (2020). Alpha synuclein connects the gut-brain axis in Parkinson's disease patients – A view on clinical aspects, cellular pathology and analytical methodology. *Frontiers in Cell and Developmental Biology*, *8*, 573696-undefined. https://doi.org/10.3389/fcell.2020.573696

Schenck, C. H., Boeve, B. F., & Mahowald, M. W. (2013). Delayed emergence of a parkinsonian disorder or dementia in 81% of older men initially diagnosed with idiopathic rapid eye movement sleep behavior disorder: A 16-year update on a previously reported series. *Sleep Medicine*, *14*, 744–748. https://doi.org/10.1016/j.sleep.2012.10.009

Schweighauser, M., Shi, Y., Tarutani, A., Kametani, F., Murzin, A. G., Ghetti, B., Matsubara, T., Tomita, T., Ando, T., Hasegawa, K., Murayama, S., Yoshida, M., Hasegawa, M., Scheres, S. H. W., & Goedert, M. (2020). Structures of α-synuclein filaments from multiple system atrophy. *Nature*, *585*, 464–469. https://doi.org/10.1038/s41586-020-2317-6

Seeras, K., Qasawa, R. N., & Prakash, S. (2019). Truncal vagotomy. In *StatPearls [Internet]*. StatPearls Publishing.

Seike, N., Yokoseki, A., Takeuchi, R., Saito, K., Miyahara, H., Miyashita, A., Ikeda, T., Aida, I., Nakajima, T., Kanazawa, M., Wakabayashi,

M., Toyoshima, Y., Takahashi, H., Matsumoto, R., Toda, T., Onodera, O., Ishikawa, A., Ikeuchi, T., & Kakita, A. (2021). Genetic variations and neuropathologic features of patients with PRKN mutations. *Movement Disorders*. https://doi.org/10.1002/mds.28521

Shannon, K. M., Keshavarzian, A., Mutlu, E., Dodiya, H. B., Daian, D., Jaglin, J. A., & Kordower, J. H. (2012). Alpha-synuclein in colonic submucosa in early untreated Parkinson's disease. *Movement Disorders*, *27*, 709–715. https://doi.org/10.1002/mds.23838

Sharma, N., & Nehru, B. (2018). Curcumin affords neuroprotection and inhibits α-synuclein aggregation in lipopolysaccharide-induced Parkinson's disease model. *Inflammopharmacology*, *26*, 349–360. https://doi.org/10.1007/s10787-017-0402-8

Sheard, J. M., Ash, S., Mellick, G. D., Silburn, P. A., & Kerr, G. K. (2013). Malnutrition in a sample of community-dwelling people with Parkinson's disease. *PLoS One*, *8*(1), e53290. https://doi.org/10.1371/journal.pone.0053290

Singh, P. K., Kotia, V., Ghosh, D., Mohite, G. M., Kumar, A., & Maji, S. K. (2013). Curcumin modulates α-synuclein aggregation and toxicity. *ACS Chemical Neuroscience*, *4*, 393–407. https://doi.org/10.1021/cn3001203

Siruguri, V., & Bhat, R. V. (2015). Assessing intake of spices by pattern of spice use, frequency of consumption and portion size of spices consumed from routinely prepared dishes in southern India. *Nutrition Journal*, *14*, 7. https://doi.org/10.1186/1475-2891-14-7

Song, W.-B., Wang, Y.-Y., Meng, F.-S., Zhang, Q.-H., Zeng, J.-Y., Xiao, L.-P., Yu, X.-P., Peng, D.-D., Su, L., Xiao, B., & Zhang, Z.-S. (2010). Curcumin protects intestinal mucosal barrier function of rat enteritis via activation of MKP-1 and attenuation of p38 and NF-κB activation. *PLoS One*, *5*(9), e12969. https://doi.org/10.1371/journal.pone.0012969

Sparreboom, A., Cox, M. C., Acharya, M. R., & Figg, W. D. (2004). Herbal remedies in the United States: Potential adverse interactions with anticancer agents. *Journal of Clinical Oncology*, *22*, 2489–2503. https://doi.org/10.1200/JCO.2004.08.182

Srinivasan, M. (1972). Effect of curcumin on blood sugar as seen in a diabetic subject. *Indian Journal of Medical Sciences*, *26*, 269–270.

Stokholm, M. G., Danielsen, E. H., Hamilton-Dutoit, S. J., & Borghammer, P. (2016). Pathological α-synuclein in gastrointestinal tissues from prodromal Parkinson disease patients. *Annals of Neurology*, *79*, 940–949. https://doi.org/10.1002/ana.24648

Surathi, P., Jhunjhunwala, K., Yadav, R., & Pal, P. K. (2016). Research in Parkinson's disease in India: A review. *Annals of Indian Academy of Neurology*, *19*, 9–20. https://doi.org/10.4103/0972-2327.167713

Surmeier, D. J., Obeso, J. A., & Halliday, G. M. (2017). Parkinson's disease is not simply a prion disorder. *Journal of Neuroscience*, *37*, 9799–9807. https://doi.org/10.1523/JNEUROSCI.1787-16.2017

Svensson, E., Henderson, V. W., Szépligeti, S., Stokholm, M. G., Klug, T. E., Sørensen, H. T., & Borghammer, P. (2018). Tonsillectomy and risk of Parkinson's disease: A danish nationwide population-based cohort study. *Movement Disorders*, *33*, 321–324. https://doi.org/10.1002/mds.27253

Svensson, E., Horváth-Puhó, E., Stokholm, M. G., Sørensen, H. T., Henderson, V. W., & Borghammer, P. (2016). Appendectomy and risk of Parkinson's disease: A nationwide cohort study with more than 10 years of follow-up. *Movement Disorders*, *31*, 1918–1922. https://doi.org/10.1002/mds.26761

Svensson, E., Horváth-Puhó, E., Thomsen, R. W., Djurhuus, J. C., Pedersen, L., Borghammer, P., & Sørensen, H. T. (2015). Vagotomy and subsequent risk of Parkinson's disease. *Annals of Neurology*, *78*, 522–529. https://doi.org/10.1002/ana.24448

Swart, C., Haylett, W., Kinnear, C., Johnson, G., Bardien, S., & Loos, B. (2014). Neurodegenerative disorders: Dysregulation of a carefully maintained balance? *Experimental Gerontology*, *58*, 279–291. https://doi.org/10.1016/j.exger.2014.09.003

Tanaka, Y., Kato, T., Nishida, H., Yamada, M., Koumura, A., Sakurai, T., Hayashi, Y., Kimura, A., Hozumi, I., Araki, H., Murase, M., Nagaki, M., Moriwaki, H., & Inuzuka, T. (2011). Is there a delayed gastric emptying of patients with early-stage, untreated Parkinson's disease? An analysis using the 13 C-acetate breath test. *Journal of Neurology*, *258*, 421–426. https://doi.org/10.1007/s00415-010-5769-z

Tapal, A., & Tiku, P. K. (2012). Complexation of curcumin with soy protein isolate and its implications on solubility and stability of curcumin. *Food Chemistry*, *130*, 960–965. https://doi.org/10.1016/j.foodchem.2011.08.025

Thevaranjan, N., Puchta, A., Schulz, C., Naidoo, A., Szamosi, J. C., Verschoor, C. P., Loukov, D., Schenck, L. P., Jury, J., Foley, K. P., Schertzer, J. D., Larché, M. J., Davidson, D. J., Verdú, E. F., Surette, M. G., & Bowdish, D. M. E. (2017). Age-associated microbial dysbiosis promotes intestinal permeability, systemic inflammation, and macrophage dysfunction. *Cell Host & Microbe*, *21*, 455–466.e4. https://doi.org/10.1016/j.chom.2017.03.002

Tian, S., Guo, R., Wei, S., Kong, Y., Wei, X., Wang, W., Shi, X., & Jiang, H. (2016). Curcumin protects against the intestinal ischemia-reperfusion injury: Involvement of the tight junction protein ZO-1 and TNF-α related mechanism. *The Korean Journal of Physiology & Pharmacology*, *20*, 147–152. https://doi.org/10.4196/kjpp.2016.20.2.147

Tuttle, M. D., Comellas, G., Nieuwkoop, A. J., Covell, D. J., Berthold, D. A., Kloepper, K. D., Courtney, J. M., Kim, J. K., Barclay, A. M., Kendall, A., Wan, W., Stubbs, G., Schwieters, C. D., Lee, V. M. Y., George, J. M., & Rienstra, C. M. (2016). Solid-state NMR structure of a pathogenic fibril of full-length human α-synuclein. *Nature Structural & Molecular Biology*, *23*, 409. https://doi.org/10.1038/nsmb.3194

Tysnes, O., Kenborg, L., Herlofson, K., Steding-Jessen, M., Horn, A., Olsen, J. H., & Reichmann, H. (2015). Does vagotomy reduce the risk of Parkinson's disease? *Annals of Neurology*, *78*, 1011–1012. https://doi.org/10.1002/ana.24531

Ulusoy, A., Phillips, R. J., Helwig, M., Klinkenberg, M., Powley, T. L., & di Monte, D. A. (2017). Brain-to-stomach transfer of α-synuclein via vagal preganglionic projections. *Acta Neuropathologica*, *133*, 381–393. https://doi.org/10.1007/s00401-016-1661-y

Ulusoy, A., Rusconi, R., Pérez-Revuelta, B. I., Musgrove, R. E., Helwig, M., Winzen-Reichert, B., & di Monte, D. A. (2013). Caudo-rostral brain spreading of α-synuclein through vagal connections. *EMBO Molecular Medicine*, *5*, 1119–1127.

Uversky, V. N., & Eliezer, D. (2009). Biophysics of Parkinson's disease: Structure and aggregation of α-synuclein. *Current Protein and Peptide Science*, *10*, 483–499.

Visanji, N. P., Marras, C., Kern, D. S., al Dakheel, A., Gao, A., Liu, L. W. C., Lang, A. E., & Hazrati, L.-N. (2015). Colonic mucosal a-synuclein lacks specificity as a biomarker for Parkinson disease. *Neurology*, *84*, 609–616. https://doi.org/10.1212/WNL.0000000000001240

Wallen, Z. D., Appah, M., Dean, M. N., Sesler, C. L., Factor, S. A., Molho, E., Zabetian, C. P., Standaert, D. G., & Payami, H. (2020). Characterizing dysbiosis of gut microbiome in PD: Evidence for overabundance of opportunistic pathogens. *NPJ Parkinson's Disease*, *6*, 1–12. https://doi.org/10.1038/s41531-020-0112-6

Wickner, R. B., Edskes, H. K., Kryndushkin, D., McGlinchey, R., Bateman, D., & Kelly, A. (2011). Prion diseases of yeast: Amyloid

structure and biology. In J. Davey (Ed.), *Seminars in Cell & Developmental Biology* (pp. 469–475). Elsevier.

Wszolek, Z. K., Pfeiffer, R. F., Tsuboi, Y., Uitti, R. J., McComb, R. D., Stoessl, A. J., Strongosky, A. J., Zimprich, A., Müller-Myhsok, B., Farrer, M. J., Gasser, T., Calne, D. B., & Dickson, D. W. (2004). Autosomal dominant parkinsonism associated with variable synuclein and tau pathology. *Neurology*, *62*(9), 1619–1622. https://doi.org/10.1212/01.WNL.0000125015.06989.DB

Xiao, Y., Chen, X., Yang, L., Zhu, X., Zou, L., Meng, F., & Ping, Q. (2013). Preparation and oral bioavailability study of curcuminoid-loaded microemulsion. *Journal of Agricultural and Food Chemistry*, *61*, 3654–3660. https://doi.org/10.1021/jf400002x

Yoshita, M. (1998). Differentiation of idiopathic Parkinson's disease from striatonigral degeneration and progressive supranuclear palsy using iodine-123 meta-iodobenzylguanidine myocardial scintigraphy. *Journal of the Neurological Sciences*, *155*, 60–67. https://doi.org/10.1016/S0022-510X(97)00278-5

Zhang, W., Tarutani, A., Newell, K. L., Murzin, A. G., Matsubara, T., Falcon, B., Vidal, R., Garringer, H. J., Shi, Y., Ikeuchi, T., Murayama, S., Ghetti, B., Hasegawa, M., Goedert, M., & Scheres, S. H. W. (2020). Novel tau filament fold in corticobasal degeneration. *Nature*, *580*, 283–287. https://doi.org/10.1038/s41586-020-2043-0

CHAPTER 5: Discussion

5.1 Overview of main findings

The present study aimed to evaluate the neuroprotective effects of curcumin in a PINK1 model of dopamine toxicity and paraquat-induced cellular damage. We hypothesized that curcumin would act as a neuroprotective agent by improving cell viability and mitochondrial function in the model. Using RT-qPCR we found that *PINK1* was significantly upregulated in the mutant, however, no significant difference in *TH* gene expression was observed between groups. Although no dopamine was detected using LC-MS, higher levels of phenylalanine, a precursor of dopamine, were observed in the mutant compared to the WT and untransfected groups. We hypothesize that the presence of this precursor will subsequently lead to increased levels of dopamine. Paraquat significantly reduced cell viability in all transfected and untransfected groups, indicating cellular damage in the model. We observed that curcumin pre-treatment was unable to rescue the paraquat-induced decrease in cell viability and mitochondrial membrane potential in untransfected and transfected groups. Both WT PINK1 and mutant PINK1 significantly reduced mitochondrial membrane potential. Finally, comparing the effect of curcumin and nanocurcumin on cell viability, we found, interestingly, that nanocurcumin as well as the empty nanoparticle elicited toxicity. In fact, pre-treatment with nanocurcumin (prior to paraquat exposure) caused a 30 % greater loss in cell viability compared to the paraquat treatment alone. Conversely, the 'curcumin only' treatment significantly increased SH-SY5Y cell viability.

5.2 PD cellular model

In the present study, our attempts to produce a cellular PD model were partially successful. The genetic aspect of the model was verified as evidenced by increased *PINK1* expression in the mutant. Paraquat was shown to significantly reduce cell viability. However, dopamine toxicity could not be clearly verified due to failure to measure this compound directly and indirectly.

Genetic models typically involve the knockdown or knockout of PD-associated genes such as *SNCA*, *LRRK2*, *DJ-1*, *PINK1*, and *PRKN* (Chia, Tan & Chao, 2020), however, overexpression models are also useful in studying disease. Unlike knockouts and knockdowns, overexpression is not as excessive to result in catastrophic cell loss and thus can be considered a more 'subtle' genetic model. Gene overexpression leads to abundant target protein expression and can increase protein activity to cause a mutant phenotype. Since gene expression is tightly regulated, with small aberrations potentially causing pathological effects, forced overexpression of individual genes may prompt the cascade of disease-causing events to elucidate the connections between genes and their biological pathways (Prelich, 2012). Therefore, for the present study, a genetic *in vitro* model was chosen as an appropriate model of PD. This experimental model involved the transfection of human SH-SY5Y

83

neuroblastoma cells with *PINK1*. The SH-SY5Y cell line has been widely utilized in PD research and was derived in 1978 from the SK-N-SH cell line (Biedler et al., 1978). Although not strictly dopaminergic neurons, differentiated SH-SY5Y cells can become 'neuron-like' and may express the catecholamines dopamine and noradrenaline, as well as dopamine-related factors including TH, dopamine receptors, and transporters (Xie, Hu & Li, 2010). This makes SH-SY5Y cells a suitable candidate for studying neurodegenerative disorders such as PD, which is characterized by a loss of dopaminergic neurons. Currently, the basis of neuronal vulnerability to dopamine in PD is not well understood. Oxidation of excess dopamine that is not catabolized or packaged is known to contribute to oxidative stress and neurodegeneration in PD brains (Cobley, Fiorello & Bailey, 2018; Monzani et al., 2019). Finally, to represent the environmental triggers of PD, we included paraquat exposure in our model to induce mitochondrial dysfunction and reduce cell viability. Therefore, in the present study, we sought to create an SH-SY5Y cellular model of PD through paraquat exposure as well as overexpression of G309D *PINK1* which has been shown previously to upregulate dopamine in catecholaminergic cells (Zhou et al., 2014).

In the present study, the G309D PINK1 plasmid was successfully sequenced, while the WT plasmid could not be verified. The four different WT plasmids (WT-A, WT-B, WT-C, and WT-Z) revealed unexpected sequencing and banding patterns, and differed from the G309D mutant in more ways than the mutation site alone. Although the WT-Z DNA was successfully transformed into DH5α *E. coli,* its sequence could not be verified possibly due to recombination of the plasmid backbone without the insert, and thus could not be used in the study. In the absence of a verifiable WT plasmid, the only feasible option was to use the WT-B plasmid which was included in the same delivery as the verified mutant and could be easily propagated in *E. coli*. Therefore, we decided to continue the study with WT-B and Mutant-B, but keeping this as a consideration when interpreting results. Repetition of the experiments with a verified WT plasmid was deferred for future work.

The mutant displayed a 34-fold increase in *PINK1* gene expression relative to the untransfected group, consistent with a previous study by Bus *et al.* (2020). However, a non-significant 0.45-fold decrease in *PINK1* expression was observed in the WT group, inconsistent with Bus *et al.* (2020) who reported an upregulation akin to the G309D mutant. This observation may be due to rearrangement of the WT PINK1 plasmid, which would prevent primer binding and amplification.

Administration of the neurotoxin paraquat led to significant decreases in cell viability after 24 h, indicating cellular damage. The concentration at which 50 % loss in cell viability was expected was calculated to be 1.7 mM. According to the literature, a wide range of paraquat concentrations including 0.25 mM, 0.5 mM, and 1.2 mM have been shown to cause a similar decrease in SH-SY5Y cell viability (Fujimori et al., 2012; van der Merwe, 2015; Bekker, 2021). Such vast differences within a common cell line could be explained by laboratory-specific experimental variables that may be

difficult to ascertain. It could be speculated that significant increases in cell viability observed in this study with 0.07 mM, 0.13 mM, and 0.26 mM paraquat treatment could be indicative of hormesis, a phenomenon whereby low doses of an environmental agent can elicit a stimulating, beneficial effect while high doses cause an inhibitory, toxic effect (Mattson, 2008).

The chosen curcumin concentration of 2.5 µM increased cell viability by 77 % and did not cause toxicity, unlike the higher 20 µM concentration treatment which decreased cell viability by 33 %. Similar observations were made by Jaroonwitchawan and colleagues who reported a 40 % decrease in SH-SY5Y cell viability with 20 µM curcumin treatment (Jaroonwitchawan et al., 2017). Therefore, the selected curcumin concentration was deemed to be appropriate.

Regarding *TH* gene expression, Zhou *et al.* (2014) reported upregulation in G309D PINK1 transfected cells and downregulation in WT PINK1 cells compared to a vector control (Zhou et al., 2014). Conversely, *TH* gene expression in the present study was not significantly different for the WT and mutant PINK1 groups compared to the untransfected control. Various reasons could account for these discrepancies. Due to the complexity of transcriptional regulatory processes, it must be noted that measures of gene expression may not directly translate to protein levels. Therefore, gene expression alone does not provide a holistic view of expression. Several PINK1 studies have reported discrepancies between TH mRNA and protein levels, including those in human iPSCs (Bus et al., 2020) and mouse models (Maynard et al., 2020). PINK1 may regulate *TH* gene expression and dopamine content through modulation of *TH* transcription factors including nuclear receptor-related 1 (Lu et al., 2018). Furthermore, TH is the rate-limiting enzyme in catecholamine synthesis and therefore, is subject to additional regulatory mechanisms to control dopamine levels. Therefore, both gene expression and protein levels of this highly regulated enzyme should be investigated, with consideration of the timing at which this occurs. Additionally, although the 24 h transfection period sufficed to detect differences in *PINK1* expression which is directly affected by transfection with *PINK1*, an extended transfection period may be required to elicit significant changes in *TH* expression. Thus, dopamine toxicity could be occurring in the mutant model, however, detection of this phenomenon requires optimization of the timing at which measurements are made.

While the mechanism of dopamine toxicity resulting from *PINK1* overexpression is unknown, loss of PINK1 disrupts dopamine metabolism by affecting its synthesis and uptake (Bus et al., 2020). The mechanism may involve the use of amino acids for energy production rather than neurotransmitter metabolism (Bus et al., 2020). Moreover, *TH* expression is regulated by several coregulators such as DJ-1 and Pitx3. PINK1 may regulate *TH* expression by interacting with and phosphorylating these proteins (Zhou et al., 2014). As the G309D PINK1 mutation causes loss of PINK1 function, overexpression of this mutant protein may render it unable to regulate *TH*, and therefore dopamine, expression.

Since *TH* gene expression was not significantly different between PINK1 groups and the control, we sought to measure dopamine levels using an alternative approach with LC-MS. Dopamine could not be detected as the extraction method isolated only compounds with masses greater than dopamine. However, we observed that the mutant PINK1 group exhibited higher levels of the dopamine precursor phenylalanine which was tentatively identified. This exploratory finding further alludes to the possibility that dopamine may still be accumulating in the model but can only be detected and measured at a specific time point/s in the pathway and requires more sensitive extraction and detection assays. Dopamine could be present at a lower level compared to other compounds such as phenylalanine as its production and transportation are highly regulated. Future studies should evaluate whether the addition of dopamine precursors to the cultured cells increases dopamine production and therefore, the sensitivity of the assays used to measure this molecule. LC-MS could not discern the difference between L-phenylalanine and its mirror image (D- form) which may be important as the former is incorporated into cellular proteins, while the latter can be used as a pain killer (Heller, 1982). Therefore, the protocol for isolating dopamine from PINK1-expressing SH-SY5Y cell culture should be optimized to include smaller molecules. Notably, these experimental results to verify dopamine toxicity reflect a static view of the dynamic process of dopamine metabolism. Conflicting evidence for TH levels in previous studies and challenges of accurately measuring dopamine in a subtle overexpression model complicates the verification of dopamine toxicity.

Although the dopamine toxicity in the model could not be shown in the present study, the G309D PINK1 mutant significantly increased *PINK1* expression, and paraquat exposure successfully reduced cell viability. This confirms a model of *PINK1* overexpression and cellular stress. The G309D mutation has been shown previously to increase dopamine content (Zhou et al., 2014), and therefore, the model sufficed to investigate the effect of curcumin treatment as detailed below.

5.3 Determining the effect of curcumin on the model

In our study, pre-treatment with curcumin was unable to significantly rescue the reduction in cell viability induced by paraquat in the untransfected group. However, curcumin pre-treatment has been shown previously to reduce the proportion of paraquat-induced SH-SY5Y cell death from 69 % to 22 % (Jaroonwitchawan et al., 2017). These conflicting results could be due to the differences in curcumin and paraquat concentrations between the studies. Notably, our chosen concentration of 2.5 µM curcumin was lower, and the 1.7 mM paraquat concentration was significantly higher than the 10 µM curcumin and 0.5 mM paraquat used in the Jaroonwitchawan *et al.* study. Additionally, paraquat toxicity could not be significantly rescued by curcumin pre-treatment in both PINK1 groups. It is possible that the paraquat toxicity and effects of *PINK1* overexpression resulted in mitochondrial and cellular damage that was too extensive to be rescued by curcumin. Higher curcumin concentrations of 10 µM and 15 µM have been shown to significantly increase cell viability in SH-SY5Y cells that have

been challenged with a stressor (Wu et al., 2020). Therefore, higher concentrations of curcumin and longer exposure times may be necessary to rescue cells from the cytotoxicity posed by paraquat and PINK1 in the present study.

Curcumin's inability to increase cell viability in the mutant PINK1 group could be indicative of the toxic effect of the mutation. While 'curcumin only' treatment did not yield significant increases in viability, this may not detract from its therapeutic potential. The similarity of curcumin treatment to the untreated control indicates a positive effect to keep cells at baseline health, even for the mutant. A theory exists which postulates that curcumin may only exert increased protective effects when cells are exposed to stress. This phenomenon has been observed in cancer studies wherein curcumin induced apoptosis in tumor cell lines but had no effect on pathology-free, non-cancer cells (Syng-Ai, Kumari & Khar, 2004). Reasons for this effect are currently unknown but it suggests that curcumin could be a suitable therapeutic agent to specifically target pathological cells.

The chosen paraquat treatment of 1.7 mM for 24 h elicited an approximate 50 % loss in cell viability in the untransfected and WT PINK1 groups. In the mutant group, paraquat treatment further reduced cell viability slightly, indicative of the mild toxic effects of the mutation. Consistent with previous findings (Zhou et al., 2014), the mutant did not significantly decrease cell viability. The loss of function mechanism of the G309D mutation differs from other *PINK1* mutations as this protein has been shown to be expressed at relatively stable levels, unlike other recessive mutations which cause drastic reductions in protein levels (Beilina et al., 2005). Beilina and colleagues (2005) predicted that the G309 site where recessive point mutations have been found is unlikely to be within the active site but in an area involved in protein folding. A G309D substitution will likely not completely destabilize the fold but may interfere with ATP binding or hydrolysis. Additionally, the authors reported that the G309D mutation resulted in only a small decrease in kinase activity, a feature that is critical to PINK1 function. Therefore, the G309D mutation may cause only mild PINK1 dysfunction, resulting in minor deleterious effects on cell function and viability as was observed in the present study.

Notably, while the MTT assay is widely used to evaluate cell viability, the assay specifically assesses mitochondrial metabolic activity as it is mitochondrial enzymes that convert the MTT molecules into formazan causing the conversion of NADH to NAD^+ (van Meerloo, Kaspers & Cloos, 2011). The cell viability results confirm an effect of paraquat on mitochondrial function, although the exact mechanism of this effect remains elusive. MPTP is another toxic herbicide linked to PD risk and is commonly used to elicit a PD-like phenotype in PD research (Bové et al., 2005). Despite the structural similarity between paraquat and MPTP, these toxic compounds are believed to cause oxidative stress through different mechanisms. Paraquat has been shown to target complex I of the mitochondrial electron transport chain (Cochemé & Murphy, 2008). This contrasts with another study suggesting that this herbicide can still exert its toxic effects after knockdown of complex I (Choi et al., 2008).

Paraquat may also be involved in redox cycling and NADPH depletion (Bonneh-Barkay et al., 2005), thereby weakening cellular antioxidant mechanisms. Therefore, mitochondrial dysfunction is central to paraquat's mechanism of toxicity. Moreover, PINK1's involvement in mitophagy (**Figure 1.5** in **Chapter 1**) necessitates the assessment of mitochondrial activity in order to understand the effects of PINK1 mutations. The cell viability assay indirectly measures mitochondrial metabolic activity which was not affected by PINK1 or rescued by curcumin. Therefore, we further assessed mitochondrial function by measuring mitochondrial membrane potential.

In the present study, differences in mitochondrial membrane potential were more apparent when we analyzed % positive fluorescence events (PE/FITC frequency) than when examining PE/FITC fluorescence intensity. As observed for cell viability, pre-treatment with curcumin was not able to rescue the cells from the paraquat-induced reduction in membrane potential in all transfection groups. This suggests that further optimization is required to improve the curcumin and/or paraquat treatments regarding concentration and exposure time. Alternatively, assuming these factors are sufficient, pre-treatment with curcumin may not be an effective strategy to rescue paraquat-induced cytotoxicity. Paraquat caused a pattern of decreased mitochondrial membrane potential to ~50 % of the control. This effect was not significant due to the large variation of data points for the control group.

The stark contrast between the effect of treatment on PE/FITC fluorescence intensity and frequency was an unexpected finding. While fluorescence intensity alone is usually reported for a JC-1 assay, this is only one of many measures, including frequency, that is recorded. In our opinion, analyzing percentage positive events in addition to fluorescence intensity provides a more holistic view of the results. In this study, paraquat and pre-treatment groups had the same intensity but lower frequency than the control. This may be indicative of a possible compensatory mechanism whereby paraquat-induced cell death causes the remaining cells to compensate for the dying or dead cells due to paraquat exposure. A recent study reported a similar compensatory mechanism in *Drosophila* larvae where some neurons were able to detect and compensate for the death of their neighbors by expanding synapses and increasing neurotransmitter release (Wang et al., 2021). It is possible that cells may compensate by overproducing JC-1 aggregates thereby restoring impaired mitochondrial function. Although fewer viable cells are present in paraquat-exposed groups, the remaining cells may produce the same ratio of JC-1 aggregates to monomers as the control cells, causing no difference in fluorescence intensity. However, this effect may only be temporary, for when maximum compensatory capacity is reached, these cells will likely eventually succumb to the toxic effects of paraquat. In view of this, several zebrafish studies have demonstrated increased antioxidant responses to specifically compensate for paraquat-induced ROS formation (Nunes et al., 2017; Wang, Souders, et al., 2018). Therefore, further studies are needed to investigate this phenomenon in SH-SY5Y cells and other PD cell and animal models.

Mitochondrial membrane potential, as assessed by PE/FITC frequency, was significantly reduced in the WT and mutant PINK1 groups compared to the untransfected control, indicative of the toxic effects of PINK1 overexpression. Dopamine toxicity in PINK1 deficient cells may cause mitochondrial depolarisation due to the opening of the mitochondrial permeability transition pore. This process requires the production of ROS (Gandhi et al., 2012). Therefore, antioxidant compounds such as curcumin may protect against depolarization and cell death in susceptible neurons, as has been shown previously (van der Merwe et al., 2017).

5.4 Curcumin versus nanocurcumin

Curcumin shows promise as an antioxidant therapy, possibly through its effect of increasing the expression and efficacy of enzymes that scavenge free radicals (Trujillo et al., 2014; Gibellini et al., 2015; Nawab et al., 2019). However, several characteristics limit its practical application in individuals living with PD. These include its poor solubility in water, rapid metabolism, and systemic expulsion, as well as its inability to cross the blood-brain barrier (Anand et al., 2007). Structural modifications, conjugates, liposomes, nanospheres, and nanoparticles are some of the developments that have been designed to overcome these obstacles (Karthikeyan, Senthil & Min, 2020). Encapsulation of curcumin into various nanocarriers increases its bioavailability and solubility, retention in the body, and reduces unintended toxicity to surrounding tissues while preserving curcumin's properties (Karthikeyan, Senthil & Min, 2020).

However, in the present study, nanocurcumin unexpectedly caused a significant reduction in SH-SY5Y cell viability. It is possible that the DMSO solvent may have degraded the biodegradable PCL polymer, unlike PBS or DMEM which preserve the nanoparticle integrity and have been used previously as a solvent for PCL nanoparticles (Omarch et al., 2019). Also, the 2.5 µM nanocurcumin used may have been too highly concentrated and caused toxicity, and therefore needs to be further optimized to reap its protective benefits. In addition, since the release of the encapsulated compound occurs slowly, the exposure time of 24 h may not suffice for the complete delivery of nanocurcumin to the cell. Alternatively, the reduction in viability may be due to the specific unloaded PCL nanoparticle used to encapsulate curcumin which also produced the same effect as the nanocurcumin (**Figure 3.14** in **Chapter 3**). Moreover, it is plausible that the sucrose used for structural integrity of the nanoparticle may have also contributed to this effect. Previous studies have reported no effect of unloaded PCL nanoparticles on cell viability in mouse macrophages (Łukasiewicz et al., 2021) and in colon cancer SW480 cells over a range of concentrations (Oritz et al., 2012). However, these studies used the nanoemulsion templating method and the interfacial polymer disposition method, respectively, for nanocurcumin synthesis as opposed to the single emulsion-solvent evaporation technique employed in the present study. Therefore, alternative methods to improve the synthesis of PCL nanoparticles should be investigated, with particular focus on their effects in SH-SY5Y cells.

Notably, ionic gelation and antisolvent precipitation have been touted as particularly efficacious techniques (Karthikeyan, Senthil & Min, 2020). Finally, it is also worth investigating if nanocurcumin can be used as a drug alone or in addition to existing PD therapies.

5.5 Implications for PD

Pre-treatment with curcumin is an experimental treatment representing a prophylactic, preventative approach against PD development. However, co-treatment and post-treatment are alternative strategies used in PD models to determine the therapeutic potential of curcumin both during disease development and after PD onset, respectively. While the choice of pre-, post-, and co-treatment is hotly debated, these approaches all aim to implement curcumin as a drug for PD management. Conversely, curcumin also has potential as a nutraceutical compound to supplement one's diet rather than a medication regime. Small, consistent doses of curcumin throughout one's lifetime may have more beneficial (and potentially less toxic) effects than current PD drugs. Low prevalence rates of neurological disease in regions such as India where individuals frequently consume curcumin alludes to the potential efficacy of this nutraceutical approach (Das et al., 2010; Surathi et al., 2016). This strategy may not only be effective in genetic forms of PD, such as *PINK1*-associated disease, but also in individuals with idiopathic PD presenting with α-synuclein pathology, a hallmark of PD. α-Synuclein pathology is found in the brain and the gut, however, it is unclear which region develops this pathology first. Due to curcumin's potential to break down, prevent aggregation, and eliminate toxic forms of α-synuclein (Shrikanth Gadad et al., 2012; Kamelabad et al., 2021), dietary supplementation with curcumin may present as an effective strategy for both the prevention and reduction of disease progression. Furthermore, curcumin's action in the gut has been shown in animal models to relieve some of the GI symptoms associated with the disease such as leaky gut and delayed gastric emptying (Kochar et al., 2014; Tian et al., 2016). This could reduce the morbidity experienced by individuals living with PD. Given the potentially greater efficacy of dietary curcumin in the gut, further research is required to determine if life-long curcumin consumption can eliminate α-synuclein from the gut to prevent or delay PD progression (Chetty et al., 2021).

Consequently, there is great potential for nutraceuticals in PD treatment. Several of these 'functional foods' have been investigated for their protective properties, including rutin, St. John's wort, resveratrol, and various vitamins (summarized in **Table 1.3**, **Chapter 1**). Of these, curcumin represents a particularly suitable candidate due to its protective effects against both disease symptoms as well as progression, and animal models can be easily used to test these effects. However, in order to validate curcumin's therapeutic application in humans, clinical trials and large epidemiological studies are required that follow up with participants consuming curcumin over a lifetime. Due to logistics and funding among other factors, this may be challenging and therefore, may require alternative strategies to advance the field of nutraceuticals.

5.6 Limitations

The main limitation of the study was that the WT plasmid could not be verified. The plasmid insert could have degraded or undergone rearrangement, which could be avoided in future experiments by transforming the viral DNA into chemically competent cells. These include NEBStable (New England Biolabs, MA, United States) or Stbl3 *E. coli* which can increase transformation efficiency. Alternatively, CRISPr (clustered regularly interspaced short palindromic repeats) or site-directed mutagenesis could be used to revert the mutant to the WT with a single base change at the mutation site. Regarding the evaluation of dopamine toxicity in the model, this study was limited in that experimental results demonstrated a static view of the dynamic process of dopamine metabolism. Although several measurements to verify the model were incorporated into the experimental design of the present study, this limitation should be taken into consideration when assessing cellular processes that evolve over time. Finally, the unloaded PCL nanoparticle reduced SH-SY5Y cell viability in this study which limited the evaluation of the curcumin-loaded nanoparticle's effects. The specific technique used for PCL nanoparticle synthesis, its concentration, and solvent may affect its toxicity which should be further investigated in SH-SY5Y cells.

Another limitation of the present study was that technical replicates were not included in experiments due to the complexity of performing assays with a large number of treatment groups. Technical replicates account for human error and variability in assay measurements related to equipment and protocols. However, biological replicates were included in all experiments of the study to account for batch effects. Lastly, the use of undifferentiated SH-SY5Y cells may have limited the cellular model, as differentiation with retinoic acid has been shown to induce more mature, neuronal-like morphological and biochemical characteristics (Xie, Hu & Li, 2010). Although differentiation can be difficult, the use of undifferentiated cells may limit its interpretation as a true PD model.

5.7 Future directions

The main findings of this study and possible avenues for future research are summarized in **Figure 5.1**. To improve the model used in the present study, SH-SY5Y cell differentiation should be performed. This will result in a homogenous cell population with neuronal morphology which may reduce cell cycle fluctuations observed in undifferentiated cells (Encinas et al., 2002). It must be noted that differentiation results in a distinct reduction in cell number amounting to a 30-40 % decrease in population size (Shipley, Mangold & Szpara, 2016). This must be taken into consideration when assessing the feasibility of performing experimental assays that also result in cell loss (e.g., with wash steps) yet require large cell numbers, such as the JC-1 mitochondrial membrane potential assay. Furthermore, the dopaminergic properties such as TH and DA-β-hydroxylase activities of

differentiated SH-SY5Y cells further enhance their suitability to study dopamine toxicity in PD within a neuronal environment (Xie, Hu & Li, 2010).
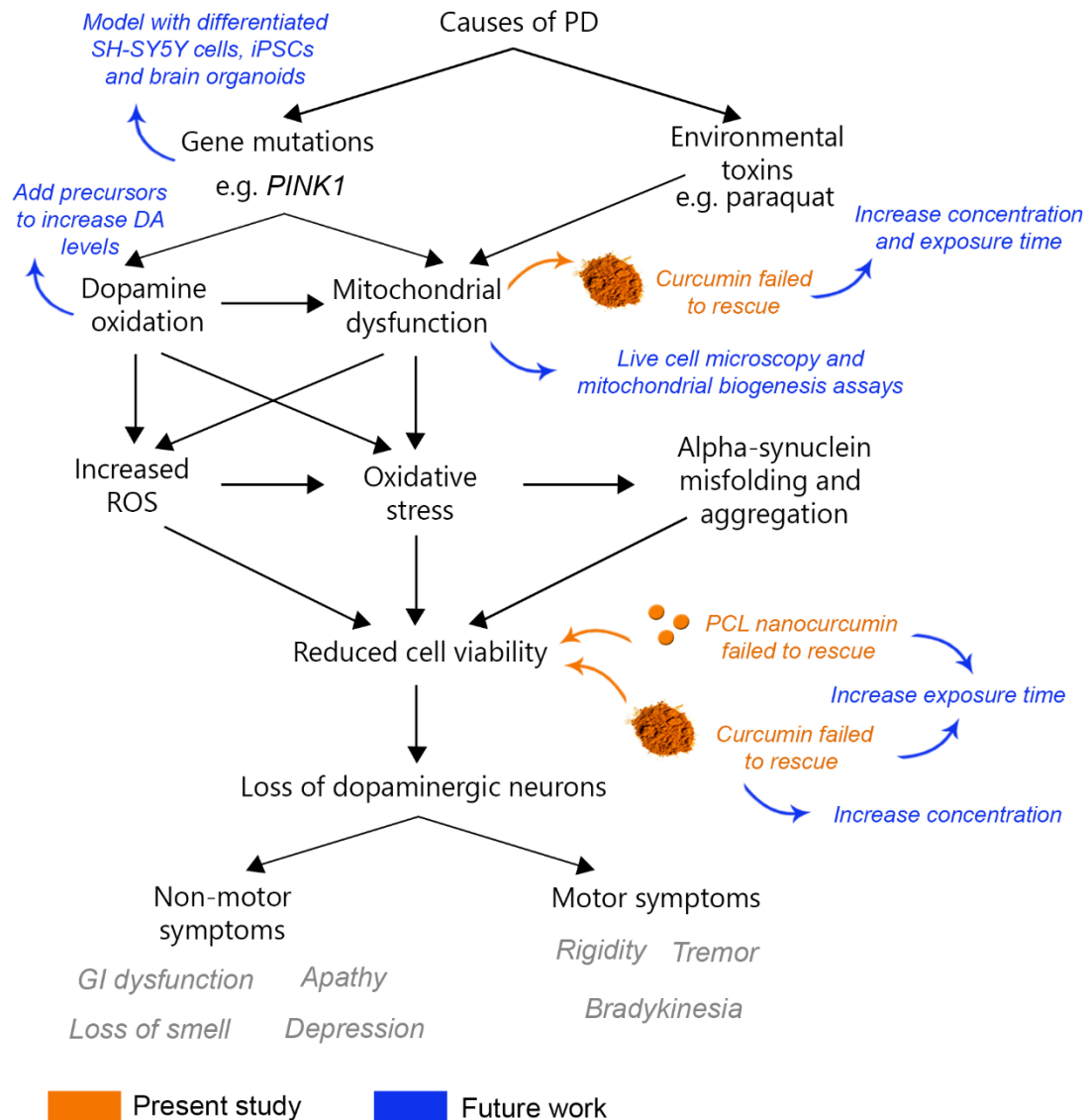
Figure 5.1 Suggestions for future work based on the present study's findings. Findings of the current study are denoted in orange while suggestions for future work are written in blue. Abbreviations: iPSCs, induced pluripotent stem cells; PD, Parkinson's disease; ROS, reactive oxygen species; PCL, polycaprolactone; GI, gastrointestinal.

While overexpression represents a useful mechanism to study the effects of PD-linked mutations (**Table 1.1** in **Chapter 1**), such artificial models of PD may not fully reflect the pathogenesis present in individuals living with PD-linked mutations of interest. Therefore, iPSCs derived from individuals with PD-linked gene mutations may be useful to verify findings made in other models. Human somatic cells can be reprogrammed into iPSCs with a cocktail of four transcription factors, namely

OCT4, SOX2, KLF4, and c-Myc (Xiao et al., 2016). These iPSCs can be differentiated into various cell types, including dopaminergic neurons. One study showed the rescue effects of the drug rapamycin on mitochondrial dysfunction in iPSC-derived neural cells from familial PD patients carrying *PINK1* mutations (Cooper et al., 2012). Future studies should utilize a similar iPSC model to establish the neuroprotective effects of curcumin on *PINK1* mutation-induced pathology.

In addition to iPSCs, the use of 3D culturing of brain organoids derived from human pluripotent stem cells is increasing in PD research (Paşca, 2018). Pluripotent stem cells may be differentiated into neural cells in 2D cultures or 3D brain organoids. In diseases such as PD where multiple brain regions are involved in pathogenesis, organoids can be patterned further to resemble particular neuronal regions, and then be combined to generate brain assembloids or 'connected groups of organoids'. This allows researchers to model interactions between brain regions and provides a more holistic understanding of complex disease pathogenesis.

The addition of dopamine precursors may increase the sensitivity of assays such as LC-MS and HPLC which may be used to detect this molecule. Alternatively, an ELISA kit for dopamine detection should be used in future work. Furthermore, curcumin treatment may have an effect on mitochondria beyond enhancing mitochondrial membrane potential. Therefore, alternative methods to examine mitochondrial function should be used to supplement mitochondrial membrane potential assays in future studies. Alternatives include live cell microscopy, assays for mitochondrial biogenesis, and confocal microscopy following mitochondrial staining. Moreover, the timing and formulation of curcumin treatment have a significant impact on laboratory experimental outcomes and therefore, must be optimized before conclusions can be made regarding the efficacy of curcumin.

5.8 Concluding remarks

Given the overwhelming evidence for mitochondrial dysfunction and oxidative stress in PD (Dias, Junn & Mouradian, 2013) compounded with ineffective long-term treatments, the search for a powerful antioxidant as a potential PD treatment is of considerable interest. The protective effects of many plant-based antioxidants show promise as PD therapies, including rutin, resveratrol, St. John's wort, and curcumin. The results of the present study demonstrate that curcumin has potential as a therapeutic compound to increase cell viability and mitochondrial function in healthy cells (which is promising), however, still requires optimization to enhance its efficacy in unhealthy cells. Consequently, further research is warranted to determine the precise mechanisms underlying curcumin's protective effects against mitochondrial dysfunction and dopamine toxicity in *PINK1* and other genetic models of PD. This plant-based compound is an attractive potential therapeutic agent due to its relatively low toxicity, and numerous beneficial properties. Nonetheless, its low bioavailability and various other biochemical characteristics limit its efficacy in the body. Although

promising due to their potential to overcome these barriers, nanocurcumin formulations require refinement and evaluation of their safety in patient-derived PD cellular models before they can be advocated for widespread therapeutic use. Investigating if curcumin or its nanoformulations can be used as a drug alone or in combination with existing PD therapies is also of importance. Replacing a portion of PD drugs in an individual's treatment regime with curcumin may improve therapeutic benefit with fewer side effects overall.

Alternatively, producing drug formulations of curcumin (such as nanoparticle-encapsulated curcumin) may not be the only approach to reap the benefits of this plant compound. Life-long and regular consumption of curcumin as a nutraceutical in one's diet may be a more effective and sustainable method to prevent or slow down PD development by removal of misfolded α-synuclein through excretion via the large intestine. This concept, illustrated in **Figure 5.2**, is explored in our review article (Chetty et al., 2021). Hence, investment in long-term epidemiological studies is warranted to investigate the potential of curcumin as a nutraceutical therapy to prevent or delay PD progression.
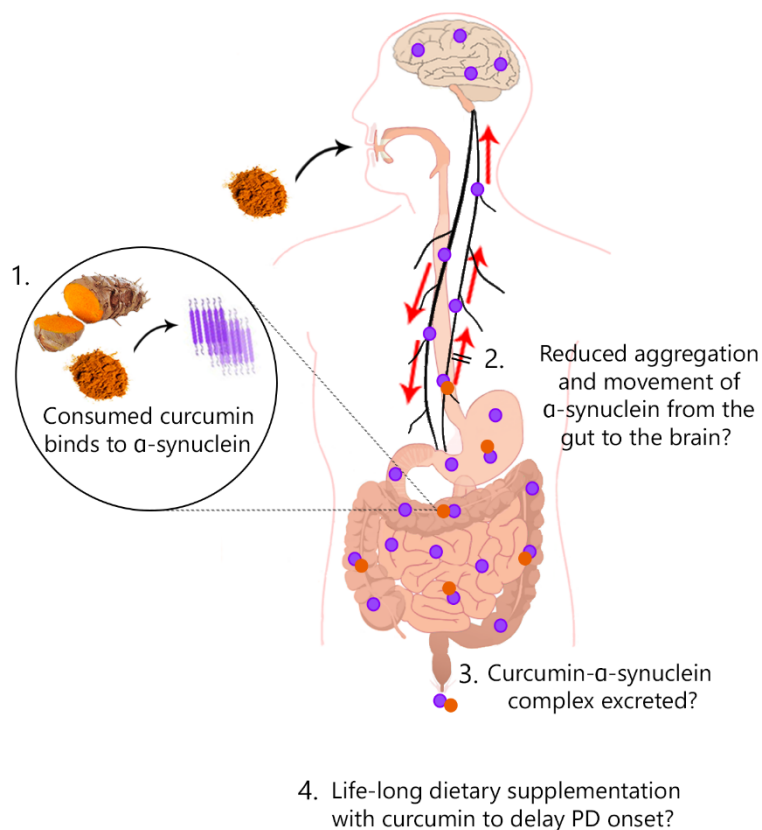
Figure 5.2 Proposed therapeutic potential of curcumin as a nutraceutical intervention against PD. Purple dots represent misfolded α-synuclein aggregates. Orange dots represent consumed curcumin.

References

Aggarwal, S., Ichikawa, H., Takada, Y., Sandur, S.K., Shishodia, S. & Aggarwal, B.B. 2006. Curcumin (diferuloylmethane) down-regulates expression of cell proliferation and antiapoptotic and metastatic gene products through suppression of IκBα kinase and Akt activation. *Molecular pharmacology*. 69(1):195–206. DOI: 10.1124/mol.105.017400.

Ahmi, Ö.Z. 2019. Experimental cell culture models for investigating neurodegenerative diseases. *Journal of Cellular Neuroscience and Oxidative Stress*. 11(2):835–851. DOI: 10.37212/jcnos.683400.

Alafuzoff, I. & Hartikainen, P. 2018. Alpha-synucleinopathies. In *Handbook of clinical neurology*. V. 145. Elsevier. 339–353. DOI: 10.1016/B978-0-12-802395-2.00024-9.

Anand, P., Kunnumakkara, A.B., Newman, R.A. & Aggarwal, B.B. 2007. Bioavailability of curcumin: problems and promises. *Molecular pharmaceutics*. 4(6):807–818. DOI: 10.1021/mp700113r.

Andersen, J.K. 2004. Oxidative stress in neurodegeneration: cause or consequence? *Nature medicine*. 10(7):S18–S25. DOI: 10.1038/nrn1434.

Anuchapreeda, S., Tima, S., Duangrat, C. & Limtrakul, P. 2008. Effect of pure curcumin, demethoxycurcumin, and bisdemethoxycurcumin on WT1 gene expression in leukemic cell lines. *Cancer chemotherapy and pharmacology*. 62(4):585. DOI: 10.1007/s00280-007-0642-1.

Arbo, B.D., André-Miral, C., Nasre-Nasser, R.G., Schimith, L.E., Santos, M.G., Costa-Silva, D., Muccillo-Baisch, A.L. & Hort, M.A. 2020. Resveratrol Derivatives as Potential Treatments for Alzheimer's and Parkinson's Disease. *Frontiers in Aging Neuroscience*. 12:103. DOI: 10.3389/fnagi.2020.00103.

Arowoogun, J., Akanni, O.O., Adefisan, A.O., Owumi, S.E., Tijani, A.S. & Adaramoye, O.A. 2021. Rutin ameliorates copper sulfate-induced brain damage via antioxidative and anti-inflammatory activities in rats. *Journal of Biochemical and Molecular Toxicology*. 35(1):e22623. DOI: 10.1002/jbt.22623.

Bahmad, H., Hadadeh, O., Chamaa, F., Cheaito, K., Darwish, B., Makkawi, A.K. & Abou-Kheir, W. 2017. Modeling Human Neurological and Neurodegenerative Diseases: From Induced Pluripotent Stem Cells to Neuronal Differentiation and Its Applications in Neurotrauma. *Front Mol Neurosci*. 10:50. DOI: 10.3389/fnmol.2017.00050.

Barnham, K.J. & Bush, A.I. 2014. Biological metals and metal-targeting compounds in major neurodegenerative diseases. *Chemical Society Reviews*. 43(19):6727–6749. DOI: 10.1039/C4CS00138A.

Beilina, A., van der Brug, M., Ahmad, R., Kesavapany, S., Miller, D.W., Petsko, G.A. & Cookson, M.R. 2005. Mutations in PTEN-induced putative kinase 1 associated with recessive parkinsonism have differential effects on protein stability. *Proceedings of the National Academy of Sciences of the United States of America*. 102(16):5703–5708. DOI: 10.1073/pnas.0500617102.

Bekker, M. 2021. An Investigation Of The Neuroprotective Properties Of Curcumin By Monitoring Autophagy And Apoptosis.

Bennett, B., McDonald, F., Beattie, E., Carney, T., Freckelton, I., White, B. & Willmott, L. 2017. Assistive technologies for people with dementia: ethical considerations. *Bulletin of the World Health Organization*. 95(11):749–755. DOI: 10.2471/BLT.16.187484.

Bhaumik, S., Jyothi, M.D. & Khar, A. 2000. Differential modulation of nitric oxide production by curcumin in host macrophages and NK cells. *FEBS letters*. 483(1):78–82.

Bhowmik, D., Kumar, K.P., Chandira, M. & Jayakar, B. 2009. Turmeric: a herbal and traditional medicine. *Archives of Applied Science Research*. 1(2):86–108.

Biedler, J., Roffler-Tarlov, S., Schachner, M. & Freedman, L. 1978. Multiple Neurotransmitter Synthesis by Human Neuroblastoma Cell Lines and Clones. *Cancer Research*. 38(11):3751–3757.

Bisaglia, M., Soriano, M.E., Arduini, I., Mammi, S. & Bubacco, L. 2010. Molecular characterization of dopamine-derived quinones reactivity toward NADH and glutathione: Implications for mitochondrial dysfunction in Parkinson disease. *Biochimica et Biophysica Acta (BBA) - Molecular Basis of Disease*. 1802(9):699–706. DOI: 10.1016/j.bbadis.2010.06.006.

Bonifati, V., Rohe, C.F., Breedveld, G.J., Fabrizio, E., de Mari, M., Tassorelli, C., Tavella, A., Marconi, R., et al. 2005. Early-onset parkinsonism associated with PINK1 mutations: frequency, genotypes, and phenotypes. *Neurology*. 65(1):87–95. DOI: 10.1212/01.wnl.0000167546.39375.82.

Bonneh-Barkay, D., Reaney, S.H., Langston, W.J. & di Monte, D.A. 2005. Redox cycling of the herbicide paraquat in microglial cultures. *Molecular Brain Research*. 134(1). DOI: 10.1016/j.molbrainres.2004.11.005.

Bové, J., Prou, D., Perier, C. & Przedborski, S. 2005. Toxin-induced models of Parkinson's disease. *NeuroRx*. 2(3):484–494. DOI: 10.1602/neurorx.2.3.484.

Braak, H., del Tredici, K., Rüb, U., de Vos, R.A.I., Steur, E.N.H.J. & Braak, E. 2003. Staging of brain pathology related to sporadic Parkinson's disease. *Neurobiology of aging*. 24(2):197–211. DOI: 10.1016/s0197-4580(02)00065-9.

Braak, H., Rüb, U., Gai, W.P. & del Tredici, K. 2003. Idiopathic Parkinson's disease: possible routes by which vulnerable neuronal types may be subject to neuroinvasion by an unknown pathogen. *Journal of neural transmission*. 110(5):517–536. DOI: 10.1007/s00702-002-0808-2.

Bromek, E., Haduch, A., Gołembiowska, K. & Daniel, W.A. 2011. Cytochrome P450 mediates dopamine formation in the brain in vivo. *Journal of neurochemistry*. 118(5):806–815. DOI: 10.1111/j.1471-4159.2011.07339.x.

Bus, C., Zizmare, L., Feldkaemper, M., Geisler, S., Zarani, M., Schaedler, A., Klose, F., Admard, J., et al. 2020. Human Dopaminergic Neurons Lacking PINK1 Exhibit Disrupted Dopamine Metabolism Related to Vitamin B6 Co-Factors. *iScience*. 23(12):101797. DOI: 10.1016/j.isci.2020.101797.

Cao, S., Wang, C., Yan, J., Li, X., Wen, J. & Hu, C. 2020. Curcumin ameliorates oxidative stress-induced intestinal barrier injury and mitochondrial damage by promoting Parkin dependent mitophagy through AMPK-TFEB signal pathway. *Free Radical Biology and Medicine*. 147:8–22. DOI: 10.1016/j.freeradbiomed.2019.12.004.

Carlsson, A., Lindqvist, M., Magnusson, T. & Waldeck, B. 1958. On the presence of 3-hydroxytyramine in brain. *Science*. 127(3296):471. DOI: 10.1126/science.127.3296.471.

Chan, N.C., Salazar, A.M., Pham, A.H., Sweredoski, M.J., Kolawa, N.J., Graham, R.L.J., Hess, S. & Chan, D.C. 2011. Broad activation of the ubiquitin–proteasome system by Parkin is critical for mitophagy. *Human molecular genetics*. 20(9):1726–1737. DOI: 10.1093/hmg/ddr048.

Chatterjee, D. & Gerlai, R. 2009. High precision liquid chromatography analysis of dopaminergic and serotoninergic responses to acute alcohol exposure in zebrafish. *Behavioural brain research*. 200(1):208–13. DOI: 10.1016/j.bbr.2009.01.016.

Chen, P.S., Peng, G.S., Li, G., Yang, S., Wu, X., Wang, C.C., Wilson, B., Lu, R.B., et al. 2006. Valproate protects dopaminergic neurons in midbrain neuron/glia cultures by stimulating the release of neurotrophic factors from astrocytes. *Molecular Psychiatry*. 11(12):1116–1125. DOI: 10.1038/sj.mp.4001893.

Chen, X., Guo, C. & Kong, J. 2012. Oxidative stress in neurodegenerative diseases. *Neural Regeneration Research*. 5(7):376–385. DOI: 10.3969/j.issn.1673-5374.2012.05.009.

Cheng, Y., Kozubek, A., Ohlsson, L., Sternby, B. & Duan, R.-D. 2007. Curcumin decreases acid sphingomyelinase activity in colon cancer Caco-2 cells. *Planta medica*. 73(08):725–730. DOI: 10.1055/s-2007-981540.

Chetty, D., Abrahams, S., Coller, R., Carr, J., Kenyon, C. & Bardien, S. 2021. Movement of prion-like α-synuclein along the gut–brain axis in Parkinson's disease: A potential target of curcumin treatment. *European Journal of Neuroscience*. 54(2):4695–4711. DOI: 10.1111/ejn.15324.

Chia, S.J., Tan, E.-K. & Chao, Y.-X. 2020. Historical Perspective: Models of Parkinson's Disease. *International Journal of Molecular Sciences*. 21(7). DOI: 10.3390/ijms21072464.

Chinese Pharmacopoeia Commission. 2005.

Choi, W.-S., Kruse, S.E., Palmiter, R.D. & Xia, Z. 2008. Mitochondrial complex I inhibition is not required for dopaminergic neuron death induced by rotenone, MPP+, or paraquat. *Proceedings of the National Academy of Sciences*. 105(39):15136–15141. DOI: 10.1073/pnas.0807581105.

Cobley, J.N., Fiorello, M.L. & Bailey, D.M. 2018. 13 reasons why the brain is susceptible to oxidative stress. *Redox Biology*. 15:490–503. DOI: 10.1016/j.redox.2018.01.008.

Cochemé, H.M. & Murphy, M.P. 2008. Complex I Is the Major Site of Mitochondrial Superoxide Production by Paraquat. *Journal of Biological Chemistry*. 283(4). DOI: 10.1074/jbc.M708597200.

Cookson, M.R. 2012. Parkinsonism due to mutations in PINK1, parkin, and DJ-1 and oxidative stress and mitochondrial pathways. *Cold Spring Harbor perspectives in medicine*. 2(9):a009415. DOI: 10.1101/cshperspect.a009415.

Cooper, O., Seo, H., Andrabi, S., Guardia-Laguarta, C., Graziotto, J., Sundberg, M., McLean, J.R., Carrillo-Reid, L., et al. 2012. Pharmacological Rescue of Mitochondrial Deficits in iPSC-Derived Neural Cells from Patients with Familial Parkinson's Disease. *Science Translational Medicine*. 4(141):141ra90. DOI: 10.1126/scitranslmed.3003985.

Creed, R.B. & Goldberg, M.S. 2018. New Developments in Genetic rat models of Parkinson's Disease. *Movement Disorders*. 33(5):717–729. DOI: 10.1002/mds.27296.

Dagda, R.K., Cherra, S.J., Kulich, S.M., Tandon, A., Park, D. & Chu, C.T. 2009. Loss of PINK1 Function Promotes Mitophagy through Effects on Oxidative Stress and Mitochondrial Fission. *Journal of Biological Chemistry*. 284(20):13843–13855. DOI: 10.1074/jbc.M808515200.

Darvesh, A.S., Carroll, R.T., Bishayee, A., Novotny, N.A., Geldenhuys, W.J. & van der Schyf, C.J. 2012. Curcumin and neurodegenerative diseases: a perspective. *Expert opinion on investigational drugs*. 21(8):1123–1140. DOI: 10.1517/13543784.2012.693479.

Das, S.K., Misra, A.K., Ray, B.K., Hazra, A., Ghosal, M.K., Chaudhuri, A., Roy, T., Banerjee, T.K., et al. 2010. Epidemiology of Parkinson disease in the city of Kolkata, India: a community-based study. *Neurology*. 75(15):1362–1369. DOI: 10.1212/WNL.0b013e3181f735a7.

Daubner, S.C., Le, T. & Wang, S. 2011. Tyrosine hydroxylase and regulation of dopamine synthesis. *Archives of Biochemistry and Biophysics*. 508(1):1–12. DOI: 10.1016/j.abb.2010.12.017.

Dehghani, Z., Meratan, A.A., Saboury, A.A. & Nemat-Gorgani, M. 2020. α-Synuclein fibrillation products trigger the release of hexokinase I from mitochondria: Protection by curcumin, and possible role in pathogenesis of Parkinson's disease. *Biochimica et Biophysica Acta (BBA) - Biomembranes*. 1862(6):183251. DOI: 10.1016/j.bbamem.2020.183251.

Devi, L., Raghavendran, V., Prabhu, B.M., Avadhani, N.G. & Anandatheerthavarada, H.K. 2008. Mitochondrial Import and Accumulation of α-Synuclein Impair Complex I in Human Dopaminergic Neuronal Cultures and Parkinson Disease Brain. *Journal of Biological Chemistry*. 283(14). DOI: 10.1074/jbc.M710012200.

Dias, V., Junn, E. & Mouradian, M.M. 2013. The Role of Oxidative Stress in Parkinson's Disease. *Journal of Parkinson's Disease*. 3(4). DOI: 10.3233/JPD-130230.

Dieffenbach, C., Lowe, T. & Dveksler, G. 1993. General concepts for PCR primer design. *Genome Research*. 3:S30–S37. DOI: 10.1101/gr.3.3.s30.

Dorsey, E.R., Elbaz, A., Nichols, E., Abd-Allah, F., Abdelalim, A., Adsuar, J.C., Ansha, M.G., Brayne, C., et al. 2018. Global, regional, and national burden of Parkinson's disease, 1990–2016: a systematic analysis for the Global Burden of Disease Study 2016. *The Lancet Neurology*. 17(11):939–953. DOI: 10.1016/S1474-4422(18)30295-3.

Du, X.-X., Xu, H.-M., Jiang, H., Song, N., Wang, J. & Xie, J.-X. 2012. Curcumin protects nigral dopaminergic neurons by iron-chelation in the 6-hydroxydopamine rat model of Parkinson's disease. *Neuroscience Bulletin*. 28(3):253–258. DOI: 10.1007/s12264-012-1238-2.

Dunn, L. & Lewis, P.A. 2008. The Shaking Palsy - Advances in Our Understanding of Parkinson's Disease. *Opticon1826*. (4). DOI: 10.5334/opt.040806.

Ebrahimi-Fakhari, D., Cantuti-Castelvetri, I., Fan, Z., Rockenstein, E., Masliah, E., Hyman, B.T., McLean, P.J. & Unni, V.K. 2011. Distinct roles in vivo for the ubiquitin–proteasome system and the autophagy–lysosomal pathway in the degradation of α-synuclein. *Journal of Neuroscience*. 31(41):14508–14520. DOI: 10.1523/JNEUROSCI.1560-11.2011.

Eglen, R. & Reisine, T. 2011. Primary cells and stem cells in drug discovery: emerging tools for high-throughput screening. *Assay And Drug Development Technologies*. 9(2):108–124. DOI: 10.1089/adt.2010.0305.

Ehringer, H. & Hornykiewicz, O. 1960. Distribution of noradrenaline and dopamine (3-hydroxytyramine) in the human brain and their behavior in diseases of the extrapyramidal system. *Klin Wochenschr*. 38:1236–1239. DOI: 10.1007/bf01485901.

Encinas, M., Iglesias, M., Liu, Y., Wang, H., Muhaisen, A., Ceña, V., Gallego, C. & Comella, J.X. 2002. Sequential Treatment of SH-SY5Y Cells with Retinoic Acid and Brain-Derived Neurotrophic Factor Gives Rise to Fully Differentiated, Neurotrophic Factor-Dependent, Human Neuron-Like Cells. *Journal of Neurochemistry*. 75(3). DOI: 10.1046/j.1471-4159.2000.0750991.x.

Esteves, A.R., Arduíno, D.M., Silva, D.F.F., Oliveira, C.R. & Cardoso, S.M. 2011. Mitochondrial Dysfunction: The Road to Alpha-Synuclein Oligomerization in PD. *Parkinson's Disease*. 2011:693761. DOI: 10.4061/2011/693761.

Fabbri, M., Ferreira, J.J., Lees, A., Stocchi, F., Poewe, W., Tolosa, E. & Rascol, O. 2018. Opicapone for the treatment of Parkinson's disease: A review of a new licensed medicine. *Movement disorders*. 33(10):1528–1539. DOI: 10.1002/mds.27475.

Falkenburger, B.H. & Schulz, J.B. 2006. Limitations of cellular models in Parkinson's disease research. *J Neural Transm Suppl*. (70):261–268. DOI: 10.1007/978-3-211-45295-0_40.

Falkenburger, B.H., Saridaki, T. & Dinter, E. 2016. Cellular models for Parkinson's disease. *Journal of neurochemistry*. 139:121–130. DOI: 10.1111/jnc.13618.

Feng, L.R. & Maguire-Zeiss, K.A. 2010. Gene Therapy in Parkinson's Disease. *CNS drugs*. 24(3):177–192. DOI: 10.2165/11533740-000000000-00000.

Fernandez, H.H. & Chen, J.J. 2007. Monoamine oxidase-B inhibition in the treatment of Parkinson's disease. *Pharmacotherapy: The Journal of Human Pharmacology and Drug Therapy*. 27(12P2):174S-185S. DOI: 10.1592/phco.27.12part2.174S.

Ferrer-Sueta, G., Campolo, N., Trujillo, M., Bartesaghi, S., Carballal, S., Romero, N., Alvarez, B. & Radi, R. 2018. Biochemistry of Peroxynitrite and Protein Tyrosine Nitration. *Chemical Reviews*. 118(3):1338–1408. DOI: 10.1021/acs.chemrev.7b00568.

Flora, G., Gupta, D. & Tiwari, A. 2013. Nanocurcumin: A Promising Therapeutic Advancement over Native Curcumin. *Critical Reviews in Therapeutic Drug Carrier Systems*. 30(4). DOI: 10.1615/CritRevTherDrugCarrierSyst.2013007236.

Forouzanfar, F., Read, M.I., Barreto, G.E. & Sahebkar, A. 2020. Neuroprotective effects of curcumin through autophagy modulation. *IUBMB Life*. 72(4):652–664. DOI: 10.1002/iub.2209.

Fujimori, K., Fukuhara, A., Inui, T. & Allhorn, M. 2012. Prevention of paraquat-induced apoptosis in human neuronal SH-SY5Y cells by lipocalin-type prostaglandin D synthase. *Journal of Neurochemistry*. 120(2). DOI: 10.1111/j.1471-4159.2011.07570.x.

Gandhi, S., Vaarmann, A., Yao, Z., Duchen, M.R., Wood, N.W. & Abramov, A.Y. 2012. Dopamine Induced Neurodegeneration in a PINK1 Model of Parkinson's Disease. *PLoS ONE*. 7(5). DOI: 10.1371/journal.pone.0037564.

Ganeshpurkar, A. & Saluja, A.K. 2017. The Pharmacological Potential of Rutin. *Saudi Pharmaceutical Journal*. 25(2). DOI: 10.1016/j.jsps.2016.04.025.

Gao, C., Wang, Y., Sun, J., Han, Y., Gong, W., Li, Y., Feng, Y., Wang, H., et al. 2020. Neuronal mitochondria-targeted delivery of curcumin by biomimetic engineered nanosystems in Alzheimer's disease mice. *Acta Biomaterialia*. 108:285–299. DOI: 10.1016/j.actbio.2020.03.029.

Genoud, S., Roberts, B.R., Gunn, A.P., Halliday, G.M., Lewis, S.J.G., Ball, H.J., Hare, D.J. & Double, K.L. 2017. Subcellular compartmentalisation of copper, iron, manganese, and zinc in the Parkinson's disease brain. *Metallomics*. 9(10):1447–1455. DOI: 10.1039/C7MT00244K.

Giannopoulos, S., Samardzic, K., Raymond, B.B.A., Djordjevic, S.P. & Rodgers, K.J. 2019. L-DOPA causes mitochondrial dysfunction in vitro: A novel mechanism of L-DOPA toxicity uncovered. *The International Journal of Biochemistry & Cell Biology*. 117:105624. DOI: 10.1016/j.biocel.2019.105624.

Gibellini, L., Bianchini, E., de Biasi, S., Nasi, M., Cossarizza, A. & Pinti, M. 2015. Natural Compounds Modulating Mitochondrial Functions. *Evidence-Based Complementary and Alternative Medicine*. 2015:527209. DOI: 10.1155/2015/527209.

Goldberg, M.S. & Lansbury Jr, P.T. 2000. Is there a cause-and-effect relationship between α-synuclein fibrillization and Parkinson's disease? *Nature Cell Biology*. 2(7):E115–E119. DOI: 10.1038/35017124.

Gonçalves, F.B. & Morais, V.A. 2021. PINK1: A Bridge between Mitochondria and Parkinson's Disease. *Life*. 11(5):371. DOI: 10.3390/life11050371.

Guijarro-Real, C., Plazas, M., Rodríguez-Burruezo, A., Prohens, J. & Fita, A. 2021. Potential In Vitro Inhibition of Selected Plant Extracts against SARS-CoV-2 Chymotripsin-Like Protease (3CLPro) Activity. *Foods*. 10(7):1503. DOI: 10.3390/foods10071503.

Guldberg, H.C. & Marsden, C.A. 1975. Catechol-O-methyl transferase: pharmacological aspects and physiological role. *Pharmacological reviews*. 27(2):135–206.

Guo, Y.-J., Dong, S.-Y., Cui, X.-X., Feng, Y., Liu, T., Yin, M., Kuo, S.-H., Tan, E.-K., et al. 2016. Resveratrol alleviates MPTP-induced motor impairments and pathological changes by autophagic degradation of α-synuclein via SIRT1-deacetylated LC3. *Molecular Nutrition & Food Research*. 60(10):2161–2175. DOI: 10.1002/mnfr.201600111.

Gustot, A., Gallea, J.I., Sarroukh, R., Celej, M.S., Ruysschaert, J.-M. & Raussens, V. 2015. Amyloid fibrils are the molecular trigger of inflammation in Parkinson's disease. *Biochemical Journal*. 471(3):323–333. DOI: 10.1042/BJ20150617.

Hall, T.A. 1999. BioEdit: A User-Friendly Biological Sequence Alignment Editor and Analysis Program for Windows 95/98/NT. *Nucleic Acids Symposium Series*. 41:95–98.

Halliwell, B. 1994. Free radicals, antioxidants, and human disease: curiosity, cause, or consequence? *The Lancet*. 344(8924):721–724. DOI: 10.1016/S0140-6736(94)92211-X.

Hamid, E., Ayele, B.A., Massi, D.G., ben Sassi, S., Tibar, H., Djonga, E.E., El-Sadig, S.M., Amer El Khedoud, W., et al. 2021. Availability of Therapies and Services for Parkinson's Disease in Africa: A Continent-Wide Survey. *Movement Disorders*. 36(10):2393–2407. DOI: 10.1002/mds.28669.

Hantikainen, E., Lagerros, Y.T., Ye, W., Serafini, M., Adami, H.-O., Bellocco, R. & Bonn, S. 2021. Dietary antioxidants and the risk of Parkinson Disease. *Neurology*. 96(5):e895–e903. DOI: 10.1212/WNL.0000000000011373.

Haque, M.E., Thomas, K.J., D'Souza, C., Callaghan, S., Kitada, T., Slack, R.S., Fraser, P., Cookson, M.R., et al. 2008. Cytoplasmic Pink1 activity protects neurons from dopaminergic neurotoxin MPTP. *Proceedings of the National Academy of Sciences*. 105(5):1716–1721. DOI: 10.1073/pnas.0705363105.

Harborne, J. 1986. Nature, distribution and function of plant flavonoids. *Progress in clinical and biology research*. 213:15–24.

He, L., Kulesskiy, E., Saarela, J., Turunen, L., Wennerberg, K., Aittokallio, T. & Tang, J. 2018. Methods for High-throughput Drug Combination Screening and Synergy Scoring. *Methods in Molecular Biology*. 1711:351–398. DOI: 10.1007/978-1-4939-7493-1_17.

Heller, B. 1982. *Patent No. Patent 4355044*. United States.

Helmschrodt, C., Becker, S., Perl, S., Schulz, A. & Richter, A. 2020. Development of a fast liquid chromatography-tandem mass spectrometry method for simultaneous quantification of

neurotransmitters in murine microdialysate. *Analytical and Bioanalytical Chemistry*. 412(28):7777–7787. DOI: 10.1007/s00216-020-02906-z.

Heo, J.-M., Ordureau, A., Paulo, J.A., Rinehart, J. & Harper, J.W. 2015. The PINK1-PARKIN mitochondrial ubiquitylation pathway drives a program of OPTN/NDP52 recruitment and TBK1 activation to promote mitophagy. *Molecular cell*. 60(1):7–20. DOI: 10.1016/j.molcel.2015.08.016.

Herlinger, E., Jameson, R.F. & Linert, W. 1995. Spontaneous autoxidation of dopamine. *Journal of the Chemical Society, Perkin Transactions 2*. (2):259–263. DOI: 10.1039/P29950000259.

Hijaz, B.A. & Volpicelli-Daley, L.A. 2020. Initiation and propagation of α-synuclein aggregation in the nervous system. *Molecular Neurodegeneration*. 15(1):19. DOI: 10.1186/s13024-020-00368-6.

Hirsch, E.C. & Hunot, S. 2009. Neuroinflammation in Parkinson's disease: a target for neuroprotection? *The Lancet Neurology*. 8(4):382–397. DOI: 10.1016/S1474-4422(09)70062-6.

Hornykiewicz, O. 2002. Dopamine miracle: from brain homogenate to dopamine replacement. *Movement Disorders*. 17(3):501–508. DOI: 10.1002/mds.10115.

Huang, N., Zhang, Y., Chen, M., Jin, H., Nie, J., Luo, Y., Zhou, S., Shi, J., et al. 2019. Resveratrol delays 6-hydroxydopamine-induced apoptosis by activating the PI3K/Akt signaling pathway. *Experimental Gerontology*. 124:110653. DOI: 10.1016/j.exger.2019.110653.

Hughes, K.C., Gao, X., Kim, I.Y., Rimm, E.B., Wang, M., Weisskopf, M.G., Schwarzschild, M.A. & Ascherio, A. 2016. Intake of antioxidant vitamins and risk of Parkinson's disease. *Movement Disorders*. 31(12):1909–1914. DOI: 10.1002/mds.26819.

Intagliata, S., Modica, M.N., Santagati, L.M. & Montenegro, L. 2019. Strategies to Improve Resveratrol Systemic and Topical Bioavailability: An Update. *Antioxidants*. 8(8):244. DOI: 10.3390/antiox8080244.

Islam, T.M. 2017. Oxidative stress and mitochondrial dysfunction-linked neurodegenerative disorders. *Neurological Research*. 39(1):73–82. DOI: 10.1080/01616412.2016.1251711.

Jankovic, J. 2008. Parkinson's disease: clinical features and diagnosis. *Journal of neurology, neurosurgery & psychiatry*. 79(4):368–376. DOI: 10.1136/jnnp.2007.131045.

Jaroonwitchawan, T., Chaicharoenaudomrung, N., Namkaew, J. & Noisa, P. 2017. Curcumin attenuates paraquat-induced cell death in human neuroblastoma cells through modulating oxidative stress and autophagy. *Neuroscience Letters*. 636:40–47. DOI: 10.1016/j.neulet.2016.10.050.

Jayaprakasha, G.K., Jena, B.S., Negi, P.S. & Sakariah, K.K. 2002. Evaluation of antioxidant activities and antimutagenicity of turmeric oil: a byproduct from curcumin production. *Zeitschrift für Naturforschung C*. 57(9–10):828–835. DOI: 10.1515/znc-2002-9-1013.

Jellinger, K.A. 1991. Pathology of Parkinson's disease. Changes other than the nigrostriatal pathway. *Mol Chem Neuropathol*. 14(3):153–197. DOI: 10.1007/bf03159935.

Jenner, P. & Olanow, C.W. 2006. The pathogenesis of cell death in Parkinson's disease. *Neurology*. 66(Issue 10, Supplement 4):S24–S36. DOI: 10.1212/WNL.66.10_suppl_4.S24.

Jinsmaa, Y., Sullivan, P., Gross, D., Cooney, A., Sharabi, Y. & Goldstein, D.S. 2014. Divalent metal ions enhance DOPAL-induced oligomerization of alpha-synuclein. *Neuroscience Letters*. 569:27–32. DOI: 10.1016/j.neulet.2014.03.016.

Jones, L.J., Gray, M., Yue, S.T., Haugland, R.P. & Singer, V.L. 2001. Sensitive determination of cell number using the CyQUANT® cell proliferation assay. *Journal of Immunological Methods*. 254(1–2):85–98. DOI: 10.1016/S0022-1759(01)00404-5.

Jost, W.H. 2020. Parkinsonian Drugs: Indications. In *NeuroPsychopharmacotherapy*. Springer International Publishing. 1–19. DOI: 10.1007/978-3-319-56015-1_216-1.

Kamada, T., Chow, T., Hiroi, T., Imaoka, S., Morimoto, K., Ohde, H. & Funae, Y. 2002. Metabolism of selegiline hydrochloride, a selective monoamine b-type inhibitor, in human liver microsomes. *Drug metabolism and pharmacokinetics*. 17(3):199–206. DOI: 10.2133/dmpk.17.199.

Kamelabad, M., Sardroodi, J., Ebrahimzadeh, A. & Ajamgard, M. 2021. Influence of curcumin and rosmarinic acid on disrupting the general properties of Alpha-Synuclein oligomer: Molecular dynamics simulation. *Journal of Molecular Graphics and Modelling*. 107:107963. DOI: 10.1016/j.jmgm.2021.107963.

Kamp, F., Exner, N., Lutz, A.K., Wender, N., Hegermann, J., Brunner, B., Nuscher, B., Bartels, T., et al. 2010. Inhibition of mitochondrial fusion by α-synuclein is rescued by PINK1, Parkin and DJ-1. *The EMBO Journal*. 29(20):3571–3589. DOI: 10.1038/emboj.2010.223.

Kane, L.A., Lazarou, M., Fogel, A.I., Li, Y., Yamano, K., Sarraf, S.A., Banerjee, S. & Youle, R.J. 2014. PINK1 phosphorylates ubiquitin to activate Parkin E3 ubiquitin ligase activity. *Journal of Cell Biology*. 205(2):143–153.

Karthikeyan, A., Senthil, N. & Min, T. 2020. Nanocurcumin: A Promising Candidate for Therapeutic Applications. *Frontiers in Pharmacology*. 11:487. DOI: 10.3389/fphar.2020.00487.

Kazlauskaite, A., Kondapalli, C., Gourlay, R., Campbell, D.G., Ritorto, M.S., Hofmann, K., Alessi, D.R., Knebel, A., et al. 2014. Parkin is activated by PINK1-dependent phosphorylation of ubiquitin at Ser65. *Biochemical Journal*. 460(1):127–141.

Kim, T.-H., Choi, J., Kim, H.-G. & Kim, H.R. 2014. Quantification of Neurotransmitters in Mouse Brain Tissue by Using Liquid Chromatography Coupled Electrospray Tandem Mass Spectrometry. *Journal of Analytical Methods in Chemistry*. 2014:506870. DOI: 10.1155/2014/506870.

Kingsbury, A.E., Bandopadhyay, R., Silveira-Moriyama, L., Ayling, H., Kallis, C., Sterlacci, W., Maeir, H., Poewe, W., et al. 2010. Brain stem pathology in Parkinson's disease: an evaluation of the Braak staging model. *Movement Disorders*. 25(15):2508–2515. DOI: 10.1002/mds.23305.

Kochar, N.I., Gonge, K., Chandewar, A. v & Khadse, C. 2014. Curcumin ameliorates gastrointestinal dysfunction and oxidative damage in diabetic rats. *Int. J. Pharmacol. Res*. 4(2):53–60. DOI: 10.7439/ijpr.v4i2.86.

Kopito, R.R. 2000. Aggresomes, inclusion bodies and protein aggregation. *Trends in cell biology*. 10(12):524–530. DOI: 10.1016/s0962-8924(00)01852-3.

Krishna, A., Biryukov, M., Trefois, C., Antony, P.M., Hussong, R., Lin, J., Heinäniemi, M., Glusman, G., et al. 2014. Systems genomics evaluation of the SH-SY5Y neuroblastoma cell line as a model for Parkinson's disease. *BMC Genomics*. 15(1):1154. DOI: 10.1186/1471-2164-15-1154.

Kunnumakkara, A.B., Guha, S., Krishnan, S., Diagaradjane, P., Gelovani, J. & Aggarwal, B.B. 2007. Curcumin potentiates antitumor activity of gemcitabine in an orthotopic model of pancreatic cancer through suppression of proliferation, angiogenesis, and inhibition of nuclear factor-κB–regulated gene products. *Cancer research*. 67(8):3853–3861. DOI: 10.1158/0008-5472.CAN-06-4257.

van Laar, V.S. & Berman, S.B. 2009. Mitochondrial dynamics in Parkinson's disease. *Experimental neurology*. 218(2):247–256. DOI: 10.1016/j.expneurol.2009.03.019.

Lane, E.L., Handley, O.J., Rosser, A.E. & Dunnett, S.B. 2008. Potential cellular and regenerative approaches for the treatment of Parkinson's disease. *Neuropsychiatric disease and treatment*. 4(5):835. DOI: 10.2147/ndt.s2013.

Larsen, K.E., Fon, E.A., Hastings, T.G., Edwards, R.H. & Sulzer, D. 2002. Methamphetamine-induced degeneration of dopaminergic neurons involves autophagy and upregulation of dopamine synthesis. *Journal of Neuroscience*. 22(20):8951–8960. DOI: 10.1523/JNEUROSCI.22-20-08951.2002.

Larsen, S.B., Hanss, Z. & Krüger, R. 2018. The genetic architecture of mitochondrial dysfunction in Parkinson's disease. *Cell and tissue research*. 373(1):21–37. DOI: 10.1007/s00441-017-2768-8.

Lazarou, M., Sliter, D.A., Kane, L.A., Sarraf, S.A., Wang, C., Burman, J.L., Sideris, D.P., Fogel, A.I., et al. 2015. The ubiquitin kinase PINK1 recruits autophagy receptors to induce mitophagy. *Nature*. 524(7565):309–314. DOI: 10.1038/nature14893.

Lee, H.S. 2006. Antiplatelet property of Curcuma longa L. rhizome-derived ar-turmerone. *Bioresource technology*. 97(12):1372–1376. DOI: 10.1016/j.biortech.2005.07.006.

Liu, J., Wang, X., Lu, Y., Duan, C., Gao, G., Lu, L. & Yang, H. 2017. Pink1 interacts with α-synuclein and abrogates α-synuclein-induced neurotoxicity by activating autophagy. *Cell Death & Disease*. 8(9):e3056–e3056. DOI: 10.1038/cddis.2017.427.

Livak, K.J. & Schmittgen, T.D. 2001. Analysis of relative gene expression data using real-time quantitative PCR and the 2− ΔΔCT method. *methods*. 25(4):402–408. DOI: 10.1006/meth.2001.1262.

Longo, D.M., Yang, Y., Watkins, P.B., Howell, B.A. & Siler, S.Q. 2016. Elucidating differences in the hepatotoxic potential of tolcapone and entacapone with DILIsym®, a mechanistic model of drug-induced liver injury. *CPT: pharmacometrics & systems pharmacology*. 5(1):31–39. DOI: 10.1002/psp4.12053.

Lotharius, J., Falsig, J., van Beek, J., Payne, S., Dringen, R., Brundin, P. & Leist, M. 2005. Progressive degeneration of human mesencephalic neuron-derived cells triggered by dopamine-dependent oxidative stress is dependent on the mixed-lineage kinase pathway. *Journal of Neuroscience*. 25(27):6329–6342. DOI: 10.1523/JNEUROSCI.1746-05.2005.

Lu, L., Jia, H., Gao, G., Duan, C., Ren, J., Li, Y. & Yang, H. 2018. Pink1 Regulates Tyrosine Hydroxylase Expression and Dopamine Synthesis. *Journal of Alzheimer's Disease*. 63(4):1361–1371. DOI: 10.3233/JAD-170832.

Luk, K.C., Song, C., O'Brien, P., Stieber, A., Branch, J.R., Brunden, K.R., Trojanowski, J.Q. & Lee, V.M.-Y. 2009. Exogenous α-synuclein fibrils seed the formation of Lewy body-like intracellular inclusions in cultured cells. *Proceedings of the National Academy of Sciences*. 106(47):20051–20056. DOI: 10.1073/pnas.0908005106.

Łukasiewicz, S., Mikołajczyk, A., Błasiak, E., Fic, E. & Dziedzicka-Wasylewska, M. 2021. Polycaprolactone Nanoparticles as Promising Candidates for Nanocarriers in Novel Nanomedicines. *Pharmaceutics*. 13(2):191. DOI: 10.3390/pharmaceutics13020191.

Lutz, A.K., Exner, N., Fett, M.E., Schlehe, J.S., Kloos, K., Lämmermann, K., Brunner, B., Kurz-Drexler, A., et al. 2009. Loss of Parkin or PINK1 Function Increases Drp1-dependent Mitochondrial Fragmentation. *Journal of Biological Chemistry*. 284(34):22938–22951. DOI: 10.1074/jbc.M109.035774.

Magalingam, K., Radhakrishnan, A. & Haleagraha, N. 2013. Rutin, a bioflavonoid antioxidant protects rat pheochromocytoma (PC-12) cells against 6-hydroxydopamine (6-OHDA)-induced neurotoxicity. *International Journal of Molecular Medicine*. 32(1):235–240. DOI: 10.3892/ijmm.2013.1375.

Magalingam, K.B., Radhakrishnan, A. & Haleagrahara, N. 2016. Protective effects of quercetin glycosides, rutin, and isoquercetrin against 6-hydroxydopamine (6-OHDA)-induced neurotoxicity in rat pheochromocytoma (PC-12) cells. *International Journal of Immunopathology and Pharmacology*. 29(1). DOI: 10.1177/0394632015613039.

Maiti, P. & Manna, J. 2014. Activation of Heat Shock Proteins by Nanocurcumin to Prevent Neurodegenerative Diseases. *Brain Disorders & Therapy*. 3(5):139. DOI: 10.4172/2168-975X.1000139.

Marsden, C.D. 1982. The mysterious motor function of the basal ganglia: The Robert Wartenberg Lecture. *Neurology*. 32(5):514–539. DOI: 10.1212/WNL.32.5.514.

Masato, A., Plotegher, N., Boassa, D. & Bubacco, L. 2019. Impaired dopamine metabolism in Parkinson's disease pathogenesis. *Molecular Neurodegeneration*. 14(1):35. DOI: 10.1186/s13024-019-0332-6.

Mattson, M.P. 2008. Hormesis defined. *Ageing Research Reviews*. 7(1):1–7. DOI: 10.1016/j.arr.2007.08.007.

Maynard, M.E., Redell, J.B., Kobori, N., Underwood, E.L., Fischer, T.D., Hood, K.N., LaRoche, V., Waxham, M.N., et al. 2020. Loss of PTEN-induced kinase 1 (Pink1) reduces hippocampal tyrosine hydroxylase and impairs learning and memory. *Experimental Neurology*. 323:113081. DOI: 10.1016/j.expneurol.2019.113081.

McBurney, R.N., Hines, W.M., VonTungeln, L.S., Schnackenberg, L.K., Beger, R.D., Moland, C.L., Han, T., Fuscoe, J.C., et al. 2012. The liver toxicity biomarker study phase I: Markers for the effects of tolcapone or entacapone. *Toxicologic pathology*. 40(6):951–964. DOI: 10.1177/0192623312444026.

van Meerloo, J., Kaspers, G.J.L. & Cloos, J. 2011. *Cell Sensitivity Assays: The MTT Assay*. 2nd ed. V. 731. J. Walker, Ed. Humana Press.

Meiser, J., Weindl, D. & Hiller, K. 2013. Complexity of dopamine metabolism. *Cell Communication and Signaling*. 11(1):34. DOI: 10.1186/1478-811X-11-34.

van der Merwe, C. 2015. Analysis of copy number variation and disease mechanisms underlying Parkinson's disease.

van der Merwe, C., van Dyk, H.C., Engelbrecht, L., van der Westhuizen, F.H., Kinnear, C., Loos, B. & Bardien, S. 2017. Curcumin Rescues a PINK1 Knock Down SH-SY5Y Cellular Model of Parkinson's Disease from Mitochondrial Dysfunction and Cell Death. *Molecular Neurobiology*. 54(4). DOI: 10.1007/s12035-016-9843-0.

Mills, R.D., Sim, C.H., Mok, S.S., Mulhern, T.D., Culvenor, J.G. & Cheng, H. 2008. Biochemical aspects of the neuroprotective mechanism of PTEN-induced kinase-1 (PINK1). *Journal of neurochemistry*. 105(1):18–33. DOI: 10.1111/j.1471-4159.2008.05249.x.

Mizuno, Y. 2020. Definition and Classification of Parkinsonian Drugs. In *NeuroPsychopharmacotherapy*. P. Riederer, G. Laux, B. Mulsant, W. Le, & T. Nagatsu, Eds. Cham: Springer International Publishing. 1–30. DOI: 10.1007/978-3-319-56015-1_213-1.

Monoranu, C.M., Apfelbacher, M., Grünblatt, E., Puppe, B., Alafuzoff, I., Ferrer, I., Al-Saraj, S., Keyvani, K., et al. 2009. pH measurement as quality control on human post mortem brain tissue: a study of the BrainNet Europe consortium. *Neuropathology and applied neurobiology*. 35(3):329–337. DOI: 10.1111/j.1365-2990.2008.01003a.x.

Montioli, R., Cellini, B., Dindo, M., Oppici, E. & Voltattorni, C.B. 2013. Interaction of human Dopa decarboxylase with L-Dopa: spectroscopic and kinetic studies as a function of pH. *BioMed research international*. 2013:161456. DOI: 10.1155/2013/161456.

Monzani, E., Nicolis, S., Dell'Acqua, S., Capucciati, A., Bacchella, C., Zucca, F.A., Mosharov, E. v, Sulzer, D., et al. 2019. Dopamine, oxidative stress and protein–quinone modifications in parkinson's and other neurodegenerative diseases. *Angewandte Chemie International Edition*. 58(20):6512–6527. DOI: 10.1002/anie.201811122.

Mori, H., Niwa, K., Zheng, Q., Yamada, Y., Sakata, K. & Yoshimi, N. 2001. Cell proliferation in cancer prevention; effects of preventive agents on estrogen-related endometrial carcinogenesis model and on an in vitro model in human colorectal cells. *Mutation Research/Fundamental and Molecular Mechanisms of Mutagenesis*. 480:201–207. DOI: 10.1016/s0027-5107(01)00200-7.

Moselhy, S.S., Razvi, S., Hasan, N., Balamash, K.S., Abulnaja, K.O., Yaghmoor, S.S., Youssri, M.A., Kumosani, T.A., et al. 2018. Multifaceted role of a marvel golden molecule, curcumin: a review.

Indian journal of pharmaceutical sciences. 80(3):400–411. DOI: 10.4172/pharmaceutical-sciences.1000372.

Mosharov, E. v, Borgkvist, A. & Sulzer, D. 2015. Presynaptic effects of levodopa and their possible role in dyskinesia. *Movement disorders*. 30(1):45–53. DOI: 10.1002/mds.26103.

Mosmann, T. 1983. Rapid colorimetric assay for cellular growth and survival: Application to proliferation and cytotoxicity assays. *Journal of Immunological Methods*. 65(1–2):55–63. DOI: 10.1016/0022-1759(83)90303-4.

Murphy, M.P. 2009. How mitochondria produce reactive oxygen species. *Biochemical Journal*. 417(1):1–13. DOI: 10.1042/BJ20081386.

Mythri, R.B. & Srinivas Bharath, M.M. 2012. Curcumin: a potential neuroprotective agent in Parkinson's disease. *Current pharmaceutical design*. 18(1):91–99. DOI: 10.2174/138161212798918995.

Nawab, A., Li, G., Liu, W., Lan, R., Wu, J., Zhao, Y., Kang, K., Kieser, B., et al. 2019. Effect of Dietary Curcumin on the Antioxidant Status of Laying Hens under High-Temperature Conditions. *Brazilian Journal of Poultry Science*. 21(2). DOI: 10.1590/1806-9061-2018-0868.

Nissinen, E. 2010. *Basic aspects of catechol-O-methyltransferase and the clinical applications of its inhibitors*. Academic Press.

Numakawa, Y., Numakawa, T., Matsumoto, T., Yagasaki, Y., Kumamaru, E., Kunugi, H., Taguchi, T. & Niki, E. 2006. Vitamin E protected cultured cortical neurons from oxidative stress-induced cell death through the activation of mitogen-activated protein kinase and phosphatidylinositol 3-kinase. *Journal of Neurochemistry*. 97(4):1191–1202. DOI: 10.1111/j.1471-4159.2006.03827.x.

Nunes, M.E., Müller, T.E., Braga, M.M., Fontana, B.D., Quadros, V.A., Marins, A., Rodrigues, C., Menezes, C., et al. 2017. Chronic Treatment with Paraquat Induces Brain Injury, Changes in Antioxidant Defenses System, and Modulates Behavioral Functions in Zebrafish. *Molecular Neurobiology*. 54(6):3925–3934. DOI: 10.1007/s12035-016-9919-x.

Oertel, W. & Schulz, J.B. 2016. Current and experimental treatments of Parkinson disease: a guide for neuroscientists. *Journal of neurochemistry*. 139:325–337. DOI: 10.1111/jnc.13750.

Olanow, C.W. 2015. Levodopa: effect on cell death and the natural history of Parkinson's disease. *Movement disorders*. 30(1):37–44. DOI: 10.1002/mds.26119.

Omarch, G., Kippie, Y., Mentor, S., Ebrahim, N., Fisher, D., Murilla, G., Swai, H. & Dube, A. 2019. Comparative in vitro transportation of pentamidine across the blood-brain barrier using

polycaprolactone nanoparticles and phosphatidylcholine liposomes. *Artificial Cells, Nanomedicine, and Biotechnology*. 47(1):1428–1436. DOI: 10.1080/21691401.2019.1596923.

Ordureau, A., Heo, J.-M., Duda, D.M., Paulo, J.A., Olszewski, J.L., Yanishevski, D., Rinehart, J., Schulman, B.A., et al. 2015. Defining roles of PARKIN and ubiquitin phosphorylation by PINK1 in mitochondrial quality control using a ubiquitin replacement strategy. *Proceedings of the National Academy of Sciences*. 112(21):6637–6642. DOI: 10.1073/pnas.1506593112.

Ozawa, K., Headlam, M.J., Mouradov, D., Watt, S.J., Beck, J.L., Rodgers, K.J., Dean, R.T., Huber, T., et al. 2005. Translational incorporation of L-3, 4-dihydroxyphenylalanine into proteins. *The FEBS journal*. 272(12):3162–3171. DOI: 10.1111/j.1742-4658.2005.04735.x.

Palazzi, L., Bruzzone, E., Bisello, G., Leri, M., Stefani, M., Bucciantini, M. & Polverino de Laureto, P. 2018. Oleuropein aglycone stabilizes the monomeric α-synuclein and favours the growth of non-toxic aggregates. *Scientific Reports*. 8(1):8337. DOI: 10.1038/s41598-018-26645-5.

Palle, S. & Neerati, P. 2018. Improved neuroprotective effect of resveratrol nanoparticles as evinced by abrogation of rotenone-induced behavioral deficits and oxidative and mitochondrial dysfunctions in rat model of Parkinson's disease. *Naunyn-Schmiedeberg's Archives of Pharmacology*. 391(4):445–453. DOI: 10.1007/s00210-018-1474-8.

Pandey, N., Strider, J., Nolan, W.C., Yan, S.X. & Galvin, J.E. 2008. Curcumin inhibits aggregation of α-synuclein. *Acta Neuropathologica*. 115(4). DOI: 10.1007/s00401-007-0332-4.

Parambi, D.G.T. 2020. Treatment of Parkinson's Disease by MAO-B Inhibitors, New Therapies and Future Challenges - A Mini-Review. *Combinatorial Chemistry & High Throughput Screening*. 23(9):847–861. DOI: 10.2174/1386207323666200402090557.

Park, H.-A. & Ellis, A.C. 2020. Dietary Antioxidants and Parkinson's Disease. *Antioxidants*. 9(7):570. DOI: 10.3390/antiox9070570.

Parkinson, J. 2002. An Essay on the Shaking Palsy. *The Journal of Neuropsychiatry and Clinical Neurosciences*. 14(2):223–236. DOI: 10.1176/jnp.14.2.223.

Paumier, K.L., Sukoff Rizzo, S.J., Berger, Z., Chen, Y., Gonzales, C., Kaftan, E., Li, L., Lotarski, S., et al. 2013. Behavioral Characterization of A53T Mice Reveals Early and Late Stage Deficits Related to Parkinson's Disease. *PLoS ONE*. 8(8):e70274. DOI: 10.1371/journal.pone.0070274.

Pickrell, A.M. & Youle, R.J. 2015. The roles of PINK1, parkin, and mitochondrial fidelity in Parkinson's disease. *Neuron*. 85(2):257–273. DOI: 10.1016/j.neuron.2014.12.007.

Pitt, J.J. 2009. Principles and applications of liquid chromatography-mass spectrometry in clinical biochemistry. *The Clinical Biochemist: Reviews*. 30(1):19–34.

Pogocki, D., Ruman, T., Danilczuk, M., Danilczuk, M., Celuch, M. & Wałajtys-Rode, E. 2007. Application of nicotine enantiomers, derivatives and analogues in therapy of neurodegenerative disorders. *European journal of pharmacology*. 563(1–3):18–39. DOI: 10.1016/j.ejphar.2007.02.038.

Oritz, R., Prados, J., Melguizo, C., Arias, J.L., Ruíz, M., Álvarez, P., Caba, O., Luque, R., et al. 2012. 5-Fluorouracil-loaded poly(ε-caprolactone) nanoparticles combined with phage E gene therapy as a new strategy against colon cancer. *International Journal of Nanomedicine*. (January):95. DOI: 10.2147/IJN.S26401.

Prelich, G. 2012. Gene Overexpression: Uses, Mechanisms, and Interpretation. *Genetics*. 190(3):841–854. DOI: 10.1534/genetics.111.136911.

Pridgeon, J.W., Olzmann, J.A., Chin, L.-S. & Li, L. 2007. PINK1 Protects against Oxidative Stress by Phosphorylating Mitochondrial Chaperone TRAP1. *PLoS Biology*. 5(7):e172. DOI: 10.1371/journal.pbio.0050172.

R Core Team. 2020.

Rajeswari, A. & Sabesan, M. 2008. Inhibition of monoamine oxidase-B by the polyphenolic compound, curcumin and its metabolite tetrahydrocurcumin, in a model of Parkinson's disease induced by MPTP neurodegeneration in mice. *Inflammopharmacology*. 16(2):96–99. DOI: 10.1007/s10787-007-1614-0.

Ramachandran, C., Rodriguez, S., Ramachandran, R., Nair, P.K.R., Fonseca, H., Khatib, Z., Escalon, E. & Melnick, S.J. 2005. Expression profiles of apoptotic genes induced by curcumin in human breast cancer and mammary epithelial cell lines. *Anticancer research*. 25(5):3293–3302.

Riveles, K., Huang, L.Z. & Quik, M. 2008. Cigarette smoke, nicotine and cotinine protect against 6-hydroxydopamine-induced toxicity in SH-SY5Y cells. *Neurotoxicology*. 29(3):421–427. DOI: 10.1016/j.neuro.2008.02.001.

Rodgers, K.J. & Dean, R.T. 2000. Metabolism of protein-bound DOPA in mammals. *The International Journal of Biochemistry & Cell Biology*. 32(9):945–955. DOI: 10.1016/s1357-2725(00)00034-0.

Rodriguez-Oroz, M.C., Jahanshahi, M., Krack, P., Litvan, I., Macias, R., Bezard, E. & Obeso, J.A. 2009. Initial clinical manifestations of Parkinson's disease: features and pathophysiological mechanisms. *Lancet Neurol*. 8(12):1128–1139. DOI: 10.1016/s1474-4422(09)70293-5.

Salehi, B., Calina, D., Docea, A.O., Koirala, N., Aryal, S., Lombardo, D., Pasqua, L., Taheri, Y., et al. 2020. Curcumin's Nanomedicine Formulations for Therapeutic Application in Neurological Diseases. *Journal of Clinical Medicine*. 9(2):430. DOI: 10.3390/jcm9020430.

Schapira, A.H. v. 2008. Mitochondria in the aetiology and pathogenesis of Parkinson's disease. *The Lancet Neurology*. 7(1):97–109. DOI: 10.1016/S1474-4422(07)70327-7.

Scholz, D., Pöltl, D., Genewsky, A., Weng, M., Waldmann, T., Schildknecht, S. & Leist, M. 2011. Rapid, complete and large-scale generation of post-mitotic neurons from the human LUHMES cell line. *Journal of neurochemistry*. 119(5):957–971. DOI: 10.1111/j.1471-4159.2011.07255.x.

Segura-Aguilar, J., Paris, I., Muñoz, P., Ferrari, E., Zecca, L. & Zucca, F.A. 2014. Protective and toxic roles of dopamine in Parkinson's disease. *Journal of neurochemistry*. 129(6):898–915. DOI: 10.1111/jnc.12686.

Shahmoradian, S.H., Lewis, A.J., Genoud, C., Hench, J., Moors, T.E., Navarro, P.P., Castaño-Díez, D., Schweighauser, G., et al. 2019. Lewy pathology in Parkinson's disease consists of crowded organelles and lipid membranes. *Nature Neuroscience*. 22(7):1099–1109. DOI: 10.1038/s41593-019-0423-2.

Sharma, S., Ali, A., Ali, J., Sahni, J.K. & Baboota, S. 2013. Rutin: therapeutic potential and recent advances in drug delivery. *Expert Opinion on Investigational Drugs*. 22(8):1063–1079. DOI: 10.1517/13543784.2013.805744.

Shipley, M.M., Mangold, C.A. & Szpara, M.L. 2016. Differentiation of the SH-SY5Y Human Neuroblastoma Cell Line. *Journal of Visualized Experiments*. (108):53193. DOI: 10.3791/53193.

Shrikanth Gadad, B., K. Subramanya, P., Pullabhatla, S., S. Shantharam, I. & K.S., R. 2012. Curcumin-glucoside, A Novel Synthetic Derivative of Curcumin, Inhibits α-Synuclein Oligomer Formation: Relevance to Parkinson's Disease. *Current Pharmaceutical Design*. 18(1). DOI: 10.2174/138161212798919093.

Siddique, Y.H., Naz, F. & Jyoti, S. 2014. Effect of Curcumin on Lifespan, Activity Pattern, Oxidative Stress, and Apoptosis in the Brains of Transgenic Drosophila Model of Parkinson's Disease. *BioMed Research International*. 2014:1–6. DOI: 10.1155/2014/606928.

Sivandzade, F., Bhalerao, A. & Cucullo, L. 2019. Analysis of the Mitochondrial Membrane Potential Using the Cationic JC-1 Dye as a Sensitive Fluorescent Probe. *BIO-PROTOCOL*. 9(1). DOI: 10.21769/BioProtoc.3128.

Sookhaklari, R., Geramizadeh, B., Abkar, M. & Moosavi, M. 2019. The neuroprotective effect of BSA-based nanocurcumin against 6-OHDA-induced cell death in SH-SY5Y cells. *Avicenna Journal Of Phytomedicine*. 9(2):92–100.

Soong, N.W., Hinton, D.R., Cortopassi, G. & Arnheim, N. 1992. Mosaicism for a specific somatic mitochondrial DNA mutation in adult human brain. *Nature genetics*. 2(4):318–323. DOI: 10.1038/ng1292-318.

Spencer, J.P.E., Jenner, P., Daniel, S.E., Lees, A.J., Marsden, D.C. & Halliwell, B. 2002. Conjugates of Catecholamines with Cysteine and GSH in Parkinson's Disease: Possible Mechanisms of Formation Involving Reactive Oxygen Species. *Journal of Neurochemistry*. 71(5):2112–2122. DOI: 10.1046/j.1471-4159.1998.71052112.x.

Stocchi, F., Vacca, L. & Radicati, F.G. 2015. How to optimize the treatment of early stage Parkinson's disease. *Translational neurodegeneration*. 4(1):4. DOI: 10.1186/2047-9158-4-4.

Surathi, P., Jhunjhunwala, K., Yadav, R. & Pal, P.K. 2016. Research in Parkinson's disease in India: A review. *Annals of Indian Academy of Neurology*. 19(1):9–20. DOI: 10.4103/0972-2327.167713.

Syng-Ai, C., Kumari, A.L. & Khar, A. 2004. Effect of curcumin on normal and tumor cells: role of glutathione and bcl-2. *Molecular cancer therapeutics*. 3(9):1101–1108.

Takanashi, M., Mochizuki, H., Yokomizo, K., Hattori, N., Mori, H., Yamamura, Y. & Mizuno, Y. 2001. Iron accumulation in the substantia nigra of autosomal recessive juvenile parkinsonism (ARJP). *Parkinsonism & related disorders*. 7(4):311–314. DOI: 10.1016/s1353-8020(00)00050-x.

Tanaka, M., Kim, Y.M., Lee, G., Junn, E., Iwatsubo, T. & Mouradian, M.M. 2004. Aggresomes formed by α-synuclein and synphilin-1 are cytoprotective. *Journal of Biological Chemistry*. 279(6):4625–4631. DOI: 10.1074/jbc.M310994200.

Taylor, S., Wakem, M., Dijkman, G., Alsarraj, M. & Nguyen, M. 2010. A practical approach to RT-qPCR—Publishing data that conform to the MIQE guidelines. *Methods*. 50(4):S1–S5. DOI: 10.1016/j.ymeth.2010.01.005.

Tayyem, R.F., Heath, D.D., Al-Delaimy, W.K. & Rock, C.L. 2006. Curcumin content of turmeric and curry powders. *Nutrition and cancer*. 55(2):126–131. DOI: 10.1207/s15327914nc5502_2.

Teo, K.C. & Ho, S.-L. 2013. Monoamine oxidase-B (MAO-B) inhibitors: implications for disease-modification in Parkinson's disease. *Translational Neurodegeneration*. 2(1):19. DOI: 10.1186/2047-9158-2-19.

Testa, C.M., Sherer, T.B. & Greenamyre, J.T. 2005. Rotenone induces oxidative stress and dopaminergic neuron damage in organotypic substantia nigra cultures. *Molecular Brain Research.* 134(1):109–118. DOI: 10.1016/j.molbrainres.2004.11.007.

Tian, S., Guo, R., Wei, S., Kong, Y., Wei, X., Wang, W., Shi, X. & Jiang, H. 2016. Curcumin protects against the intestinal ischemia-reperfusion injury: involvement of the tight junction protein ZO-1 and TNF-α related mechanism. *The Korean Journal of Physiology & Pharmacology*. 20(2):147–152. DOI: 10.4196/kjpp.2016.20.2.147.

Toulorge, D., Guerreiro, S., Hild, A., Maskos, U., Hirsch, E.C. & Michel, P.P. 2011. Neuroprotection of midbrain dopamine neurons by nicotine is gated by cytoplasmic Ca2+. *The FASEB Journal*. 25(8):2563–2573. DOI: 10.1096/fj.11-182824.

Trujillo, J., Granados-Castro, L.F., Zazueta, C., Andérica-Romero, A.C., Chirino, Y.I. & Pedraza-Chaverrí, J. 2014. Mitochondria as a Target in the Therapeutic Properties of Curcumin. *Archiv der Pharmazie*. 347(12):873–884. DOI: 10.1002/ardp.201400266.

Tysnes, O.-B. & Storstein, A. 2017. Epidemiology of Parkinson's disease. *Journal of Neural Transmission*. 124(8):901–905. DOI: 10.1007/s00702-017-1686-y.

Umerska, A., Gaucher, C., Oyarzun-Ampuero, F., Fries-Raeth, I., Colin, F., Villamizar-Sarmiento, M., Maincent, P. & Sapin-Minet, A. 2018. Polymeric Nanoparticles for Increasing Oral Bioavailability of Curcumin. *Antioxidants*. 7(4):46. DOI: 10.3390/antiox7040046.

Uversky, V.N. & Eliezer, D. 2009. Biophysics of Parkinson's disease: structure and aggregation of α-synuclein. *Current Protein and Peptide Science*. 10(5):483–499. DOI: 10.2174/138920309789351921.

Valencia, C.A., Pervaiz, M.A., Husami, A., Qian, Y. & Zhang, K. 2013. Sanger Sequencing Principles, History, and Landmarks. 3–11. DOI: 10.1007/978-1-4614-9032-6_1.

Valente, E.M., Abou-Sleiman, P.M., Caputo, V., Muqit, M.M.K., Harvey, K., Gispert, S., Ali, Z., del Turco, D., et al. 2004. Hereditary early-onset Parkinson's disease caused by mutations in PINK1. *Science*. 304(5674):1158–1160.

Walsh, D.W.M., Siebenwirth, C., Greubel, C., Ilicic, K., Reindl, J., Girst, S., Muggiolu, G., Simon, M., et al. 2017. Live cell imaging of mitochondria following targeted irradiation in situ reveals rapid and highly localized loss of membrane potential. *Scientific Reports*. 7(1):46684. DOI: 10.1038/srep46684.

Wang, F.-Y., Wang, P., Zhao, D.-F., Gonzalez, F.J., Fan, Y.-F., Xia, Y.-L., Ge, G.-B. & Yang, L. 2021. Analytical methodologies for sensing catechol-O-methyltransferase activity and their applications. *Journal of Pharmaceutical Analysis*. 11(1):15–27. DOI: 10.1016/j.jpha.2020.03.012.

Wang, H., Dong, X., Liu, Z., Zhu, S., Liu, H., Fan, W., Hu, Y., Hu, T., et al. 2018. Resveratrol Suppresses Rotenone-induced Neurotoxicity Through Activation of SIRT1/Akt1 Signaling Pathway. *The Anatomical Record*. 301(6):1115–1125. DOI: 10.1002/ar.23781.

Wang, M., Boddapati, S., Emadi, S. & Sierks, M. 2010. Curcumin reduces α-synuclein induced cytotoxicity in Parkinson's disease cell model. *BMC Neuroscience*. 11(1):57. DOI: 10.1186/1471-2202-11-57.

Wang, T., Li, C., Han, B., Wang, Z., Meng, X., Zhang, L., He, J. & Fu, F. 2020. Neuroprotective effects of Danshensu on rotenone-induced Parkinson's disease models in vitro and in vivo. *BMC Complementary Medicine and Therapies*. 20(1):20. DOI: 10.1186/s12906-019-2738-7.

Wang, X.H., Souders, C.L., Zhao, Y.H. & Martyniuk, C.J. 2018. Paraquat affects mitochondrial bioenergetics, dopamine system expression, and locomotor activity in zebrafish (Danio rerio). *Chemosphere*. 191:106–117. DOI: 10.1016/j.chemosphere.2017.10.032.

Wang, Y., Lobb-Rabe, M., Ashley, J., Anand, V. & Carrillo, R.A. 2021. Structural and Functional Synaptic Plasticity Induced by Convergent Synapse Loss in the Drosophila Neuromuscular Circuit. *The Journal of Neuroscience*. 41(7):1401–1417. DOI: 10.1523/JNEUROSCI.1492-20.2020.

Wickremaratchi, M.M., Knipe, M.D.W., Sastry, B.S.D., Morgan, E., Jones, A., Salmon, R., Weiser, R., Moran, M., et al. 2011. The motor phenotype of Parkinson's disease in relation to age at onset. *Movement disorders*. 26(3):457–463. DOI: 10.1002/mds.23469.

Wood-Kaczmar, A., Gandhi, S., Yao, Z., Abramov, A.S.Y., Miljan, E.A., Keen, G., Stanyer, L., Hargreaves, I., et al. 2008. PINK1 Is Necessary for Long Term Survival and Mitochondrial Function in Human Dopaminergic Neurons. *PLoS ONE*. 3(6):e2455. DOI: 10.1371/journal.pone.0002455.

Wu, L., Jiang, C., Kang, Y., Dai, Y., Fang, W. & Huang, P. 2020. Curcumin exerts protective effects against hypoxia-reoxygenation injury via the enhancement of apurinic/apyrimidinic endonuclease1 in SH-SY5Y cells: Involvement of the PI3K/AKT pathway. *International Journal of Molecular Medicine*. 45(4):993–1004. DOI: 10.3892/ijmm.2020.4483.

Xiao, B., Ng, H.H., Takahashi, R. & Tan, E.-K. 2016. Induced pluripotent stem cells in Parkinson's disease: scientific and clinical challenges. *Journal of Neurology, Neurosurgery & Psychiatry*. 87(7):697–702. DOI: 10.1136/jnnp-2015-312036.

Xicoy, H., Wieringa, B. & Martens, G.J.M. 2017. The SH-SY5Y cell line in Parkinson's disease research: a systematic review. *Molecular Neurodegeneration*. 12(1):10. DOI: 10.1186/s13024-017-0149-0.

Xie, H., Hu, L. & Li, G. 2010. SH-SY5Y human neuroblastoma cell line: in vitrocell model of dopaminergic neurons in Parkinson's disease. *Chinese medical journal*. 123(8):1086–1092.

Xu, X., Huang, J., Li, J., Liu, L., Han, C., Shen, Y., Zhang, G., Jiang, H., et al. 2016. Induced pluripotent stem cells and Parkinson's disease: modelling and treatment. *Cell proliferation*. 49(1):14–26. DOI: 10.1111/cpr.12229.

Yu, X., Chen, L., Tang, M., Yang, Z., Fu, A., Wang, Z. & Wang, H. 2019. Revealing the Effects of Curcumin on SH-SY5Y Neuronal Cells: A Combined Study from Cellular Viability, Morphology, and Biomechanics. *Journal of Agricultural and Food Chemistry*. 67(15):4273–4279. DOI: 10.1021/acs.jafc.9b00314.

Yue, G.G.L., Chan, B.C.L., Hon, P.-M., Lee, M.Y.H., Fung, K.-P., Leung, P.-C. & Lau, C.B.S. 2010. Evaluation of in vitro anti-proliferative and immunomodulatory activities of compounds isolated from Curcuma longa. *Food and Chemical Toxicology*. 48(8–9):2011–2020. DOI: 10.1016/j.fct.2010.04.039.

Zarow, C., Lyness, S.A., Mortimer, J.A. & Chui, H.C. 2003. Neuronal loss is greater in the locus coeruleus than nucleus basalis and substantia nigra in Alzheimer and Parkinson diseases. *Arch Neurol*. 60(3):337–341. DOI: 10.1001/archneur.60.3.337.

Zecca, L., Youdim, M.B.H., Riederer, P., Connor, J.R. & Crichton, R.R. 2004. Iron, brain ageing and neurodegenerative disorders. *Nature Reviews Neuroscience*. 5(11):863–873.

Zeng, W., Zhang, W., Lu, F., Gao, L. & Gao, G. 2017. Resveratrol attenuates MPP+-induced mitochondrial dysfunction and cell apoptosis via AKT/GSK-3β pathway in SN4741 cells. *Neuroscience Letters*. 637:50–56. DOI: 10.1016/j.neulet.2016.11.054.

Zhang, J., Fan, W., Wang, H., Bao, L., Li, G., Li, T., Song, S., Li, H., et al. 2015. Resveratrol Protects PC12 Cell against 6-OHDA Damage via CXCR4 Signaling Pathway. *Evidence-Based Complementary and Alternative Medicine*. 2015. DOI: 10.1155/2015/730121.

Zhang, P., Chan, W., Ang, I.L., Wei, R., Lam, M.M.T., Lei, K.M.K. & Poon, T.C.W. 2019. Revisiting Fragmentation Reactions of Protonated α-Amino Acids by High-Resolution Electrospray Ionization Tandem Mass Spectrometry with Collision-Induced Dissociation. *Scientific Reports*. 9(1):6453. DOI: 10.1038/s41598-019-42777-8.

Zhou, Z.D., Lan, Y.H., Tan, E.K. & Lim, T.M. 2010. Iron species-mediated dopamine oxidation, proteasome inhibition, and dopaminergic cell demise: implications for iron-related dopaminergic neuron degeneration. *Free Radical Biology and Medicine*. 49(12):1856–1871. DOI: 10.1016/j.freeradbiomed.2010.09.010.

Zhou, Z.D., Refai, F.S., Xie, S.P., Ng, S.H., Chan, C.H.S., Ho, P.G.H., Zhang, X.D., Lim, T.M., et al. 2014. Mutant PINK1 upregulates tyrosine hydroxylase and dopamine levels, leading to vulnerability of dopaminergic neurons. *Free Radical Biology and Medicine*. 68:220–233. DOI: 10.1016/j.freeradbiomed.2013.12.015.

Zonyane, S., Fawole, O.A., la Grange, C., Stander, M.A., Opara, U.L. & Makunga, N.P. 2020. The Implication of Chemotypic Variation on the Anti-Oxidant and Anti-Cancer Activities of Sutherlandia frutescens (L.) R.Br. (Fabaceae) from Different Geographic Locations. *Antioxidants*. 9(2):152. DOI: 10.3390/antiox9020152.

Zorova, L.D., Popkov, V.A., Plotnikov, E.Y., Silachev, D.N., Pevzner, I.B., Jankauskas, S.S., Babenko, V.A., Zorov, S.D., et al. 2018. Mitochondrial membrane potential. *Analytical Biochemistry*. 552:50–59. DOI: 10.1016/j.ab.2017.07.009.

Zucca, F.A., Segura-Aguilar, J., Ferrari, E., Muñoz, P., Paris, I., Sulzer, D., Sarna, T., Casella, L., et al. 2017. Interactions of iron, dopamine and neuromelanin pathways in brain aging and Parkinson's disease. *Progress in neurobiology*. 155:96–119. DOI: 10.1016/j.pneurobio.2015.09.012.

Appendix I.   List of reagents

Bacterial and DNA reagents:

LB media
5 g bactotryptone
2.5 g yeast extract
5 g NaCl

100 mg/ml Ampicillin
100 mg ampicillin
1 ml dH$_2$O

Agarose gel
1 g SeaKem® LE Agarose powder
100 ml 1X sodium borate (SB) buffer
Heat in a microwave until dissolved

Cell culture reagents:

Culturing medium
Dulbecco's Modified Eagle Medium (DMEM) supplemented with:
10 % Fetal bovine serum (FBS)
1 % Penicillin-Streptomycin

Freezing medium
90 % FBS
10 % DMSO

Supplementary Table 1. Amino acid composition of high glucose Dulbeccos's Modified Eagle's Medium. Taken from https://www.thermofisher.com/za/en/home/technical-resources/media-formulation.8.html

Amino acid	Molecular Weight	Concentration (mg/L)	Concentration (mM)
Glycine	75.0	30.0	0.4
L-Arginine hydrochloride	211.0	84.0	0.39810428

118

L-Cystine 2HCl	313.0	63.0	0.20127796
L-Glutamine	146.0	584.0	4.0
L-Histidine hydrochloride-H2O	210.0	42.0	0.2
L-Isoleucine	131.0	105.0	0.8015267
L-Leucine	131.0	105.0	0.8015267
L-Lysine hydrochloride	183.0	146.0	0.7978142
L-Methionine	149.0	30.0	0.20134228
L-Phenylalanine	165.0	66.0	0.4
L-Serine	105.0	42.0	0.4
L-Threonine	119.0	95.0	0.79831934
L-Tryptophan	204.0	16.0	0.078431375
L-Tyrosine disodium salt dihydrate	261.0	104.0	0.39846742
L-Valine	117.0	94.0	0.8034188

Immunofluorescence reagents:

1X PBS
1 PBS tablet
200 ml dH$_2$O

0.5 % BSA
500 mg BSA
100 ml PBS

0.25 % Triton X-100
100 ul Triton X-100
40 ml PBS

4 % formaldehyde
4 ml formaldehyde
8 ml distilled water

10 µg/ml DAPI

2 ul 5mg/ml DAPI

998 µl PBS

Cellular treatments:

5 mg/ml MTT dye

10 mg of Thiazolyl Blue Tetrazolium Bromide

2 ml PBS

20 µM Curcumin

Dissolve 50 mg curcumin in 13.6 ml DMSO

50 mM Paraquat

Dissolve 12.5 mg paraquat in 1 ml dH$_2$O

1 mg/ml unloaded polycaprolactone nanoparticle

Dissolve 1mg of nanoparticle in 1 ml DMSO

1 mg/ml curcumin loaded polycaprolactone nanoparticle

Dissolve 1mg of nanocurcumin in 1 ml DMSO
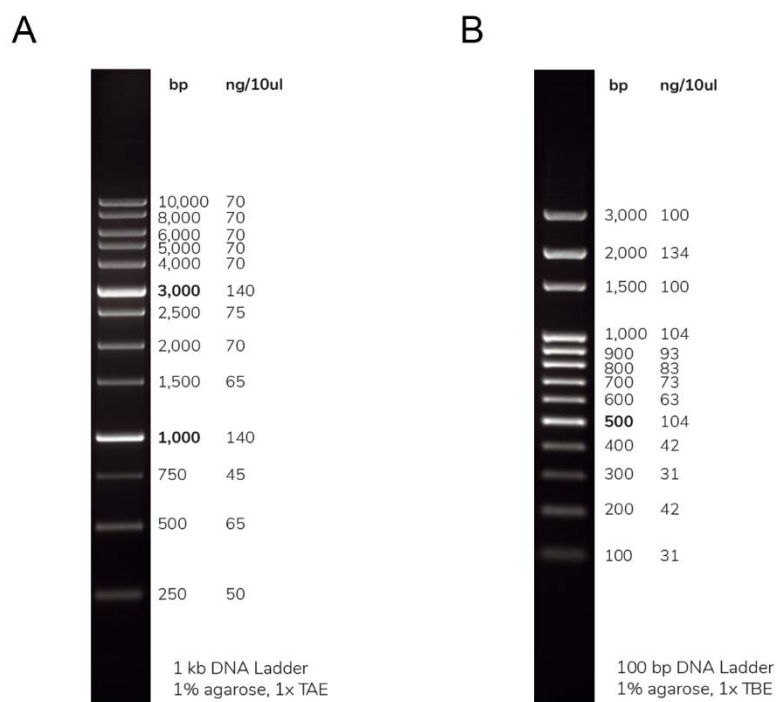
Supplementary Figure 1. DNA ladders used for sizing of DNA products in agarose gel electrophoresis. A – The 1 kb DNA ladder (Solis Biodyne) is composed of 13 DNA fragments ranging from 250 bp to 10 kb. The 1 kb and 3 kb reference bands serve for easy orientation. **B** – The 100 bp DNA ladder (Solis Biodyne) is composed of 13 DNA fragments ranging from 100 bp to 3 kb. The 500 bp reference band serves for easy orientation.

Appendix II.   PINK1 data

Supplementary Table 2: List of sequencing primers

Primer	Sequence (5'-3')	Tm (°C)	Ta (°C)
PINK1 G309D FOR	ATCCAAGAGAGGTCCCAAGC	59.08	54.08
PINK1 G309D REV	TTTGCATGGCTTTCTTCTCCG	59.46	54.46
PP2F661	ATGTGGAACATCTCGGCAGG	60.11	55.11
PP2R1525	GATGAAGCACATTTGCGGCT	59.83	54.83
PP8F934	CGGACGCTGTTCCTCGTTAT	60.18	55.18
PP8R1506	TACTCGGGCAGATGGTCTCT	59.74	54.74
PP1F479	AGTCCATTGGTAAGGGCTGC	60.03	55.03
PP1R683	GAACCTGCCGAGATGTTCCA	60.04	55.04
PP2F322	CTGGGCCTCATCGAGGAAAA	59.75	54.75
PP2R496	AGCCCTTACCAATGGACTGC	60.03	55.03
PP1F1504	GTAGCCGCAAATGTGCTTCA	59.48	54.48
PP1R1640	TTCTCTGTGAGCCTGTTGGC	60.25	55.25
PP6F1576	AAGATGGTTGGCTGGCTCCT	61.50	56.50
PP6R1694	TCACACTCCAGGTTAGCCAGA	60.48	55.48

Tm, melting temperature; Ta, annealing temperature

Supplementary Table 3. List of universal primers.

Primer	Sequence (5'-3')	Tm (°C)	Ta (°C)
CMV-F	CGCAAATGGGCGGTAGGCGTG	60.21	55.21
pBABE3	ACCCTAACTGACACACATTCC	52.40	47.40

Tm, melting temperature; Ta, annealing temperature
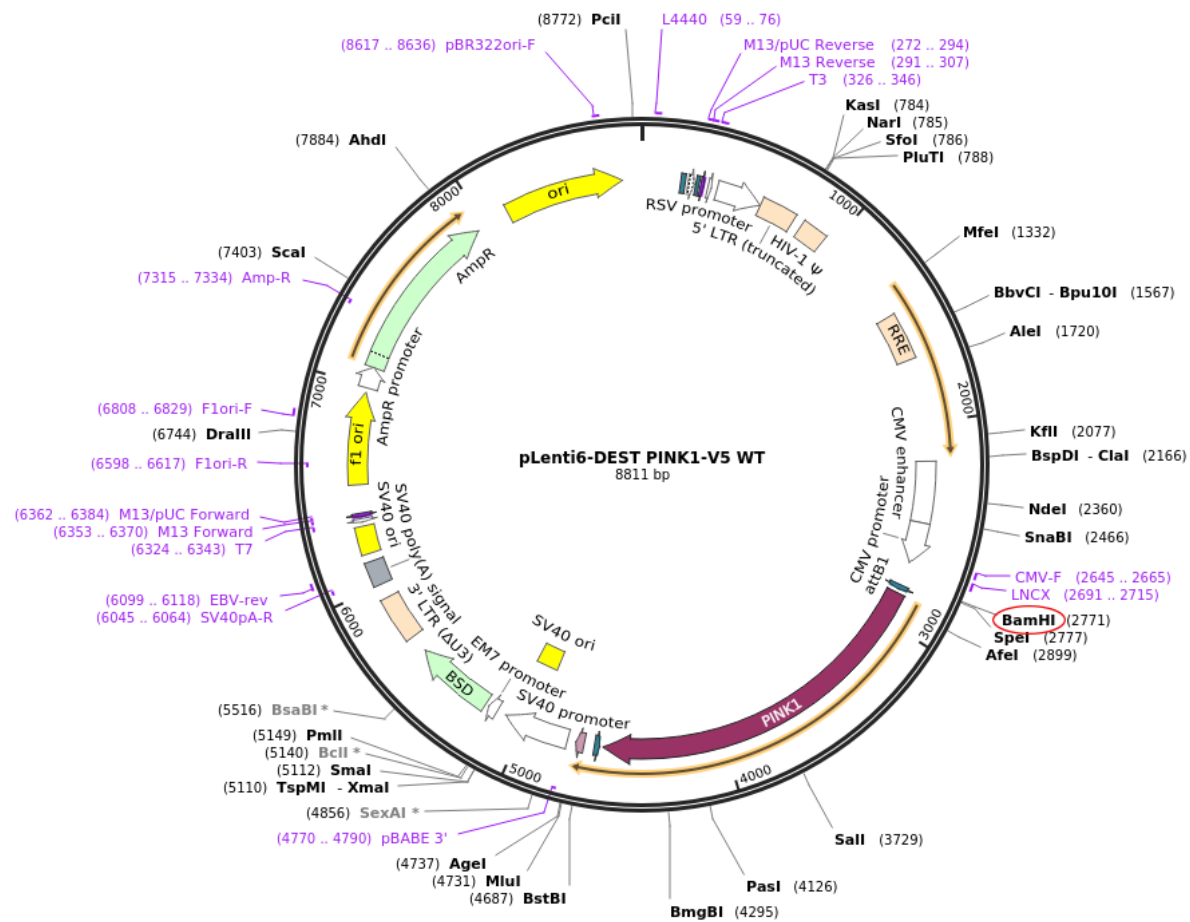
Supplementary Figure 2. Plasmid map of pLenti6-DEST PINK1-V5 WT.

Supplementary Table 4. Troubleshooting of WT and G309D PINK1 plasmids.

Plasmid	Date received	Source	Problem	Solution
WT-A (*E. coli* stab)	May 2020	Addgene, United States	These bacterial stabs could only be plated two months following arrival in South Africa due to closure of the lab during the nationwide lockdown. Due to delayed processing, these bacteria struggled to grow on both media with and without antibiotics.	Addgene agreed to send another batch of plasmids
Mutant-A (*E. coli* stab)	May 2020	Addgene, United States		
WT-B (*E. coli* stab)	August 2020	Addgene, United States	Good growth on selection media but unable to verify by sequencing, PCR, or restriction digest	Addgene agreed to send another WT
Mutant-B (*E. coli*	August 2020	Addgene, United States	Verified by sequencing, PCR, and restriction digest	Chosen for use in all experiments

stab)				
WT-C (*E. coli* stab)	May 2021	Addgene, United States	Unable to verify by restriction digest and failed to grow after first plating from bacterial stab.	Addgene agreed to send an aliquot of WT plasmid DNA for transformation
WT-D (DNA)	June 2021	Addgene, United States	WT-D DNA required transformation into chemically competent *E. coli* which was not available	Wait for Stbl3 *E. coli* delivery for transformation but use WT-B for all experiments in the interim
WT-Z (DNA)	June 2021	Dr Zhi Dong Zhou, Dr Saw Wuan-Ting (Duke-NUS Medical School, Singapore)	WT-Z could not be verified by restriction digest following transformation into DH5α *E. coli*	Wait for Stbl3 *E. coli* delivery for transformation but use WT-B for all experiments in the interim.
Mutant-Z (DNA)	June 2021	Dr Zhi Dong Zhou, Dr Saw Wuan-Ting (Duke-NUS Medical School, Singapore)	WT-Z could not be verified by restriction digest following transformation into DH5α *E. coli*	Wait for Stbl3 *E. coli* delivery for transformation but use WT-B for all experiments in the interim.

Supplementary Table 5. List of PD-linked hPINK1 mutations and their protein and nucleotide locations. Compiled from NCBI ClinVar search of the PINK1 gene

https://www.ncbi.nlm.nih.gov/clinvar

PINK1 mutation	Protein location	Nucleotide and protein change	Protein change
A168P	N-lobe	502G>C	Ala168Pro
M318L	N-lobe	952A>T	Met318Leu
T257I	Activation loop/N-lobe	770C>T	Thr257Ile
L268V	N-lobe	802C>G	Leu268Val
H271Q	N-lobe	813C>A	His271Gln
A280T	N-lobe	838G>A	Ala280Thr
T313M	N-lobe	938C>T	Thr313Met
L268V	N-lobe	802C>G	Leu268Val
H271Q	N-lobe	813C>A	His271Gln
A280T	N-lobe	838G>A	Ala280Thr
P296L	N-lobe	887C>T	Pro296Leu
G309D	N-lobe	926G>A	Gly309Asp
A339T	C-lobe	1015G>A	Ala339Thr

M341I	C-lobe	1023G>A	Met341Ile
L347P	C-lobe	1040T>C	Leu347Pro
F385L	C-lobe	1153T>C	Phe385Leu
C388R	C-lobe	1162T>C	Cys388Arg
P399L	C-lobe	1196C>T	Pro399Leu
R407Q	C-lobe	1220G>A	Arg407Gln
Y431H	C-lobe	1291T>C	Tyr431His
W437X	C-lobe	1311G>A	Trp437Ter
Q5X	MTS	13C>T	Gln5Ter
G23S	MTS	67G>A	Gly23Ser
G26R	MTS	76G>C	Gly26Arg
G30R	MTS	88G>C	Gly30Arg
R42C	Between MTS and OMS	124C>T	Arg42Cys
A54E	Between MTS and OMS	161C>A	Ala54Glu
S73L	OMS	218C>T	Ser73Leu
C92fs	OMS	273del	Cys92fs
L108fs	TMS	322del	Leu108fs
Q115L	Between TMS and kinase domain	344A>T	Gln115Leu
T145M	Between TMS and kinase domain	434C>T	Thr145Met
G150D	Between TMS and kinase domain	449G>A	Gly150Asp
R152W	Between TMS and kinase domain	454C>T	Arg152Trp
G163D	N-lobe	488G>A	Gly163Asp
K186N	N-lobe	558G>C	Lys186Asn
G189R	N-lobe	565G>A	Gly189Arg
P196L	N-lobe	587C>T	Pro196Leu
A200fs	N-lobe	599del	Ala200fs
R207Q	N-lobe	620G>A	Arg207Gln
R207fs	N-lobe	620del	Arg207fs
P209L	N-lobe	626C>T	Pro209Leu
P215L	N-lobe	644C>T	Pro215Leu
A217D	N-lobe	650C>A	Ala217Asp
W222X	N-lobe	665G>A	Trp222Ter
A232V	N-lobe	695C>T	Ala232Val
M237V	N-lobe	709A>G	Met237Val
R246X	N-lobe	736C>T	Arg246Ter
L249V	N-lobe	745T>G	Leu249Val
T257I	N-lobe	770C>T	Thr257Ile
Y258X	N-lobe	774C>A	Tyr258Ter
Q367X	N-lobe	799C>T	Gln267Ter
R276W	N-lobe	826C>T	Arg276Trp

R276Q	N-lobe	827G>A	Arg276Gln
R279C	N-lobe	835C>T	Arg279Cys
R279H	N-lobe	836G>A	Arg279His
S284Y	N-lobe	851C>A	Ser284Tyr
P289T	N-lobe	865C>A	Pro289Thr
L308Q	N-lobe	923T>A	Leu308Gln
R312Q	N-lobe	935G>A	Arg312Gln
T313M	N-lobe	938C>T	Thr313Met
M318L	N-lobe	952A>T	Met318Leu
Y321C	C-lobe	962A>G	Tyr321Cys
S335G	C-lobe	1003A>G	Ser335Gly
A340T	C-lobe	1018G>A	Ala340Thr
A359T	C-lobe	1075G>A	Ala359Thr
D366N	C-lobe	1096G>A	Asp366Asn
A3838T	C-lobe	1147G>A	Ala383Thr
Y404X	Activation loop	1212C>G	Tyr404Ter
G411S	Activation loop	1231G>A	Gly411Ser
Q456X	C-lobe	1366C>T	Gln456Ter
E476K	C-lobe	1426G>A	Glu476Lys
R492X	C-lobe	1474C>T	Arg492Ter
R501Q	C-lobe	1502G>A	Arg501Gln
N521T	C-terminal region	1562A>C	Asn521Thr
D525fs	C-terminal region	1570_1573dup	Asp525fs
D525N	C-terminal region	1573G>A	Asp525Asn
K526N	C-terminal region	1578G>C	Lys526Asn
M527T	C-terminal region	1580T>C	Met527Thr
W577R	C-terminal region	1729T>C	Trp577Arg

Abbreviations: hPINK1, human PINK1; MTS, mitochondrial targeting sequence; OMS, mitochondria membrane localization sequence; TMS, transmembrane sequence.

Appendix III. Supplementary data

1. PCR of WT plasmids
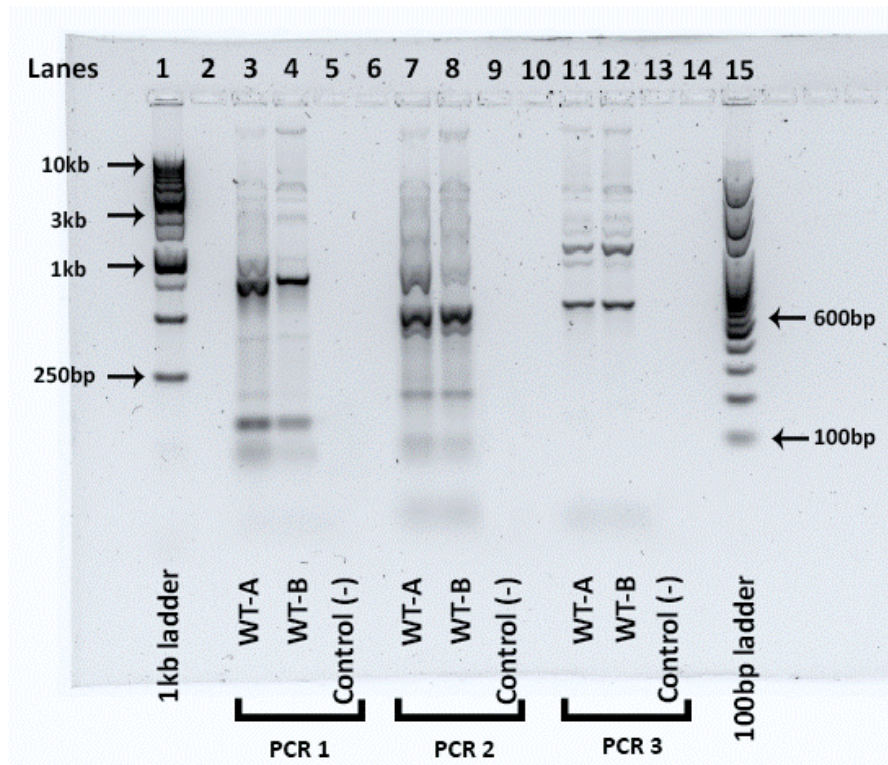
Supplementary Figure 3. Polymerase Chain Reaction products of WT-A and WT-B PINK1.

 Lane 1: 1 kb DNA ladder; Lane 3-5: PCR 1; Lane 7-9: PCR 2; Lane 11-13: PCR 3; Lane 15: 100 bp DNA ladder; Lane 2, 6, 10, and 14: Blank.

2. LC-MS mass spectra
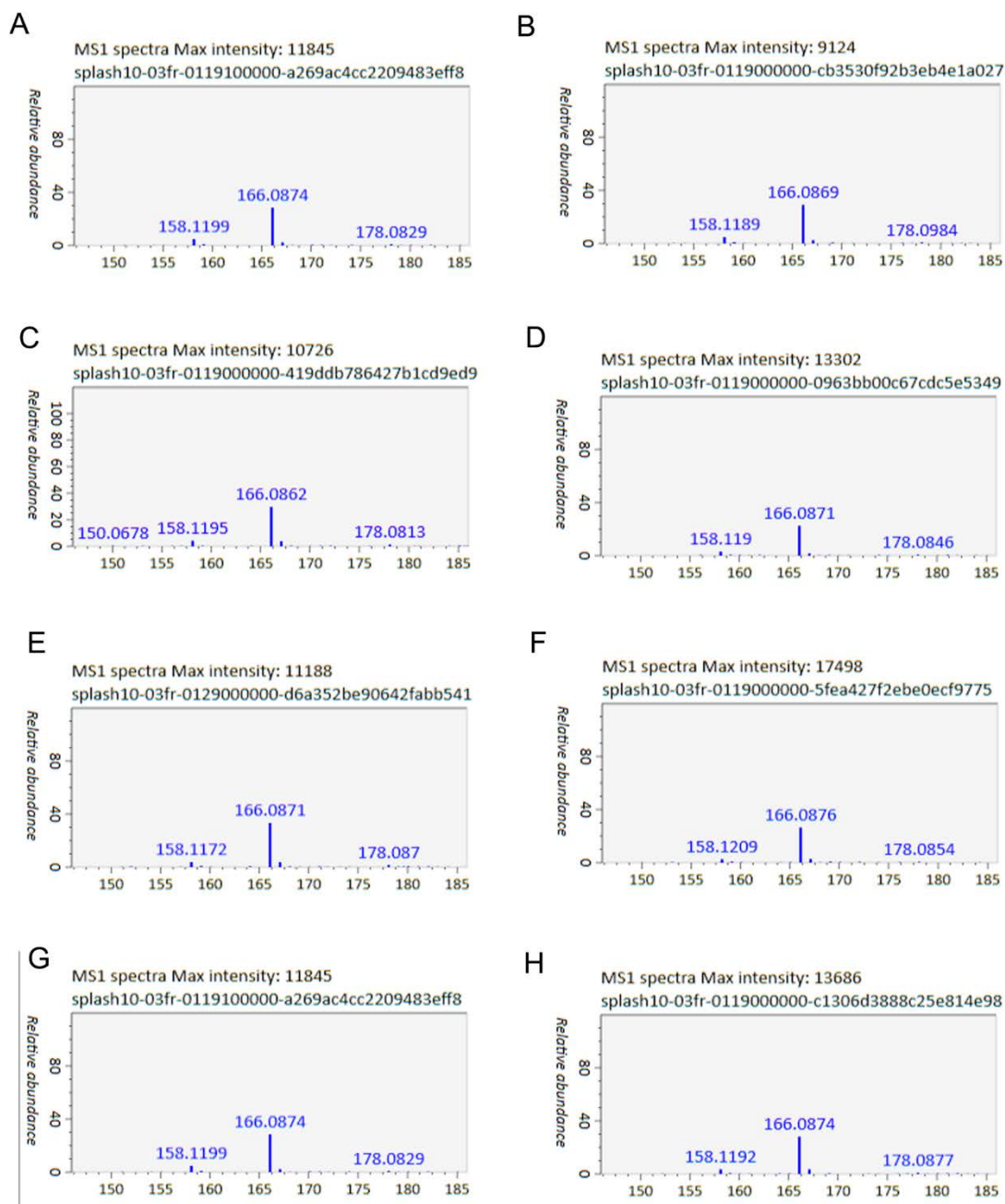
Supplementary Figure 4. Relative abundance of phenylalanine detected in cell culture medium control (A-B), untransfected (C-D), WT PINK1, (E-F) and G309D PINK1 (G-H) SH-SY5Y cells.
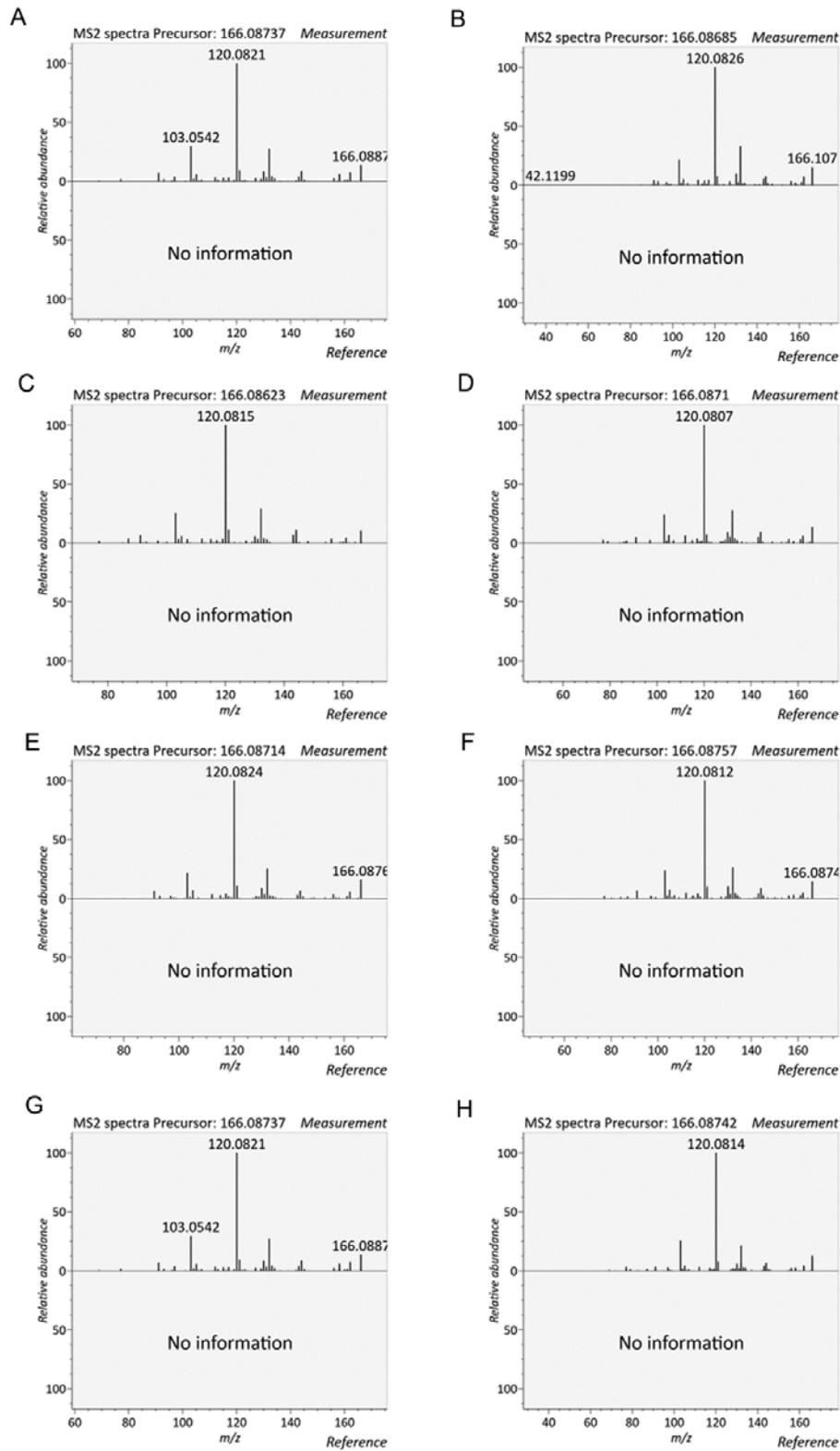
Supplementary Figure 5. Fragment ions of phenylalanine detected in cell culture medium control (A-B), untransfected (C-D), WT PINK1, (E-F) and G309D PINK1 (G-H) SH-SY5Y cells.

Supplementary Table 6. Compounds unique to the mutant PINK1, and both WT and mutant PINK1 compared to the untransfected control as determined through LC-MS.

Observed m/z	Sample	Molecular Formula [M+H]⁺	Theoretical m/z	Mass tolerance error (PPM)
349.14090	G309D 1	C18H17N6O2	349.1413	-1.14
		C2H17N14O7	349.1405	1.25
		C3H13N18O3	349.1418	-2.58
		C4H19N11O8	349.1418	-2.6
		C17H21N2O6	349.14	2.69
		C16H15N9O	349.14	2.7
		C20H19N3O3	349.1426	-4.99
		H15N17O6	349.1391	5.09
		C5H15N15O4	349.1431	-6.43
		C6H21N8O9	349.1431	-6.44
		C15H19N5O5	349.1386	6.53
		C14H13N12	349.1386	6.55
349.13930	G309D 2	H15N17O6	349.1391	0.51
		C16H15N9O	349.14	-1.88
		C17H21N2O6	349.14	-1.89
		C15H19N5O5	349.1386	1.95
		C14H13N12	349.1386	1.97
		C2H17N14O7	349.1405	-3.33
		C18H17N6O2	349.1413	-5.72
		C14H23NO9	349.1373	5.78
		C13H17N8O4	349.1373	5.8
356.06670	G309D 1	C5H16N4O14	356.0663	1.12
		C4H10N11O9	356.0663	1.13
		C3H4N18O4	356.0663	1.15
		C20H10N3O4	356.0671	-1.21
		C18H8N6O3	356.0658	2.56
		C5H6N15O5	356.0676	-2.62
		C6H12N8O10	356.0676	-2.64
		C3H14N7O13	356.065	4.89
		C2H8N14O8	356.065	4.91
		C21H6N7	356.0685	-4.97
		C22H12O5	356.0685	-4.98
		C17H12N2O7	356.0645	6.32
		C16H6N9O2	356.0644	6.33
		C6H2N19O	356.069	-6.38
		C7H8N12O6	356.069	-6.39
		C8H14N5O11	356.069	-6.41
356.06760	G309D 2	C5H6N15O5	356.0676	-0.09

		C6H12N8O10	356.0676	-0.11
		C20H10N3O4	356.0671	1.32
		C21H6N7	356.0685	-2.44
		C5H16N4O14	356.0663	3.65
		C4H10N11O9	356.0663	3.66
		C3H4N18O4	356.0663	3.68
		C6H2N19O	356.069	-3.85
		C7H8N12O6	356.069	-3.86
		C8H14N5O11	356.069	-3.88
		C18H8N6O3	356.0658	5.09
		C23H8N4O	356.0698	-6.21
361.32890	G309D 1	C17H41N6O2	361.3291	-0.55
		C15H39N9O	361.3278	3.16
		C19H43N3O3	361.3304	-4.27
		C13H37N12	361.3264	6.88
361.32780	G309D 1	C15H39N9O	361.3278	0.12
		C17H41N6O2	361.3291	-3.6
		C13H37N12	361.3264	3.84
525.37600	G309D 1	C25H43N13	525.3764	-0.83
		C26H49N6O5	525.3764	-0.84
		C25H53N2O9	525.3751	1.7
		C24H47N9O4	525.3751	1.71
		C27H45N10O	525.3778	-3.39
		C28H51N3O6	525.3778	-3.4
		C23H51N5O8	525.3738	4.26
		C22H45N12O3	525.3738	4.27
		C37H49O2	525.3733	5.22
		C29H47N7O2	525.3791	-5.95
		C30H53O7	525.3791	-5.96
		C21H49N8O7	525.3724	6.81
		C20H43N15O2	525.3724	6.82
		C14H43N19O3	525.3796	-6.9
525.37570	G309D 2	C25H53N2O9	525.3751	1.13
		C24H47N9O4	525.3751	1.14
		C25H43N13	525.3764	-1.41
		C26H49N6O5	525.3764	-1.42
		C23H51N5O8	525.3738	3.69
		C22H45N12O3	525.3738	3.7
		C27H45N10O	525.3778	-3.96
		C28H51N3O6	525.3778	-3.97
		C37H49O2	525.3733	4.65
		C21H49N8O7	525.3724	6.24

		C20H43N15O2	525.3724	6.25
		C29H47N7O2	525.3791	-6.52
		C30H53O7	525.3791	-6.53
556.17580	G309D 1	C34H20N8O	556.176	-0.37
		C35H26NO6	556.176	-0.38
		C20H32N2O16	556.1752	1.11
		C19H26N9O11	556.1752	1.12
		C18H20N16O6	556.1752	1.13
		C19H16N20O2	556.1765	-1.28
		C20H22N13O7	556.1765	-1.29
		C21H28N6O12	556.1765	-1.3
		C33H24N4O5	556.1747	2.03
		C32H18N11	556.1747	2.04
556.17580	G309D 2	Same as above		
610.18490	G309D 1	C6H28N17O17	610.1849	-0.01
		C35H20N11O	610.1852	-0.54
		C36H26N4O6	610.1852	-0.55
		C21H32N5O16	610.1844	0.81
		C20H26N12O11	610.1844	0.82
		C19H20N19O6	610.1844	0.83
		C21H22N16O7	610.1857	-1.37
		C22H28N9O12	610.1857	-1.38
		C23H34N2O17	610.1857	-1.39
		C35H30O10	610.1839	1.64
		C34H24N7O5	610.1839	1.65
		C33H18N14	610.1839	1.66
		C4H26N20O16	610.1836	2.19
		C8H30N14O18	610.1863	-2.21
		C37H22N8O2	610.1866	-2.74
		C38H28NO7	610.1866	-2.75
610.18410	G309D 2	C35H30O10	610.1839	0.33
		C34H24N7O5	610.1839	0.34
		C33H18N14	610.1839	0.35
		C19H20N19O6	610.1844	-0.48
		C20H26N12O11	610.1844	-0.49
		C21H32N5O16	610.1844	-0.5
		C4H26N20O16	610.1836	0.88
		C6H28N17O17	610.1849	-1.32
		C20H36NO20	610.1831	1.69
		C19H30N8O15	610.1831	1.7
		C18H24N15O10	610.1831	1.71
		C35H20N11O	610.1852	-1.85

		C36H26N4O6	610.1852	-1.86
		C33H28N3O9	610.1826	2.53
Unique to WT and G309D compared to UT				
175.01710	WT 1	C11HN3	175.017	0.3
		C13H3O	175.0184	-7.37
175.01650	WT 2	C11HN3	175.017	-3.13
175.01710	G309D 1	C11HN3	175.017	0.3
175.01670	G309D 2	C11HN3	175.017	-1.98
280.14010	WT 1	C11H22NO7	280.1396	1.69
		C10H16N8O2	280.1396	1.71
		C12H18N5O3	280.141	-3.09
		C9H20N4O6	280.1383	6.48
280.14060	WT 2	C12H18N5O3	280.141	-1.3
		C11H22NO7	280.1396	3.47
		C10H16N8O2	280.1396	3.49
		C14H20N2O4	280.1423	-6.09
280.14060	G309D 1	C12H18N5O3	280.141	-1.3
		C11H22NO7	280.1396	3.47
		C10H16N8O2	280.1396	3.49
		C14H20N2O4	280.1423	-6.09
280.13980	G309D 2	C11H22NO7	280.1396	0.62
		C10H16N8O2	280.1396	0.64
		C12H18N5O3	280.141	-4.16
		C9H20N4O6	280.1383	5.41
		C8H14N11O	280.1383	5.43
374.30390	WT 1	C22H38N4O	374.3046	-1.77
		C21H42O5	374.3032	1.8
		C20H36N7	374.3032	1.82
		C24H40NO2	374.3059	-5.36
		C19H40N3O4	374.3019	5.39
374.30420	WT 2	C22H38N4O	374.3046	-0.97
		C21H42O5	374.3032	2.61
		C20H36N7	374.3032	2.62
		C24H40NO2	374.3059	-4.55
		C19H40N3O4	374.3019	6.19
374.30290	G309D 1	C20H36N7	374.3032	-0.85
		C21H42O5	374.3032	-0.87
		C19H40N3O4	374.3019	2.72
		C22H38N4O	374.3046	-4.44
		C17H38N6O3	374.3005	6.31
374.30450	G309D 2	C22H38N4O	374.3046	-0.17
		C21H42O5	374.3032	3.41

133

		C20H36N7	374.3032	3.42
		C24H40NO2	374.3059	-3.75
		C19H40N3O4	374.3019	6.99
678.68890	WT 1	C45H90O3	678.689	-0.14
		C43H88N3O2	678.6877	1.84
		C41H86N6O	678.6863	3.81
		C48H88N	678.6917	-4.09
		C39H84N9	678.685	5.79
678.68650	WT 2	C41H86N6O	678.6863	0.28
		C43H88N3O2	678.6877	-1.7
		C39H84N9	678.685	2.26
		C45H90O3	678.689	-3.68
678.68700	G309D 1	C43H88N3O2	678.6877	-0.96
		C41H86N6O	678.6863	1.01
		C45H90O3	678.689	-2.94
		C39H84N9	678.685	2.99
		C48H88N	678.6917	-6.89
678.68710	G309D 2	C43H88N3O2	678.6877	-0.82
		C41H86N6O	678.6863	1.16
		C45H90O3	678.689	-2.79
		C39H84N9	678.685	3.14
		C48H88N	678.6917	-6.74

Abbreviations: WT, wild-type; UT, untransfected; m/z, mass to charge ratio.

3. Flow cytometry optimization
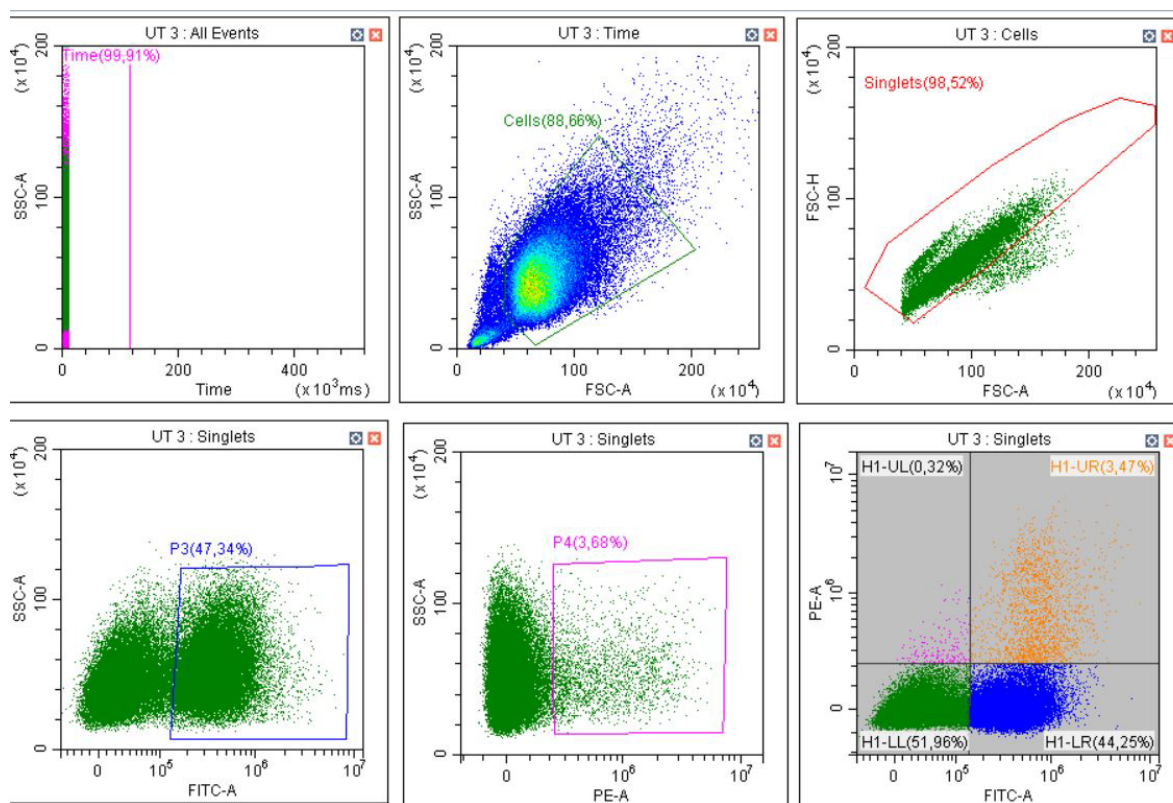
Supplementary Figure 6. Gating strategy for flow cytometry. Refinement criteria included time, cells, singlets, and FITC and PE events. This gating strategy was used for flow cytometry analysis of all samples.

Abbreviations: FITC, fluorescein; PE, phycoerythrin; UT, untransfected.

Appendix IV. Nanocurcumin synthesis

Nanocurcumin was produced by and obtained from our collaborator Dr Sarah D'Souza at the University of Western Cape, South Africa.

Supplementary Table 7. Properties of unloaded and loaded curcumin polycaprolactone nanoparticles. Upon incorporation of curcumin, the nanoparticle size, PDI and ZP were reduced, as previously observed (Umerska et al., 2018). Low PDI values (< 0.3) suggest more uniform, or monodisperse, particle sizes. ZP is directly related to the charges of the raw materials comprising the particles. Stable nanoparticles, as observed when loaded with curcumin, have ZP values between -20 mV and 20 mV.

	Nanoparticle	Curcumin loaded nanoparticle
Size (nm)	404 ± 110	292 ± 27
Polydispersity index (PDI)	0.34 ± 0.17	0.13 ± 0.07
Zeta potential (ZP) (mV)	-22.2 ± 9.67	-14.4 ± 1.80

Abbreviations: PDI, polydispersity index; ZP, zeta potential

Appendix V.   Laboratory protocols

1.   Culturing human neuroblastoma SH-SY5Y cells

The inner surfaces of the laminar flow hood were cleaned with 70 % ethanol to prevent contamination and sterile 25 cm^2 CellBIND flasks (Corning, United States) were correctly labelled. Cell culture media was prepared by adding 10 % FBS and 1 % penicillin streptomycin to DMEM (Thermo Fisher Scientific, United States). A volume of 1 ml media was added to each cryovial of frozen cells to thaw cells quickly. A volume of 4 ml media was added to each flask, followed by 1 ml of cells which was pipetted directly into each flask. Flasks were incubated at 37 °C, 5 % CO_2 until 80-90 % confluent, with media changes and washes with phosphate buffered saline (PBS) as needed.

1.1. Trypsinizing the cells

Once confluent, the media was pipetted out of the flask and the cells were washed with 5 ml PBS to remove excess media. Thereafter, 3 ml trypsin was added to the flask and incubated for 5 mins to lift bound cells off the flask surface. A volume of 4 ml media was added to the flask to neutralize the trypsin, and the cell/trypsin mixture was pipetted into a 15 ml centrifuge tube. The tube was centrifuged at 1006 x g for 3 min. The supernatant was discarded, and the pellet of cells was resuspended in media for transfer into a bigger flask or use in a culture plate for further experiments.

Appendix VI. R script

```
onewayanova <- aov(variable ~ factor, data = data, projections = FALSE, qr = TRUE,

        contrasts = NULL)
```

Footnote: variable=Viability (dependent variable); factor=Concentration (categorical group variable)

```
twowayanova<-aov(variable1~ as.factor(group1)*as.factor(group2),data=data)
```

Footnote: variable1=Viability (dependent variable); group1=Transfection (categorical group variable 1) group2=Treatment (categorical group variable 2)

```
shapiro.test(res)
```

```
leveneTest(variable1 ~ group,data=data)
```

Footnote: variable1=Viability (dependent variable); group=Treatment (categorical group variable)

```
posthoc <- lsmeans(anova,

        pairwise ~ group,

        adjust="posthoc")
```

Footnote: group=Treatment (dependent variable); posthoc=Bonferroni or Dunnett

```
TukeyHSD(anova)
```

```
robustlinearmodel <- MASS::rlm(formula = value ~ group1 + group2,data=dataset)
```

Footnote: value= Cellular Viability (numeric of type num or integer); group1= Transfection status (categorical group variable) and group2= Treatment groups (categorical group variable)